An Experimental Study on Hydro-Mechanical Characteristics of Compacted Bentonite-Sand Mixtures

Dissertation
as a requirement for the degree of

Doktor – Ingenieur

at the Faculty of Civil Engineering

Bauhaus-University Weimar

submitted by

Agus Setianto Samingan
from Jakarta / Indonesia

Weimar

Reviewers:

1. Prof. Dr.-Ing. habil. T. Schanz
2. Prof. D.G. Fredlund
3. Prof. P. Delage

Day of Defense: 29 July 2005

To my parents, my wife Sofia, and my daughter Zahira

VORWORT DES HERAUSGEBERS

Die vorliegende Promotionsarbeit ist dem Forschungsgebiet der „Experimentellen Bodenmechanik“ zuzuordnen. Mittelpunkt bildet die Untersuchung von expansiven Materialien unter Berücksichtigung deren nicht vollständiger Sättigung. Derartige Arbeiten beziehen sich oft auf die Anwendung dieser Materialien im Rahmen der untertägigen Lagerung hoch toxischer Abfälle. Im Gegensatz zur Anwendung in der unmittelbaren Nähe des Abfalls wird in dieser Arbeit der Einsatz in Verschlussbauwerken behandelt. Aus diesem Grund werden Einflüsse der Temperatur nicht betrachtet.

Im Rahmen der untertägigen Endlagerung hoch toxischer Abfälle ist eine wichtige Zielsetzung die möglichst vollständige Abkapslung des Abfalls von der Biosphäre. Besonders alte Bergwerke bieten sich hierfür an, und werden weltweit favorisiert. Ein wichtiges Bauwerk im Gesamtkonzept ist das so genannte „Verschlussbauwerk“, gewisser Maßen die Eingangstür zu einem Endlager.

Neben Aufgaben der Lastabtragung in das umgebende Gebirge und der Lagestabilität steht die Verringerung der Durchströmbarkeit im Vordergrund. Bevorzugt werden Baustoffe, die unter Fluidzutritt quellen und dadurch ihre Permeabilität drastisch reduzieren. Eine der technischen Möglichkeiten bilden Mischungen aus Sand und aktivem Ton, hier besonders unterschiedliche Bentonite. Der ursprünglich „trocken“ eingebaute Baustoff erfährt bei einer Fluidbeaufschlagung eine progressive Aufsättigung. Deshalb ist eine Beschreibung der konstitutiven Eigenschaften unter Berücksichtigung des Sättigungsgrades von entscheidender Bedeutung.

Neben der Permeabilität ist die Entwicklung der Volumenänderung (Quellpotential) bzw. des Quelldrucks, der Kompressibilität mit der Sättigung von Bedeutung.

Teilgesättigte Materialien erfordern eine Diskussion der zu ihrer Beschreibung notwendigen Definition der „effektiven“ Spannungen. Dieser für trockene oder vollständig gesättigte Materialien eingeführte Begriff muss bei Berücksichtigung der Teilsättigung erweitert werden. Der in dieser Arbeit verfolgte Ansatz beinhaltet die Berücksichtigung der so genannten „Saugspannung“. Diese umfasst wiederum verschiedene Komponenten, die sich auf unterschiedliche zu Grunde liegende Prozesse beziehen (Kapillarwirkung, physico-chemische Interaktion zwischen Ton und Porenfluids: osmotischer Anteil). Eine zentrale Bedeutung kommt der Beziehung

zwischen Sättigung bzw. dem Wassergehalt und der Saugspannung zu. Diese Beziehung ist abhängig von der Belastungsrichtung und der Belastungsgeschichte.

Die vorliegende Arbeit umfasst, neben Entwicklung und Einführung der sehr komplexen Versuchstechnik, drei wesentliche eigenständige Arbeitspakete:

a. Die Untersuchung der „Saugspannung“ für teilgesättigte expansive Materialien, und hierbei besonders die Analyse der zu Grunde liegenden physikalisch-chemischen Prozesse (Kapitel 8).

b. Untersuchungen zur Be- und Entwässerung von expansiven Materialien für unterschiedliche Randbedingungen bezüglich der Volumendehnung (Kapitel 9).

c. Untersuchungen zum Quelldruck und der Kompressibilität teilgesättigter, expansiver Materialien.

Die von Herrn Samingan erzielten Ergebnisse, an Baustoffen, wie sie im nationalen deutschen Konzept verwendet werden sollen, ermöglichen es erstmalig, einen „begründeten“ quantitativen Entwurf für Dichtelemente durchzuführen.

Besonders hervorzuheben ist an dieser Stelle die Ableitung konstitutiver Modellparameter aus den experimentellen Untersuchungen, dies es uns in Zusammenarbeit mit unseren Partnern ermöglichte, konkrete Aufgabenstellungen mittels numerischer Modellierungen zu behandeln.

Die Arbeiten wurden durch die Förderung des BMBF erst ermöglicht. Besonderer Dank gilt dem Projektträger, vertreten durch Dr. H. Pitterich (FZ Karlsruhe).

Weimar, im August 2005 Tom Schanz

ABSTRACT

Nuclear and hazardous waste disposal issues have become universal issues and problems related to the final disposal of these waste including finding a suitable site, natural and engineered barriers used, construction of the repository, long-term performance assessment have gained increasing attention all over the world. High-level radioactive and hazardous waste are required to be buried in deep geological repositories. In Germany, the ongoing researches have assessed the suitability of salt-stone formation in the country as a host rock candidate for its nuclear waste repository. Bentonite-based materials have been proposed to be used as sealing and buffer elements for the nuclear waste repository. Several hydro-mechanical processes will take place in the field and influence behaviour of the sealing and buffer elements of the repository.

In this dissertation, a study on the hydro-mechanical characterisation of bentonite-sand mixtures is presented. Mixtures of a calcium-type bentonite, named Calcigel, and quartz sand were used in the investigation. Series of experiments including basic and physico-chemical characterisation, microstructure and fabric studies, suction and swelling pressure measurements, wetting and drying test, one-dimensional compression-rebound test, one-dimensional cyclic wetting-drying test under constant vertical stress, and saturated permeability test were conducted.

The experimental data obtained are analysed and several characteristics of the material are brought out in this dissertation. Conclusions regarding basic behaviour of the materials are drawn based on the results of microstructure and fabric studies. Factors influencing the magnitude of suction and swelling pressure of the materials are outlined and discussed. The suction-induced compression and rebound characteristics of the material are described. The wetting and drying behaviour as influenced by the material boundary conditions are discussed. Permeability characteristics of the materials are examined based on several available permeability models.

Several mechanical and hydraulic parameters that can be used in modelling using some available constitutive modelling approaches are derived based on the experimental data. At the end, conclusions regarding the hydro-mechanical characteristics of the materials are drawn and suggestions for future studies are made.

ZUSAMMENFASSUNG

Die (End-) Verwahrung von hoch toxischem chemischen und radioaktiven Abfällen hat aktuell weltweit an Bedeutung gewonnen und insbesondere Fragen bezüglich der „optimalen Einlagerung“, der Art der Versiegelung, die Konstruktion der Endlagerstätten sowie das Verhalten während „langer“ Zeiträume, sind Schwerpunkte der Forschung. Hoch radioaktive und chemische Abfälle sollen in der Mehrzahl der Konzepte in Kanistern versiegelt und unterirdisch in großer Tiefe in geeigneten geologischen Schichten gelagert werden. Aktuelle Forschungen in Deutschland haben ergeben, dass z.B. Salz-Gestein ein zuverlässiger Wirtsgesteins-Kandidat für die sicher Endlagerung des radioaktiven Abfalls ist. Bentonit basierendes Material wird derzeit als Versiegelung bzw. als Puffermaterial für hoch toxisches und radioaktives Abfallmaterial genutzt. Komplexe, gekoppelte hydromechanische Prozesse beeinflussen das Verhalten der Versiegelung sowie die Pufferwirkung der Endlagerstätte.

In der vorliegenden Dissertation wird eine Studie über die hydromechanischen Eigenschaften von Betonit- Sand-Gemischen dargestellt. Die untersuchten Mischungen bestehen aus unterschiedlichen Anteilen von Kalzium-Bentonit, das so genannte Calcigel, und Quarzsand. Porosimetrieuntersuchungen und Studien mit dem ESEM ergaben Aufschluss über die Struktur und die physikalisch-chemischen Kennwerte des Gefüges auf der Mikroskala. Auf der Makroskala wurde u.a. die Saugspannungs-Wassergehaltsbeziehung der Gemische untersucht. Außerdem wurden zyklische Trocknungs- und Bewässerungsversuche, Kompressionsversuche im Ödometergerät und gesättigte Permeabilitätsversuche durchgeführt. Der Quelldruck und das Quellpotential wurden für unterschiedliche Belastungspfade untersucht.

Die erzielten experimentellen Ergebnisse wurden im Rahmen der zu Grunde liegenden theoretischen Modelle ausgewertet und interpretiert. Wegweisende Erkenntnisse der Arbeit beziehen sich auf die Saugspannungs-Wassergehaltsbeziehung für unterschiedliche Versuchsrandbedingungen (freie Volumenänderung versus vollständig behinderte Volumenänderung) und die Entwicklung des Quelldrucks in Abhängigkeit der Saugspannung.

Die erzielten Ergebnisse wurden zur Kalibrierung von zwei unterschiedlichen konstitutiven Ansätzen benutzt. Zusätzlich durchgeführte Versuche konnten abschliessend erfolgreich simuliert werden.

ACKNOWLEDGEMENTS

Praise be to God, the most gracious and the most merciful, for His helps that enable me to finish this work. I would like to thank first and foremost my supervisor, Prof. Tom Schanz, for his meticulous guidance throughout my period of candidature. I am especially grateful with the opportunities given to me to carry out the works and compile my *promotion*. I would like to acknowledge the financial support provided by Bundesministerium fur Bildung und Forschung (BMBF) through a project grant No. 02C0881.

My gratitude should also be extended to the members of the Laboratory of Soil Mechanics including the research and laboratory staffs. I thank Dr. Tripathy who designed the high pressure oedometer cell that was used in the experimental work. I would also like to pass my recognition to Dr. Datcheva who provided a significant role in the derivation of modelling parameters. Thanks also to Ms. Tscheschlok and Mr. Hoppe for their assistance in the experiments. My gratitude goes also to Ms. Lins, Mr. Zimerrer, and Mr. Arifin for their shares of ideas. Uncountable helps from my roommate Mr. Wolff are gratefully acknowledged.

My thanks are also for Prof. Fredlund, Prof. Sridharan, and Prof. Nagaraj for the discussion during their short visits to Weimar. Many thanks go to Prof. Delage for his agreement to be an external reviewer of this dissertation together with Prof. Fredlund. I would like pass my gratefulness to all parties who indirectly assisted me during my period of stay in Weimar.

At last but not at least, I would like to gratitude my wife, Sofia, who has been accompanying me patiently, and my daughter, Zahira, for her entertaining and cheerful behaviour at home.

LIST OF CONTENTS

LIST OF FIGURES

LIST OF TABLES

LIST OF SYMBOLS

a	:	A soil (or fitting) parameter used in the van Genuchten and Fredlund and Xing SWCC equation.
A	:	Attractive forces.
A_p	:	Void ratio at the reference net mean stress (p_c) with respect to changes in net mean stress.
A_s	:	Void ratio at the reference suction (s_c) with respect to changes in suction.
B	:	Bentonite content.
c_{app}	:	Apparent effective cohesion of soil.
c_M	:	Slope of $\Delta M_w/\Delta M_{w\ max}$ versus $t^{0.5}$ curve at the earlier stage of swelling pressure test.
c_p	:	Slope of $P_s/P_{s\ max}$ versus $t^{0.5}$ curve at the earlier stage of swelling pressure test.
c_{RH}	:	Intercept in the rectangular hyperbola method of consolidation analysis.
c_v	:	Coefficient of consolidation.
c'	:	Saturated effective cohesion of soil.
C	:	A correction factor in the Fredlund and Xing SWCC equation.
$C_{K\text{-}C}$	:	Kozeny-Carman empirical coefficient.
C_1	:	A soil parameter controlling the change in A_p with suction and the change in A_s with net mean stress.
C_2	:	A soil parameter controlling the change in A_p with suction and the change in N_s with net mean stress.
C_3	:	A soil parameter controlling the change in N_p with suction and the change in N_s with net mean stress.
C_4	:	A soil parameter controlling the change in A_s with net mean stress and the change in N_p with suction.
C_o	:	Bulk concentration of permeant.
$C_p^{\,a}$	:	Adsorptive coefficient.
$C_p^{\,c}$	:	Capillary coefficient.
D	:	Soil grain diameter.
D_{ave}	:	Average soil pore diameter.

D_p : Soil pore diameter.

e : Soil void ratio.

e_b : Bentonite void ratio.

e_c : Cluster void ratio.

e_{co} : Initial cluster void ratio (i.e., equal to e_{mo}).

e_m : Soil micro-structural void ratio.

e_M : Soil macro-structural void ratio.

e_o : Soil initial void ratio.

e_T : Total void ratio (i.e., equal to e).

E : Modulus of elasticity of the soil structure with respect to changes in net mean stress.

E_w : Modulus of elasticity of the water phase with respect to changes in net mean stress.

F : A function used in the crack assessment.

G_s : Specific gravity.

G_{ss} : Specific gravity of sand.

H : Modulus of elasticity of the soil structure with respect to changes in suction.

H_w : Modulus of elasticity of the water phase with respect to changes in suction.

f_D : Micro-macro interaction function for suction decrease.

f_I : Micro-macro interaction function for suction increase.

f_{Do}, f_{D1} : Material parameters for f_D.

f_{Io}, f_{I1} : Material parameters for f_I.

g : Gravitational acceleration.

k : A parameter which takes into account the increase in tensile strength with increasing suction.

k_{ave} : Average saturated coefficient of permeability.

k_s : Saturated coefficient of permeability with respect to water phase.

k_{sc} : Computed saturated coefficient of permeability with respect to water phase.

k_{rw} : Relative permeability for wetting fluid.

k_w : Unsaturated coefficient of permeability with respect to water phase.

K : Intrinsic permeability.

K_m : Coefficient of volume change for the microstructure of an expansive soil.

K_{min} : Minimum bulk modulus of soil.

K_o : Coefficient of earth pressure at rest.

K_t : Coefficient of volume change for the macrostructure (or soil structure) of an

expansive soil with respect to changes in net mean stress.

m : A soil (or fitting) parameter used in the van Genuchten and Fredlund and Xing SWCC equation.

m_{RH} : Slope in the rectangular hyperbola method of consolidation analysis.

m_1^s : Coefficient of volume change of the soil structure with respect to changes in net mean stress.

m_2^s : Coefficient of volume change of the soil structure with respect to changes in suction.

$m_{1\,oed}^s$: Coefficient of volume change of the soil structure with respect to changes in net mean stress for K_o-conditions.

$m_{2\,oed}^s$: Coefficient of volume change of the soil structure with respect to changes in suction for K_o-conditions.

m_1^w : Coefficient of volume change of the water phase with respect to changes in net mean stress.

m_2^w : Coefficient of volume change of the water phase with respect to changes in suction.

$m_{1\,oed}^w$: Coefficient of volume change of the water phase with respect to changes in net mean stress for K_o-conditions.

$m_{2\,oed}^w$: Coefficient of volume change of the water phase with respect to changes in suction for K_o-conditions.

M : Critical state line parameter.

M_w : Molecular weight of water.

n : A soil (or fitting) parameter used in the van Genuchten and Fredlund and Xing SWCC equation.

n_D : A material parameter for f_D.

n_I : A material parameter for f_I.

n_M : Soil macro-porosity.

n_T : Soil total porosity.

n_w^a : Adsorptive water-filled porosity.

N : Average number of clay particles per clay cluster.

N_p : Slope of the void ratio versus net mean stress curve in logarithmic scale.

N_s : Slope of the void ratio versus suction curve in logarithmic scale.

p : Net mean stress.

p_c : Reference net mean stress (i.e., also called p_{ref}).

P_{int} : Mercury intrusion pressure.

p_o : Yield stress or apparent pre-consolidation pressure.

p_o^* : Saturated yield stress or saturated pre-consolidation pressure.

$\hat{p}$	:	Micro-structural effective stress.
P	:	Pressure.
P_s	:	Swelling pressure.
$P_{s\,max}$	:	Maximum swelling pressure.
q	:	Rate of water transfer.
$q_{measured}$	:	Measured flow rate of water.
$q_{K\text{-}C}$	:	Estimated flow rate of water based on Kozeny-Carman model.
r	:	A fitting parameter describing changes in λ with suction.
r^2	:	Coefficient of determination.
R	:	Repulsive forces.
$R_{corrected}$	:	Corrected psychrometer reading.
R_g	:	Universal gas constant.
R_{psy}	:	Uncorrected psychrometer reading.
RH	:	Relative humidity.
s	:	Suction.
s_b	:	Air entry value.
s_c	:	Reference suction.
s_{cap}	:	A capillary component of suction.
s_m	:	Matric suction.
s_r	:	Suction corresponding to the residual volumetric water content (or residual degree of saturation).
s_t	:	Total suction.
S_e	:	Effective degree of saturation.
SEE	:	Standard error of estimate.
S_r	:	Degree of saturation.
S_{ra}	:	An adsorptive component of degree of saturation.
S_{rb}	:	Bentonite degree of saturation.
S_{rc}	:	A capillary component of degree of saturation.
S_{res}	:	Residual degree of saturation.
S_o	:	Specific surface area of soil particles.
t	:	Elapsed time.
t_s	:	Tensile strength.
T	:	Temperature.
T_{HG}	:	Surface tension of mercury.

T_w : Surface tension of water.

u_a : Pore-air pressure.

u_f : Liquid pressure.

u_v : Partial pressure of pore-water vapour.

u_{vo} : Saturation pressure of pore-water vapour.

u_w : Pore-water pressure.

V_a : Volume of air phase in a soil element.

V_o : Initial total volume of a soil element.

V_p : Soil pore volume.

V_v : Volume of void in a soil element.

V_w : Volume of water phase in a soil element.

w : Soil water content.

w_b : Bentonite water content.

w_{fp} : Filter paper water content.

w_m : Soil mixture water content.

α : A non-associativity parameter.

α_i : A parameter expressing the change in κ with suction.

α_m : A material parameter in the elastic micro-structural volumetric strain versus micro-structural effective stress.

α_p : Ratio of swelling pressure increment to suction decrement.

α_{sp} : A parameter expressing the change in κ_s with net mean stress.

α_{ss} : A parameter expressing the change in κ_s with suction.

β : A fitting parameter describing changes in λ with suction.

β_m : A material parameter in the elastic micro-structural volumetric strain versus micro-structural effective stress.

δ_b : A coefficient in the Brooks and Corey permeability function.

δ_v : Vertical deformation.

ΔM_w : Absorbed water.

ΔM_{wmax} : Maximum absorbed water.

ε_a : Axial strain.

ε_r : Radial strain.

ε_v : Volumetric strain.

$\varepsilon_{vertical}$: Vertical strain.

ε_{vm}^{e} : Elastic micro-structural volumetric strain.

ε_{vM}^{p} : Plastic volumetric strain of the macrostructure (or soil structure)

ε_{vp} : Volumetric strain induced by changes in net mean stress for virgin states of the soil.

ε_{vs} : Volumetric strain induced by changes in suction for virgin states of the soil.

ε_{vLC}^{p} : Plastic volumetric strain induced by the activation of LC yield curve.

ε_{vSI}^{p} : Plastic volumetric strain induced by the activation of SI yield curve.

ε_{vSD}^{p} : Plastic volumetric strain induced by the activation of SD yield curve.

θ_s : Saturated volumetric water content.

θ_w : Volumetric water content.

Θ : Normalised (or effective) volumetric water content.

κ : Compressive index for the macrostructure (or soil structure) with respect to changes in net mean stress.

$\kappa(o)$: Saturated compressive index for the macrostructure (or soil structure) with respect to changes in net mean stress.

κ_m : Compressive index for the microstructure of an expansive soil.

κ_s : Compressive index for the macrostructure (or soil structure) with respect to changes in suction.

$\kappa_s(o)$: Compressive index for the macrostructure (or soil structure) with respect to changes in suction at zero mean stress and zero suction.

λ : Slope of virgin compression line with respect to changes in net mean stress.

λ_b : Pore-size distribution index of soils.

λ_s : Slope of virgin compression line with respect to changes in suction.

$\lambda(o)$: Slope of saturated virgin compression line with respect to changes in net mean stress.

μ_w : Absolute viscosity of water.

π : Osmotic suction.

ρ : A parameter which takes into account the decrease in tensile strength with increasing temperature.

ρ_d : Soil dry density.

ρ_{db} : Bentonite dry density.

ρ_w : Density of water.

σ : Total stress.

σ' : Effective stress.

σ^*	:	'True' effective stress.
σ_m	:	Mean stress.
σ_{net}	:	Net stress.
σ_v	:	Total vertical stress (or vertical pressure).
$\sigma\parallel$	:	Total stress parallel to the direction of cracks.
$\sigma\perp$		Total stress perpendicular to the direction of cracks.
υ	:	Poisson's ratio.
ϑ	:	A dummy variable in the Mualem permeability function formulation.
φ_{HG}	:	Contact angle between mercury and the soil pore surface.
φ_w	:	Contact angle between water and the soil pore surface.
ϕ^b	:	An angle indicating the increase in shear strength with increasing suction.
ϕ'	:	Saturated effective cohesion of soil.
χ	:	Bishop's effective stress parameter.

CHAPTER 1

INTRODUCTION

1.1 Background

Nuclear (or radioactive) waste disposal issues have gained a universal attention since many nuclear power plants around the world are approaching the end of their operational stage. Issues pertaining to suitability of sites planned for the final disposal, natural as well as engineered barriers used, construction, operation, and long-term performance prediction have triggered intensive research studies in this field. Several governmental and private institutions have been established in many countries to deal with all these aspects. The issues for the toxic waste disposal programme basically remain the same since the volume of these wastes also increases with increasing industrialisation.

Classification of radioactive and hazardous wastes has been established. The classification provides a standard based on criteria which vary from country to country regarding how and in which way the waste should be stored or disposed. Some radioactive wastes are classified as low-level waste so that these wastes can be stored in several near-surface repositories. On the other hand, the high-level radioactive and hazardous waste requires deep geological repositories for the disposal. There is a need to establish high-level radioactive programmes to ensure robustness of the disposal system adopted and to assess long-term safety of the whole repository construction. In the deep geological disposal concept, the long-term performance of the repository is influenced by many factors including characteristics of host rocks where the repository is seated, characteristics of the sealing and buffer elements used, quality of the canisters where the waste is stored, and interactions between all of these components during construction and most importantly during repository lifetime.

In some concepts, the engineered barriers (i.e., the sealing and buffer elements) of the repository are expected to play a role in retarding any possible flow of substances in the beginning of operation of the repository. After that, the natural barriers (i.e., the host rocks) will take over the role. Therefore, it is important to investigate the materials that have been proposed to be used as sealing and buffer elements for the repository beside the studies performed on the host rock site characterisation. In the field, the sealing and buffer materials will undergo complex and coupled thermo-hydro-chemo-mechanical processes. Interactions between the host rocks, sealing and buffer elements, and probably with some substances from the waste will also take place.

In Germany, bentonite-based materials (including bentonite-sand mixtures) have been proposed to be used as sealing and buffer elements for the highly toxic waste (including nuclear waste) repository in the country. Research studies on the characterisation of the materials are underway in several research institutions as well as in several universities. The characterisation includes characterisation with respect to geotechnical, geological, hydraulic, chemical, physico-chemical, and thermal aspects of the material. The work presented in this doctoral dissertation is a part of the characterisation which mainly focussed on the hydro-mechanical aspects of the bentonite-based materials from the geotechnical engineering point of view. The experimental work carried out in this study was financially supported by Bundesministrium für Bildung und Forschung (BMBF) or the Federal Ministry for Education and Research through a project grant No. 02C0881.

1.2 Objectives and Scopes

The general objective of the study is to investigate the hydro-mechanical behaviour of bentonite-sand mixtures regarding the use of these materials as sealing and buffer elements for the final highly toxic waste (including nuclear waste) repository in Germany. The study has a primary focus on the experimental characterisation of the materials. The characterisation focussed on mixtures of a calcium-type bentonite, named Calcigel (or Montigel earlier), and quartz sand. The detailed scopes of the investigation are as follows:

- Determination of the basic and physico-chemical properties of the bentonite and sand used. Although these properties are not used directly in the analysis of experimental results, the results provide basic information that can be used for other purposes.

- Microstructure and fabric studies of the materials. The results gained from these studies provide information on how the materials behave in response to hydro-mechanical processes.

- Measurements of suction of bentonite-sand mixtures. Suction is a stress state variable of unsaturated soils. Since the bentonite-sand mixtures used in the repository are initially unsaturated, suction is present.

- Characterisation of the hydro-mechanical properties of the materials by considering several possible mechanisms that occur in the field.

- Derivation of several parameters that can be used in the constitutive modelling of the materials. It must be noted that although some experiments performed might not represent the real field processes, the data obtained are useful in the derivation of modelling parameters.

- The chemical and temperature aspects are not focuses of the current study. However, the experimental results presented in this dissertation can be used in conjunction with the data with respect to the chemical and temperature effects that may be obtained in the future.

1.3 Organisation of the Dissertation

The dissertation is composed by twelve chapters. The first chapter (i.e., this chapter) outlines the background, objectives, and scopes of the study, and the organisation of the dissertation. The second chapter presents literature review on radioactive and highly toxic waste disposal facilities in Germany and other countries. In the third chapter, theories relevant to the hydro-mechanical behaviour of the materials are described. These include physico-chemical characteristics, structure, fabric, mineralogy, clay-water interactions, and swelling and collapse mechanisms. The fourth chapter presents constitutive models that can be used to model the behaviour of expansive soils (including the compacted bentonite-sand mixtures). Several hydraulic models which are pertinent to the study are also presented and discussed.

In the fifth chapter, a literature review on experimental techniques that are relevant to the study is presented. Based on this, the experiments were carried out. The sixth chapter describes the basic and physico-chemical properties of the materials. The preparation of specimens used and the experiments performed in this study are described. The chapter also presents the microstructure and fabric studies performed on the material and discusses the results. In the seventh chapter, experimental techniques and procedures adopted are elaborated. The experimental results are presented and discussed in Chapter 8 to Chapter 10. Several parameters that can be used in the modelling are derived in the eleventh chapter. The twelfth chapter presents conclusions drawn based on the results from this study and suggestions for future research studies.

CHAPTER 2

RADIOACTIVE AND TOXIC WASTE DISPOSAL FACILITIES IN GERMANY AND OTHER COUNTRIES

2.1 General

Radioactive waste cover all non reusable materials containing radio-nuclides with concentrations higher than those that have been regulated by the authorities based on environmental considerations. The radioactive waste is mainly divided into two categories; namely, low and intermediate level waste (LILW), and high level waste (HLW). The classification of the two categories may vary from country to country depending on the local regulations but general classifications can be made based on alpha and beta/gamma concentrations (IAEA, 1994).

The LLW is defined as radioactive waste containing low beta/gamma contaminated material with a possible long-lived alpha contamination. In the absence of alpha-contaminated material, no special treatment is required for this level of waste. The ILW is a radioactive waste with higher concentrations of beta/gamma and sometimes accompanied by alpha emitters. This level of waste commonly produces heat and requires remote treatment. The HLW is considered as a long-lived waste category and possesses high concentrations of beta/gamma and alpha emitters. Due to its high radiation level, isolated treatment is compulsory. Significant increase in temperature may occur as a result of the radioactivity.

In Germany, the classification of radioactive waste is not based on the dose rate as in the IAEA classification system. The waste is rather grouped primarily based on the radioactive inventory and the heat produced by radioactive decay (Enviros, 2003). The radioactive waste is divided into two categories; namely, negligible heat developing waste with low level radioactive contents and heat developing waste with high radioactive contents. On the other hand, the European Union (EU) has prepared a classification system for solid radioactive waste, which will simplify information exchange between its member states. In the EU classification system, solid radioactive waste is classified into three classes; namely, transition radioactive waste, low and intermediate-level waste (LILW), and high-level waste (HLW).

By definition, toxic waste includes the radioactive waste but with a more general meaning. The toxic or hazardous waste comprise all waste resulting from any processes

such as chemical processes, physical processes, etc. that should be treated and stored with care.

2.2 Storage and Disposal of Nuclear/Radioactive and Toxic Waste

The nuclear/radioactive and toxic waste are disposed by insulating them such that during the active lifetime of the radioactive waste or during the hazardous period of the toxic waste, the biosphere in the vicinity of the waste, by any possible ways, will not be polluted virtually to a limit above which the effects cannot be tolerated by the environment. The commonly adopted systems include surface disposal facilities and deep repositories.

The surface disposal facilities comprise landfills where hazardous (usually non-radioactive) waste is stored in bulk or containerised forms and disposed in excavated trenches or compartments. The deep geological repositories, normally located at 500-1000 m deep, are generally used for storage of radioactive waste, especially those categorised as ILW and HLW. The deep geological storage systems are chosen based on considerations that the locations must be stable enough against any natural disasters and human intrusions (Allègre, 1999). An ideal HLW repository should be located in a quite 'impermeable' formation with respect to water by taking account that soluble radioactive elements can move easily with water itself and can be strongly absorbed by the formation. For these reasons, it has been found that geological formations with sedimentary salt or clay layers are the most suitable hosts for the repository system. The system is normally comprised of galleries that can be opened or completely closed. For the HLW, the disposal system adopted nowadays allows access to the galleries for a certain time before the final closure.

2.2.1 Radioactive Waste Disposal Concepts in America, Asia-Pacific and Europe

Concerns about radioactive waste have grown up in U.S.A. since the country has been generating various types of equipment for military purposes. Since 1982, under the Nuclear Waste Policy Act (NWPA), the U.S. Department of Energy (DOE) has been responsible in storing and disposing the nuclear waste especially those grouped as HLW through its Office of Civilian Nuclear Waste Management (OCRWM) (Enviros, 2003). The Nuclear Regulatory Commission (NRC), an independent agency which was established in 1974, has been responsible for regulating civilian use of nuclear materials. After preliminary studies were performed on several proposed sites for the disposal, in 1987, the US government eventually decided to choose Yucca Mountain in the state of Nevada as the final location for the spent nuclear fuel and HLW disposal. Since then, research studies have been carried out and aimed at investigating aspects related to suitability of the site. The conceptual design of the project is shown in Figure 2.1 (DOE, 2002). The installation is located in a volcanic tuff rock at a depth of 300 m and far above

the ground water table. The repository consists of concrete-lined galleries inside which the protected canisters are placed. The disposal is planned to begin after 2010. In 1999, the Waste Isolation Pilot Plant (WIPP), the world's first underground disposal licensed to be a permanent and safe repository for U.S. nuclear waste, began operations. The project is located in a dessert of South-eastern New Mexico, seated in a thick salt formation at a depth of about 700 m.

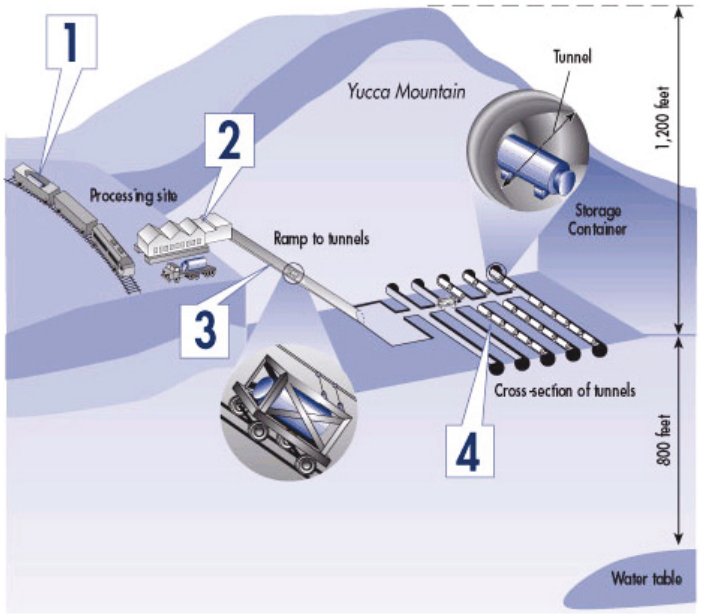

Figure 2.1 The conceptual design of the Yucca Mountain facility (DOE, 2002)

In Canada, the Atomic Energy of Canada Limited (AECL) has been given responsibility for research and development of HLW deep underground disposal facilities (Enviros, 2003). The planned repository for nuclear waste disposal in Canada is expected to be seated in intrusive igneous rock of the Canadian Shield at a depth of 500-1000 m (AECL, 2002). The site is tectonically inactive and is located in Ontario. A network of horizontal tunnels and disposal rooms would be built to enclose waste containers. The network would subsequently be filled and sealed with buffer and backfill materials. A mixture of bentonite and silica sand at a ratio of 50/50 would be used as buffer for the disposal whereas a mix of glacial rock clay and crushed granite aggregate together with engineered barriers would provide sealing of the rest of the vault.

The deep geological disposal concept in Japan has been established based on an additional seismic consideration since the country is located in a tectonically active zone. A multi-barrier system (Figure 2.2) has been designed to sit in crystalline rock or pre-neugene (hard rocks) located at a depth of 1000 m and in soft rock of neugene sediments at a depth of 500 m (JNC, 1999a). The galleries make it possible for the canisters to be placed vertically and horizontally. A compacted mixture of bentonite and silica sand in a proportion of 70/30 with dry density of 1.6 Mg/m^3 has been selected as buffer material for

the repository. The deep geological disposal construction located at the Tokai prototype nuclear power plant is now in progress and would be ready for operation in several years.

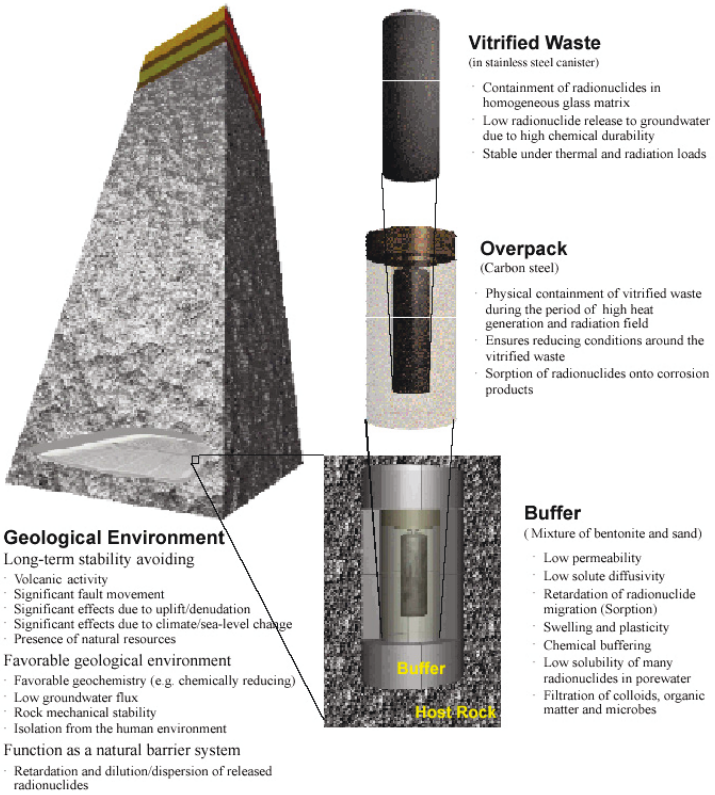

Figure 2.2 Japan's multi-barrier concept (JNC, 1999a)

In Australia, there are only low-level and intermediate-level radioactive waste (LLW and ILW). The LLW and some ILW with short-lived materials are stored in several near-surface repositories whereas the long-lived ILW are disposed in other above-ground built facilities. The long-lived ILW are much less in volume as compared to the LLW. Since 1998, the issues of civil radiation protection in Australia have been undertaken by the Australian Radiation Protection and Nuclear Safety Agency (ARPANSA) (Enviros, 2003). At the moment, a near-surface disposal site at the Mt. Walton East Intractable Waste Disposal Facility for LLW is in operation. In 2000, several sites were short-listed as a candidate for the LLW and ILW repository and an environmental impact statement (EIS) related to the repositories was also submitted to the government, which was subsequently approved in 2003. However, the government finally cancelled the approval of the sites due to regulatory issues in 2004.

In Europe, several countries, among them are Belgium, Finland, France, Spain, Sweden, Switzerland, United Kingdom, and Germany, have initiated establishment of nuclear waste repositories. Surface or near-surface disposal concepts (Figure 2.3) are meant for the LILW whereas deep geological repository (Figure 2.4) is designed to store the long-lived radioactive materials for several thousands of years (ONDRAF/NIRAS,

2003). Although the classification of radioactive waste has been standardised in the European Union, concepts upon which repositories are designed vary between the member countries. Accordingly, each member country has its own agencies and authorities dealing with these issues.

In Belgium, the Belgian Agency for Radioactive Waste and Fissile Materials (ONDRAF/NIRAS) was established in 1980 to manage a multi-year national program of the long-term waste disposal management (Enviros, 2003). The multi-barrier concept adopted in Belgium relies on the capability of Boom clay formation to retard any flows of substances into and from the stored waste. The engineered barrier provided is expected to perform up to a few thousand years after which the natural barrier will provide a major role (ONDRAF/NIRAS, 2001). The temporary land-burial facilities for ILW and LLW have been planned to be located in a Boom clay formation at Mol-Dessel (i.e, called as the CILVA facility) until a suitable repository is developed and begins operation expectedly in the year 2030. The facility at Mol is operated by BELGOPROCESS and is also meant for the HLW returned from reprocessing in France and the existing HLW produced previously in Belgium.

In Finland, the Finnish Radiation and Nuclear Safety Authority (STUK) is responsible for assessment of the waste management plans and activities (Enviros, 2003). The STUK appointed Posiva, a commercial company, to carry out all disposal-related works. After all technical assessments, Posiva finally called for a repository to be built at a depth of 400-700 m at Olkiluoto site in the city of Eurajoki. The repository is planned to be in operation starting from 2020 and is supposed to be sealed in the year 2050.

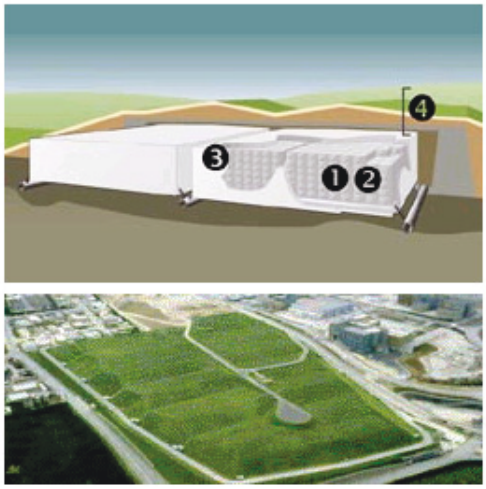

Figure 2.3 A typical surface disposal facility according to the EU's concept: (1) waste conditioned in concrete; (2) steel container; (3) concrete structure; and (4) several impermeable layers (ONDRAF/NIRAS, 2003)

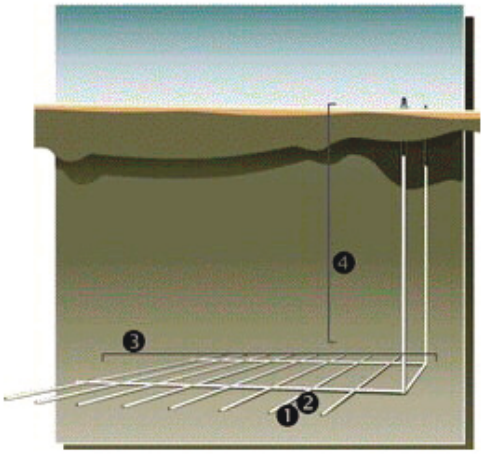

Figure 2.4 A typical deep geological repository according to the EU's concept: (1) vitrified waste; (2) steel container; (3) disposal infrastructure; and (4) geological formations (ONDRAF/NIRAS, 2003)

The French nuclear waste program has been assigned to the National Radioactive Waste Management Agency (ANDRA) which was established in 1979. ANDRA is basically a part of the French Atomic Energy Commission (CEA) which is responsible for all radioactive waste disposal-related issues (Enviros, 2003). ANDRA has identified four geological formations suitable for HLW disposal; namely, clay, salt, granite, and schist formations (ANDRA, 2003). A site, known as the Centre de la Manche, which is located in northern France, had been used for disposing LLW in the near surface facilities for several decades. The site was closed in 1994 and a replacement site near Soulaines in Northeast France has been appointed. For HLW, three sites that are located in a granite layer below sedimentary cover have been selected by ANDRA for further examination. The three sites are Vienne in marl at Bure, Haute Marne, Gard near Marcoule, and in Marl. The selected site is expected to be in active operation by the year 2010. The French government had initially approved the site at Bure in 1999 after which a fatal accident (i.e., shaft sinking) occurred in 2001. The site was suspended in 2002 and began in operation again in 2003 after the introduction of new safety practices and equipment.

The nuclear programme in Spain is managed by the Ministry of Industry and Energy assisted by three state-owned companies; namely, CIEMAT which takes care of research and development issues, ENUSA which deals with front-end issues, and ENRESA which is directly in touch with waste-related matters (Enviros, 2003). A near-surface disposal facility for LILW known as El Cabril has been in operation since 1992 and is located 100 km away from Cordoba. No decision has been made regarding the final disposal concept and the final location for the HLW repository. No decision has also been made thus far regarding a concept of final disposal repository but ENRESA has targeted that the plan is to be announced in 2010.

The Swedish Nuclear Fuel and Waste Management Company (SKB) was established in 1970s to manage radioactive waste in Sweden (Enviros, 2003). A final near-surface repository for LILW has been set up at a location near Forsmark nuclear power plant whereas the Swedish HLW are shipped to the interim store known as CLAB (Figure 2.5) which is situated in the vicinity of the reactor site at Oskarshamn. The facility is located in a granite layer at a depth of 30 m. Final disposal concept for the HLW repository has been outlined in a proposed SKB plan which describes that the HLW from spent nuclear fuel is to be encapsulated in high-integrity copper canisters. The canisters would subsequently be placed in a repository that would be located at a depth of 500 m in crystalline rocks. No final location has been selected for the HLW repository. Compacted mixture of bentonite IBECO C with a water content of 18% and a dry density of 1.69 Mg/m^3 has been selected for the sealing material (Gray, 1993).

In Switzerland, LILW and HLW are to be disposed underground in a suitable rock formation at a minimum depth of 100 m. The regulatory body which deals with nuclear issues in the country is the Swiss Federal Nuclear Safety Inspectorate (HSK) of the Federal Office of Energy (BFE). The National Cooperative for the Storage of Radioactive Waste (NAGRA) was established in 1972 to manage the disposal of all Swiss radioactive waste returned from reprocessing in France and United Kingdom (Enviros, 2003). NAGRA has considered a crystalline rock formation in northern part of the country as a feasible location for the HLW repositories.

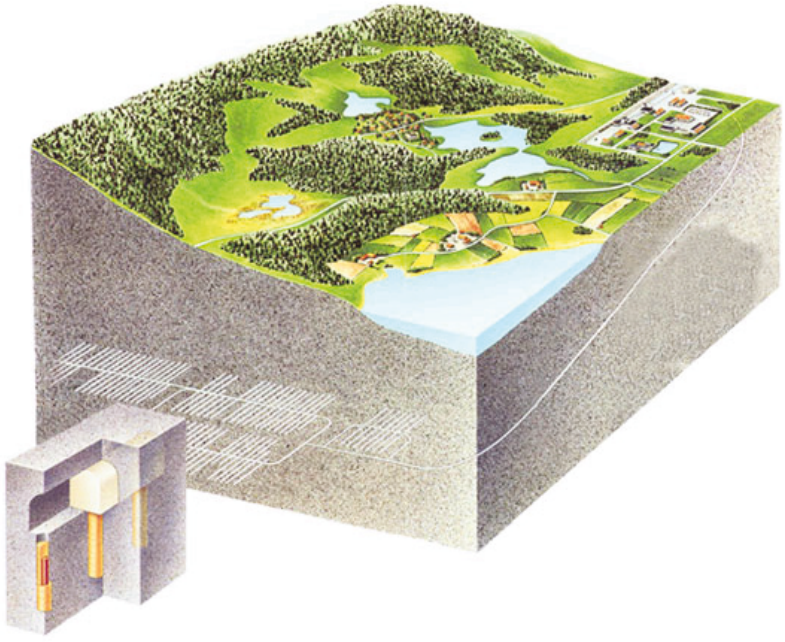

Figure 2.5 CLAB facility in Sweden (SKB, 2003)

In the United Kingdom, the British Nuclear Fuels (BNFL), a government-owned corporation, is responsible for the reprocessed HLW disposal in the country whereas

LLIW disposal are managed by the Nuclear Industry Radioactive Waste Executive (NIREX), a government institution which had been established in 1990 (Enviros, 2003). NIREX has been searching for a potential location near Sellafield in Cumbria and plans operation of a repository for LLIW by the year 2010. However, the proposal was refused in 1997 after being inquired by public and new concepts have to be established. For HLW, a current concept of reprocessing and storing the waste in surface storage for at least 50 years is continued. A final disposal for the HLW would be a deep geological repository, which is expected to be required by the year 2040.

2.2.2 Radioactive Waste Disposal Concept in Germany

Deutsche Gesellschaft zum Bau und Betrieb von Erdlagern für Abfallstoffe mbH (DBE) or the German Company for Construction and Operation of Waste Repositories, an organisation appointed by the federal government as represented by *Bundesamt für Strahlenschutz* (BfS) or the Federal Office for Radiation Protection, since 1979, has been in contract, to establish final repositories for the German nuclear waste (Enviros, 2003). BfS is under jurisdiction of the Federal Environmen Ministry (BMU). DBE has ascertained the applicability of the former Konrad iron ore mine near Salzgitter as an underground disposal for the negligible heat developing waste whereas another site at Gorleben salt dome in the province of Lower Saxony had been planned to be used for both negligible heat developing and heat developing waste.

Prior to German reunification, another site, known as Morsleben, had been appointed since 1970 to be used as a final repository for the East German's low and medium radioactive waste. The site was also used as an interim storage facility for spent fuel in the country. Located in the province of Saxony-Anhalt, the repository has been under extensive inspections and investigations by BfS after the reunification, despite suspended disposal activities following appeal from the government of Saxony-Anhalt in 1998.

The Gorleben disposal facilities are located at a depth ranging from 800 to 900 m and were initially expected to be in operation starting from 2030. Although, it has been proven to be suitable for the German nuclear waste disposal, it has been facing strong opposition from the government of Lower Saxony. In 1998, the federal government stated that the Gorleben site's suitability was still questionable and other potential sites for the disposal should be found and examined.

2.2.2.1 Selection of Suitable Site for the Final Repository in Germany

BMU decided that all radioactive waste shall be disposed in deep geological formations. AkEnd (2002) proposed that there should be only one repository in the country for this purpose. Based on the half-lives of radio-nuclides resulting from the nuclear waste and the evolution of geological system where the repository is to be seated,

the AkEnd Committee decided that the final repository shall be able to isolate the waste within a minimum period of one million years. The following general requirements have been defined in AkEnd (2002) for selecting the suitable site for the final repository in Germany.

- No or slow transport of harmful substances including radio-nuclides into and out of the isolating rock zone and low flow rate of the groundwater at repository level.
- There must be a large volume of isolating rock zone, a long distance from water-bearing formations, and safety requirements in the case of barrier failure. These factors are related to the configuration of host rocks and isolating rock zone.
- Good spatial characteristics of the host rocks. This requirement is related to the reliability of safety assessment, repository design, and effort of exploration required.
- Good predictability of the host rock behaviour. This requirement is related to the long-term safety assessment of the repository.
- Favourable mechanical characteristics of the host rocks to minimise damage of the barrier systems (i.e., the host rocks) caused by the construction and operation of the repository.
- Low tendency of the formation of water flow paths and good gas compatibility. These are to ensure the integrity of repository system such that the system is robust against any possible loads and stresses and possible generated gas by the stored waste.
- Good thermal characteristics. This is to ensure the temperature redistribution when a high temperature is generated in the repository such that no damage due to thermal and thermo-mechanical loads can be expected to occur.
- High radionuclide retention capacity and favourable hydro-chemical characteristics of the host rocks.

The criteria that have been setup by the committee lead to a decision to consider two rock formations; namely salt-stone and clay-stone formations as candidates for the final repository site in Germany. The following aspects have been listed regarding the feasibility of salt-stone and clay-stone formations as host rocks at a workshop entitled 'Workshop *Gegenüberstellung von Endlagerkonzepten im Salz und Tongestein* (GEIST)' in the city of Peine in January 2005.

- The salt-stone formation is a homogeneous system as compared to the clay-stone formation which has complex geophysical characteristics. The salt-stone formation in Germany is generally located at greater depths compared to the clay-stone formation.

- Based on the previous and on-going research studies, the salt-stone formation has better thermal properties compared to the clay-stone formation. The characteristics of salt-stone formation are found to be less affected by temperature.

- The clay-stone formation has a wider permeability range and is generally more permeable than the salt-stone formation. The liquid transport mechanisms in the clay-stone formation are dominated by diffusion processes with sorption properties of the clay-stone being relevant while in the salt-stone formation, advection-type transports dominate.

- The clay-stone formation has been found to provide better long-term barrier effects which are beneficial over the salt-stone formation. However, the structural integrity of the repository system as a whole (i.e., the repository and the host rocks) is better in the case of salt-stone formation. More research studies are needed in the case of clay-stone formation.

- Data on the properties of host rocks are more available in the case of salt-stone formation that enables modelling of the repository performance to be performed better and more confidently.

- The techniques pertaining to the final deposition of the nuclear waste have been studied and demonstrated in the case of the salt-stone formation whereas for the clay-stone formation the techniques are still merely a concept.

- The feasibility study indicates that the repository construction and operation costs are cheaper in the case of salt-stone formation compared to those of the clay-stone formation.

2.2.2.2 Design Concepts of the Final Repository

There are two different design concepts of nuclear waste repository in Germany. The first design is based on a concept which considers separation of different functions provided by different elements of the construction (sealing element, buffer element, and host rocks) whereas the other approach is based on a concept which considers the functionality of repository construction and its elements as a whole (Sitz et al., 2003). The second concept appears to be more suitable considering that coupled thermo-hydro-chemo-mechanical processes not individual processes that take place and determine the construction stability. The available design concepts for the German repository were used as considerations in the design of Sondershausen field test (see Subchapter 2.5).

2.3 Bentonite and Bentonite-Sand as Buffer and Sealing Materials

By definition, bentonite is a native, colloidal, hydrated aluminium silicate, frequently generated from alteration of volcanic ash, with smectite group minerals

(mostly montmorillonite and other minerals such as hectorite, saponite, beidelite, and nontronite) as its major constituents. Details of physico-chemical properties of bentonite can be found in Chapter 3 of the dissertation. Since montmorillonite is the main mineral of the bentonite, its characteristics are predominantly reflected in the properties of bentonite as a whole.

Pusch (1979) noted that several properties of bentonite such as low permeability and easy handling can be favourable for the use of this material as buffer and sealing element for nuclear waste disposal. Commonly, compacted bentonite in a form of heavily compacted bricks or pellet is preferable since it is easy to handle during placement. Since compacted bentonite is a low permeable material, it is expected that hydro-geological transport of radio nuclides through groundwater (i.e., advective process), is minimised. Moreover, the high ion exchange capacity of bentonite enables ions from radionuclide to be absorbed such that their transport is even more retarded. During the development of heat resulting from the radioactive decay of the stored waste, bentonite as buffer material is expected to transfer the excessive heat to the host rocks and thus reduces the generated thermal gradient. Highly plastic nature and high strength provide additional advantages with respect to fissures-resulting deformability developed due to geological movement of the host rocks and self-sealing behaviour, and any possible applied load that may act in the deep geological repository. Therefore, Pusch (1979) suggested the use of bentonite, especially in a form of highly compacted bricks as sealing material for nuclear waste disposal.

However, excessive swelling pressure developed as bentonite is moistened during operation stage of the repository should be limited as it might cause damage to the repository itself. Yong et al. (1986) addressed this issue besides requirements of low shrinkage characteristic of the buffer material pertaining to the development of fissures during heat development, good compressibility of the buffer material for ensuring easy handling, and good deformability to warrant stress dissipation that may be generated in the system. These factors lead to the use of mixtures of bentonite and sand. The addition of sand has been found to be advantageous regarding ease of handling, manufacturing, and economic factors. Moreover, the addition of sand improves the thermal conductivity whilst for a given dry density the swelling pressure of a bentonite-sand mixture is lower than that of the pure bentonite. The coefficient of permeability of the compacted bentonite-sand mixture may also be lower compared to that of the compacted pure bentonite depending on the percentage of sand added and dry density of the compacted mixture. Thus, the optimum percentage of sand added must be investigated. JNC (1999b) proposed the use of a heavily compacted mixture of bentonite and silica sand as buffer material for the Japan's nuclear waste disposal concept while AECL (1994) suggested the use high density mixture of 50% bentonite and 50% silica sand for Canada's repository concept.

2.4 Previous and Ongoing Studies on Characterisation of Buffer and Sealing Materials

Most of investigations performed to select and characterise the material used as buffer and sealing element for the repository are carried out in conjunction with observations and feasibility studies aimed at selecting the most ideal site for nuclear waste disposal facility. Due to the complexity of behaviour of the buffer and sealing materials (i.e., the bentonite and the bentonite-sand mixtures), internationally collaborative and interdisciplinary research studies are commonly performed for this purpose. Objective of the research studies on this field is mainly to derive parameters from laboratory test data that are required for modelling and in the case of large scale tests, the parameters are usually obtained by back-calculation. The parameters are utilised to predict the short-term as well as the long-term behaviour of the repository.

In U.S.A., along with the establishment of the Yucca Project in 1993, an underground laboratory, which was built at a depth of 300 m, has been used to investigate geologic features and hydrogeology of the Yucca Mountain itself (DOE, 2002). Relevant processes of saturated and unsaturated water movement and the possibility of water and other solutions to be in contact and flow with radio nuclides as also affected by natural and human intrusions are investigated together with the effects of heat on water movements and the response of host rocks to heat and stresses.

The underground research laboratory in Canada, known as Whiteshell facilities in Manitoba, had been constructed by AECL at a depth of 420 m in the Canadian granite shield in attempt to investigate several aspects related to disposal of HLW (AECL, 2002). These include geological characterisation of the site, water and solute transport research, chemistry and microbiology of the groundwater, temperature- and time-dependent rock deformation and failure, damage study, and study on clay- and concrete-based materials for its sealing and buffer elements. Although the facilities have been decommissioned, research studies in the area of sealing and buffer elements for nuclear waste disposal in Canada are still underway, mainly in universities. With respect to geotechnical engineering aspects, a research group at the Geotechnical Engineering Department, University of Manitoba has been conducting research on the characterisation of a bentonite-sand mixture for sealing element in the Canadian Shield. The research involves triaxial tests under high confining pressures and temperature on saturated and unsaturated compacted specimens of bentonite-sand mixture in a proportion of 50/50. Experimental data that have been obtained are also used to develop a constitutive model which can further be utilised in numerical modelling for predicting the long-term performance of the nuclear waste disposal repository.

Besides the laboratory experiments carried out in Canada, two large-scale tests; namely, a buffer-container experiment and an isothermal test were conducted at the

Atomic Energy of Canada's underground research laboratory near Lac du Bonnet in Manitoba. The experiments were aimed at examining various aspects related to the construction of a deep geological repository in the granitic rocks in the Canadian shield and the application of sealing technology in that environment. The results of both the buffer-container and isothermal tests have been reported and discussed in Dixon et al. (2002).

In Europe, an international co-operation of research on nuclear waste disposal concept, known as Stripa Project, had been established and led by Swedish Nuclear Fuel and Waste Management Co. (SKB) Sweden (Enviros, 2003). The project which consisted of three overlapped phases; namely, Phase 1 (from 1980 to 1985), Phase 2 (from 1983-1988), and Phase 3 (from 1986-1992), had been undertaken with contribution from Canada, Finland, France, United Kingdom, Japan, and the United States. A half-scale mock-up test, known as Buffer Mass Test (BMT) was performed at Stripa which is shown in Figure 2.6 (Pusch et al., 1985 and Gray, 1993). The test was aimed at assessing performance of the buffer material (i.e., bentonite) under possible field conditions by also considering the methods of preparation, handling, and installation. A 30-m long gallery seated at a depth of 340 m had been constructed to have six 3-m deep and 76-cm diameter shafts in which electrical heaters were placed. The heaters simulating the heat emitted by the nuclear waste canister were sealed and buffered using compacted unsaturated sodium bentonite blocks (i.e., MX-80 bentonite from Wyoming). Swelling pressures developed in the bentonite and water pressures exerted in the granitic host rocks as well as temperature changes during the experiment were monitored. In addition, the water content of the bentonite, relative movement of each component, and fractures were also measured (Gray, 1993). Upon testing, the physical and chemical properties of the material that had undergone thermo-hydraulic treatments during experiment were re-investigated in the laboratory for comparison to those obtained for the as-prepared conditions. Generally, no significant changes in those properties were evident.

Another European multi-national research project on deep geological waste disposal repository, known as Full-scale High-level Waste Engineered Barrier Experiment (FEBEX) project, has been underway since 1995 at Grimsel underground research laboratory in Switzerland with participation from Spain (Figure 2.7). The whole Grimsel test site is an international collaboration of several countries; namely, Switzerland, Germany, France, Japan, Sweden, Spain, Taiwan, Czech Republic, and U.S.A. The FEBEX project demonstrates the feasibility of engineered barrier system for HLW disposal and studies focussing on thermo-hydro-mechanical (THM) and thrmo-hydro-geochemical (THG) coupled processes in the real situation. An in-situ test is being undertaken in the northern zone of the test site (Figure 2.7), upon which a predictive modelling has been performed to back-calculate the results obtained from the field measurements. A smaller mock-up test (Figure 2.8) is also being carried out at CIEMAT Spain for the same purposes. In both experiments, temperature, swelling pressure, fluid

pressure, relative humidity, and deformation were recorded. Besides the mock-up test, laboratory tests were also performed to provide basic parameters required for the numerical modelling (FEBEX, 2000). All these studies were carried out on FEBEX bentonite, a bentonite from Almería Spain, as used in the form of compacted blocks.

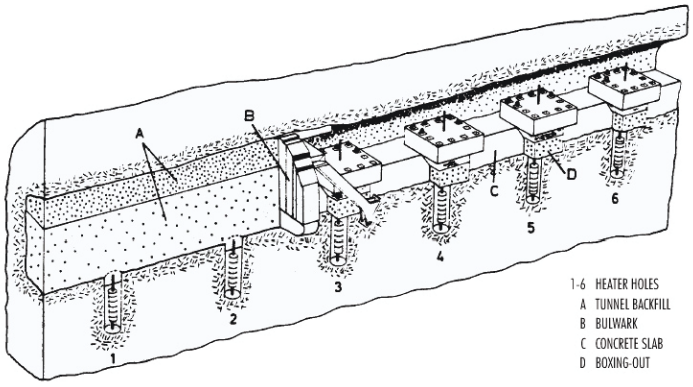

Figure 2.6 Buffer Mass Test (BMT) conducted at Stripa (Pusch et al., 1985)

Apart from these two multinational projects in Europe, many individual institutions and universities have also performed studies on the same subjects. Before the commencement of FEBEX project, Switzerland's representative for the project, NAGRA, had performed separate investigations on MX-80 bentonite and a natural calcium-type bentonite from southern part of Germany, Montigel (now Calcigel) (Schmidt et al., 1992). The investigations consisted of physical properties characterisation and also stiffness (Müller-Vonmoos and Kahr, 1982; Studer et al., 1984, Brenner, 1988), swelling and shrinkage (Bucher and Spiegel, 1984; Bucher et al., 1985; Bucher et al., 1986; Kahr et al., 1986; Kraehenbuehl et al., 1987; Brenner, 1988; Grauer, 1988; Hasenpatt, 1988; Pusch and Güven, 1988; Haas, 1991), liquid transport mechanisms (Bucher and Spiegel, 1984; Pusch, 1985, Bucher et al., 1986) as well as the time-dependent behaviour, chemical, and chemical process characterisation (Müller-Vonmoos and Kahr, 1982; Wanner, 1986; Milodowski et al., 1990, Müller-Vonmoos et al., 1991).

From academic institutions, the Polytechnics University of Catalonia (UPC) in Spain, for instance, has been performing intensive research on the hydro-thermo-mechanical characterisation of compacted Boom clay, compacted bentonite, and compacted bentonite-sand mixtures. The research includes swelling pressure investigation as affected by temperature, soil-water characteristic curves, compressibility, shear strengths, and saturated as well as unsaturated permeabilities. A computer program, named CODE_BRIGHT, has purposely been developed to numerically analyse the performance of buffer materials in the field based on the experimental data.

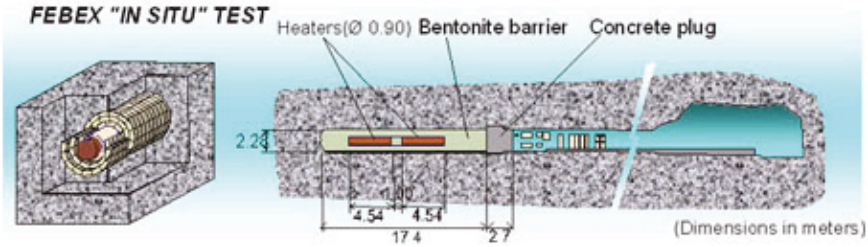

Figure 2.7 In-situ test at the Grimsel underground laboratory (Grimsel, 2003)

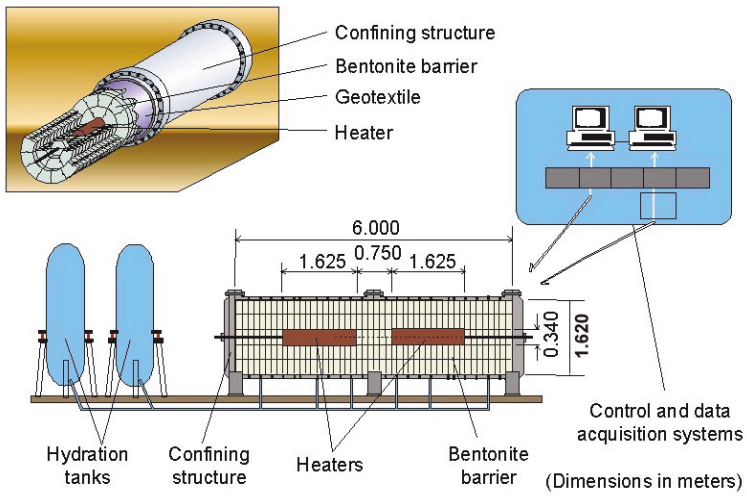

Figure 2.8 Layout of the mock-up test for FEBEX project (Grimsel, 2003)

In France, several universities such as *Ecole Nationale des Ponts et Chaussées* (ENPC) and *Institut National Polytechnique de Lorraine* (INPL) have been conducting investigations on bentonite and bentonite-sand mixtures for the use as sealing and buffer elements for nuclear disposal systems. Research studies at ENPC have been performed mainly on compressibility and volume change behaviour of compacted expansive material (i.e., bentonite and other clays), upon which a model for volume change of expansive soil was proposed (Cui et al., 2002b). Complimentarily, studies conducted at INPL focus on hydro-mechanical, thermo-mechanical, and hydro-chemical characterisation of unsaturated bentonite-silt mixture, including a study of the effect of aging on the material behaviour (Cuisinier and Masrouri, 2002).

Recently, Centre of Experimental Geotechnics (CTE) at the Czech Technical University (CTU) has set up a mock-up test in which bentonite-based material in a form of compacted blocks are used (Figure 2.9). The material under investigation is a mixture of 85% bentonite, 10% silica sand and 5% graphite by dry mass. The resulting compacted blocks after static compaction have a dry density of 1.8 Mg/m^3. Several sensors have been installed in attempt to measure temperature, water content, and development of swelling pressure with time during experiment (CEG, 2002).

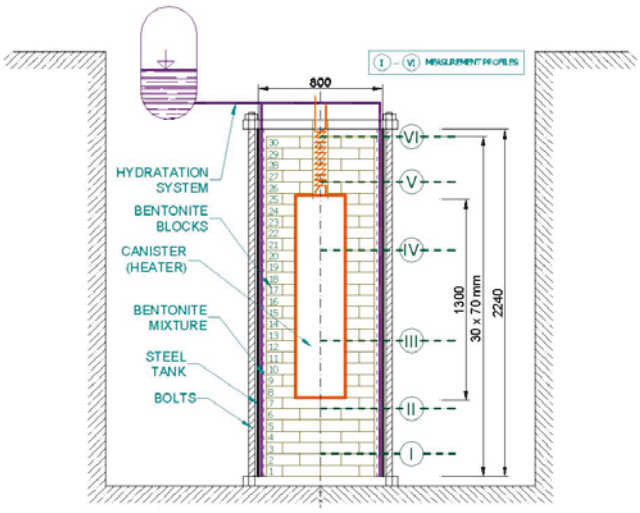

Figure 2.9 Layout of the mock-up test at CEG Czech Republic (CEG, 2002)

2.5 Recent Studies on Bentonite-Based Materials in Germany

In Germany, research studies on the characterisation of bentonite-based materials have been performed along with the investigations carried out pertaining to the feasibility studies for the planned final repository at Gorleben and also by individual universities and research institutions. The study conducted at the Gorleben repository mainly consisted of hydro-geological and geophysical investigations. Subsequently, a number of universities and institutions have been intensively carrying out more deeply research on the characterisation of bentonite-based materials that are planned to be used as buffer and sealing materials for the final HLW repository in the country.

In the Technical University of Freiberg (TU Freiberg), Sitz (1997) performed an investigation on several bentonite-based materials including Calcigel and MX-80 for the long-time stability of the materials when used as buffer and sealing materials for the HLW repository in saline environment (i.e., salt-stone formation). The research studies composed of measurements of the maximum swelling pressures using different liquids, measurement of coefficients of permeability with different permeating liquids, and measurement of shear strengths. The experimental data for different dry densities were presented in Sitz (1997). Following that, a mock-up test was set up at a location in the city of Sodershausen aiming at investigating response of the repository construction as a whole to mechanical and hydraulic loadings and interaction between the repository construction and the saline environment (Sitz, 2003). The study did not focus on the temperature influence which in fact changes the properties of bentonite-sand bricks used and affects the long-term stability of the whole repository.

The Sondershausen construction was designed based on criteria as described by Wittke (1996) and Wittke et al. (1998). The proposed concept was planned to be adopted as a general concept of radioactive and hazardous waste disposal barrier in Germany

(Figure 2.10). The layout of the Sondershausen mock-up test is shown in Figure 2.11. According to this concept, the sealing construction should be able to carry any possible loadings and should be impermeable enough to retard flows of any liquids or gasses during its operation. The initial intrinsic permeability of the sealing and buffer elements should be as low as $2x10^{-16}$ m^2 and the canister material should be resistant to corrosion that may result from aggressive salt solution from the surrounding host rocks. In addition, escalated temperature up to 70 ^oC during the operation stage and as high as 83 ^oC in the post operation stage of the construction must be considered to influence stability of the whole construction. Based on these criteria except the temperature influence consideration, the repository construction was pressurised with salt solutions and its responses by means of changes in water content and relative humidity, stresses and deformations, and flow of the solutions were measured.

Parallel to the abovementioned studies, a series of investigation on physico-chemical properties of several bentonites has been undertaken by *Gesellschaft für Anlagen und Reaktorsicherheit* (GRS)*mbH*. The main objectives of the investigation were to characterise the physico-chemical characteristics of MX-80 and Calcigel bentonites and salt stone including the swelling behaviour of the materials with respect to several liquids that may be encountered in the real field situations (Herbert and Moog, 2002a). Swelling pressures of the materials against several salt and granitic solutions were determined using a newly developed swelling pressure equipment. A model of cation exchange during permeation of bentonites with the solutions was also proposed.

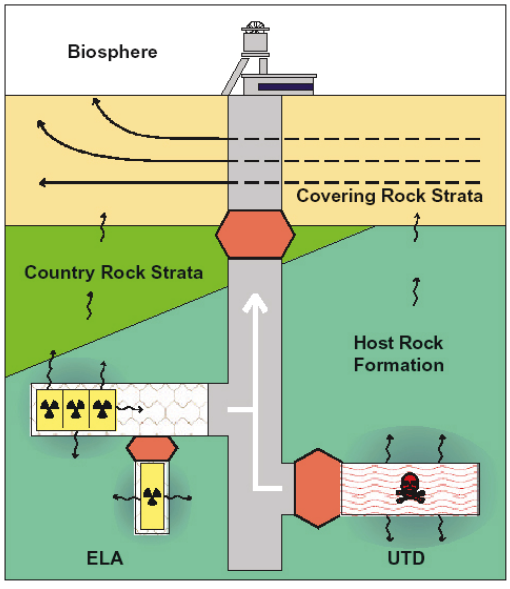

Figure 2.10 Nuclear and hazardous waste disposal barrier concept in Germany (Herbert and Moog, 2002b)

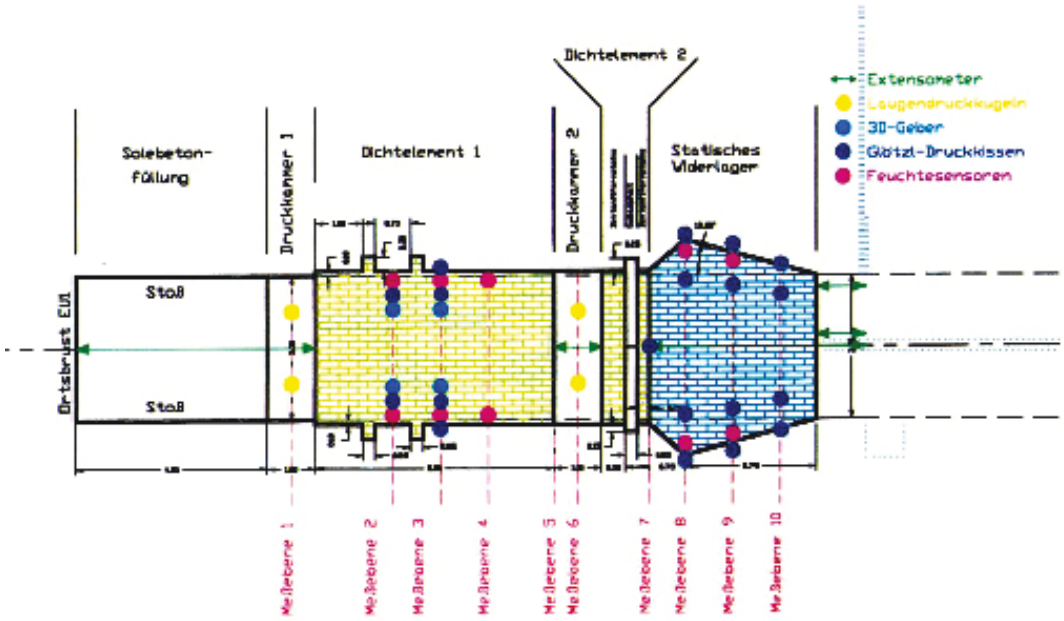

Figure 2.11 Layout of the Sondershausen mock-up test (Sitz, 2003)

Besides the experimental characterisation of potential materials for the waste disposal sealing and buffer elements, numerical investigations are also performed and focus mainly on the prediction of the long-term performance of the sealing material and the whole sealing construction. A computer program, called as RockFlow-CHM (Xie et al., 2003) has been coded for this purpose. A preliminary assessment of the computer code to calculate swelling and shrinking of a bentonite-based material and changes in the degree of saturation as well as void ratio during wetting and drying cycles has been performed and presented (Xie et al., 2004).

2.6 Focus of Current Investigation

Current investigation at the Laboratory of Soil Mechanics Bauhaus-University Weimar as brought out partly in this dissertation focuses on the hydro-mechanical characterisation of bentonite-based materials (i.e., Calcigel-sand mixtures) that can potentially be used as sealing and buffer elements in the nuclear waste disposal facilities in Germany. The study involves research on the material behaviour in the light of geotechnical engineering aspects including characterisation of the material at saturated and unsaturated states. The study also focuses on identifying several parameters that can be used for the prediction of stability of the repository construction. The detailed information on research objectives and scopes has been given in Chapter 1 and experimental program planned for the study can be found in Chapter 6.

CHAPTER 3

HYDRO-MECHANICAL BEHAVIOUR OF EXPANSIVE SOILS

3.1 General

This chapter discusses theories that are relevant to the investigation into hydro-mechanical behaviour of compacted bentonite-sand mixtures. The physico-chemical characteristics of clay and bentonite are described. Description of the mechanisms pertaining to the hydro-mechanical processes which may be encountered by the compacted bentonite-sand mixtures is also provided.

The hydro-mechanical behaviour of compacted bentonite-sand mixtures (or other expansive soils) is influenced by behaviour of the soil at microscopic level. The behaviour at this scale signifies the soil behaviour under saturated conditions (Gens and Alonso, 1992). Under unsaturated conditions, the presence of air influences the macroscopic hydro-mechanical behaviour of expansive soils. Therefore, it is necessary to provide separate descriptions of the behaviour of expansive soils under saturated and unsaturated states.

3.2 Physico-Chemical Characteristics of Clay and Bentonite

Soil generally consists of three phases; namely, solid phase, water phase, and air phase. Fredlund and Morgenstern (1977) introduced the fourth phase of the soil, which is called contractile skin in analysing an unsaturated soil element. The properties of a soil depend mainly on the properties of its solid and water phases and the interaction between them. The solid phase consists of different fractions that can range from gravel and boulders to clay particles. It has long been known that despite its size, the clay fraction has an important role in controlling the behaviour of a soil (Mitchell, 1993).

Pure clays can be classified into two main groups; namely, expansive (montmorillonitic) clays and non-expansive (kaolinitic and illitic) clays. The illitic clays are present in much smaller quantities compared to other clays (i.e., the montmorillonitic and kaolinitic clays) (Mitchell, 1993). In-situ, pure clays are commonly found in the form of mixture of the two groups. Both the montmorillonitic and kaolinitic clays are primarily composed by crystalline minerals. The components that form the clay minerals are silicon, aluminum, ferrous and ferric ion, magnesium, oxygen, and hydroxyls. Factors affecting the characteristics of pure clays are structure, mineralogy, and fabric of the clay, and clay-water interaction.

3.2.1 Structure and Mineralogy

The structure of clays mainly consists of arrangements of silica and alumina units (Figure 3.1). The silica unit is composed by a silicon atom (Si) surrounded by four oxygen atoms forming a tetrahedron with Si at the center. The alumina unit comprises an aluminum atom (Al) and six hydroxyls in an octahedral coordination. The arrangement of silica tetrahedral and alumina octahedral units influence the characteristics of clay soils. The two main groups of clay (i.e., the montmorillonitic and the kaolinitic clays) behave quite differently one from the other under physico-chemical changes induced by environment (Sridharan and Prakash, 2000). The montmorillonitic clays exhibit much greater swelling under water imbibitions than the kaolinitic clays.

Due to its swelling capability, bentonite is commonly categorised as montmorillonitic clay. Bentonite mainly consists of smectite mineral which is an arrangement of one alumina octahedral layer sandwiched between two silica tetrahedral layers (Figure 3.2). This type of arrangement is continuous in the lateral and horizontal directions and stacked one above another in the vertical direction. Bonding between layers is provided by van der Waals forces and by cations. These types of bond are weak and can be easily broken by absorption of water or other polar liquids (Mitchell, 1993). In between the stacks, there exist exchangeable cations which balance the negative charge of the unit layers resulting from isomorphous substitutions in the octahedral sheets and possibly unit layers of water (H_2O). The isomorphous substitution occurs when silicon atoms in a tetrahedral layer are substituted by aluminium atoms, or when aluminium atoms in an octahedral layer are replaced by magnesium or other divalent atoms. As a result, the tetrahedral layer or the octahedral layer becomes negatively charged.

Two properties controlling the behaviour of clays are specific surface area and cation exchange capacity. The specific surface area (SSA) of a soil is defined as the surface area of one gram of soil dry mass and has a unit of m^2/g. The cation exchange capacity (CEC) of a clay is defined as an ability of the clay to retain cations. The CEC has a unit of meq/100 g. The exchangeable cations present in a clay or the CEC value, and the SSA value of a clay are reflected in its liquid limit (Nagaraj and Miura, 2001). Therefore, the liquid limit indirectly represents the swelling capability of the clay in terms of swelling potential and swelling pressure. A sodium montmorillonite or a sodium bentonite in which sodium ion (Na^+) is its predominant exchangeable cation has a higher CEC and a larger SSA compared to a calcium bentonite with calcium ion (Ca^{2+}) as its predominant exchangeable cation (Mitchell, 1993). Consequently, the liquid limit of the sodium bentonite is higher than that of the calcium bentonite.

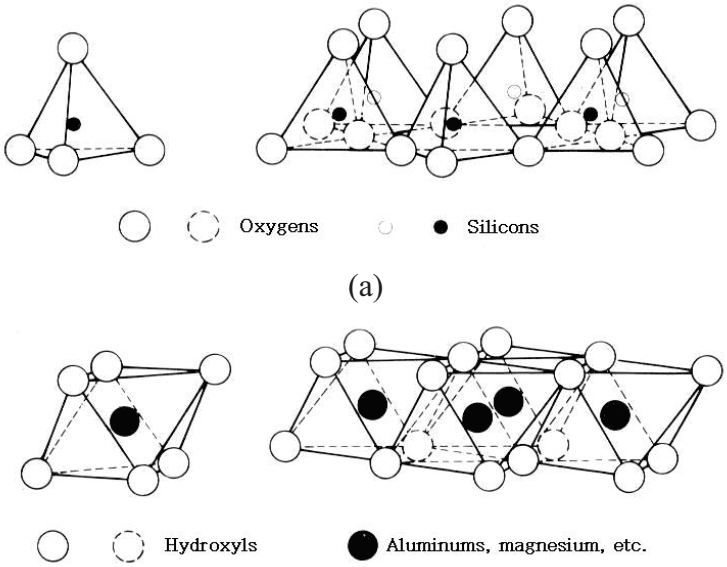

Figure 3.1 Silica and alumina units composing a clay unit (Mitchell, 1993): (a) silica tetrahedron and silica tetrahedral arrangement, and (b) alumina octahedron and alumina octahedral arrangement

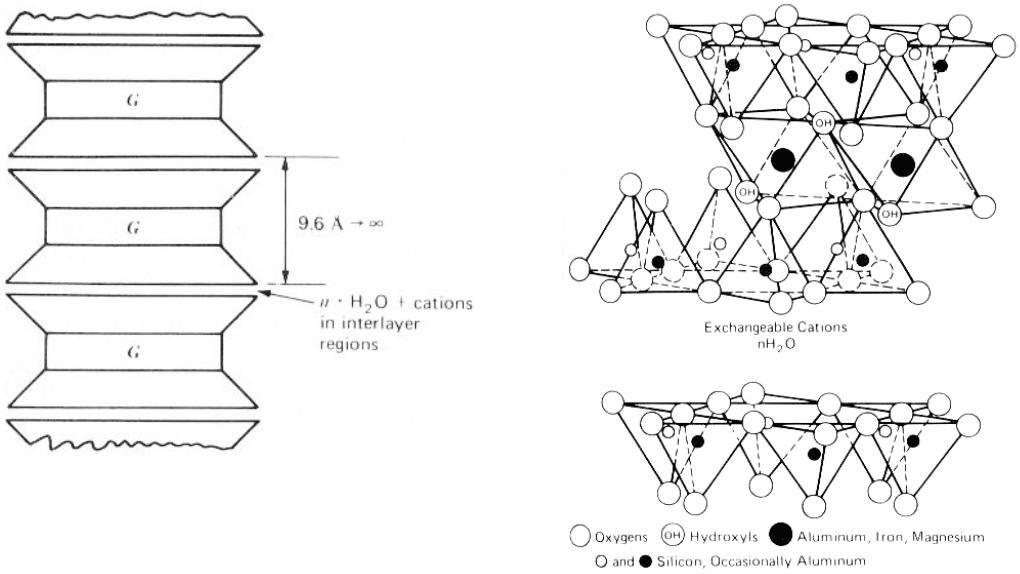

Figure 3.2 Schematic diagram of montmorillonite (Mitchell, 1993)

3.2.2 Fabric

The soil fabric is defined as the arrangement of soil particles, groups of particle, and pores in the soil (Mitchell, 1993). Fabric is correlated with soil particle associations. The soil particle associations exist in a clay suspension and in a soil as a multi-grained fabric. Van Olphen (1977) divided particle associations in clay suspensions into four main

categories. The first category is dispersed arrangement where no face-to-face association of clay particles exists. The second category is aggregated arrangement where several clay particles are grouped with face-to-face association to form an aggregate. The third category is flocculated arrangement where edge-to-edge and edge-to-face association of aggregates exist. The last category is deflocculated arrangement where no aggregations of clay particles exist. Three other modes of association can exist which are mainly combinations of the main types of clay particle association (Figure 3.3).

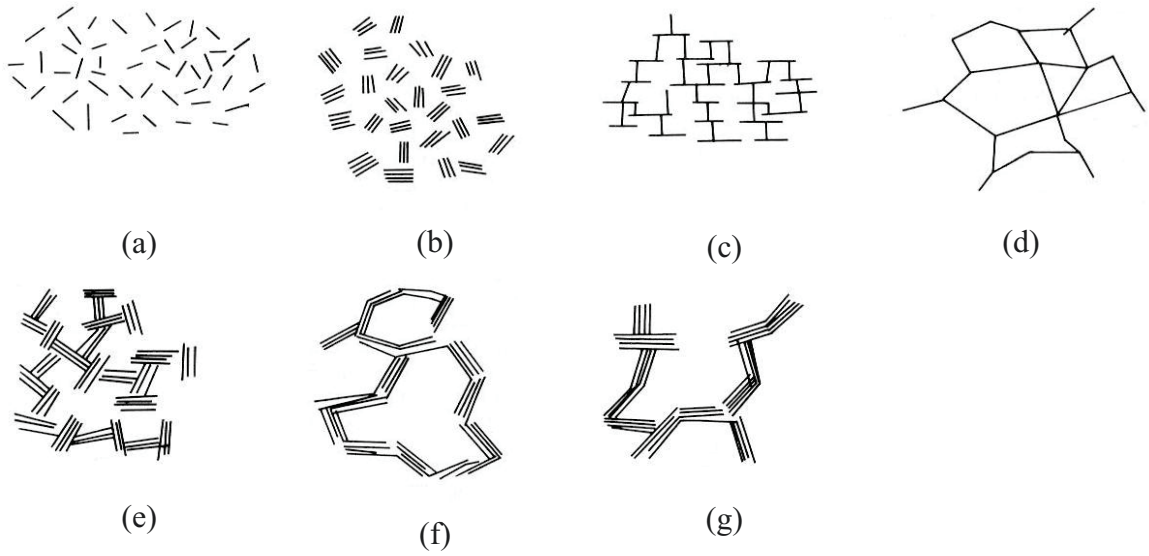

Figure 3.3 Types of particle associations in clay suspensions (van Olphen, 1977): (a) dispersed deflocculated, (b) aggregated deflocculated, (c) dispersed edge-to-face flocculated, (d) dispersed edge-to-edge flocculated, (e) aggregated edge-to-face flocculated, (f) aggregated edge-to-edge flocculated, and (g) aggregated edge-to-face and edge-to-edge flocculated

Collins and McGown (1974) presented several types of particle associations of soils. It was stated that the single-grained fully dispersed fabric cannot be found in fine-grained soils (or clays). The clay particles always form multi-grained aggregates. A clay soil was found to consist of elementary fabric arrangements, particle assemblages and pore spaces. Based on this, Mitchell (1993) divided the fabric of soil into three scales; namely, micro-fabric, mini-fabric, and macro-fabric. The micro-fabric of a soil consists of regular aggregations of soil particles and small pores within the aggregates. The mini-fabric is composed of aggregations of the micro-fabric and pores in a larger scale, which are called intra-assemblage pores. The macro-fabric of a clay soil contains cracks, fissures, and other structures that are called trans-assemblage pores. The maximum size of micro-fabric is a few tens of micrometers whereas the mini-fabric has a size of up to a few hundreds of micrometers.

Yong (1999) suggested a structure and pore hierarchy of expansive clays based on water potential concept (see Subchapter 3.5.1.1). It was stated that the smallest unit of a

clay was the 2:1 clay unit layer. Several clay unit layers formed a clay unit particle and several clay unit particles constituted a clay ped with micro-pores. According to the model by Yong (1999), a clay cluster is an assemblage of several clay peds where macro-pores are located in between. Micro-pores are the pores in a smaller scale (i.e., pores in the clay peds). The micro- and macro-pores interact each other in response to any hydro-mechanical processes imposed to the expansive soil.

3.2.3 Clay-Pore Fluid Interaction

The interaction between micro- and macro-pores is mainly governed by movement of pore fluid (i.e., water) into and out of the macro-pores and the interaction between the clay particles and water. The interaction between clay particles and water is caused by unbalanced forces at the interface between soil and water. Dissolved ions that are present in the bulk soil-water also contribute to the clay-water interaction. Low (1961) and Mitchell (1993) described several possible mechanisms of the clay-water interaction. The possible clay-water interaction mechanisms are hydrogen bonding, hydration of exchangeable cations, osmotic attraction, charged surface-dipole attraction, and attraction caused by London dispersion forces (or van der Waals bonds).

The hydrogen bonding is formed due to the presence of oxygens or hydroxyls on the surface of clay minerals. The oxygens attract the positive poles while the hydroxyls attract the negative poles of water molecules. The hydration of exchangeable cations occurs as water is attracted to the negatively charged clay surfaces. This mechanism results in hydration forces which are dominant at low water content. The osmotic attraction mechanism occurs as a result of osmotic process. Ions present near the clay surface are subject to electrostatic attraction force fields. Therefore, the ions cannot freely diffuse from the vicinity of clay surface. As a result, equalisation of ion concentration occurs and is caused by the movement of water molecules to the clay surface through a diffusion process.

The mechanism of charged surface-dipole attraction is caused by the orientation of water dipoles. The positive poles of the water molecules will be orientated towards the negatively charged clay surfaces. The degree of orientation of water dipoles is highest on the clay surfaces and decreases with distance from the clay surfaces. The structural disorder at the mid-plane between two adjacent parallel clay platelets is filled with cations such that the negative poles of water molecules at the midplane are in equilibrium with the cations. The clay-water interaction due to the van der Waals forces arises from attraction between two atoms. The van der Waals forces attract water molecules and bond them to the clay surfaces.

The clay-water interactions described above occurs at the microscopic level when pure clay is considered to consist of parallel arrangement of single clay platelets.

However, mixtures of clay, silt, and sand as well as possibly with organic matters are the most often encountered in the field. Therefore, although even the characteristics of pure clay is reflected in the behaviour of a soil mixture, adoption of the ideal microscopic behaviour of clays may not be sufficient in generalising macroscopic measurable phenomena of a soil mixture. Examples of this type of soil mixture which are of interest in the current investigation are mixtures of bentonite and sand.

3.3 Bentonite-Sand Mixture

Compacted bentonite-sand mixture is an example of a bentonite-based material which is widely used as clay liner for landfills and as sealing and buffer elements for nuclear waste and highly toxic waste containments. The behaviour of compacted bentonite-sand mixtures is controlled largely by the properties of bentonite. However, at a certain composition (or bentonite content) the behaviour of compacted mixture is influenced by the properties of the sand. The presence of sand in the mixture improves the shear strength and thermal properties of the compacted mixture. The swelling pressure and swelling potential of the compacted mixture of bentonite and sand are lower than those of the compacted pure bentonite at the same dry density (or void ratio).

The influence of sand on the mechanical behaviour of a mixture takes effect at a low bentonite content, i.e., when the inter-granular contact between sand grains exists. This type of mixture is often referred to as ‘bentonite-enhanced sand’ in which properties of the mixture (e.g., shear strength, coefficient of permeability, and swelling potential) at different dry density are influenced by load-deformation characteristics of the sand (Stewart et al., 1999). Graham et al. (1995) and Blatz et al. (2000) studied the influence of suction on the shear strength and stiffness of an unsaturated compacted bentonite-sand mixture.

Depending on the bentonite percentage of the mixture, the state of sand grains in the compacted mixture can be classified into two categories (Figure 3.4). The first state occurs when the bentonite content is high enough such that the sand grains are covered by the bentonite particles. At this state, there is no sand-grain contact. In the second state, the inter-granular contacts between sand grains exist. Taking into consideration that the specific surface area of the bentonite is much higher compared to that of the sand, this state is only possible at very low bentonite contents.

There is a limiting bentonite content beyond which bentonite dominates the behavior of a mixture. This occurs at a particular dry density (or void ratio) of the compacted mixture depending on the swelling properties of the bentonite. In a particular composition and dry density, the presence of sand may also reduce the coefficient of permeability of the compacted mixture. The coefficient of permeability of the compacted bentonite-sand mixture may become even lower than that of the compacted pure bentonite

at the same dry density. Studds et al. (1998) reported that a 'bentonite-enhanced sand' with 10% bentonite content had a lower coefficient of permeability than the mixture with 20% bentonite content.

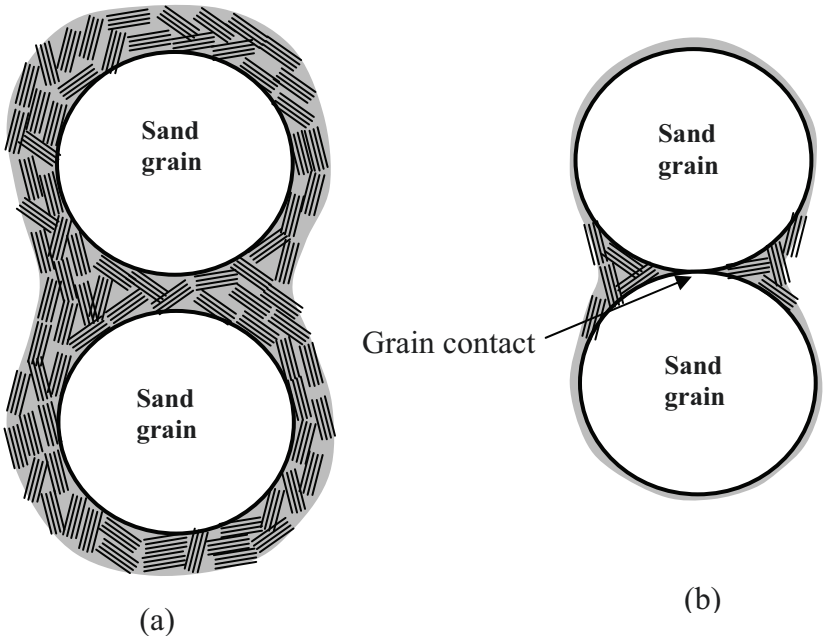

Figure 3.4 Two possible states of sand grains in a deflocculated clay system: (a) clay particles 'coating' sand grains and (b) clay particles 'welding' sand grains

Komine and Ogata (2003) suggested that swelling upon wetting takes place when the pores in a compacted bentonite-sand mixture are filled with swollen bentonite (i.e., self-sealing effect). It can be expected that a mixture of bentonite and sand with low bentonite content shows no swelling under certain vertical stress. The vertical stress can be regarded as the swelling pressure at a particular equilibrium void ratio or in other words swelling pressure is a manifestation of swelling potential or swelling (Mesri et al., 1994). Consequently, the term swelling potential may then be taken to include both the swelling and swelling pressure (Sridharan et al. 1986).

It is clear that although swelling of a bentonite-sand mixture is initiated by the swelling of clay minerals in the bentonite, it is actually a macroscopic response of the mixture to the applied hydro-mechanical processes. It will be described later on that the macroscopic behaviour of an expansive soil can be linked to its behaviour at microscopic level provided that interaction between the two levels is known.

3.4 Hydro-Mechanical Behaviour of Saturated Expansive Soils

As described earlier, the micro-pores in an expansive soil are essentially saturated and the effective stress concept for saturated soils consequently holds. The existence of repulsive and attractive forces in expansive soils has an influence on the formulation of

effective stress for expansive soils. In this subchapter, the effective stress concept for expansive soils is described and the swelling and collapse mechanisms in response to changes in the effective stress are discussed.

3.4.1 Effective Stress Concept of Saturated Expansive Soils

The compressibility and shear strength properties of clays (or most of the soils) are controlled by the physico-chemical properties and stress history of the soil. The effective stress determines the states of saturated soils that are represented by water content and void ratio (or dry density). The general expression of effective stress (σ') as defined by Terzaghi (1936) is as follows:

$$\sigma' = \sigma - u_w \tag{3.1}$$

where σ is the total stress and u_w is the pore-water pressure.

The effective stress concept expressed in Equation (3.1) represents a part of the total stress (σ) which is carried by the soil grains (or represents the grain contact pressure). However, grain contacts may not really exist in clays and this leads to inter-granular stress and inter-particle stress concepts in the formulation of effective stress concept for expansive soils.

3.4.1.1 Inter-Granular and Inter-Particle Stresses

The term of effective stress has been associated with inter-granular and inter-particle stresses (Mitchell, 1993). The inter-granular pressure is analysed by considering static equilibrium of normal forces acting perpendicular to a wavy plane passing between soil particles. According to the equilibrium conditions, the inter-granular stress is defined as the 'true' effective stress (σ^*) which is expressed in the following equation (Lambe and Whitman, 1969).

$$\sigma^* = \left(\sigma - u_w\right) - (R - A) \tag{3.2}$$

where R is the repulsive forces including the long range double layer repulsion and the short range repulsion mainly due to hydration forces, and A is the attractive forces resulting from the long range van der Waals and electrostatic attractions and the short range attractions due to chemical and cementation bondings.

The magnitude of van der Waals forces is inversely proportional to the distance from a point under consideration to the clay surface, to the power of seven. Therefore, the forces can be considered to be operative in short distance. The electrostatic attractions are caused by attractions between particle edges and particle surfaces. In the situations where there are no granular contacts, the contact pressure becomes zero and the effective stress is defined as (R - A) since the 'true' effective stress is zero (Achari et al., 1999).

3.4.1.2 Physico-Chemical State Variables

The 'true' effective stress or the inter-granular stress cannot be regarded as state variable since it is not developed based on an appropriate cubical element of unsaturated soil which is commonly adopted in continuum mechanics using the concept of continuous stress fields (Fredlund, 1987). Barbour and Fredlund (1989) showed that the effective stress (σ - u_w) and the net repulsive force (R - A) can be considered as the physico-chemical stress state variables for saturated clays. The effective stress considered by Barbour and Fredlund (1989) was a net pressure difference between the total stress and the pressure of free pore-fluid or (σ - u_f). It was suggested that (R - A) be determined by measuring the osmotic pressure (or the osmotic suction) (π) of the bulk solution. The physico-chemical stress state variables proposed by Barbour and Fredlund (1989) were supported by the compression test data provided by Mesri and Olson (1971) (Figure 3.5).

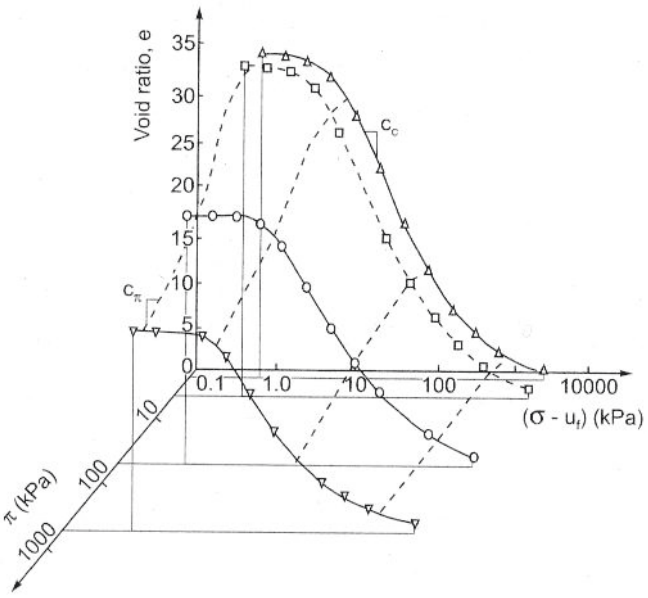

Figure 3.5 Three-dimensional constitutive surface for Na-montmorillonite tested by Mesri and Olson (1971) (replotted by Barbour and Fredlund, 1989)

3.4.2 Swelling Mechanisms in Saturated Expansive Soils

Swelling of clay, in general, is caused by a reduction in effective stress due to unloading or addition of water (Mitchell, 1993). Swelling due to the addition of water can be broadly divided into two categories. The first category is crystalline swelling caused by hydration of exchangeable cations and the second category is macroscopic swelling which proceeds beyond crystalline swelling. Many studies have focused on crystalline swelling (e.g., Madsen and Müller-Vonmoos, 1989 and Slade and Quirk, 1991). The development of crystalline swelling proceeds due to absorption of three to four mono-layers of water molecules in the inter-laminar pores. The absorption of three to four water

layers occurs in step; correspondingly, the development of crystalline swelling is also stepwise. In the case when the swelling is restrained, there is a development of swelling pressure and in the case of crystalline swelling; the swelling pressure developed is very high, reaching several thousands of kPa (Iwata et al., 1995). However, this type of swelling pressure acts at a short range (up to about 10 Å separation distance) (Yong, 1999). The macroscopic swelling proceeds beyond crystalline swelling as a result of a difference in chemical potential of water in the outer (or bulk) solution and in the space between clay platelets. Therefore, it represents the osmotic concept. The magnitude of macroscopic swelling can be computed using diffuse double layer (DDL) theory proposed by Gouy (1910) and Chapman (1913).

The DDL theory describes that the charged surface of a clay platelet and the vicinal distributed charge of ions form a diffuse double layer. The theory assumes that ions in the diffuse double layers are regarded as point charges and the ion distribution is assumed to follow the Boltzmann distribution equation (Iwata et al., 1995). The electrical potential is assumed to be determined by the Poisson equation in a similar form to that used in the electromagnetism theory. No interactions between ions in the diffuse double layers and parallel clay platelet arrangements are two other assumptions used. According to the DDL theory, the electrical potential at the mid-plane between two adjacent clay platelets is related to the distance between the two platelets. Relationship between the mid-plane electrical potential and the distance between two clay platelets is a function of the properties of clay and its pore-water. Two approaches have been adopted to use the DDL theory in describing the behaviour of clay soils. The first approach considers a single DDL without interaction between one DDL and another (e.g., Komine and Ogata, 2003 and Xie et al., 2004) whereas the second approach considers interacting DDLs (e.g., Sridharan and Jayadeva, 1982 and Tripathy et al., 2004). The first approach may be applicable in the case of clay suspension while the second approach appears to be more applicable for compacted clays.

Schofield (1946) utilised the DDL theory to determine swelling pressure of clays while Bolt (1956) used the DDL theory to describe the compressibility of pure clays. Bolt (1956) observed discrepancy between the results computed using the DDL theory and the experimental data. The disagreement is attributed to some factors that are not accounted for in the model. These involve the deviation from parallel clay platelet arrangement, the attractive forces being ignored, the over-estimation of ion concentration near clay surfaces, the interaction between ions as being neglected by taking the Poisson equation for the electric potential function, the possible termination of diffuse double layer by air-water interface as clay desaturates (Iwata et al., 1995). In the latest case, there is no compatibility between the external loading and the internal physico-chemical state of the soil-water system, which only occurs when DDL is fully developed in the saturated system (Nagaraj et al., 1988). Under these conditions, the DDL is said to be truncated. Iwata et al. (1995) provided a tedious method for computing the electrical potential

distribution of the truncated DDL based on the Gouy-Chapman theory. The ion distribution was calculated based on water adsorption model which also considers the Maxwell-Boltzmann law of energy distribution.

The DDL theory was subsequently modified to account for some of these factors. The attraction due to van der Waals forces is accounted for in a model by Derjaguin and Landau (1941) and Verwey and Overbeek (1948), which is known as DLVO theory. The overestimation of ion concentration was considered by Stern (1924) and further by van Olphen (1977). Sridharan and Jayadeva (1982) empirically related the mid-plane electrical potential with the distance between two adjacent clay platelets and provided procedures to obtain the compressibility of clays using the DDL theory. Tripathy et al. (2004) proposed semi-empirical correlations between the mid-plane electrical potential and the distance for compacted specimens of several different bentonites. Several new equations for the relationships between the mid-plane electrical potential and the distance between two adjacent clay platelets were introduced. Several published experimental data on swelling pressure of bentonites were used to best-fit the equations. Using the method proposed by Tripathy et al. (2004), the factors that are not accounted for in the original DDL theory may empirically be taken into account. Therefore, although the DDL theory considers only the microscopic behaviour of the simplistic parallel clay platelets arrangement, it may be modified and used for predicting some of the macroscopic behaviour of expansive soils such as swelling pressure and compressibility.

3.4.3 Collapse Mechanism in Saturated Expansive Soils

When an expansive soil is wetted the pore-water pressure is increased causing a decrease in its effective stress (i.e., according to the single-valued effective stress concept described in Subchapter 3.5.2.1). The decrease in effective stress causes swelling of expansive soils. The collapse of soil upon wetting is therefore considered to be an apparent contradiction to the principle of effective stress (Mitchell, 1993). According to the (single-valued) effective stress principle, a reduction in the effective stress normally yields an increase in void ratio. Collapse is controlled by the behaviour of soil as a particulate material. In order for collapse to occur, soil fabric should be open and unsaturated. The collapse phenomenon can also be observed when an unsaturated soil is stabilised at a high enough total stress such that its structure becomes meta-stable. A strong binding induced by cementing agent may also hold soil particles together in a dry state and collapse will be observed when the soil is wetted since the bonding is broken.

According to the above explanation, collapse of soil under certain total stress only occurs when hydraulic process (i.e., wetting process) is involved. The apparent collapse that may be observed in saturated clay system when it is in contact with a solution under certain total stress is only due to the osmotic process which occurs in the soil pores. The phenomenon is possible when a solution of a lower osmotic potential than that of the soil

pore-water is introduced into the saturated soil. The osmotic process takes place as a result of a difference between the osmotic potential of the soil and that of the bulk solution. However, this phenomenon should not be confused with collapse since the process is an osmotic consolidation process and the effective stress is increased during the process.

The following is another explanation of collapse mechanism of expansive soils. During wetting, normal and shear stresses develop in the soil. The normal stress acts perpendicular to the contact plane between the clay clusters. The shear stress operates parallel to the contact plane between the clay clusters. Collapse occurs when the ratio of shearing force to normal force exceeds the friction coefficient of the soil at particle level. At these conditions, the shear stress induces a relative movement between clay clusters. However, the shear force developed at particle level when an expansive soil is wetted should not be confused with the shear force induced at macroscopic level. Therefore, collapse may also occur when a soil is wetted after it is loaded isotropically under unsaturated conditions.

3.5 Unsaturated Expansive Soils

The characteristics of an unsaturated expansive soil are related to the characteristics of its saturated micro-structures and the interactions between microscopic and macroscopic responses of the soil to the applied hydro-mechanical processes. Unsaturated expansive soils exhibit large volumetric changes upon wetting. Unlike the case of unsaturated non-swelling soils, the large volumetric swelling taking place in the unsaturated swelling soils is mostly irreversible (Gens and Alonso, 1992).

The ideal microscopic behaviour of saturated expansive soils as described for instance in the DDL theory may not sufficiently explain the macroscopic behaviour of unsaturated expansive soils. This is particularly true at intermediate suctions during wetting of an expansive soil as a result of the existence of macro-structures in the soil. The DDL is truncated due to the presence of air in the macro-pores. The truncated DDL induces changes in the distribution of ions in the diffuse double layer. Figure 3.6 shows a possible representation of a compacted bentonite-sand mixture. According to the figure, a compacted bentonite-sand mixture consists of arrangements of clay clusters, sand grains, and possibly silts with macro-pores (or inter-aggregate pores) in between. Each clay cluster consists of clay particles with intra-aggregate pores (or intra-cluster pores) in between. Clay particle is an arrangement of clay unit layers with inter-layer pores in between. Both the intra-aggregate and inter-layer pores are saturated and therefore both can be considered as micro-level pores.

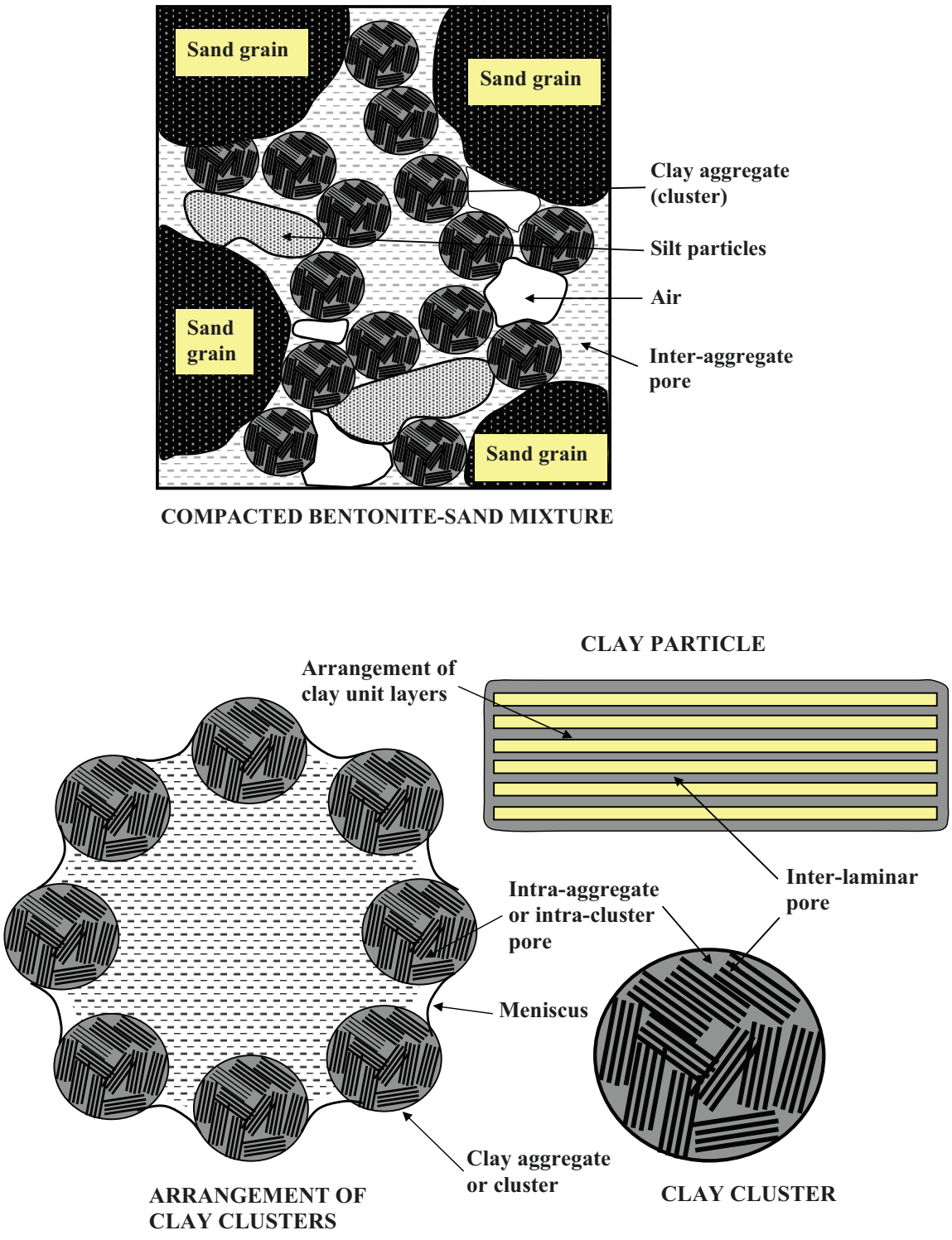

Figure 3.6 Schematic view of possible representation of unsaturated bentonite-sand mixture (modified from Nagaraj and Srinivasa Murthy, 1985)

The compacted bentonite-sand mixture at a state shown in Figure 3.6 has a non-zero value of suction. The multi-level structure of soil pores in the compacted bentonite-sand

mixture suggests that suction at a transient stage may be different in the different levels of pores. In the subsequent subchapter, a general concept of suction in expansive soils based on the classical definition of suction and a microscopic view of suction in expansive soils are described.

3.5.1 Concept of Suction

General concept of suction was initially developed by soil physicist in the early 1900's (e.g., Buckingham, 1907; Edlefsen and Anderson, 1943 and Bolt and Miller, 1958). Aitchison (1965) provided general definitions of soil suction and suction components from a thermodynamics standpoint. Suction or total suction (s_t) is defined as the total free energy of the soil water determined as the ratio of the partial pressure of the water vapour in equilibrium with a solution identical in composition to the soil water, to the partial pressure of the water vapour in equilibrium with a pool of free pure water.

Total suction consists of two components; namely, matric and osmotic components (Equation (3.3)). The matric component of total suction (s_m) is defined as the component of free energy of the soil water, which is determined as the ratio of partial pressure of the water vapour in equilibrium with the soil water, relative to partial pressure of the water vapour in equilibrium with a solution identical in composition with a pool of soil water. Osmotic suction (π) is the component of free energy of the soil water which is derived from the ratio of partial pressure of the water vapour in equilibrium with a pool of solution identical in composition with the soil water, relative to partial pressure of water vapour in equilibrium with a pool of pure water.

$$s_t = s_m + \pi \tag{3.3}$$

By this definition, the matric suction component is related to the air-water interface (or surface tension) giving rise to the capillary phenomenon. Matric suction is defined as the difference between pore-air pressure (u_a) and pore-water pressure (u_w) in the soil. For non-swelling soils (e.g., sands) osmotic suction can be generated by saturating the soil with a salt solution at a particular salt concentration. By increasing the pore-air pressure (u_a) and maintaining the pore-water pressure (u_w) at a certain value, matric suction is applied and is associated with the difference between u_a and u_w (or u_a - u_w) provided there is no change in the soil-water composition.

3.5.1.1 Concept of Suction in Expansive Soils

The general concept of soil suction described above does not appear to fully apply in the case of expansive soils. Expansive soils have a high surface charge and therefore without introducing salt solutions to expansive soils, osmotic suction inherently exists (Iwata et al., 1995). As described in the earlier subchapters, based on the concept of a simplified two clay-platelet arrangement, cations are attracted to the particle surfaces and

distributed in accordance with the Boltzmann distribution equation (Mitchell, 1993). Near the clay surface, the concentration of cations is high and then decreases rapidly and approaches a constant value at a finite distance from the unit layer surface. According to this concept, the concentration of cations at this point (or at the mid-plane between two interacting unit layers), controls the magnitude of osmotic suction. As water is added to the bentonite, swelling occurs and the concentration of cations at the mid-plane decreases and therefore the osmotic suction decreases.

Yong (1999) stated that the term water potential was more appropriate than suction for expansive soils. While suction has a positive value, water potential has a negative value. Matric potential consists of capillary action and sorptive forces while osmotic potential is due to the soluble salts which can freely move, if there is no true semi-permeable membrane for the ions (i.e., the salts in the macro-pores). The presence of water meniscus or capillary action is not necessary for soil to have matric potential since in the absence of capillary action there is still the presence of sorptive forces (Yong, 1999). Since at equilibrium the potential of water in the liquid and vapour forms is the same at all points within the soil, the total water potential of the soil, which is manifested by the total water potential of the vapour space just above or in the soil, will be balanced by the sum of matric and osmotic potential components of the soil pore-water. However, the magnitude of each component may vary within the soil depending on the distance between points in the soil under consideration to the surface of clay particles. Therefore, on the outer surface of the soil, capillary still exists to balance the water potential of the air space if the relative humidity of the air space is less than 100%. On the outer surface of the soil, the influence of sorptive forces on the magnitude of total water potential is not as significant as its influence on the magnitude of total water potential at a point within a short distance from the clay particles. Hence, air-water interface (or water meniscus) has to exist to counter the unbalanced force that is still present in the system.

Schick (2004) presents a model to separate components constituting suction in expansive soils. According to the model, suction in expansive soils consists of two components; namely, a component which is related to capillary phenomenon and an adsorption component. The response of an expansive soil following wetting (i.e., the increase in water content and void ratio or degree of saturation) due to the decrease in suction can be quantified separately for each component of suction using the model.

On the thermodynamic basis, Iwata et al. (1995) describes an interdependency of osmotic suction, sorptive forces, and swelling due to an increase in water potential on the surface charge of clays. Therefore, the magnitude of matric potential, osmotic potential and total water potential, and consequently their alterations are a response to water content changes that are coupled and controlled by the properties of clay minerals. Since matric potential includes the effects of capillary and sorptive forces, and osmotic potential is due to the presence of salts (or ions) in the macro-pores, the total water potential of an

expansive soil is equal to the sum of the matric and osmotic potential components. Therefore, the total suction is equal to the sum of the matric and osmotic suction of the soil.

3.5.1.2 Micro-Structural Consideration of Suction in Expansive Soils

The classical description of suction and suction components in an expansive soil assumes that the soil consists of uniform clay unit layers that are arranged in a parallel manner. However, even in the case of pure sedimented clay, aggregation occurs and there is a development of micro-structure in the soil. Consider a schematic picture of a compacted bentonite-sand mixture shown in Figure 3.6. A stable structure of compacted mixture exits when there is a balance between repulsive and attractive forces under any applied external pressure. The measured suction represents the energy status (or potential) of water at this equilibrium state.

At the 'as-compacted' state, bentonite-sand mixtures may exhibit a non-uniform distribution of water potential (or total suction). At this state, the inter-aggregate pore-water in the clay clusters is held by capillary menisci. The pore-water has a different potential in the intra-aggregate (or the intra-cluster) pore-water and the inter-laminar pore-water, due to incomplete hydration. The total suction measured under this condition corresponds to the status of pore-water under transient conditions and most likely represents the potential of pore-water in the inter-aggregate pores.

The potential of water in the inter-aggregate pores is higher (or the total suction is lower) than that in the intra-aggregate and the inter-laminar pores. This is primarily due to a difference in the cation concentration between the inter-aggregate pore-water and the intra-aggregate pore-water. As time elapses, there is a redistribution of pore-water where internal flow of water occurs under a water potential gradient. Eventually, a 'true' internal equilibrium conditions is achieved. The 'true' equilibrium conditions are achieved when suction is the same at all levels of pores in the soil.

Figure 3.7 shows a possible total suction evolution associated with the internal redistribution of water in the pores. The movement of pore-water from one potential to another potential increases the size of clay clusters and thus decreases the inter-aggregate pore volumes. The void ratio of the compacted mixture as a whole may or may not change but water content remains unaltered. At the 'true' equilibirum state, the total suction represents an equilibrium condition and is higher than that at the initial 'as-compacted' state. The time to reach the 'true' equilibrium state depends on the size of pores, the degree of interaction between the pore-water and the clay unit layers (i.e., the chemistry of pore fluid and the type of clay), and the permeability at micro and macro scales.

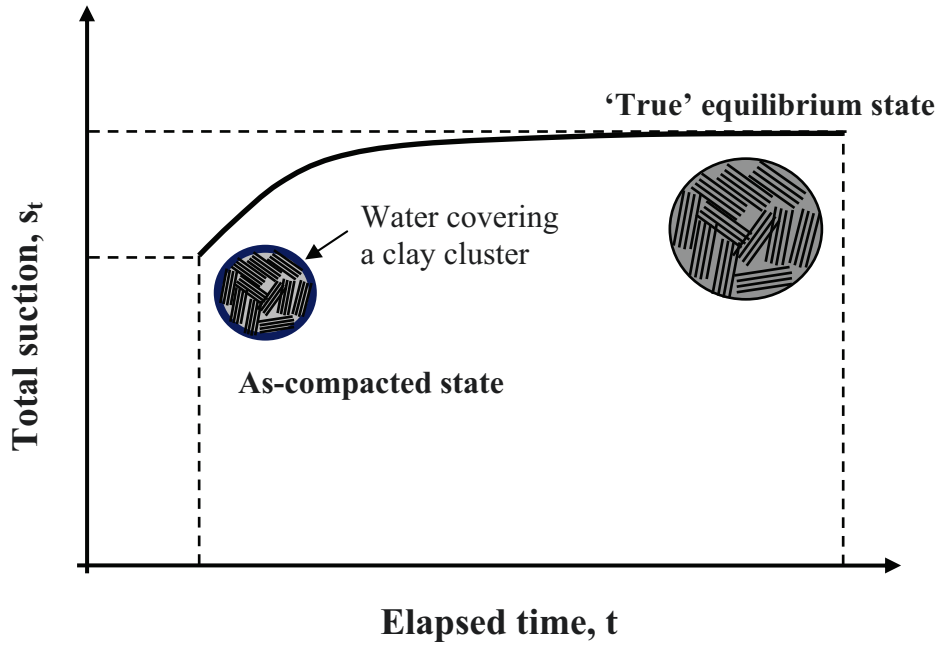

Figure 3.7 Total suction change with time due to internal pore-water redistribution

The presence of rigid clay particles strongly controls the behaviour of the soil. The properties of clay minerals can be represented by the consistency limits (i.e., Atterberg limits) (Sridharan and Nagaraj, 1999). Atterberg limits indicate variation of the soil properties with water content. Some examples are shear strength (Sridharan and Nagaraj, 1999), compressive and rebound indices (Schofield and Wroth, 1968; Nagaraj and Miura, 2001), and coefficient of permeability (Nagaraj and Miura, 2001).

Water content is related to total suction and the magnitude of total suction at any water content can be correlated to the total suction at a reference state. Nelson and Miller (1992) used liquid and plastic limits as the reference states and reported that at the liquid limit clay had suction in the range between 0.5 kPa and 1 kPa. At the plastic limit, suction in the clay was about 250 kPa. Fleureau et al. (2002) conducted drying and wetting cycles on several slurried clay specimens and found that on the drying path, the initially slurried specimens had a suction of about 7 kPa at liquid limit, whereas at the plastic limit, suction reached as much as 1000 kPa. The liquid limit represents the water-holding capacity of clay and defines the micro-level interactions of the clay particles. The liquid limit appears to be the more preferable value to use to assess clay properties. The use of cone penetrometer method has enabled the liquid limit determination of fine-grained soils to become more consistent.

3.5.2 Stress State Concept of Unsaturated Expansive Soils

The difference between effective stress concept of saturated and unsaturated soils is due to the presence of air phase in unsaturated soils. Similar to the effective stress concept

of saturated expansive soils, the formulation of effective stress concept for unsaturated expansive soils is also based on the grain contact pressure concept (Khalili et al., 2004). The stress state concepts of unsaturated soils (and unsaturated expansive soils) that have been proposed so far have attempted to be directed into a single-valued effective stress or a general one stress state variable approach (Fredlund and Rahardjo, 1993). Another approach is an independent stress state variables approach which gains greater acceptance in constitutive modelling nowadays.

3.5.2.1 Single-Valued Effective Stress Concept

The most frequently used effective stress formulation for unsaturated soils was proposed by Bishop (1959).

$$\sigma' = \left(\sigma - u_a\right) + \chi\left(u_a - u_w\right) = \sigma_{net} + \chi s \tag{3.4}$$

where u_a is the pore-air pressure, χ is the effective stress parameter related to the degree of saturation of the soil, which has a value of unity for a saturated soil and zero for a dry soil, σ_{net} is the net stress, and s is the soil suction.

The single-valued effective stress concept has subsequently adopted by many researchers (e.g., Kohgo et al., 1993; Bolzon et al., 1996; and Khalili et al., 2004) who describes applicability of the concept to describe soil mechanics phenomena. Some of the phenomena such as dilation and collapse were claimed to be explainable using the single-valued effective stress concept as long as an appropriate plasticity model was incorporated (Khalili, 2004). However, no evidence has been provided thus far to validate general used of the single-valued effective stress concept in explaining unsaturated soil behaviour.

The relationship between parameter χ and degree of saturation of a soil is normally obtained experimentally. Bishop and Henkel (1962) demonstrated the dependency of parameter χ on the soil type. Therefore, the magnitude of χ value is related not only to the soil degree of saturation per se but also to the soil structure (Khalili et al., 2004). Further, Fredlund and Rahardjo (1993) indicated difficulties related to the use of single effective stress equation to describe unsaturated soil behaviour. It was pointed out that the χ value was even related to stress and suction paths to which the soil was subjected. These factors lead to the use of independent stress state variables for unsaturated soils.

3.5.2.2 Two-Independent Stress State Variable Approach

Coleman (1962) and Matyas and Radhakrishna (1968) were amongst the first to use the two-independent stress state variable approach for unsaturated soils. Fredlund and Morgenstern (1977) provided a theoretical analysis of stress state variables for unsaturated soils based on the multi-phase continuum mechanics by taking the contractile

skin as the fourth phase of the soil. The analysis concluded that any two of three possible stress variables can be used to describe the stress state of an unsaturated soil. The possible combinations of stress state variables that can be used are: 1) (σ - u_a) and (u_a - u_w); 2) (σ - u_w) and (u_a - u_w); and 3) (σ - u_a) and (σ - u_w). The first combination has been used much more frequently than the other combinations.

The two-independent stress state variable approach has subsequently been adopted by many researchers (e.g., Alonso et al., 1990; Gens and Alonso, 1992; Alonso et al., 1999; Cui et al., 2002b; and Vu and Fredlund, 2004). The concept has also been applicable for saturated and dry soils as special cases of unsaturated soils (Fredlund and Rahardjo, 1993).

3.5.3 Relationship between Swelling, Collapse, and Suction in Unsaturated Expansive Soils

Swelling of an expansive soil at unsaturated state is initiated at the micro-structural level of pores. The macroscopic measurable effect is a result of interactions between changes in the micro- and macro-pores as a response to the applied hydro-mechanical processes. When an expansive soil is dry, hydration forces due to unhydrated exchangeable cations near the clay surface dominate. An increase in water content satisfies these forces and increases the interlayer separation distance to about three to four monolayers of water molecules or about 10 Å and as a result, crystalline swelling occurs (Yong, 1999).

If after complete absorption of three to four water layers in the interlayer space the volume of soil is restrained against swelling, theoretically, the swelling pressure exerted provides a measure of the osmotic suction. The hydration forces provide an additional driving force for water in a similar manner to capillary forces and osmotic suction. Besides the hydration forces, other contributing forces arise from van der Waals force fields and other short-range attractive forces. All these forces are operative at a short range from clay particles and control the magnitude of sorptive forces.

The increased water potential (or total suction) value upon wetting is compensated by swelling in the case of free swell condition or by an increase of swelling pressure in the case of constrained swelling. When there is no more swelling or further swelling pressure development, water potentials are macroscopically the same at all points in the soil. The non-zero value of water potential is represented by the measured swelling pressure in the case of constant volume conditions. Capillary meniscus may not be present within the soil which is most likely at saturation. Consequently, the swelling pressure represents the sum of osmotic potential and sorptive forces at equilibrium.

In the case of free swell conditions, there is a reduction of suction towards a zero value (Fredlund and Rahardjo, 1993). Under zero applied stress, the saturation process of

an expansive soil may take an extremely long time or else the expansive soil never reaches full saturation. The change in water uptake has essentially vanished near saturation. However, there still exists capillary force that may be relatively small. Although the soil is close to full saturation, it may have a low coefficient of permeability since the inter-aggregate pore volume is reduced as a result of sealing of the inter-aggregate pores by the swollen clay particles (i.e., the self-sealing effect). The hydraulic gradient responsible for driving the flow of water into the soil specimen is low since the matric suction is low.

According to the above explanation it is clear that the transient process of swelling or swelling pressure development in an unsaturated expansive soil following wetting is related to the initial osmotic potential and sorptive forces of the soil. The capillary component of suction may have an influence on the end value of swelling or swelling pressure. Generally swelling or swelling pressure increases with decreasing suction. However, results of swelling pressure tests reported by Romero et al. (2003) and Lloret et al. (2003) indicate that swelling pressure may also drop with decreasing suction indicating a collapse phenomenon.

As has been explained in Subchapter 3.4.3, collapse appears to be contradictory to the effective stress principle. This is particularly true when using the single-valued effective stress in the analysis of stress-deformation problems of unsaturated soils. Although it has been cited that collapse is soil behaviour at particle level, the concept of two independent stress state variables can be used to explain the collapse behaviour of soils at macroscopic level (Fredlund and Rahardjo, 1993; Shuai and Fredlund, 1998; and Vu and Fredlund, 2004). The quantification of swelling or swelling pressure and shrinking and collapse of an expansive soil with certain initial conditions (i.e., water content, void ration or dry density, and suction) following certain hydro-mechanical paths requires a constitutive model. In Chapter 4, several models that have been proposed for modelling expansive soil behaviour with respect to hydro-mechanical loadings are described.

3.5.4 Features of Unsaturated Expansive Soils

The modelling of expansive soils required knowledge about the features of unsaturated expansive soils. Alonso (1998) listed several main features of expansive soils that have to be considered when developing a constitutive model for behavioural prediction purposes.

1. Behaviour under simple paths:

    - For a given soil, dry density, and confining stress, the final swelling upon wetting depends on the initial water content (or the initial suction) of the soil.

The higher is the initial water content of the specimen; the lower will be the swelling (Holz and Gibbs, 1956).

- For a given soil, dry density, and initial water content (or initial suction), the swelling strain is influenced by the stress level acting on the soil. The higher is the stress level; the lower will be the swelling strain upon wetting (Holtz and Gibbs, 1956).

- For a given soil, confining stress, and initial water content (or initial suction), the swelling strain upon wetting depends on the initial dry density of the soil. The higher is the initial dry density of the soil; the lower will be the swelling strain upon wetting (Holtz and Gibbs, 1956).

- Final swelling pressure depends on the initial dry density of the soil without pronounced effects of initial water content (Holtz and Gibbs, 1956; Sridharan et al., 1986; and Mesri et al., 1994). At high initial water content, swelling pressure tends to be equal to the initial suction of the soil which is in concordance with the effective stress concept.

- During progressive wetting process, swelling pressure may reach an absolute maximum value at an intermediate water content (or suction) and may decay to reach a residual value. This behaviour has been observed by many researchers such as Alonso et al. (2001), Romero et al. (2003), and Lloret et al. (2003).

2. Behaviour under complex paths involving changes in suction and mechanical loading:

   - At low stress level, wetting-drying cycles induce an accumulation of expansion (or swelling). This particular feature of expansive soil has been addressed and presented in Alonso et al. (2001).

   - At high stress level, there is an accumulation of contraction (or shrinkage) of the soil after cyclic wetting and drying. The experimental evidence shown in e.g., Dif and Bluemel (1991) and Alonso et al. (2001) is a proof of this particular behaviour of expansive soils.

3. Long-term and osmotic effects:

   - The long-term effects as addressed in Alonso (1998) are related to primary and secondary behaviour of expansive soils such as compression under saturated and unsaturated state, swelling, and swelling pressure development. The experimental proof of this behaviour can be found in e.g., Komornik and

Zeitlen (1979). The secondary effects have also been addressed and modelled by Navarro and Alonso (2001) as a local dehydration process.

- The osmotic effects are mainly related to the effects of pore solute concentration on the mechanical behaviour of expansive soils. The consequence of this consideration is that whether osmotic suction has to be considered separately as stress state variable in the modelling of unsaturated behaviour of expansive soils. Barbour and Fredlund (1989) showed that osmotic suction can be considered as one of the stress state variables for saturated expansive soils.

CHAPTER 4

MODELLING CONSTITUTIVE BEHAVIOUR OF EXPANSIVE SOILS

4.1 General

In this chapter, three constitutive models that have been proposed for modelling the behaviour of expansive soils are described. The constitutive models presented are those which are based on macroscopic measurable response of expansive soils to hydro-mechanical loading or unloading (i.e., phenomenological approach). The first constitutive model is an elasto-plastic constitutive model for expansive soils. The second constitutive model presented herein is a volume change model which is based on the soil phase continuity requirements. The third constitutive model is a non-linear elastic model which has been proposed for heavily compacted clays. Additionally, models of soil-water characteristic curves and saturated and unsaturated permeability that may be used for deriving permeability functions for the material investigated herein are also presented. The permeability models presented include the classical Kozeny-Carman model, cluster model, and gel model for saturated permeability, the macroscopic model for unsaturated permeability, and the statistical model for saturated and unsaturated permeability.

4.2 Constitutive Model I: An Elasto-Plastic Model for Unsaturated Expansive Soils (Barcelona Expansive Model or BExM)

The elasto-plastic model is a phenomenological approach which has been used as a framework to study soil behaviour. In the phenomenological approach, the macroscopic behaviour which is represented by several measurable responses of soil to stress, temperature, and other variables are correlated to the variables under considerations through several soil properties. Alonso et al. (1990) proposed a general elasto-plastic model for unsaturated soils which is known as Barcelona Basic Model (BBM). Using this model, the behaviour of unsaturated soils such as swelling and collapse can be modelled quite satisfactorily. It was realised later on that expansive soils posses double structures which require modifications to the model. The BBM model was modified to take into account the more realistic behaviour of expansive soils. The new model is called Barcelona Expansive Model (BExM) (Gens and Alonso, 1992 and Alonso et al., 1999). Both the BBM and the BExM use two stress state variables for unsaturated soils based on previous works such as by Matyas and Radhakrishna (1968), and Fredlund and

Morgenstern (1977). The assumptions used in the development of the BExM are (Gens and Alonso, 1992; Alonso, 1998; and Alonso et al., 1999):

1. Expansive soils consist of two levels of pores; namely, macro-pores and micro-pores. Micro-pores are considered to remain saturated.

2. Expansive soils behave elastically at micro level. The behaviour of the micro-structural level is purely volumetric and isotropic against changes in isotropic stress and suction. Since the micro-structural level is saturated, the effective stress principle holds for the micro-structure and the micro-structural deformation of the soil in response to a change in suction is likely to be equivalent to that induced by a change in applied stress.

3. Micro- and macro-structures are at mechanical, hydraulic, and chemical equilibrium.

4. Micro-structural behaviour is independent of the macro-structure but the reverse is not true. These facts suggest that there exist interactions between the micro- and macro-structures of expansive soils.

5. Suction is regarded as the difference between pore-air and pore-water pressure in the soil and hence it represents capillary phenomenon.

4.2.1 Elastic Volume Change Formulation

An expansive soil exhibits micro- and macro-structural deformation when subjected to changes in stress and/or suction. The volumetric deformation consists of two components; namely, elastic and plastic components of deformation. The following equation expresses the elastic micro-structural volumetric deformation as a response to changes in the effective stress (Alonso, 1998 and Alonso et al., 1999).

$$d\varepsilon^{e}_{vm} = \frac{de_m}{(1+e_m)} = \frac{d\hat{p}}{K_m} = \frac{\kappa_m}{(1+e_m)}\frac{d\hat{p}}{\hat{p}} = \beta_m \exp(-\alpha_m \hat{p})\, d\hat{p} \qquad (4.1)$$

where e^{e}_{vm} is the elastic micro-structural volumetric strain, e_m is the micro void ratio, K_m is the coefficient of volume change for the microstructure, κ_m is the compressive index for the microstructure, α_m and β_m are material parameters, and $\hat{p}$ is a micro-structural effective stress and is defined in the following equation (Alonso, 1998).

$$\hat{p} = p + s_t \qquad (4.2)$$

where p is the net mean stress ($p = \sigma_m - u_a$) and σ_m is the mean stress ($\sigma_m = 1/3(\sigma_1 + \sigma_2 + \sigma_3)$), and s_t is total suction.

Macro-structural volumetric change reflects the volumetric change of soil structure and is characterised by the measured volume change or void ratio (e). The total void ratio

(or void ratio) consists of micro-structural void ratio (e_m) and macro-structural void ratio (e_M). The macro-structural void ratio changes as a response to changes in stress and suction. The change in stress and suction induces elastic and plastic macro-structural volumetric strains. The elastic component of the macro-structural (or soil structure) volumetric deformation is formulated in the following equation.

$$d\varepsilon_{vM}^{e} = \frac{dp}{K_t} + \frac{ds}{K_s} = \frac{\kappa}{(1+e_M)}\frac{dp}{p} + \frac{\kappa_s}{(1+e_M)}\frac{ds}{(s+p_{atm})} \tag{4.3}$$

where K_t and K_s is the coefficient of volume change with respect to a change in net mean stress and suction, respectively, κ and κ_s is the compressive index with respect to a change in net mean stress and suction, respectively.

In the above equation, p_{atm} is the atmospheric pressure, which is added to avoid infinite values as s approaches zero (Alonso et al., 1999). The behaviour of expansive soils described in this dissertation is limited to the behaviour in the p-s-e three-dimensional stress space under oedometric conditions. An extension of the model for the triaxial stress space has been described in Gens and Alonso (1992) and Alonso et al. (1999) based on the extension proposed earlier in the BBM model by Alonso et al. (1990).

4.2.2 Plastic Behaviour and Loading-Collapse (LC) Yield Curve

Consider a soil specimen at a given suction value, which is compressed isotropically along its virgin compression line. The volumetric strain of the specimen during compression is expressed using the following equation (Alonso et al., 1990).

$$d\varepsilon_{vp} = -\lambda(s)\frac{dp}{p} \tag{4.4}$$

where $\lambda(s)$ is termed as the slope of virgin compression line at suction s.

Similarly, the virgin compression line for changes in suction is formulated in the following equation with $\lambda_s(p)$ representing the stiffness parameter for changes in suction for virgin states of the soil (Alonso et al., 1990), which is also thought to be a function of net means stress (p).

$$d\varepsilon_{vs} = -\lambda_s(p)\frac{ds}{(s+p_{atm})} \tag{4.5}$$

Under a monotonic loading, an expansive soil reaches its pre-consolidation pressure which marks its yield stress for a particular void ratio. A yield curve can be drawn through a number of pre-consolidation pressures (or yield stresses) that are obtained from compression tests on several 'identical' specimens under different suctions. The yield

curve obtained is called the loading-collapse (LC) yield curve. Generally, the yield stress increases with increasing suction. The variation of yield stress (p_o) with suction for isotropic loading as formulated in Alonso et al. (1990) is expressed in the following equation.

$$p_o = p_c \left(\frac{p_o^*}{p_c} \right)^{\frac{\lambda(o)-\kappa}{\lambda(s)-\kappa}} \tag{4.6}$$

where p^*_o is the saturated yield stress, p_c is a reference net mean stress, and $\lambda(o)$ is slope of the saturated virgin compression line

Equation (4.6) has been derived with assumptions that only λ varies with suction whereas κ is constant. The variation of λ with suction follows an asymptotic equation which is formulated as (Alonso et al., 1990):

$$\lambda(s) = \lambda(o)\left[r + (1-r)e^{-\beta s} \right] \tag{4.7}$$

where r and β are the fitting parameters.

The macro-structural plastic deformation occurs when the LC yield curve is activated. However, wetting and drying can also induce plastic deformation. This leads to a requirement of two additional yield curves; namely, SI and SD yield curves which are associated with suction increase and suction decrease, respectively (Figure 4.1) (Alonso et al., 1999). By assuming that the SI and SD yield curves coincide (Alonso et al., 1999), the following equation is used to formulate the both yield curves.

$$\hat{p} - s_i = 0 \tag{4.8}$$

4.2.3 Coupling between Micro- and Macro-Structural Levels of Deformation

During drying or wetting there is an interaction between micro-pores and macro-pores of an expansive soil. The relationship between the micro-structural and the macro-structural deformation is assumed to depend only on the value of p/p_o. The interaction is represented by the micro-macro-structural interaction functions. A possible representation of the interaction functions is shown in Figure 4.2 (Alonso et al., 1999). The influence of micro-structural swelling is less pronounced in a dense specimen. Therefore, the interaction function for suction decrease (f_D) is taken as decreasing with increasing p/p_o. More shrinkage of a soil specimen on drying occurs when the stress level is higher and consequently, the interaction function for suction increase (f_I) is taken as increasing with increasing p/p_o. At a value of p/p_o equal to unity, an expansive soil exhibits an open structure and is at a possible state to collapse. At this state, the $d\varepsilon_{vM}/d\varepsilon_{vm}$ is assumed to be zero.

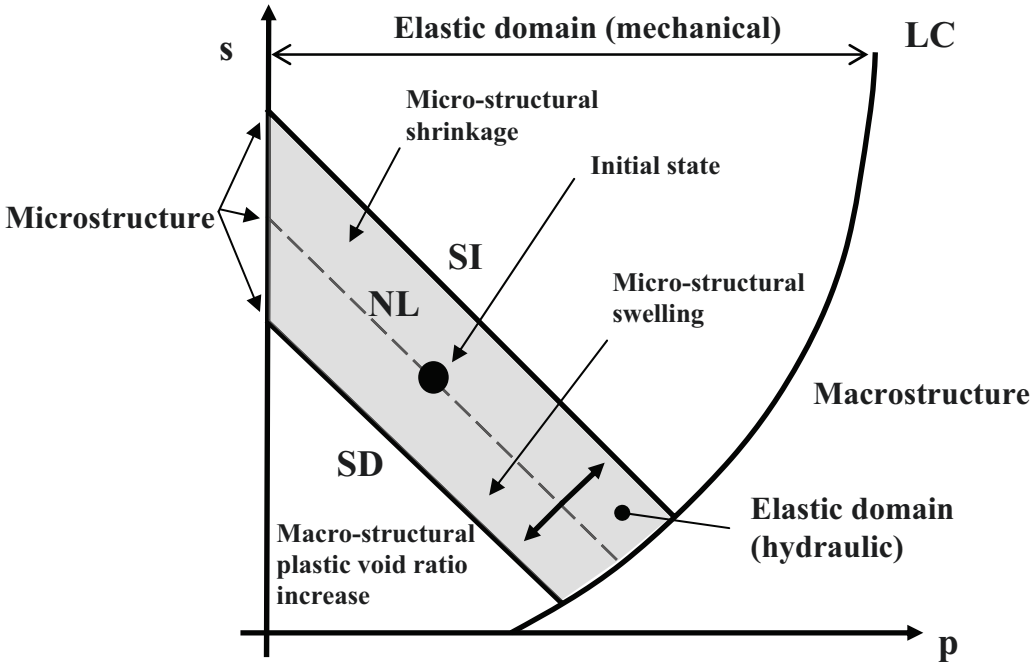

Figure 4.1 Graphical representation of the Barcelona Expansive Model (BExM)

During a cyclic drying-wetting test, SI and SD are alternately activated. The general fact is that the amount of irreversible deformation reduces with an increasing number of cycle. When suction cycles are performed on an expansive soil specimen under low pressure, the plastic strain during wetting predominates. This leads to an expansion of the specimen. On the other hand, the opposite occurs at high pressure. The suction cycles (i.e., at the low and high pressures) will finally end at an equilibrium state which is marked as a large dot in Figure 4.2.

The following equations express the plastic volumetric strain induced by the activations of SI and SD during cyclic drying-wetting tests.

$$d\varepsilon_{vM}^{p} = f_I d\varepsilon_{vm}^{e} \tag{4.9}$$

$$d\varepsilon_{vM}^{p} = f_D \, d\varepsilon_{vm}^{e} \tag{4.10}$$

Equation (4.9) and Equation (4.10) infer that the macro-structural plastic deformation is caused by the elastic micro-structural deformation. The following equations have been suggested for f_I and f_D (Alonso, 1992).

$$f_D = f_{Do} + f_{D1}\left(1 - \frac{p}{p_o}\right)^{n_D} \tag{4.11}$$

$$f_I = f_{Io} + f_{I1}\left(1 - \frac{p}{p_o}\right)^{n_I} \tag{4.12}$$

where f_{Do}, f_{D1}, n_D, f_{Io}, f_{I1}, and n_I are material parameters.

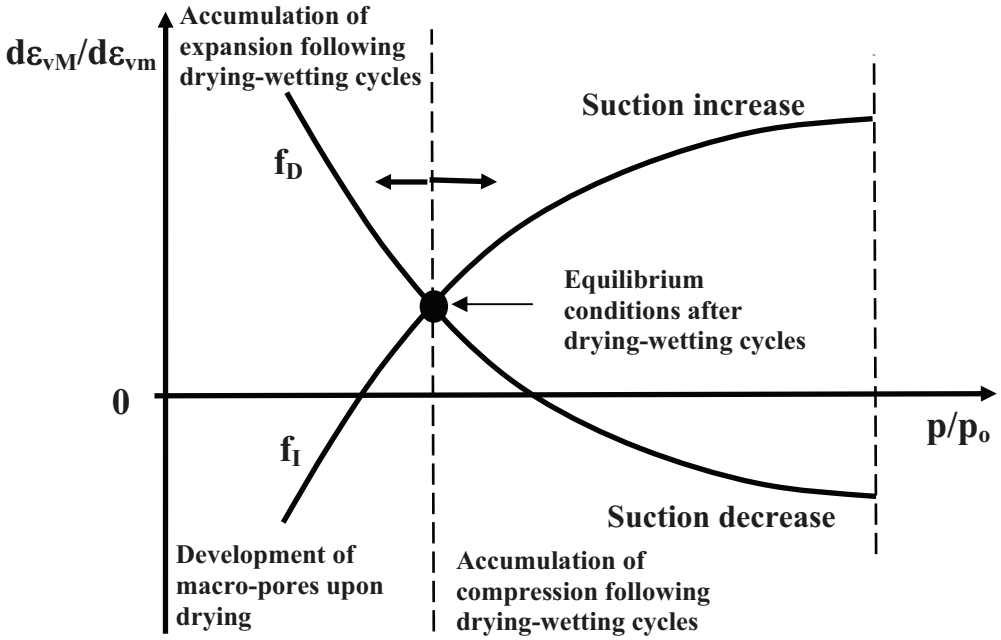

Figure 4.2 Possible interaction functions

4.2.4 Hardening Laws

It is assumed that hardening for the LC yield curve is caused by the activations of SI, SD, and LC yield curves whereas the SI and SD hardenings are only governed by the activations of SI and SD yield curves. Equations (4.13) and (4.14) define the hardening laws for SI and SD yield curves, and LC yield curve, respectively (Alonso et al., 1999 and Alonso et al., 2001). In Equation (4.13) and Equation (4.14), the function f refers to either SI (i.e., f_I) or SD (i.e., f_D).

$$ds_i = ds_o = \frac{K_m}{f} d\alpha_1 = \frac{K_m}{f}\left(d\varepsilon_{vSI}^p + d\varepsilon_{vSD}^p\right) \tag{4.13}$$

$$\frac{dp_o^*}{p_o^*} = \frac{(1+e_M)}{\lambda(o)-\kappa} d\alpha_2 = \frac{(1+e_M)}{\lambda(o)-\kappa}\left(d\varepsilon_{vSI}^p + d\varepsilon_{vSD}^p + d\varepsilon_{vLC}^p\right) \tag{4.14}$$

4.3 Constitutive Model II: A Volume Change Model Based On the Soil Phase Continuity Requirements

Fredlund and Rahardjo (1993) proposed a formulation of volume change of unsaturated soils undergoing monotonic loadings by assuming the unsaturated soil element as a continuous system of solid, water, and air phases, and contractile skin. The proposed volume change theory has been used by Shuai and Fredlund (1998) and Vu and Fredlund (2004) for simulating swelling pressure measurements on expansive soils. By neglecting the volume change of the contractile skin and assuming it to be internal to the unsaturated soil element, the following continuity requirement is obtained.

$$\frac{\Delta V_v}{V_o} = \frac{\Delta V_w}{V_o} + \frac{\Delta V_a}{V_o} \tag{4.15}$$

where V_v, V_w, and V_a is the volume of void, water phase, and air phase, respectively, and V_o is the initial total volume of the soil element.

An incremental procedure using small increments of stress and strain can be used to analyse the volume change of an unsaturated soil subjected to monotonic loadings (Fredlund and Rahardjo, 1993). The procedure can be adopted to use linear elastic formulations to solve a nonlinear stress-strain problem. Based on the continuity requirements, the total volume change of an unsaturated soil element is equal to the sum of volume changes associated with each phase (i.e., solid, water, and air phases). The volume changes associated with any two of the three phases must be measured whereas the third volume change can be computed. Normally, the total volume change (i.e., the volume change of the soil structure or ΔV_v) and the volume change with respect to water phase (ΔV_w) are measured such that the volume change associated with the air phase (ΔV_a) can be computed.

4.3.1 Soil Structure Volume Change

The constitutive relations for unsaturated soils are formulated using an extension of Hooke's law for saturated soils. In the formulation, the appropriate stress state variables for unsaturated soils, i.e., net stress and suction (Fredlund and Morgenstern, 1977), are used. For the general three-dimensional case, the change in volumetric strain ($d\varepsilon_v$) as a response to changes in net mean stress (p) and suction (s) is expressed in the following equation (Fredlund and Rahardjo, 1993).

$$d\varepsilon_v = \frac{\Delta V_v}{V_o} = m_1^s dp + m_2^s ds \tag{4.16}$$

where m_1^s and m_2^s refers to coefficient of volume change associated with the soil structure with respect to a change in net mean stress and suction, respectively. The values are

related to the soil elastic parameters and are formulated as follows (Fredlund and Rahardjo, 1993):

$$m_1^s = \frac{\partial \varepsilon_v}{\partial p} = \frac{3(1-2\upsilon)}{E} \tag{4.17}$$

$$m_2^s = \frac{\partial \varepsilon_v}{\partial s} = \frac{3}{H} \tag{4.18}$$

with E and H represents the modulus of elasticity of the soil structure with respect to a change in net mean stress and suction, respectively, and υ is the Poisson's ratio of the soil.

For the oedometric conditions (i.e., K_o-conditions), the following form is obtained (Fredlund and Rahardjo, 1993).

$$d\varepsilon_v = d\varepsilon_{vertical} = m_{1\,oed}^s d(\sigma_v - u_a) + m_{2\,oed}^s ds \tag{4.19}$$

where m^s_{1oed} and m^s_{2oed} can be related to the elasticity parameters of soil using the following equations (Fredlund and Rahardjo, 1993).

$$m_{1\,oed}^s = \frac{\partial \varepsilon_{vertical}}{\partial(\sigma_v - u_a)} = \frac{(1+\upsilon)(1-2\upsilon)}{(1-\upsilon)E} \tag{4.20}$$

$$m_{2\,oed}^s = \frac{\partial \varepsilon_{vertical}}{\partial s} = \frac{(1+\upsilon)}{(1-\upsilon)H} \tag{4.21}$$

4.3.2 Water Phase Volume Change

In the formulation of volume change, water phase is assumed to be incompressible and therefore the volume change of water phase represents the net water inflow into and outflow from the soil element. Equations for the water phase volume change take a similar form to those used to describe the volume change of the soil structure. The following equations are used to describe the volume change of water phase for general three-dimensional case (Fredlund and Rahardjo, 1993).

$$\frac{dV_w}{V_o} = m_1^w dp + m_2^w ds \tag{4.22}$$

where V_w is the volume of water and V_o is the initial total volume of the soil element. The parameters m_{1w} and m_{2w} is the coefficient of water volume change for changes in net mean stress and suction, respectively and the values are related to the elasticity parameters of soil using the following equations (Fredlund and Rahardjo, 1993).

$$m_1^w = \frac{\partial(V_w/V_o)}{\partial p} = \frac{3}{E_w} \tag{4.23}$$

$$m_2^w = \frac{\partial\left(V_w/V_o\right)}{\partial s} = \frac{1}{H_w} \tag{4.24}$$

where E_w and H_w is the water volumetric change modulus associated with a change in net mean stress and suction, respectively.

For the K_o-condition, the following equations are obtained (Fredlund and Rahardjo, 1993).

$$\frac{dV_w}{V_o} = m_{1\,oed}^w d\left(\sigma_v - u_a\right) + m_{2\,oed}^w ds \tag{4.25}$$

where $m^s{}_{1oed}$ and $m^s{}_{2oed}$ can be related to the soil elasticity parameters using the following equations (Fredlund and Rahardjo, 1993).

$$m_{1\,oed}^w = \frac{\partial\left(V_w/V_o\right)}{\partial\left(\sigma_v - u_a\right)} = \frac{\left(1+\upsilon\right)}{\left(1-\upsilon\right)E_w} \tag{4.26}$$

$$m_{2\,oed}^w = \frac{\partial\left(V_w/V_o\right)}{\partial s} = \frac{1}{H_w} - \frac{2\left(E/H\right)}{\left(1-\upsilon\right)E_w} \tag{4.27}$$

4.3.3 Constitutive Surfaces for Soil Structure and Water Phase

The constitutive relations for both the soil structure and water phase can be visualised as three-dimensional constitutive surfaces (Figure 4.3). The uniqueness of the constitutive surfaces for monotonic loading has been proved by Matyas and Radhakrishna (1968), Barden et al. (1969), and Fredlund and Morgenstern (1977). However, it is practically impossible to develop a complete unique constitutive surface for loading and unloading cases (Fredlund and Rahardjo, 1993). The non-uniqueness of the constitutive surface is due to hysteresis. The hystereis phenomenon leads to different constitutive relationships for loading and unloading. The hysteresis of a saturated soil structure during loading and unloading is reflected in the different compression and rebound curves. The presence of hysteresis of the soil structure and water phase in response to the hydro-mechanical loading and unloading results in the different volumetric deformation coefficients for both cases. However, it appears that the uniqueness of constitutive surfaces for volume decrease (i.e., loading) can also be proved for the case of volume increase (i.e., unloading).

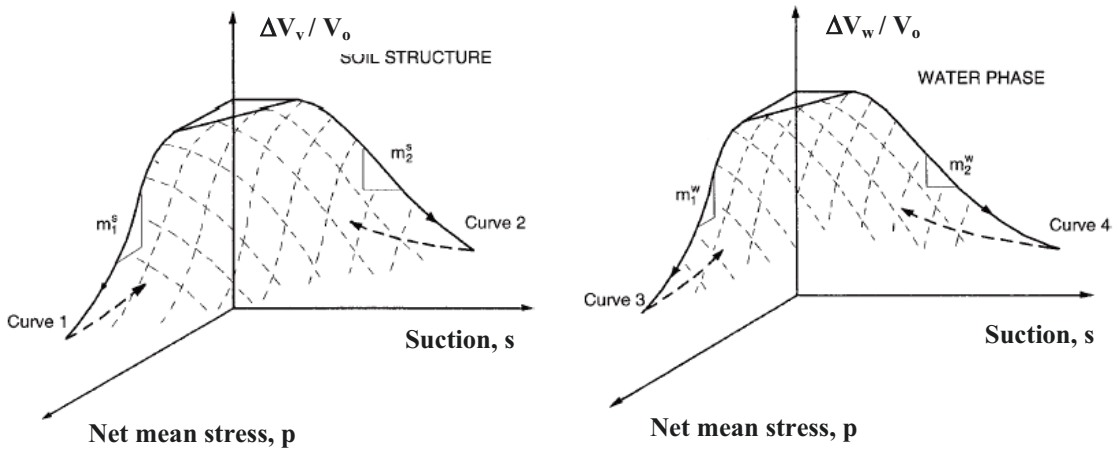

Figure 4.3 Three-dimensional constitutive surfaces for: (a) soil structure and (b) water phase

4.4 Constitutive Model III: A Non-Linear Elastic Model for Heavily Compacted Clays

The non-linear elastic model for heavily compacted clays described herein is a model which was proposed by Cui et al. (2002b). The model was developed based on experimental evidence from tests on a heavily compacted bentonite. It was observed that the heavily compacted bentonite specimens did not exhibit significant hysteresis on wetting-drying and loading-unloading tests. The observed phenomena were thought to be associated with the dominant physico-chemical effects of clay particles.

4.4.1 Concept of Critical Swelling Curve (CSC)

The critical swelling curve (CSC) is simply defined as a curve of zero swelling (Figure 4.4). At a certain combination of suction and mean stress on the CSC, a soil specimen exhibits a zero swelling upon hydration with pure water. According to the model, there is a threshold suction below which no volume change of the specimen occurs upon wetting under a constant net mean stress. Therefore, wetting performed on a specimen which is located above the CSC results in swelling. When the applied stress is high enough, suction reduction results in collapse.

4.4.2 Volume Change Formulations for Mechanical Loading and Unloading

Elastic volume change of an unsaturated expansive soil specimen during loading and unloading under constant suction is expressed as an elastic change of void ratio with stress as defined in the following power law (Cui et al., 2002b).

$$e = A_p(s)\left(\frac{p}{p_c}\right)^{N_p(s)} \tag{4.28}$$

where A_p is the void ratio at the reference net mean stress (p_c) of unity and N_p is the slope of the void ratio versus net mean stress curve on a logarithmic plot.

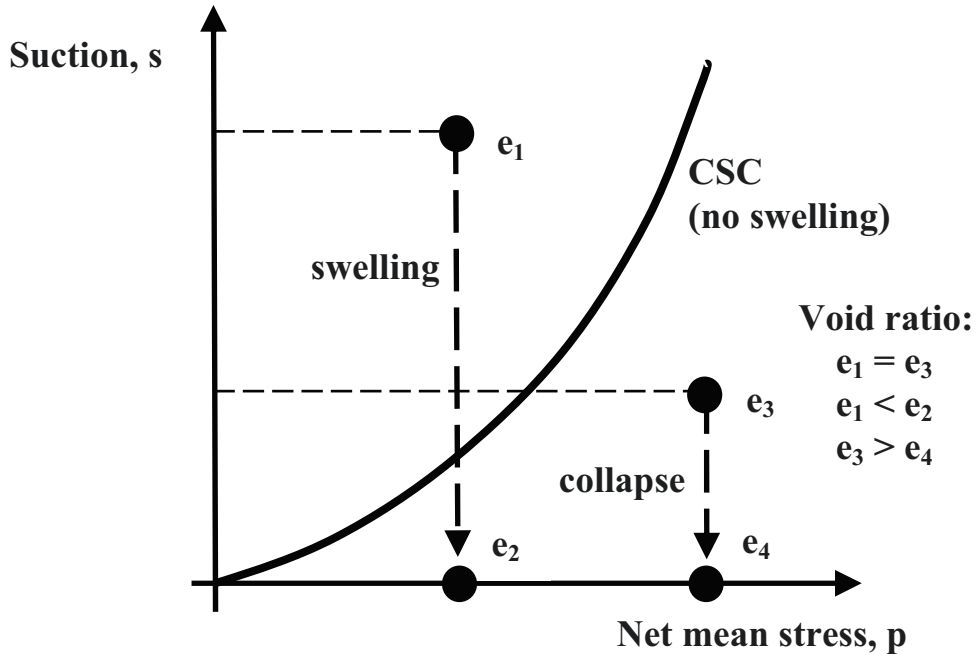

Figure 4.4 Concept of Critical Swelling Curve (CSC)

Based on the experimental data, Cui et al. (2002b) suggested the following empirical formula to relate A_p and N_p with suction.

$$A_p(s) = C_1\left(\frac{s}{s_c}\right)^{C_2} \tag{4.29}$$

$$N_p(s) = C_3 \ln\left(\frac{s}{s_c}\right) + C_4 \tag{4.30}$$

where fitting parameters C_1, C_2, C_3, and C_4 have to be obtained from the experimental data.

The change in volumetric strain induced by a change in net mean stress (i.e., mechanical loading) under constant suction can be formulated using the following equation (Cui et al., 2002b).

$$\begin{aligned} d\varepsilon_v &= A_p(s)N_p(s)\frac{1}{(1+e)}\left(\frac{p}{p_c}\right)^{\left[N_p(s)-1\right]}\frac{dp}{p_c} \\ &= C_1\left(\frac{s}{s_c}\right)\left[C_3\ln\left(\frac{s}{s_c}\right)+C_4\right]\frac{1}{(1+e)}\left(\frac{p}{p_c}\right)^{\left[C_3\ln\left(\frac{s}{s_c}\right)+C_4-1\right]}\frac{dp}{p_c} \end{aligned} \tag{4.31}$$

4.4.3 Volume Change Formulations for Wetting and Drying (Hydraulic Loading and Unloading)

It was assumed that the volume change of an expansive soil specimen for changes in suction takes a similar form to that for changes in net mean stress. The following equation is obtained for the relationship between void ratio and suction for wetting and drying with s_c represents the reference suction (Cui et al., 2002b).

$$e = A_s(p)\left(\frac{s}{s_c}\right)^{N_s(p)} \tag{4.32}$$

The A_s and N_s values can be obtained using Equations (4.33) and (4.34), respectively (Cui et al., 2002b).

$$A_s(p) = C_1\left(\frac{p}{p_c}\right)^{C_4} \tag{4.33}$$

$$N_s(p) = C_3 \ln\left(\frac{p}{p_c}\right) + C_2 \tag{4.34}$$

4.4.4 CSC Formulation

In the formulation of the CSC, it is assumed that Equations (4.28) to (4.34) are valid for the whole range of suction. Another assumption is that the stress under which a soil specimen with an initial void ratio of e and an initial suction of s is hydrated with pure water (i.e., swell under load test) corresponds to the swelling pressure at the equilibrium void ratio. The following equation is obtained and it represents the CSC of the specimen (Cui et al., 2002b).

$$\left(\frac{s}{s_c}\right) = \left[\frac{A_p(o)\left(\frac{p}{p_c}\right)N_p(o)}{C_1\left(\frac{p}{p_c}\right)^{C_4}}\right]^{\frac{1}{C_3\ln\left(\frac{p}{p_c}\right)+C_2}} \tag{4.35}$$

where $A_p(o)$ and $N_p(o)$ is the void ratio at a zero suction and at a p/p_c equal to unity and the slope of virgin compression curve when plotted in a logarithmic scale, respectively.

Assessment of Equation (4.35) shows that the model gives an unrealistic estimate of swelling at a very low pressure since the CSC does not pass the origin (Cui et al., 2002b).

4.5 Soil-Water Characteristic Curve (SWCC)

The soil-water characteristic curve (SWCC) represents the ability of a soil to retain water at various suction values. The SWCC is represented as a relationship between water content or volumetric water content or degree of saturation versus suction. The SWCC has been related to many geotechnical properties of soils such as shear strength, permeability, and compressibility (Fredlund and Rahardjo, 1993). The SWCC is also required when solving transient water and solute transport problems.

4.5.1 Typical Soil-Water Characteristic Curve (SWCC) of Non-Expansive Soils

Figure 4.5 represents a typical SWCC of non-expansive soils which is drawn as a relationship between degree of saturation and suction (Leong and Rahardjo, 1997a). The SWCC normally exhibits a sigmoidal function. The curves of water content and volumetric water content versus suction for non-expansive soils essentially follow a similar shape since suction decrease or increase induces insignificant changes in void ratio of the soils. Several parameters that can be defined from the SWCC are also given in the figure. The suction corresponding to the oven-dried conditions (i.e., zero water content or zero degree of saturation) is 1 000 000 kPa. This value is supported by experimental evidence and theoretical thermodynamics considerations (Croney and Coleman, 1961).

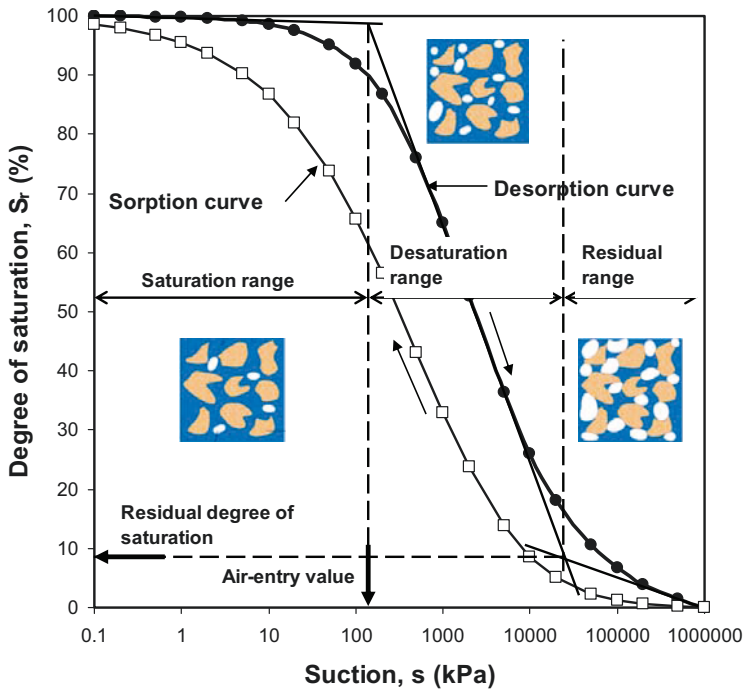

Figure 4.5 Typical soil-water characteristic curves of non-expansive soils

4.5.2 Soil-Water Characteristic Curve (SWCC) of Expansive Soils

During drying and wetting, the void ratio of expansive soils changes. The amount of water drained out of the specimen during drying from saturated conditions is accompanied by a reduction in the void ratio of the soil. Therefore, although a significant reduction in the amount of water in the specimen takes place, the soil remains saturated up to a large value of suction. This is due to dominant pysico-chemical effects of the clay-water system at the microscopic level. Figure 4.6 shows a typical soil-water characteristic curve of expansive soils drawn partly based on the experimental data obtained by Fleureau et al. (2002).

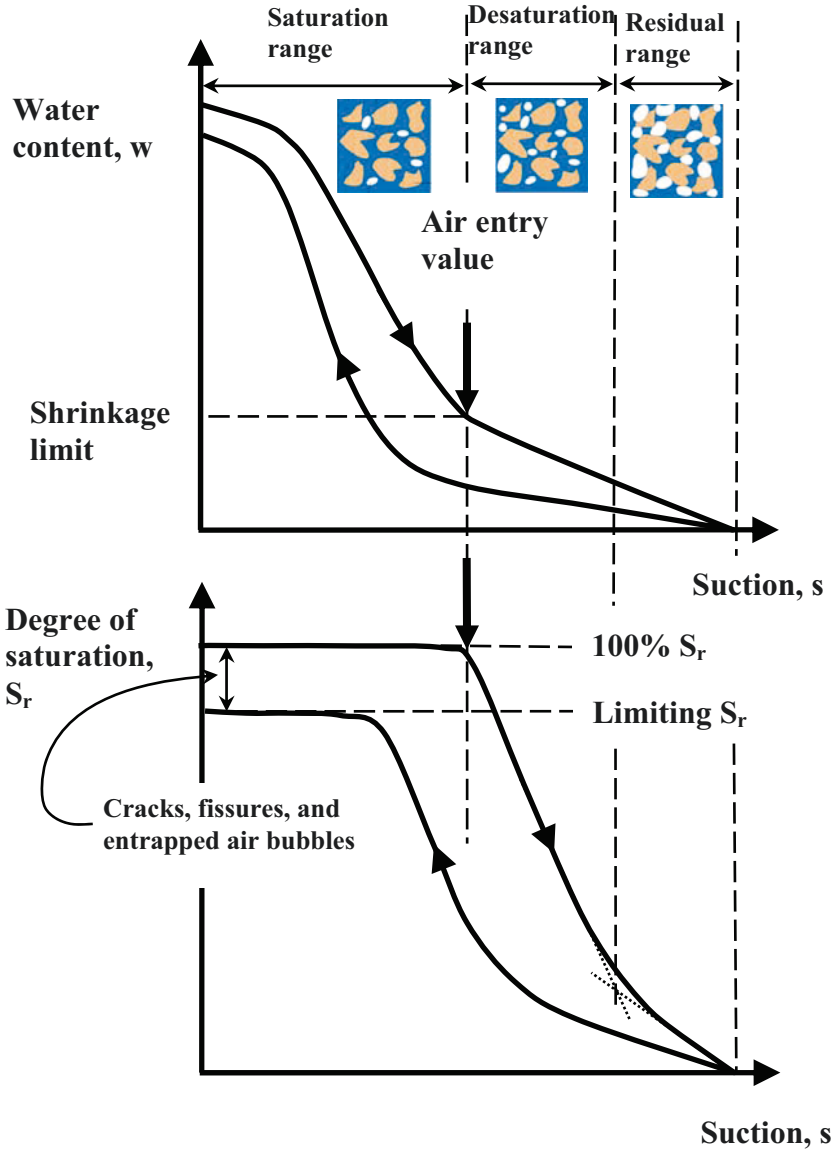

Figure 4.6 Typical soil-water characteristic curves of expansive soils

Based on several drying and wetting curves obtained on a number of slurried and compacted clay specimens, Fleureau et al. (2002) found that the air-entry value of expansive soils is located close to a suction corresponding to the shrinkage limit of the soils. Further analysis of the data indicates that there should be a limiting degree of saturation during wetting on an expansive soil specimen when no load is applied to the specimen due to cracks, fissures, and entrapped air bubbles in the specimen. Or else, the saturation conditions of the specimen might be reached at a very low value of suction at which suction is balanced by the self weight of the specimen.

4.5.3 Soil-Water Characteristic Curve (SWCC) Models

Numerous parametric models or equations have been developed for representing the SWCC. The most famous and most frequently used equations for representing the SWCC are the van Genuchten (1980) and Fredlund and Xing (1994) SWCC equations. The van Genuchten (1980) SWCC equation is expressed in Equation (4.36) while the Fredlund and Xing (1994) SWCC equation is given in Equation (4.37).

$$\Theta = \frac{\theta_w - \theta_{res}}{\theta_s - \theta_{res}} = \left[\frac{1}{1 + \left(\frac{s}{a} \right)^n} \right]^m = \left[1 + \left(\frac{s}{a} \right)^{\frac{1}{m-1}} \right]^{-m} \tag{4.36}$$

where Θ is the normalised volumetric water content or the effective degree of saturation (S_e), θ_w is the volumetric water content, θ_{res} is the residual volumetric water content, s is the soil suction, a (kPa), n, and m are fitting parameters. Parameter a in the above equation is also called the reference suction.

$$\Theta = \frac{\theta_w}{\theta_s} = \theta_w = C(s) \frac{1}{\left\{ \ln \left[\exp(1) + \left(\frac{s}{a} \right)^n \right] \right\}^m}$$
$$C(s) = 1 - \frac{\ln \left(1 + \frac{s}{s_r} \right)}{\ln \left(1 + \frac{1\,000\,000}{s_r} \right)} \tag{4.37}$$

where s_r represents the suction corresponding to the residual volumetric water content (or residual degree of saturation).

The Fredlund and Xing (1994) SWCC equation has a better theoretical basis since it was developed by taking into consideration the pore-size distribution of the soil. The C coefficient is used in the equation to give a zero volumetric water content at a suction of 1 000 000 kPa which approximately corresponds to oven-dried conditions of the soil

(Croney and Coleman, 1961). Leong and Rahardjo (1997a) assessed the van Genuchten (1980) and Fredlund and Xing (1994) SWCC equations together with some other SWCC equations and found that the Fredlund and Xing (1994) SWCC equation gave the best fit to the experimental data. Leong and Rahardjo (1997a) also found that the equation gave excellent fit if the correction factor *C(s)* was taken as unity.

Schick (2004) introduced a two-component model of SWCC for expansive soils. According to the model, the decrease in water content (or degree of saturation) of an expansive soil during drying process consisted of the decrease in water content (or degree of saturation) induced by the reduction in adsorptive component of suction and that caused by the reduction in capillary component of suction.

$$\begin{aligned} S_r &= S_r^a + S_r^c \\ S_r^a &= C_p^a \frac{n_w^a}{n_T} \\ S_r^c &= \left(1 - S_r^a\right) C_p^c \frac{100}{\left\{\ln\left[\exp(1) + \left(\frac{s}{a}\right)^n\right]\right\}^m} \end{aligned} \tag{4.38}$$

where S_r^a and S_r^c is the portion of degree of saturation associated with the adsorptive and capillary components of suction, respectively, n_w^a is the adsorptive water-filled porosity, n_T is the soil total porosity, and C_p^a and C_p^c is the adsorptive and capillary coefficient, respectively, formulated using the following equations.

$$C_p^a = 1 - \frac{\ln\left(1 + \frac{s}{s_{cap}}\right)}{\ln\left(1 + \frac{1\,000\,000}{s_{cap}}\right)} \tag{4.39}$$

$$C_p^c = 1 - \frac{\ln\left(1 + \frac{s}{s_{cap}}\right)}{\ln 2} \tag{4.40}$$

where s_{cap} is the capillary component of suction.

4.6 Permeability Models

The response of an unsaturated expansive soil to hydro-mechanical processes such as volume change or swelling pressure development can be predicted using the constitutive models presented in the earlier subchapters. However, the volume change (i.e., swelling and shrinking) and the development of swelling pressure are time-dependent processes. To predict satisfactorily the transient stage of the response of a soil

to the hydro-mechanical processes, information pertaining to the transport properties of the soil are required.

The transport of water in expansive soils may occur in two phases; namely in liquid phase (i.e., advection process) and in vapour phase (i.e., diffusion process). The transport property related to the liquid phase water transport is the coefficient of permeability whereas the coefficient of diffusivity can be used to describe the transport of water in the vapour phase. However, both the coefficient of permeability and the coefficient of diffusivity depend on the void ratio of the soil.

Vu and Fredlund (2004) proposed a coupled equation for water flow (i.e., in liquid phase) in expansive soils.

$$\frac{m_1^w}{m_1^s}\frac{\partial \varepsilon_v}{\partial t} + \left(m_2^w - \frac{m_1^w m_2^s}{m_1^s} \right) \frac{\partial s}{\partial t} - \nabla \left[k_w \nabla \left(\frac{u_w}{\rho_w g} + h \right) \right] = 0 \qquad (4.41)$$

where h is the elevation.

Equation (4.41) has been used to model one-, two-, and three-dimensional heave in expansive soils (Vu and Fredlund, 2004). The equation is applicable for both saturated and unsaturated soils under transient and steady-state seepage conditions. In the model, information pertaining to the volume change of both soil structure and water phase (i.e., m_{1w}, m_{1s}, m_{2w}, and m_{2s}) and the unsaturated coefficient of permeability (i.e., k_w) are required. The unsaturated coefficient of permeability can be computed using the saturated coefficient of permeability and the soil-water characteristic curve (Childs and Collis-George, 1950; Burdine, 1953; Brooks and Corey, 1964; Mualem, 1976; van Genuchten, 1980; Fredlund and Rahardjo, 1993; Fredlund et al., 1994; Leong and Rahardjo, 1997b; and Agus et al., 2003).

4.6.1 Kozeny-Carman Model for Saturated Permeability Function

Numerous models were proposed to relate permeability (or intrinsic permeability) of soils with void ratio (e.g., Hazen, 1892; Slichter, 1898; Terzaghi, 1925; Kozeny, 1927; and Carman, 1938). The models were initially developed for a purpose to estimate coefficient of permeability of soils with respect to water from grain size and porosity (or void ratio) of the soils. The Kozeny-Carman model was developed based on the following assumptions.

1. Darcy's law is valid for flow of water in saturated soils.
2. The Hagen-Poiseuille equation for viscous flow through tubes is valid.
3. The tortuosity of flow channels is constant.
4. The flow channels have the same size.

5. Soil particles are rigid and no interactions between soil particles and permeating fluid occur.

The Kozeny-Carman model for flow of water is expressed in the following equation (Carrier III, 2003).

$$k_s = K\left(\frac{\rho_w g}{\mu_w}\right) = \left(\frac{\rho_w g}{\mu_w}\right)\left(\frac{1}{C_{K-C}}\right)\left(\frac{1}{S_o^{\,2}}\right)\frac{e^3}{(1+e)} \tag{4.42}$$

where k_s is the saturated coefficient of permeability, K is the intrinsic permeability, ρ_w is the density of water, g is the gravitational acceleration, μ_w is the absolute viscosity of water, $C_{K\text{-}C}$ is the Kozeny-Carman empirical coefficient (i.e., equal to 5), S_o is the specific surface area of soil particles per unit volume of the soil, and e is the soil void ratio.

Carrier III (2003) found that the Kozeny-Carman model (Kozeny, 1927 and Carman, 1938) had the best theoretical basis as compared to the other models. This is due to the fact that the grain-size distribution of the soil is some how taken into account by using the specific surface area. The Kozeny-Carman formula, like other formula (e.g., Hazen, Slichter, and Terzaghi formula), is inaccurate when used for predicting the permeability of soils with platy particles such as clays, extreme grain-size distribution with high percentage of fines, and for anisotropic soils.

4.6.2 Cluster Model for Saturated Permeability Function

Olsen (1962) found discrepancies between the measured saturated coefficient of permeability and that predicted using the Kozeny-Carman formula (Equation (4.42)) for clays. Factors that might influence the flow of water though clay soils were described in Olsen (1962) and included possible errors in Darcy's law, interaction between viscous and electric flows between water and clay particles (i.e., electrokinetic coupling), possible higher viscosity of water near the clay surfaces, non-constant tortuosity of the water flow paths as induced for instance by the anisotropic shapes and orientations of clay particles, and the existence of clusters that may induce unequal pore sizes in the soil. It was found that the deviation of Equation (4.42) from the measured data was attributed to the presence of clay clusters in the soil. Some other abovementioned factors that might induce the discrepancies were found to be insignificant.

Based on the conclusion drawn regarding the factor that influences at most the deviation of the Kozeny-Carman equation for predicting the water flow though clay soils, a saturated permeability model, called cluster model, was proposed (Olsen, 1962). According to Olsen (1962), the ratio of measured flow rate to the Kozeny-Carman estimated value can be described using the following equation.

$$\frac{q_{measured}}{q_{K-C}} = N^{2/3} \frac{\left(1-\frac{e_m}{e_T}\right)^3}{\left(1+e_m\right)^{4/3}} \tag{4.43}$$

where $q_{measured}$ is the measured flow rate of water, $q_{K\text{-}C}$ is the predicted flow rate using the Kozeny-Carman model, N is the average number clay particles per cluster, e_m (or e_c in the original model) is the cluster void ratio (i.e., the intra-cluster or the intra-aggregate or the micro-pore void ratio), and e_T is the total void ratio.

For a particular soil, the ratio of flow rate as given in Equation (4.43) is equal to the ratio of the measured k_s to the computed k_s using the Kozeny-Carman model. Therefore, to compute the saturated coefficient of permeability of a clay using Equation (4.43), the parameter N and the two void ratios (i.e., the cluster and the total void ratios) must be known. The number of clay particles per cluster (N) was assumed to be constant for a specific soil permeant system. The clay-permeant dispersion systems were considered to affect the decrease in both cluster and initial cluster void ratios. Olsen (1962) assumed relationship between the total, cluster (or intra-cluster or micro), and inter-cluster (or macro) void ratios in which the cluster void ratio begins to decrease when the inter-cluster void ratio is equal to 0.43 (Figure 4.7). The following equation has been formulated for the total, cluster, and inter-cluster void ratio idealised relationship from the original assumption proposed by Olsen (1962) shown in Figure 4.7.

$$\begin{aligned} e_c = e_m = e_{co} = e_{mo} \qquad & for\ e_T = e > e_{co} + 0.43 \\ e_c = e_m = e_{co} = \frac{e_{co}}{\left(e_{co}+0.43\right)} e_T \quad & for\ e_T = e \le e_{co} + 0.43 \end{aligned} \tag{4.44}$$

where e_{co} (or e_{mo}) is the initial cluster (or micro) void ratio, e_T (or e) is the total void ratio.

The relationship given in Equation (4.44) may be reasonable for expansive soils during loading and unloading (or compression and rebound) since only macro-structure void ratio is primarily affected by the mechanical load. When an expansive soil is subjected to changes in suction, the changes in micro-structural void ratio (or cluster void ratio) is governed by the changes in micro-structural effective stress as given in Equation (4.1). Therefore, the use of Equation (4.44) underestimates the magnitude of e_c.

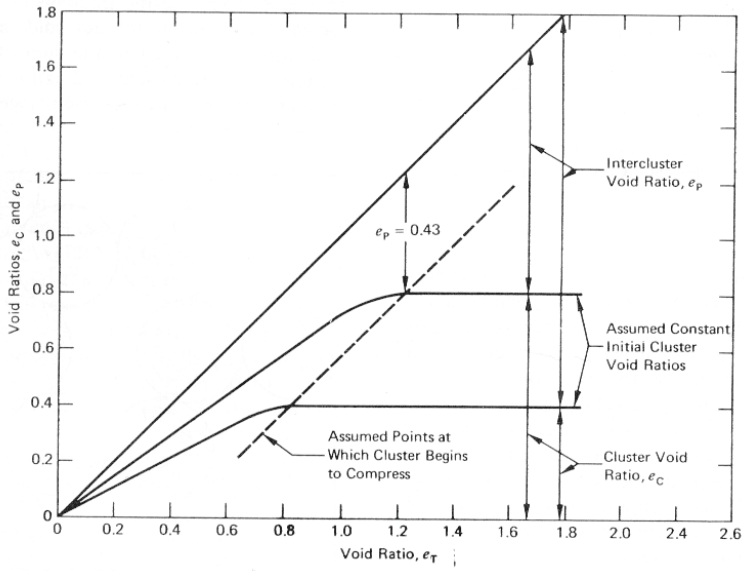

Figure 4.7 Assumed relationship between total, cluster (or intra-cluster or micro), and inter-cluster (or macro) void ratio (Olsen, 1962)

Achari et al. (1999) used the modified diffused double layer (DDL) theory in conjunction with the true effective stress concept proposed by Lambe and Whitman (1969) (see Chapter 3 for details) for computing the cluster void ratio. The repulsive force was computed from the basic DDL theory whereas the attractive force is considered to be governed by the van der Waals attractive forces. The following empirical relationship was used to compute the N value as a function of effective stress and concentration of permeant.

$$N = \frac{2.43 \times 10^{11}}{\left(\sigma - u_w\right)^2 \sqrt{C_o}} \tag{4.45}$$

where (σ - u_w) is the effective stress in kPa and C_o is the bulk concentration of permeant in g equivalent/m^3.

An iterative procedure was set up by Achari et al. (1999) to solve the DDL equation and to compute the saturated coefficient of permeability. The combination of DDL theory, true effective stress concept, and cluster model proposed by Achari et al. (1999) to compute k_s is limited to homoionic clay and ionic solutions.

4.6.3 Gel Model for Saturated Permeability Function

Pusch (2001) observed that there was a formation of clay gels when a bentonite is in contact with water. The presence of gels influence the interconnectivity of pores in the bentonite and affects its permeability. It was found that sodium montmorillonite possessed a lower permeability compared to calcium montmorillonite at the same void

ratio indicating the less volume of interconnected pores in the sodium montmorillonite. According to Pusch (2001), a compacted bentonite specimen consisted of several packs of clusters with different densities and with clay gel-filling voids in between. The densities of bentonite packs and clay gels can be evaluated by taking a digital micrograph of an ultra thin section of the specimen. An image analysis is required for further interpretation of the digital photo. Generally, the gel density is a function of dry density of the specimen and the pore-water chemistry. The average coefficient of permeability (k_{ave}) of an expansive soil with elements of different density and permeability can be computed using the following equation.

$$k_{ave} = \frac{1}{m}\sum_{i=1}^{m} n\left(\sum_{j-1}^{n}\frac{1}{k_{ij}}\right)^{-1} \tag{4.46}$$

where m is the number of elements in flow direction, n is the number of elements perpendicular to the flow direction, and k_{ij} is the coefficient of permeability of each element computed based on the image analysis of the digital micrograph.

4.6.4 Macroscopic Model for Unsaturated Permeability Function

The macroscopic model for unsaturated permeability computation was first proposed by Brooks and Corey (1964) based on the work of Burdine (1953). The model was developed with an objective to derive an analytical expression for the unsaturated permeability function (Mualem, 1976 and Leong and Rahardjo, 1997b). Assumptions used in the derivation of macroscopic model are:

1. A similarity occurs between laminar flow (i.e., microscopic level) to flow in porous media (i.e., macroscopic level).
2. Darcy's law is valid for flow of water and air in unsaturated porous media (or soils).
3. Pore fluid consists of two phases; namely, water and air, and both are separated by a curved interface.
4. Water can only flow though pores filled with water and air can only flow through air-filled soil pores.
5. Soil particles are rigid and no interactions between soil particles and permeating fluid occur.

In the Brooks and Corey (1964) macroscopic model, the soil-water characteristic curve (SWCC) was expressed as a relationship between degree of saturation (S_r) and matric suction using the following equation.

$$S_e = 100\left(\frac{S_r - S_{res}}{100 - S_{res}}\right) = 100\left(\frac{s_b}{s}\right)^{\lambda_b} \tag{4.47}$$

where S_e is the effective degree of saturation with respect to water phase in percent, S_{res} is the residual degree of saturation in percent, s is the soil suction, s_b is a fitting parameter that might be closed to the air-entry value of the soil (Corey and Brooks, 1997), and λ_b is a constant which is a soil property and called pore-size distribution index.

The unsaturated coefficient of permeability with respect to water phase (k_w) had the following form for suction greater than s_b.

$$k_{rw}\left(S_e\right) = \frac{k_s}{k_w} = S_e^{\delta_b} \tag{4.48}$$

where k_{rw} is the relative permeability with respect to water phase, k_s is the saturated coefficient of permeability, and δ is a constant. Brooks and Corey (1964) calculated that δ_b was equal to $(2 + 3\lambda_b)/\lambda_b$.

Brooks and Corey (1964) assessed the macroscopic model for predicting the unsaturated coefficient of permeability of various soils. It was found that the model gave good estimate of unsaturated permeability for sandy soils where the s_b value (or the air-entry value) can be distinguished easily in the SWCC. In the macroscopic model, the effect of pore-size distribution of the soil is neglected and therefore the model oversimplifies the flow of water in the unsaturated soils.

4.6.5 Statistical Model for Saturated and Unsaturated Permeability Functions

The statistical model has been derived by taking into account the effect of pore-size distribution on both the SWCC and the permeability function. Childs and Collis-George (1950) developed a statistical model for computing the permeability function of soils based on the following assumptions (Leong and Rahardjo, 1997b).

1. The soil consists of pores that are distributed and interconnected randomly according to a statistical distribution function.
2. The Hagen-Poiseuille equation for viscous flow through tubes is valid.
3. Darcy's law is valid for flow of water in saturated and unsaturated soils.
4. The pore-size distribution of soils is related to the SWCC using Kelvin capillary law.
5. Water can only flow though pores filled with water and air can only flow through air-filled soil pores.

6. Soil particles are rigid and no interactions between soil particles and permeating fluid occur.

Based on the above assumptions, an equation describing the flow of water in saturated and unsaturated soils was developed. The following generic equation was used to calculate the saturated coefficient of permeability from the pore-size distribution of soil (Childs and Collis-George, 1950 and Lu and Likos, 2003).

$$k_s = K\left(\frac{\mu_w}{\rho_w g}\right) = \frac{\rho_w g}{32\mu_w}\frac{n^2}{m^2}\sum_{i=1}^{m}(2i-1)\,D_{pi}^2 \tag{4.49}$$

where ρ_w is the density of water, μ_w is the absolute viscosity of water, g is the gravitational acceleration, n is the soil porosity, m is the number of pore classes, and D_{pi} is the mean diameter of pores of class i. The smallest diameter of pores is represented by D_{pn}.

Marshall (1958) modified the Childs and Collis-George equation for flow in unsaturated soils. The following equation was derived for computing the unsaturated coefficient of permeability using the Childs and Collis-George (1950) statistical model (Kunze, 1968 and Fredlund and Rahardjo, 1993).

$$k_w(\theta_w) = \frac{k_s}{k_{sc}}\frac{T_w^2}{2\mu_w\rho_w g}\frac{\theta_s}{N^2}\sum_{j=i}^{m}\left[\frac{(2j+1-2i)}{s^2}\right] \tag{4.50}$$

where k_s/k_{sc} is the ratio of measured saturated coefficient of permeability (k_s) to the computed value (k_{sc}), T_w is the surface tension of water, j and i are counters, m is the total number of pore size intervals between the saturated volumetric water content (θ_s) to the lowest volumetric water content (θ_l), θ_w is the volumetric water content, and N is the number of intervals between θ_s and zero volumetric water content.

Mualem (1976) analysed the statistical model and showed that the analytical form of Equation (4.50) is:

$$k_{rw}(\theta_w) = \frac{k_w(\theta_w)}{k_s} = \frac{\int_0^{\theta_w}\frac{(\theta_w-\vartheta)}{s^2}d\vartheta}{\int_0^{\theta_s}\frac{(\theta_s-\vartheta)}{s^2}d\vartheta} \tag{4.51}$$

where ϑ is a dummy integration variable.

Mualem (1976) proposed the following equation for computing the unsaturated coefficient of permeability from the saturated coefficient of permeability and the SWCC.

$$k_{rw}\left(\theta_w\right) = \Theta^{1/2}\left(\frac{\int_0^{\theta_w}\frac{d\theta_w}{s^2}}{\int_0^{\theta_s}\frac{d\theta_w}{s^2}}\right)^2 \tag{4.52}$$

where Θ is a coefficient (i.e., the normalised volumetric water content = θ_w/θ_s) to account for the tortosity.

Van Genuchten (1980) proposed a closed-form equation for permeability function based on the Mualem (1976) model. The equation, which is also known as van Genuchten-Mualem equation, was established by taking the van Genuchten (1980) SWCC equation to describe the relationship between effective degree of saturation and suction (Equation (4.36)) when $m = 1 - 1/n$.

$$k_{rw}\left(s\right) = \frac{\left\{1-\left(\frac{s}{a}\right)^n - 1\left[1+\left(\frac{s}{a}\right)^n\right]^{-m}\right\}^2}{\left[1+\left(\frac{s}{a}\right)\right]^{\frac{m}{2}}} \tag{4.53}$$

The van Genuchten-Mualem model can also be expressed as a relationship between relative permeability versus effective degree of saturation:

$$k_{rw}\left(\Theta\right) = \sqrt{\Theta}\left[1-\left(1-\Theta^{1/m}\right)^m\right]^2 = \sqrt{\frac{S_e}{100}}\left\{1-\left[1-\left(\frac{S_e}{100}\right)^{\frac{1}{m}}\right]^m\right\}^2 \tag{4.54}$$

where S_e is the effective degree of saturation in percent.

Leong and Rahardjo (1997b) found that the statistical models gave the best agreement with the experimental data. Agus et al. (2003b) assessed several statistical models combined with several SWCC equations to estimate the permeability functions of various types of soil ranging from sands and gravels to clays. It was found that the Mualem (1976) statistical model gave the best fit to most of the soils when used in conjunction with the Fredlund and Xing (1994) SWCC equation. The statistical model using a combination of the Fredlund and Xing (1994) SWCC equation and the Mualem (1976) statistical model is further called Fredlund and Xing-Mualem statistical model.

CHAPTER 5

LITERATURE REVIEW ON EXPERIMENTAL TECHNIQUES RELEVANT TO THIS STUDY

5.1 General

This chapter presents literature review on the experimental techniques relevant to this study. Several techniques for measuring suction that could also be used in the study are described. Swelling pressure measurements using various techniques cited in literature are also elaborated in this chapter. Relevant suction control techniques that can also be adopted in this investigation and the applications in oedometer tests are described and discussed.

5.2 Measurements of Suction

Suction measurements are challenging for geotechnical engineers. This is particularly true when measuring low values of total suction. Figure 5.1 shows approximate range of various methods commonly used for measuring suction. No single piece of equipment covers the entire range of total suction that may be encountered. Measurements of suction can be divided into two main categories; namely, direct method for measuring matric suction and indirect method for measuring matric, osmotic, and total suctions. Generally, measuring matric suction is more desirable in the low suction range (i.e., below 100 kPa) where the contribution of capillary component of suction is significant. In the high suction range, surface area effects are dominant and measurement of matric suction is difficult. Suction which is relevant in the study of expansive soils ranges from 1000 to 700 000 kPa (Likos and Lu, 2003).

5.2.1 Direct Measurement of Matric Suction

Matric suction of a soil is determined directly by measuring the negative pore-water pressure of the soil. The measurement requires a separation between water and air phase, normally by means of a ceramic disk or a ceramic cup. The maximum value of matric suction that can be measured is limited by the air entry value of the ceramic disk (or the ceramic cup) used. However, cavitation poses another restriction to the technique when used for measuring high matric suctions. This occurs when the negative pore-water pressure in the soil approaches the water vapour pressure at the ambient temperature and facilitates the movement of water from liquid to vapour form. Theoretically, the

maximum matric suction that can be measured using this method is 101.3 kPa (Fredlund and Rahardjo, 1993).

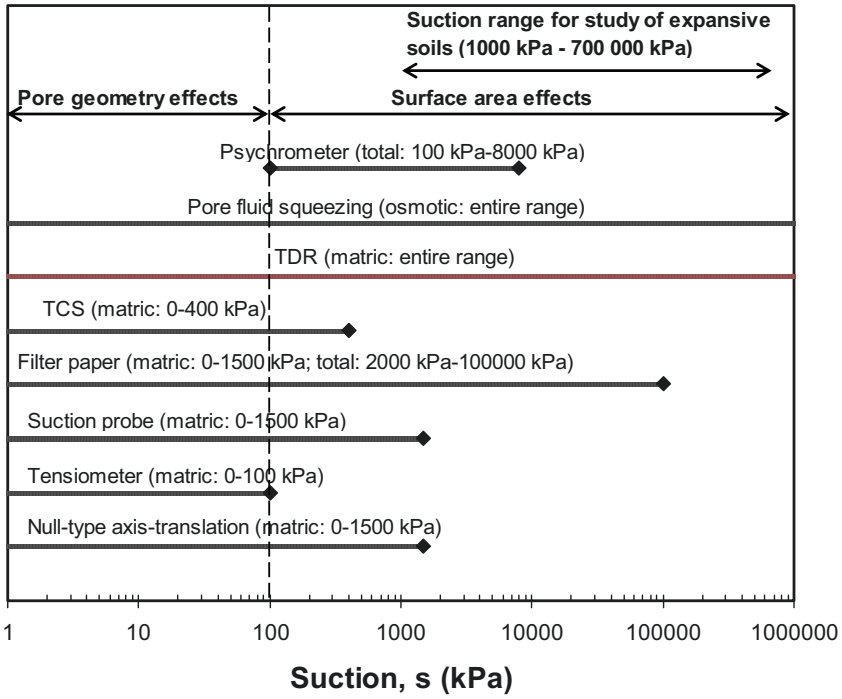

Figure 5.1 Suction measurement range of various methods

5.2.1.1 Tensiometer

Tensiometer is normally used for directly measuring the negative pore-water pressure of soil. The principle of suction measurement using tensiometer is that once pressure equilibrium between the soil and the tensiometer is achieved, water in the tensiometer will be in tension of the same magnitude as the negative pore-water pressure in the soil. Since a true semi-permeable membrane for soluble salts does not exist in tensiometer, the effect of osmotic component of suction is not measured. Thus, the measurement only provides the value of matric suction component in the soil. Due to the cavitation problem, the use of a ceramic cup with a higher air entry value will not increase the measurement range of the tensiometer. Therefore, the technique can only measure matric suction up to about 100 kPa.

Improvements have been made to the tensiometer technique to enable measurements of matric suction greater than 100 kPa to be performed. Osmotic tensiometer proposed by Peck and Rabbidge (1966) used an aqueous solution of polyethylene glycol (PEG) that provided a ‘pre-stressing’ to the tensiometer. Higher matric suction can be measured depending on the pre-stressing pressure exerted. This pressure acts as a reference pressure in the tensiometer. However, alteration of the

reference pressure with time and temperature poses difficulties and restricts the use of osmotic tensiometer in practice (Bocking and Fredlund, 1980).

5.2.1.2 Axis-translation Technique

Matric suction is mostly associated with the soil matrix and is defined as the difference between pore-air and hydrostatic pore-water pressure of the soil. Therefore, measuring negative pore-water pressure can be avoided by increasing the pore-air pressure while maintaining the pore-water pressure to a positive reference pressure (i.e., axis-translation technique) (Hilf, 1956). The measurement of matric suction using this technique is only limited by the air entry value of the ceramic disk used since cavitation can be avoided due to elevated pore-water pressure. Ceramic disks with a maximum air-entry value of 1500 kPa are available in the market (Soilmoisture Equipment Corp., 2002). Olson and Langfelder (1965) developed a pressure plate apparatus for measuring matric suction using the axis-translation technique. Since water pressure in the water compartment is maintained as close as possible at a zero value, the technique is called null-type axis-translation technique (Fredlund, 1989).

5.2.1.3 Suction Probe

Ridley and Burland (1993) developed a suction probe for measuring matric suction of soil. In the suction probe, the volume of water reservoir beneath the ceramic disk (or ceramic cup) is minimised. Water in the water reservoir is pre-pressurised such that benefit of the high tensile strength of water can be utilised (Marinho and Chandler, 1995). Similar technique has been adopted by Guan and Fredlund (1997). Recently, Meilani et al. (2002) developed a mini suction probe for measuring matric suction along the specimen's height during triaxial test on an unsaturated soil. The sensor used a 5-bar ceramic disk which was thinned down to about 1 mm thick using sandpaper. The fast response of the system was ensured by minimising the volume of water compartment beneath the ceramic disk. Similar to the null-type axis-translation technique, the upper limit of matric suction that can be measured using this technique is governed by the air-entry value of the ceramic disk (or ceramic cup) used.

5.2.2 Indirect Measurement of Matric Suction

The indirect measurement of matric suction is commonly performed using; for instance, a standard porous sensor made of a special material (e.g., nylon, fibreglass, gypsum, clay ceramics, sintered glass, metal, and filter paper). The measurement is performed by equilibrating the porous sensor with the matric suction in the soil. Hence, the water content of the porous sensor represents the magnitude of matric suction of the soil.

5.2.2.1 Thermal Conductivity Sensor (TCS)

The measurement of water content of the porous sensor can be done by measuring the electrical or thermal properties of the porous sensor. The measurement of matric suction based on the electrical properties is sensitive to the presence of dissolved salts (i.e., osmotic suction effects) in the soil pore-water (Richards, 1974). Therefore, the use of the thermal properties of the porous sensor is preferred.

Thermal conductivity sensor (TCS) is an equipment proposed by Shaw and Baver (1939) to measure matric suction using this principle (Feng et al., 2002). Since then, many researchers have used the technique and examined other materials that can be used to enclose the TCS (Phene et al., 1971; Lee and Fredlund, 1984; Fredlund and Wong, 1989; Rahardjo et al., 1989). The sensor is enclosed in a porous medium that is brought into equilibrium with the matric suction in the soil (Johnston, 1942). The thermal conductivity of the porous block is measured, which is a function of water content of the porous block in equilibrium with the soil.

The suction equilibrium is only possible when the porous block is in intimate contact with the soil (Ridley and Wray, 1996). Therefore, the technique measures matric suction. Calibration curve must first be established to relate thermal conductivity of the porous sensor with matric suction of the soil. Since water content-matric suction relationship differs from one soil to another, each soil requires a calibration curve to relate the thermal conductivity of the sensor with matric suction of the soil tested. A study by Feng et al. (2002) on the use of TCS for measuring suction indicates that the TCS exhibits hysteresis.

5.2.2.2 Time Domain Reflectometry (TDR)

Time domain reflectometry (TDR) was first suggested for measuring volumetric water content of soils by Topp et al. (1980). Since then, the method has been used by a number of researchers involving various disciplines (e.g., Dalton et al., 1984; Kalinski and Kelly, 1993; Benson and Bosscher, 1999; Amente, et al., 2000; and Yu and Drnevich, 2004). In the TDR technique, apparent dielectric constant of the soil (i.e., the bulk soil water) is measured, which is related to volumetric water content of the soil (Topp et al., 1980). A fundamental assumption used in the application of TDR technology is that the dielectric properties of the soil water are similar to those of bulk water (White et al., 1994). Pore-water of clay soils is known to exhibit dissolved salts that influences the TDR readings. Moreover, for a quite large range of water content and suction encountered in clay soils, water is held in the pores that are located within the clay clusters (i.e., intra-cluster pores). The pore-water held in the pores between the clay clusters is the bulk pore-water, which gives rise to the capillary phenomenon (i.e., matric suction) in the absence

of a true semi permeable membrane. Therefore, TDR practically measures matric suction instead of total suction.

Similar to TCS, TDR requires soil-water characteristic curve of the soil tested to relate the measured volumetric water content to matric suction. Yu and Drnevich (2004) improved the technique such that gravimetric water content of the soil specimen can also be measured without separately testing the soil for determining its specific gravity and dry density. With this improvement, field measurements of gravimetric water content can be carried out in a faster way. The method has recently been approved and standardised in ASTM D-6780 (ASTM, 2003). The advantage of the technique is mainly that reliable measurements of volumetric water content can be conducted within a short time duration (Benson and Bosscher, 1999). However, the technique requires a very sophisticated electronic device and the accuracy of TDR for measuring matric suction depends on the precise determination of SWCC of the soil tested.

5.2.2.3 In-contact filter paper technique

Filter paper technique was established for measuring soil suction by soil scientists and agronomists (e.g., Gardner, 1937; Fawcett and Collis-George, 1967; Al-Khafaf and Hanks, 1974; Hamblin, 1981; Greacen et al., 1987; and Deka et al., 1995). In geotechnical engineering fields, many researchers have also used the technique as a routine method for suction measurement (e.g., McKeen, 1980; Chandler and Gutierez, 1986; Chandler et al., 1992; Houston et al., 1994; Fredlund et al., 1995; Ridley, 1995; and Leong et al., 2002).

The in-contact filter paper technique is used for measuring matric suction of soils. In the in-contact filter paper technique, water content of an initially dry filter paper increases due to a flow of water in liquid form from the soil to the filter paper until both come into equilibrium. Therefore, a good contact between the filter paper and the soil has to be established. The in-contact filter paper method becomes inaccurate in high matric suction range since water transport is dominated by vapour transport (Fredlund et al., 1995). The water content of filter paper is converted to matric suction using an in-contact filter paper calibration curve. The calibration curve for the filter paper matric suction measurement is commonly established using a pressure plate apparatus (e.g., Al-Khafaf and Hanks, 1974; Hamblin, 1981; Greacen et al., 1987; Deka et al. 1995; and Leong et al., 2002). Leong et al. (2002) found that the filter paper technique exhibits hysteresis. Therefore, the calibration curve for initially dry filter paper is different from that of the initially wet filter paper. It is also important to note that only ash-less filter papers should be used in the filter paper technique. Although there are a number of ash-less filter papers available, only Whatman 42 and Sleicher and Schuell 59 (or SS 59) filter papers are commonly used (Leong et al, 2002).

5.2.3 Indirect Measurement of Osmotic Suction

Osmotic suction can be measured using several indirect methods. The first method for measuring osmotic suction is called saturation extract method. In the technique, distilled water is added to slurry up a soil. The soil water is subsequently drained out to measure its electrical conductivity. The electrical conductivity of the soil water is converted to suction using an osmotic suction-electrical conductivity conversion curve such as that provided by USDA (1950). In the second method, the soil pore-water can also be extracted using a pore-fluid squeezer. The technique is called squeezing technique. The squeezing technique was used by a number of researchers for measuring osmotic suction of soils (e.g., Krahn and Fredlund, 1972; Iyer, 1990; and Leong et al., 2003). Krahn and Fredlund (1972) found that despite its simplicity, the saturation extract method had a poor accuracy for determining in situ osmotic suction whereas the results of squeezing technique were sensitive to the extraction pressure used. The determination of osmotic suction by measuring the electrical conductivity is generally applicable for the entire range of osmotic suction.

5.2.4 Indirect Measurement of Total Suction

Various techniques have been used to indirectly measure total suction of soils. Among the indirect total suction measurement techniques are non-contact filter paper method, psychrometer, relative humidity sensor, and chilled-mirror hygrometer technique. The indirect measurements of total suction require determination of other parameters such as water content (i.e., in the non-contact filter paper technique), dew point (i.e., in the psychrometer), and relative humidity and temperature (i.e., in the relative humidity sensor and the chilled-mirror hygrometer technique).

5.2.4.1 Non-Contact Filter Paper Method

When a filter paper is placed without contact with a soil specimen in a closed container, the vapour space above the soil specimen acts as a true semi-permeable membrane which is only permeable to water vapour but not to ions from the pore-water. Therefore, in this technique, total suction is measured. The calibration curve for the non-contact filter paper technique is established using vapour equilibrium technique (e.g., Gardner, 1937; Fawcett and Collis-George, 1967; Al-Khafaf and Hanks, 1974; Chandler and Gutierez, 1986; Houston et al., 1994; and Leong et al., 2002). While the in-contact filter paper method is inaccurate in the high matric suction range, sensitivity of the non-contact filter paper technique diminishes at low total suction. Houston et al. (1994) found that the calibration curve of the non-contact filter paper is different from that of the in-contact filter paper. This phenomenon is similar to the findings of Leong et al. (2002). Ridley and Wray (1996) found that the non-contact filter paper technique is insensitive when used for measuring low total suctions due to possible vapour and temperature non-

equilibrium during measurement. Generally, similar filter papers as used in the in-contact filter paper technique can be used in the non-contact filter paper technique. Both the in-contact and non-contact filter paper techniques have been standardised in ASTM D 5298-94 (ASTM, 1997).

5.2.4.2 Psychrometer Technique

There are two main types of psychrometers; namely, thermocouple psychrometer and thermistor or transistor psychrometer. The thermocouple psychrometer was first introduced by Spanner (1951). The device makes use of Peltier and Seebeck effects. The Peltier effect is a temperature drop induced by an electrical current passing across a junction made of two different metal wires, which is a function of relative humidity of vapour space where measurement is conducted. When the electrical current is stopped, evaporation of water droplets that have condensed in the junction evaporates causing a further drop in temperature. The drop in temperature of the junction causes an electromotive force which is a function of relative humidity of the vapour space. The thermistor/transistor psychrometer was developed by Richards (1965). In the thermistor/transistor psychrometer, two identical thermistors are used. A drop of water is required to be placed onto the first thermistor (i.e., the wet bulb) whereas the other (i.e., the dry bulb) is let dry. Evaporation takes place as both bulbs are exposed to vapour space in the soil, which results in an electromotive force being generated. Figure 5.2(a) and Figure 5.2(b) show schematic drawing of the thermocouple and thermistor/transistor psyhcrometers, respectively.

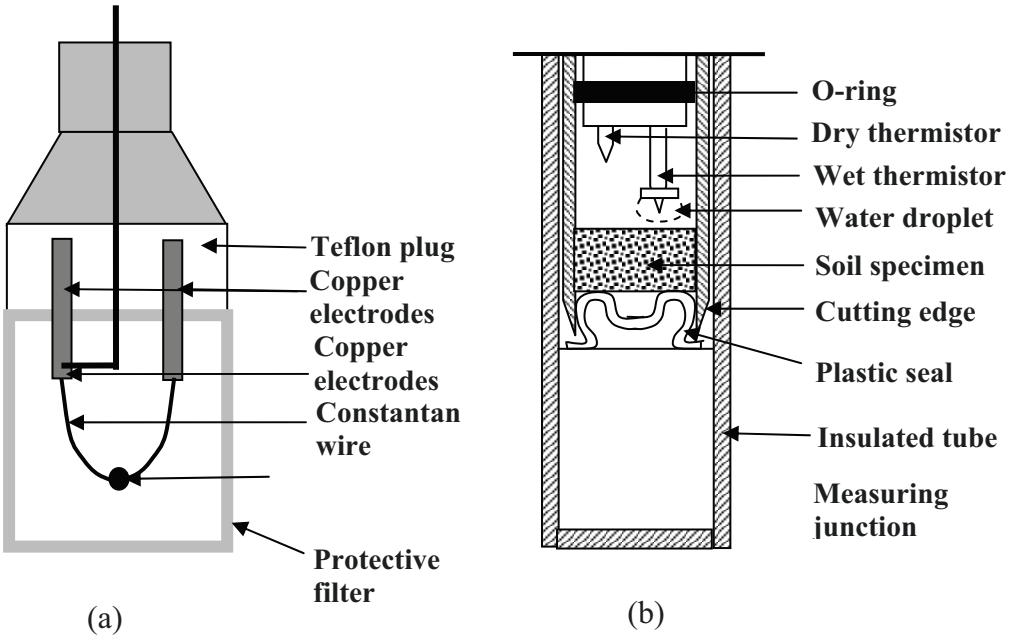

Figure 5.2 Schematic drawing of: (a) thermocouple psychrometer and (b) thermistor/transistor psychrometer

The psychrometer technique has been widely used by many researchers (e.g., Rawlins and Dalton, 1967; Brown, 1970; Krahn and Fredlund, 1972; Campbell et al., 1973; Hamilton et al., 1981; Brown and Bartos, 1982; Lee and Wray, 1995; Zerhouni, 1995; Ridley and Wray, 1996; Harrison and Blight, 2000; Tang et al., 1997 and Tang et al., 2002). There are many positive aspects, but few negative aspects associated with the accuracy of psychrometers for measuring total suction. The psychrometer technique can be used to measure total suction as high as 8500 kPa. The measurement of low total suctions (i.e., lower than 1000 kPa) using this technique requires an accurate means to maintain temperature at a constant value. Ridley and Wray (1996) noted that inaccuracies of the psychrometer technique may be caused by the insensitivity of psychrometer due to temperature effects. On the other hand, variability in the electromotive force generated induces error in high suction range. Furthermore, there may exist a possibility of deterioration in the sensitivity of psychrometer due to corrosion problem (Hamilton, 1981 and Zerhouni, 1995). Unlike the filter paper method, no reports of hysteresis of the psychrometer technique for total suction measurement have been found in literature.

5.2.4.3 Relative Humidity Sensor

The relative humidity (RH) sensor is usually used in meteorological fields for measuring the dew point of air. Many types of RH sensor are available commercially. Examples of the RH sensors are products of Vaisala Oyj (Vaisala, 2002). The relative humidity (RH) and temperature of vapour space of the soil are measured and total suction (s_t) can be computed using Kelvin's law (Fredlund and Rahardjo, 1993).

$$s_t = \frac{-R_g\, T}{M_w(1/\rho_w)} \ln\left(\frac{RH}{100}\right) \tag{5.1}$$

where s_t is total suction in kPa, R_g the universal gas constant (i.e., 8.31432 J/mol K), T the absolute measured temperature in degrees K, M_w the molecular weight of water (i.e., 18.016 kg/kmol), ρ_w the unit weight of water in kg/m^3 as a function of temperature and RH is the measured relative humidity in percent defined as u_v/u_{vo} where u_v is the partial pressure of pore-water vapour in the specimen and u_{vo} is the saturation pressure of water vapour over a flat surface of water at the same temperature.

Polymer capacitance technology is recently used in this type of sensors as the technology provides high reliability to the relative humidity measurement, insignificant hysteresis, and insensitivity to temperature fluctuation where measurement is conducted (Wiederhold, 1997 and Benson and Bosscher, 1999). Albrecht et al. (2003) used a polymer capacitance sensor for measuring relative humidity of a number of soils ranging from sand to clay. The polymer capacitance sensor consists of two electrodes that are separated by a thermoset polymer film. Depending on the RH value being measured, the film adsorbs or release water. The RH value is determined by measuring changing

capacitance of the polymer film. With this technology, a rapid response of the sensor in measuring relative humidity is obtained. The following figure shows the polymer capacitance sensor used by Albrecht et al. (2003).

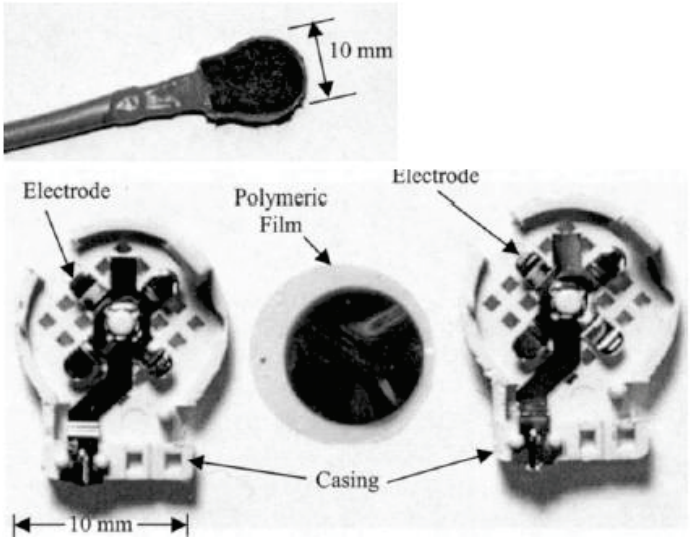

Figure 5.3 A polymer capacitance relative humidity sensor (Albrecht et al, 2003)

5.2.4.4 Chilled-Mirror Hygrometer Technique

Chilled-mirror hygrometer technique was first introduced to measure relative humidity of food products (e.g., Hand, 1994 and Zhang, et al., 1996) and pharmaceuticals (e.g., Ahlneck and Zografi, 1990 and Friedel and Cundell, 1998). It has been used in soil science to quantify water potential of soils (Gee et al., 1992 and Brye, 2003). In geotechnical engineering applications, the technique has been used for measuring total suction of soils (Leong et al., 2003; Albrecht et al., 2003; and Schanz et al., 2004). Albrecht et al. (2003) used the chilled-mirror hygrometer to assess the performance of a polymer capacitance sensor for measuring relative humidity of soils.

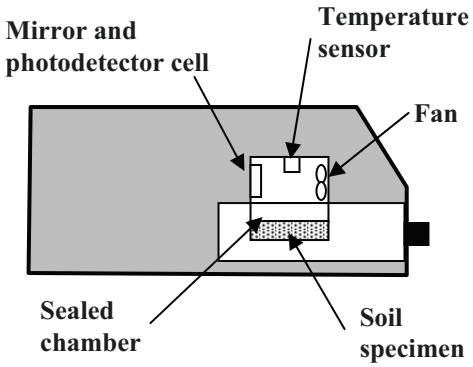

Figure 5.4 Schematic drawing of a chilled-mirror hygrometer technique

The chilled-mirror hygrometer as schematically shown in Figure 5.4 measures dew point and temperature of the headspace above the specimen. The specimen is contained in a special closed chamber. The dew point is measured using a mirror which can detect the first appearance of condensation of water vapour. Temperature of the mirror is precisely controlled by a thermoelectric cooler. A light beam directed onto the mirror is used to detect the first appearance of water vapour condensation. A photo-detector cell is employed to measure the change in reflectance of the mirror caused by the condensed water vapour. The temperature of specimen which is considered to be equal to the temperature of vapour space is measured via an infrared thermocouple. The relative humidity or the water activity of the specimen is computed from the measured dew point and temperature. To speed up equilibration time, an internal fan is used in the device to circulate the water vapour in the vapour space above the specimen. Leong et al. (2003) reported that the technique could be used to quantify total suction as low as about 150 kPa. The value is considered small in the case of low total suction measurement where much larger error can be expected (see Subchapter 5.2.6). By considering the error of total suction measurement and the way of how the isothermal equilibrium between the specimen and the vapour space is maintained, the technique is considered to be the most accurate means for measuring total suction.

5.2.5 Suction Measurement Techniques used in This Study

Four suction measurement techniques; namely, filter paper technique, psychrometer, relative humidity (RH) sensor, and chilled-mirror hygrometer technique were used in this study. The filter paper technique was used because of its simplicity and 'costless-ness'. The psychrometer technique and the RH sensor were used because the two methods have possibilities for field total suction measurement since the sensors are small and easy to handle. The chilled-mirror hygrometer technique was used as it uses the latest technology for measuring total suction. The method is considered to be the most accurate method of total suction measurement (see Chapter 8).

5.2.6 Error and Accuracy in Suction Measurements

Since good contact between filter paper and soil specimen affects the accuracy of matric suction measurement using the in-contact filter paper technique, error in the matric suction measurement is expected to be less in the low matric suction range. As the contact between the filter paper and the soil specimen diminishes in the high matric suction range, the accuracy reduces. Fredlund et al. (1995) found that measurement of matric suction on a compacted till using the in-contact filter paper technique resulted in inaccurate values at matric suctions higher than 90 kPa. Moreover, the determination of high matric suctions (e.g., above 1500 kPa) requires extrapolation of the filter paper calibration curve since no data points could be obtained at high matric suctions due to limitation of the pressure plate apparatus used for calibration. Similarly, the non-contact

filter paper calibration curve needs to be extrapolated for low total suction measurement. These factors result in inaccuracies in the filter paper suction measurements.

Accuracy of techniques used for measuring total suction depends on how an isothermal equilibrium between the specimen, the vapour space, and the sensor used can be maintained. The chilled-mirror hygrometer technique is thought to have the best accuracy since it provides the greatest possibility of maintaining isothermal equilibrium between the specimen and the vapour space. This is due to the fact that the specimen used is small and the vapour space is also minimised.

In a closed system, the amount of water vapour is constant and thus the partial pressure of water vapour (u_v) is also constant. A difference in temperature (or a temperature gradient) between the specimen and the vapour space causes movement of water resulting in a change in the saturated water vapour (u_{vo}) while the change in u_v is zero. The measurement of total suction is performed by measuring the *RH* of the vapour space. A difference in the total suction from the actual total suction of the specimen is consequently measured. A change in the total suction (or the error in suction measurement) due to a temperature gradient can be estimated by taking the first derivative of Equation (5.1) with respect to temperature (Croney et al., 1952).

$$\frac{d(\ln s_t)}{dT} = \frac{1}{T} - \frac{1}{u_{vo}\ln(RH)}\frac{d(u_{vo})}{dT} \tag{5.2}$$

The change in total suction or the error in total suction measurement due to different values of temperature gradient is shown in Figure 5.5. If the error is limited, for instance, to 30% of the measured value, the measurement of total suction will be limited to a value of about 850 kPa assuming that a 0.5 ^{o}C temperature gradient exists between the specimen and the vapour space. The temperature gradient of 0.5 ^{o}C can likely be maintained in a temperature-controlled laboratory, whereas the determination of low total suctions in the field by measuring relative humidity will most likely result in inaccurate values due to the fundamental limitations of the techniques. The accurate measurement of total suction as low as 100 kPa with 30 % error requires a means to control temperature within $\pm$0.04 ^{o}C according to Equation (5.1) and Equation (5.2).

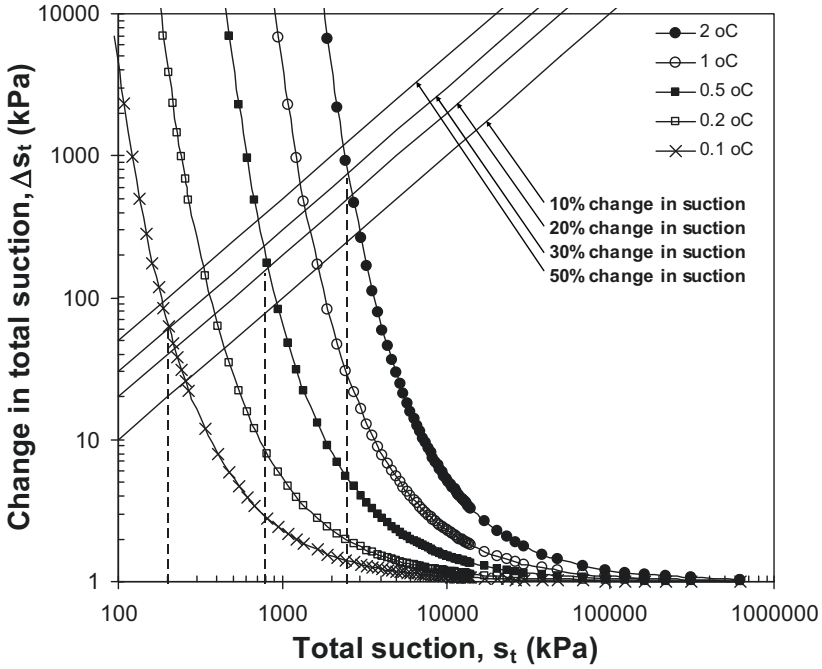

Figure 5.5 Change in total suction or error in total suction measurement due to temperature gradient

5.3 Suction Control Techniques

Various ways have been adopted for controlling matric or total suction in soil specimen during unsaturated soil experiments. Three methods that are commonly used for the suction control are described in this subchapter. The description includes axis-translation and osmotic techniques for the matric suction control and vapour equilibrium technique for the total suction control.

5.3.1 Axis-Translation Technique (ATT) for Matric Suction Control

The axis-translation technique (ATT) was first proposed by Hilf (1956). The main reason for the use of this technique is to avoid cavitation when controlling matric suction greater than 100 kPa. In this technique, the pore-water pressure in the soil is increased to a positive reference gauge pressure (u_w). Matric suction in the soil is applied by increasing the pore-air pressure (u_a). A high-air entry ceramic disk is normally used to provide separation between water and air pressures. Therefore, the maximum matric suction that can be applied using this technique is limited to 1500 kPa (i.e., the maximum air entry value of ceramic disks available in the market). The ceramic disk is not an impermeable membrane to dissolve salts (or ions) in the soil. Therefore, water flow due to osmotic effects is bypassed since in this case, the water flow is an advective process.

The applicability of ATT for matric suction control in various unsaturated soil tests has been proved (e.g., Gan and Fredlund, 1988; Huang and Fredlund, 1998; Agus et al., 2001; and Agus et al., 2003b). The technique was found to be suitable for soils with a continuous air phase (Olson and Langfelder, 1965 and Bocking and Fredlund, 1980). The use of ATT for applying high matric suction to a 'compressible' and 'quasi-impermeable' soil at high degree of saturation (i.e., where air phase in the soil is discontinuous) may isotropically compress the soil. The effects can be avoided by slowly and step-wisely increasing the pore-air pressure such that the response of pore-water pressure to the increased pore-air pressure takes place before the soil particles are compressed. Mongiovi and Tarantino (1998) confirmed the applicability of the ATT for testing unsaturated soils with low degree of saturation. The ATT has been used for controlling matric suction during unsaturated oedometer test (e.g., Romero et al, 2003), triaxial test (e.g., Wong et al., 2001), direct shear test (e.g., Gan and Fredlund, 1988), permeability test (e.g., Huang et al., 1998 and Agus et al., 2003a). The technique was also used in the determination of soil-water characteristic curves (e.g., Agus et al., 2001; Wang and Benson, 2004; Leong et al., 2004; and Schanz et al., 2004).

The key factor of the applicability of this method for controlling matric suction lies on the continuity between water phase in the soil specimen tested and that in the pores of the ceramic disk used. Thus, good contact between the soil specimen and the ceramic disk must be warranted throughout the experiment. Continuity of water supply may determine, to a certain extent, the performance of this technique when used for wetting test on a soil with a high initial suction. The soil specimen with a high initial suction will draw a large amount of water from the water reservoir through the ceramic disk. This may induce an instantaneous cavitation of the ceramic disk. Desaturation of the ceramic disk poses another problem to the applicability of ATT. The ceramic disk must be saturated prior to use. In general, distilled deaired water must be used in the saturation as well as during experiment. The saturation of ceramic disk used can be ensured by subjecting the ceramic disk to a matric suction as high as its air-entry value. When no rapid flow of air is observed, the ceramic disk is saturated.

However, even when the ceramic disk is fully saturated and the distilled deaired water is used throughout the test, air can still diffuse through water in the ceramic disk. The rate of air flow through water is described by Fick's law (Fredlund and Rahardjo, 1993). Quantification of the amount of diffused air is important particularly when measurement of volumetric flow of water into and out of the soil specimen during test is of concern. A correction to account for the diffused air is required in a prolonged unsaturated soil experiment such as in unsaturated permeability test (Huang and Fredlund, 1998). When equilibrium conditions of a soil specimen at a certain matric suction is judged based on the specimen mass, it is not necessary to quantify the amount of diffused air. However, the diffused air collected in the water pressure line as air bubbles lengthens the matric suction equilibration time. Cavitation may also grow as a result of an excessive

accumulation of air bubbles beneath the ceramic disk. This will induce a loss of contact between the soil specimen and the ceramic disk. Periodical flushing of air bubbles beneath the ceramic disk is necessary such that the continuity of pore-water in the soil and water in the water pressure line can be maintained. Additionally, the air pressure line should be connected to an air saturator such that the relative humidity of the air used is high enough to minimise evaporation.

Procedures for measuring the rate of diffusion of air through water (or through a saturated ceramic disk) have been described in Fredlund and Rahardjo (1993). Romero (2001) reported that the air diffusion rate varied fairly with applied matric suction. The coefficient of diffusion of a 5-bar ceramic disk was found to be in the range of 10^{-11} to 10^{-10} m^2/s at 20°C. The rate of diffused air as presented in Fredlund and Rahardjo (1993) infers that the rate of air diffusion during matric suction equalisation is a function of applied water pressure. The higher is the applied water pressure; the lower will be the rate of air diffusion.

Pressure plate is an apparatus for measuring soil-water characteristic curve that uses the axis-translation principle (Fredlund and Rahardjo, 1993). The method was proposed by Richards (1931). In general, there are two main types of pressure plate apparatus; namely, pressure plate apparatus with a flexible base and pressure plate apparatus with a fixed base. Both types of pressure plate apparatus can be used to determine drying as well as wetting paths of soils. However, wetting can be done more easily in the fixed-base pressure plate apparatus compared to the flexible-membrane pressure plate apparatus since flushing can be performed in a much better way (Leong et al., 2004). Moreover, since water pressure in the flexible base pressure plate is always maintained to a value closed to the atmospheric pressure, flushing should be done more frequently as the system has the highest rate of air diffusion through the ceramic disk.

5.3.2 Osmotic Technique for Matric Suction Control

The osmotic technique is used as an alternative to the ATT for controlling matric suction in the soil. The technique was first adopted by soil scientist (Zur, 1966) and later in geotechnical engineering field by Kassiff and Ben Shalom (1971), Delage et al. (1992), and Cuisinier and Masrouri (2004) on oedometer apparatus. Cui and Delage (1996) and Cunningham et al. (2003) used the osmotic technique for controlling matric suction of soils in triaxial tests. In the osmotic technique, water drainage of the soil specimen tested is generated by osmosis process due to a difference in concentration between the pore-water and the solution used. Polyethylene glycol (PEG) solution is normally used in the osmotic technique. The PEG solution is circulated through the top and bottom boundaries of the soil specimen using a pump. The technique requires a semi-permeable membrane which separates the pore-water and the PEG solution. The value of matric suction applied depends on the concentration of PEG solution used. The relationship between the PEG

solution concentration and the osmotic pressure is used to calculate the applied matric suction. Cui and Delage (1996) proved the continuity between osmotic and axis-translation techniques when used for matric suction control. The applicability of osmotic technique for controlling matric suction as high as 12600 kPa has been proved by Delage et al. (1998).

The difficulty associated with the osmotic technique is that it requires a sophisticated means for circulating the PEG solution along boundaries of the specimen tested. The concentration of PEG solution used should also be monitored during experiment. Delage et al. (1998) reported that the use of osmotic technique for controlling high matric suction (or high PEG concentration) required a special care as the PEG solution with a high concentration has a high viscosity. The equilibration time for suction equalisation using this method is quite long and can be longer than 10 days (Cuisinier and Masrouri, 2004).

5.3.3 Vapour Equilibrium Technique (VET) for Total Suction Control

The limitation of both axis-translation and osmotic techniques for applying high suction to the soil leads to the use of vapour equilibrium technique (VET). The technique has been used by a number of researchers for applying total suction to soil specimens in unsaturated soil tests (e.g., Croney et al., 1952; Agus et al., 2001; Blatz et al., 2002; Cuisioner and Masrouri, 2002; Lloret et al, 2003; and Cuisinier and Masrouri, 2004). The VET has been used for controlling total suction during unsaturated oedometer test (e.g., Cuisioner and Masrouri, 2002; Lloret et al., 2003; and Cuisinier and Masrouri, 2004), triaxial test (e.g., Blatz and Graham, 2003), and for the determination of soil-water characteristic curve of expansive soils (Croney et al., 1952; Agus et al., 2001; Blatz et al., 2002; and Schanz et al., 2004). The thermodynamic relationship between total suction and relative humidity (*RH*) or Kelvin's law (Equation (5.1)) is the basic formula used in the VET. The equilibrium requirement states that the potential of water in its liquid (i.e., pore-water) and vapour (i.e., water vapour in the pore space) forms must be the same. Therefore, water exchange between the soil pore-water and the vapour space includes the effect of capillary action, solute (osmotic suction), and sorptive forces. This is because the vapour space is essentially a true semi-permeable membrane which is only permeable to water (in vapour form) but not to ions in the soil water.

Salt (non-volatile) or acidic (volatile) solutions can be used to control *RH* of the vapour space (or total suction) in the soil. The *RH* values generated above aqueous salt solutions at different temperatures can be obtained from Greenspan (1977), Horvath (1985), Lide and Frederikse (1994), and ASTM E-104 (ASTM, 1997). Lang (1967) provides a relationship between total suction and molality of sodium chloride (NaCl) solution at different temperatures. The *RH* values over the surface of acidic solutions (i.e., sulphuric acid or H_2SO_4 solutions) for different temperatures are available in Lide and

Frederikse (1994). Due to safety concern, the salt solutions are preferred over the acidic solutions. The total suction corresponding to a particular *RH* value can be calculated using Kelvin's law (Equation (5.1)).

Generally, the VET can be used to control almost the whole range of total suction. However, the use of VET for applying total suction less than 2000 kPa suffers from inaccuracies since the technique is extremely sensitive to temperature gradient that exists between the salt solution, the vapour space, and the soil specimen (Agus and Schanz, 2003a). Equation (5.1) and Equation (5.2) can be used to estimate the minimum value of total suction that can be controlled using the vapour equilibrium technique by assuming that the soil specimen, the vapour space, and the solution used are at an isothermal equilibrium.

5.3.4 Suction Control Technique Used in This Study

Suction of the soil specimens tested in this study was controlled using the ATT and VET. The osmotic technique for controlling matric suction was not used due to the abovementioned drawbacks of the technique and the unavailability of required equipments.

5.4 Measurement of Swelling Pressure

Several methods for measuring swelling pressure of expansive soils have been adopted by a number of researchers (e.g., Kassiff and Ben Shalom, 1971; Bucher und Spiegel, 1984; Sridharan et al., 1986; Sitz, 1997; Gattermann, 1998; Herbert and Moog, 2002a; and Lloret et al., 2003). The methods are broadly classified into three main categories; namely constant volume, swell-under-load, and swell-load methods (Sridharan, et al., 1986). Different methods measure different values of swelling pressure (Figure 5.6).

5.4.1 Constant Volume Method

In the constant volume method, swelling pressure of an expansive soil can be determined by saturating the specimen with distilled water or with other solutions in one step. The test is referred to as one-step constant volume swelling pressure (CVSP) test. Various techniques have been adopted for saturating soil specimens in the CVSP tests. Among these, there are at least three methods that have recently been cited in literatures; namely, high water (or liquid) pressure, water flooding, and water circulation methods. Development of 'rigid' constant volume swelling pressure cells has enabled the determination of swelling pressure using the constant volume method to become easier. The soil specimen can also be wetted in the CVSP test by decreasing its suction in steps. Swelling pressure development with decreasing suction can be measured using this method. The method is referred to as multi-step constant volume swelling pressure test.

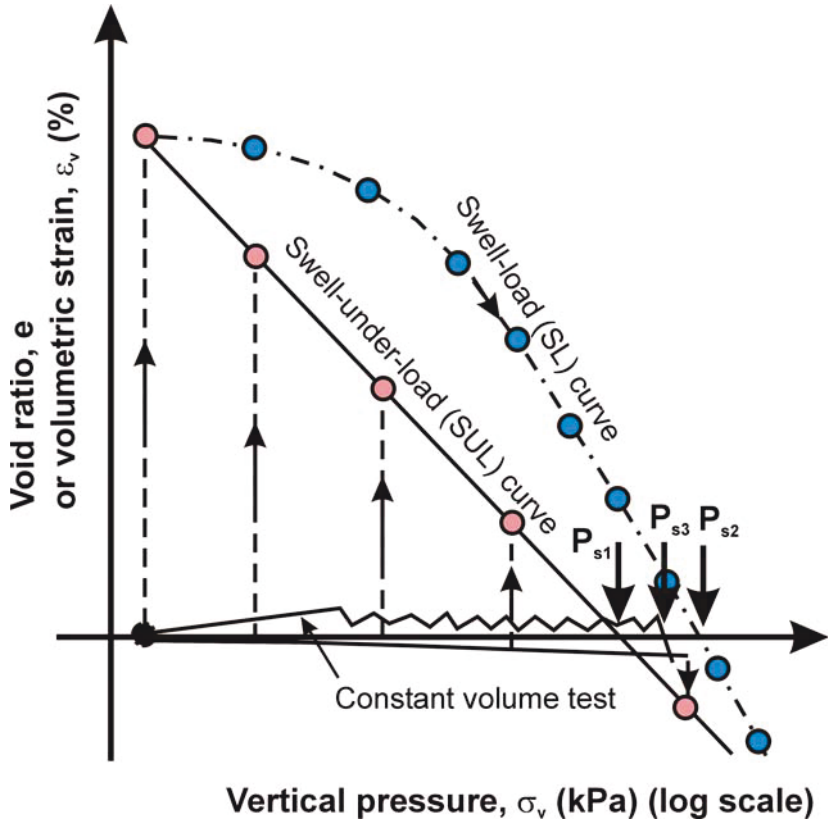

Figure 5.6 Swelling pressures measured using different methods

Correction to account for specimen's disturbance can be applied to the CVSP test results. To establish the specimen's disturbance correction, the specimen needs to be further loaded and unloaded in the similar way to the procedures for obtaining the compression and rebound curves of the specimen (Fredlund and Rahardjo, 1993 and Shuai and Fredlund, 1998).

5.4.1.1 One-Step Constant Volume Swelling Pressure (CVSP) Test by Applying High Liquid Pressure

In this technique, high water (or liquid) pressure is used to saturate the specimen. The method has been used by Bucher und Spiegel (1984), Sitz (1997), and Herbert and Moog (2002a). The test requires a liquid pump, which is able to deliver high liquid pressures to the specimen. Sitz (1997) used a CVSP test system for measuring swelling pressures of bentonites and bentonite-sand mixture (Figure 5.7). The system was similar to that used by Bucher and Spiegel (1984) but it was designed with higher cell stiffness to be able to sustain higher liquid pressures and was made of a more corrosive resistant material. The system enabled the swelling pressure of soils to be determined with respect to different types of liquid. After the placement of specimen in the cell, a liquid pressure as high as 500 kPa was applied from the bottom of the specimen. The specimen was let to reach equilibrium of total pressure (swelling and fluid pressures) as measured by the load

cell. The liquid pressure was subsequently increased by 500 kPa and similar procedures were repeated. The final applied liquid pressure was 3000 kPa. A relationship between the measured total pressure and the applied liquid pressure was obtained. Swelling pressure was defined as the total pressure at zero liquid pressure. The value was extrapolated from the total versus liquid pressures relationship.

A displacement transducer was used to measure possible volume change of the specimen during swelling pressure test. It was anticipated that the use of high liquid pressures (in some cases higher than the measured swelling pressures) might change the volume of specimen. A correction factor was applied to calculate the reduced dry density of the specimen by taking into account the specimen deformation at the end of the test. The system was able to measure swelling pressure of compacted bentonite and bentonite-sand mixtures (i.e., at a maximum dry density of 2 Mg/m^3) as high as about 8000 kPa. The main drawback of the swelling pressure measurement technique by Sitz (1997) is its long test duration. One complete test on one specimen required months to almost one-year. Therefore, the reproducible of the results could not be proved since not many specimens could be tested.

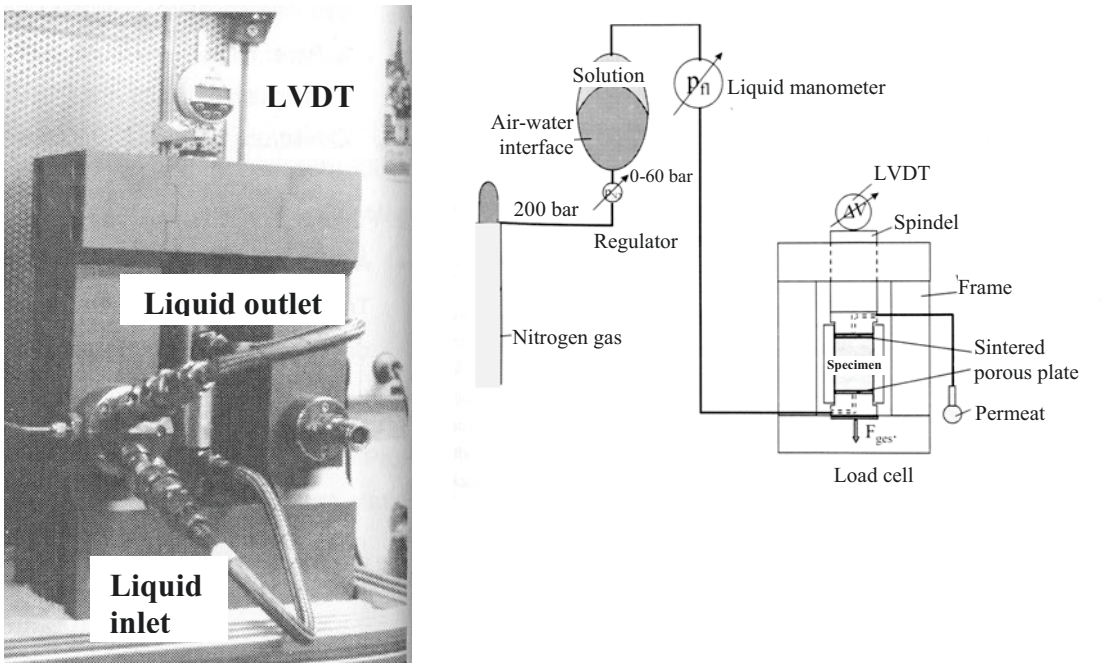

Figure 5.7 Constant volume swelling pressure cell and the system used by Sitz (1997)

Herbert and Moog (2002a) developed a new apparatus for measuring swelling pressure of expansive soils (Figure 5.8). The system also used high liquid pressures to supply water (or other liquids) to the specimen. The specimen was compacted directly in the swelling pressure cell. Water or other liquid was infiltrated into the specimen at a slow rate using a high pressure liquid chromatography (HPLC) pump. The liquid pressure increased as the expansive soil tested swelled internally (i.e., the self-sealing effect)

during experiment. The internal swelling causes a reduction in pore volume of the specimen. The infiltration was terminated at a maximum liquid pressure of 100 000 kPa (i.e., the liquid pressure expected to occur in the field). The high liquid pressure could be reached in about four days. The liquid pressure was subsequently reduced to zero and the pressure measured by the load cell at the end of the test was deemed to be the swelling pressure of the specimen. The system was able to measure swelling pressure of compacted bentonite and bentonite-sand mixtures (i.e., at a maximum dry density of 2 Mg/m^3) as high as 3500 kPa with different types of solution.

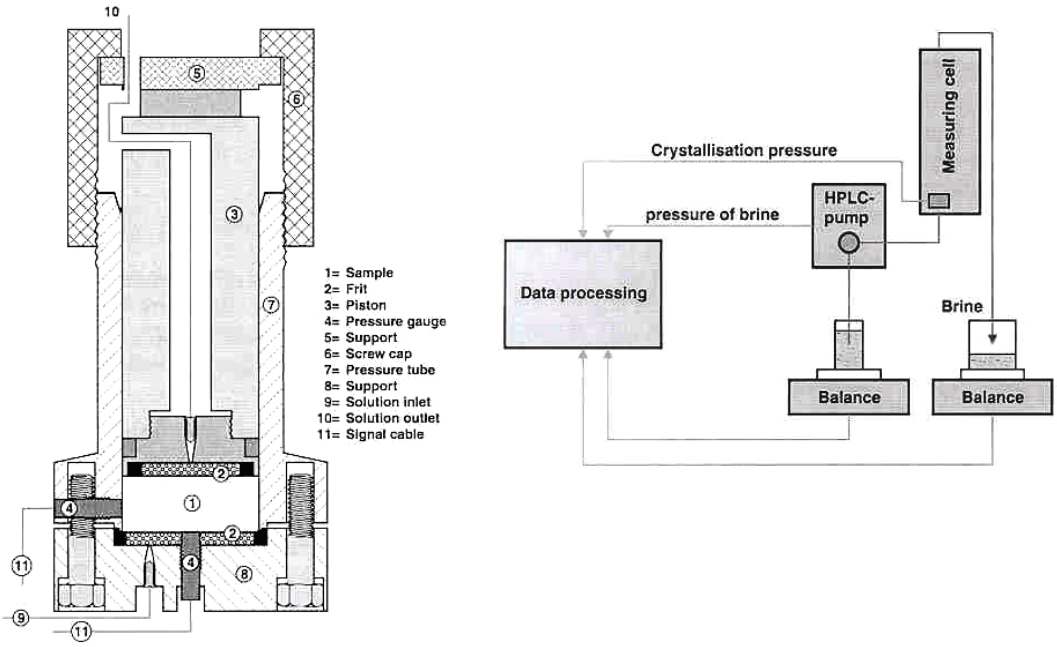

Figure 5.8 Schematic diagram of constant volume swelling pressure cell and the system used by Herbert and Moog (2002a)

The amount of water (or other liquids) entering the specimen during swelling pressure measurement can be quantified in a better way using the system developed by Herbert and Moog (2002a) compared to that used by Sitz (1997). This is because the system measured the amount of liquid in both the influent and effluent ends of the specimen. The liquid uptake could be computed by subtracting the liquid input with the liquid output. Therefore, the specimen conditions during and at the end of the measurement could be identified more precisely.

5.4.1.2 One-Step Constant Volume Swelling Pressure (CVSP) Test using Water Flooding Method

Water flooding method is commonly used in the swelling pressure test on an oedometer apparatus. In this method, the saturation of soil specimen tested can be reached more possibly compared to the swelling pressure test using high liquid pressures. The

specimen is allowed to swell in distilled water (or other solutions) and the swelling is controlled (to a zero value) by addition of loads (Sridharan et al., 1986). The load is added further to reach a certain value where no further swelling is observed. The load at the end of test corresponds to the swelling pressure of the specimen tested.

Gattermann (1998) recently used the water flooding method to measure swelling pressure of highly compacted specimens of two bentonites. The apparatus used is shown in Figure 5.9. Two different types of specimens were tested in the investigation. The first type of specimen was monolith cylindrical specimens. The second type of specimen was cylindrical specimens with columns with different sizes that were cut in the specimen to allow deformation to occur. Specimens with a maximum dry density of 1.9 Mg/m^3 were tested.

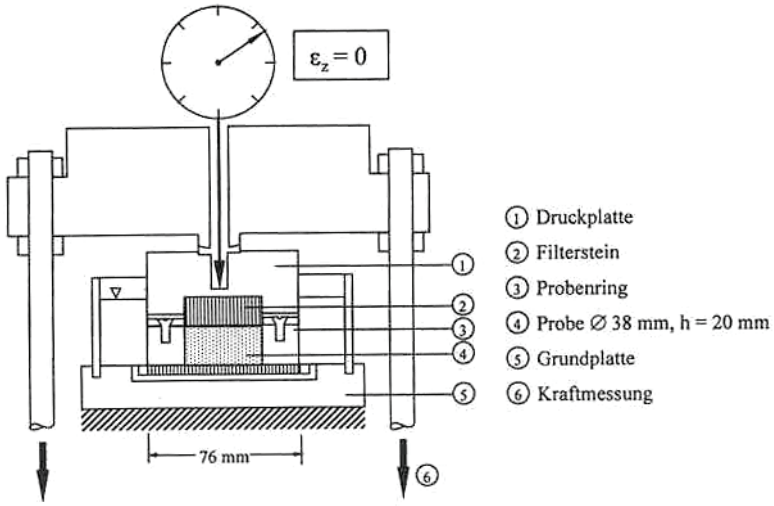

Figure 5.9 Schematic diagram of swelling pressure apparatus using water flooding method by Gattermann (1998)

As an alternative, the swelling of the soil specimen during wetting can also be restrained and a load cell can be used to measure swelling pressure. The equipment required for this technique may be in a similar form to that used by Bucher and Spiegel (1984), Sitz (1997), and Herbert and Moog (2002a).

5.4.1.3 One-Step Constant Volume Swelling Pressure (CVSP) Test using Water Circulation Method

In this method, water is circulated through the top and bottom boundaries of the soil specimen tested. Water is absorbed by the soil specimen as a result of water potential (or suction) gradient between the distilled water supplied and the soil specimen tested. The method is advantageous when used for testing a soil specimen with a high initial suction but also with a high initial degree of saturation. Moreover, the swelling pressure test using

this method can be performed along with the multi-step swelling pressure test where the development of swelling pressure with decreasing suction is investigated (see the next subchapter).

5.4.1.4 Multi-Step Constant Volume Swelling Pressure (CVSP) Test

The multi-step CVSP test is performed in attempt to study the development of swelling pressure with decreasing suction. The test can be combined with the use of axis-translation technique (ATT) (Romero et al., 2003) and vapour equilibrium technique (VET) (Lloret et al., 2003) to decrease suction of the soil specimen tested. Romero et al. (2003) measured swelling pressure of Boom clay by decreasing suction of the specimen using the ATT. The test was performed in a modified oedometer cell where swelling pressures in both the vertical and radial directions could be measured (Figure 5.10). The equipment used by Lloret et al. (2003) for measuring swelling pressure using the VET is shown in Figure 5.11. The system was a modification of a standard oedometer apparatus with a fixed lever arm which was equipped with a load cell to measure swelling pressure. In the tests by Lloret et al. (2003), water vapour generated above salt solution was circulated through the top and bottom boundaries of the specimen using an air pump. The circulation of water vapour speeded up the equilibration time.

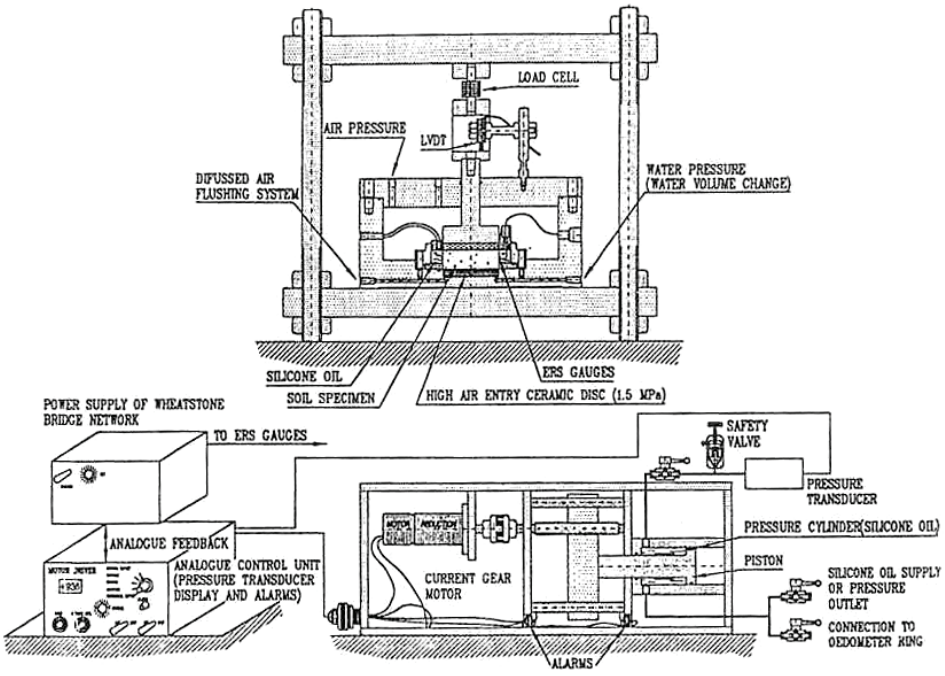

Figure 5.10 Schematic drawing of swelling pressure test setup using multi-step method and axis-translation technique (Romero et al., 2003)

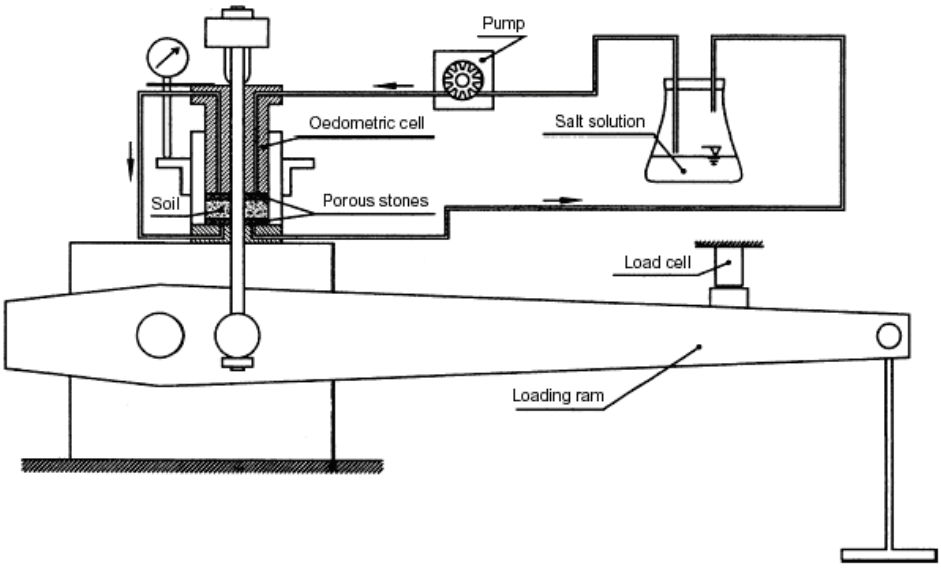

Figure 5.11 Schematic drawing of swelling pressure test setup using multi-step method and vapour equilibrium technique (Lloret et al., 2003)

5.4.2 Swell-Under-Load (SUL) Method

The swell-under-load (SUL) method is also referred to as a method of equilibrium void ratios for different consolidation pressures (Sridharan et al., 1986). Several 'identical' specimens are loaded at different vertical loads in oedometer cells. After the equilibrium of each soil specimen under the corresponding vertical load has been reached, water is added to the cells to flood the soil specimens. The specimens are allowed to swell or collapse under the corresponding vertical loads. New equilibrium void ratios of the specimens will be reached. The equilibrium void ratio versus applied vertical stress of different soil specimens tested will form a curve (normally a straight line) on a semi-logarithmic plot. The line intersects the horizontal line drawn through the average initial void ratio (or the zero volume change) at a certain point (i.e., point P_{s1} in Figure 5.6). The vertical pressure corresponding to this point is called swelling pressure determined from the swell-under-load method.

5.4.3 Swell-Load (SL) Method

The swell-load (SL) method for determining swelling pressure is normally performed along with the conventional oedometer test. A soil specimen is allowed to swell usually under a seating load of approximately 7 kPa. After the swelling has reached its equilibrium value, the soil specimen is subsequently loaded and unloaded to determine its compression and rebound curves (Figure 5.6). The compression curve intersects the horizontal line drawn through the initial void ratio (or the zero volume change) at point P_{s2} in Figure 5.6 which signifies the swelling pressure measured by the swell-load method.

5.4.4 Swelling Pressure Test Methods Used in This Study

In this study, the three methods of swelling pressure measurement were performed. The one-step water circulation method was adopted to saturate specimens for measuring swelling pressure under constant volume conditions. The multi-step method was also used to study the development of swelling pressure with decreasing suction. The method was combined with the ATT and VET for applying suction to the soil specimens.

5.5 Controlled-Suction Oedometer Test

Oodometer tests can be performed not only on saturated but also on unsaturated soil specimens. The oedometer tests on specimens under unsaturated conditions are normally carried out to investigate the effect of suction on compression and rebound characteristics of the soil. Controlled-suction oedometer tests have been performed by a number of researchers (e.g., Kassiff and Ben Shalom; 1971; Romero et al., 2003; Cuisioner and Masrouri, 2002; Romero et al., 2003; Lloret et al., 2003; and Cuisinier and Masrouri, 2004). Romero et al. (2003) tested several expansive soil specimens at different suction values using the axis-translation technique (ATT) (Figure 5.12). The test was conducted to investigate suction effects on the compression and rebound behaviour of compacted Boom clay specimens under non-isothermal conditions. It was reported that an excessive evaporation occurred when testing a specimen at 80 ^{o}C inducing difficulties in achieving matric suction equilibrium conditions of the specimen. The excessive evaporation is also thought to introduce severe problems when dry air is used in the ATT as has been addressed before (see Subchapter 5.3.1). Since in the controlled-suction oedometer tests using the ATT, equilibrium is normally deemed based on the volumetric measurement of water inflow and outflow, the decrease in water content (or degree of saturation) of the specimen during equalisation will be underestimated since water also moves in its vapour form through evaporation.

Kassiff and Ben Shalom (1971) and Cuisinier and Masrouri (2004) used the osmotic technique for controlling matric suction of the specimen during oedometer test. As mentioned in Subchapter 5.3.2, the problem associated with this technique is mainly the circulation of PEG solution used through boundaries of the specimen and the control of PEG concentration which alters during experiment. Lloret et al. (2003) and Cuisinier and Masrouri (2004) used the vapour equilibrium technique (VET) for total suction control during oedometer test. The problem with VET for total suction control has been described in Subchapter 5.3.3 where the use of this technique should be limited to 2000 kPa total suction (Agus and Schanz, 2003a). Cuisinier and Masrouri (2004) recommended that the use of VET be limited to a lower total suction of 10000 kPa due to inconsistency of the technique for applying total suction lower than that value.

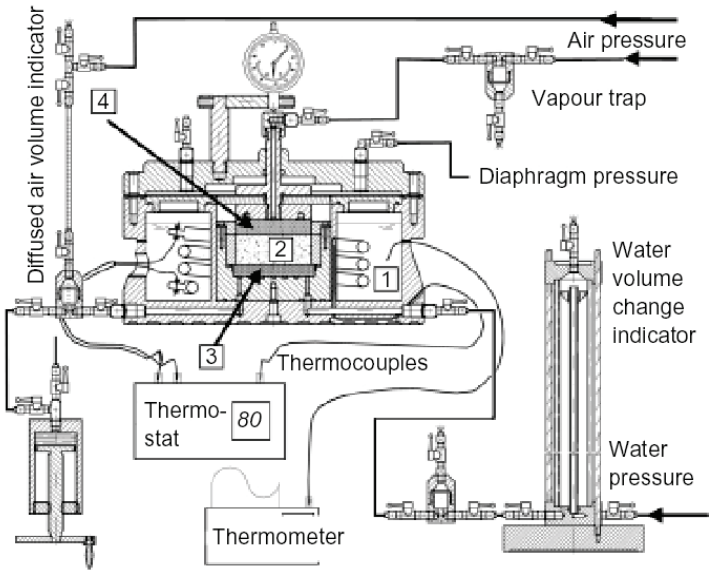

Figure 5.12 Controlled-suction oedometer test system using axis-translation technique (Romero et al., 2003)

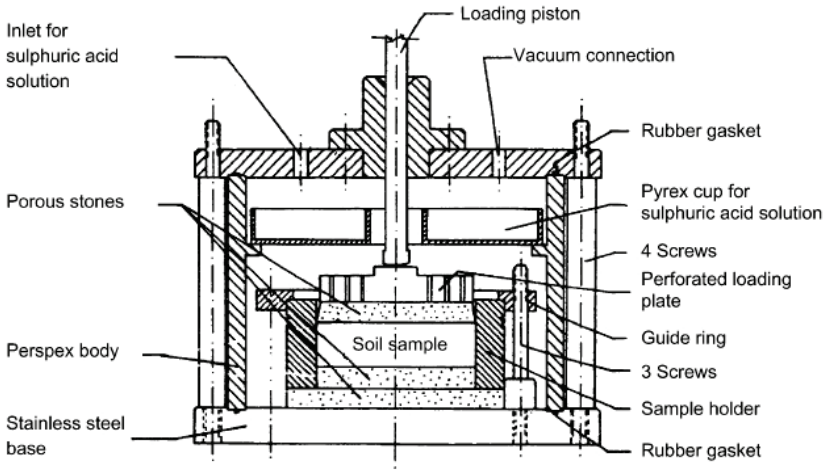

Figure 5.13 Oedometer cell with vapour equilibrium technique (Lloret et al., 2003)

In this study, oedometer tests were performed using both the ATT and VET for applying matric and total suction, respectively. The tests have been named as compression-rebound (CR) tests throughout the dissertation (see Chapter 7).

CHAPTER 6

MATERIALS USED AND EXPERIMENTAL PROGRAM

6.1 General

This chapter discusses basic characterisation of the materials that were used and experiments that were performed in the investigation. Several basic properties of the materials used were obtained through experiments and several others are collected from literatures. The experiments performed in this study were planned based on several possible hydro-mechanical mechanisms that are likely to occur in the field (i.e., in the nuclear waste disposal facilities). Several other experiments were performed for investigating the behaviour of the material, although the real mechanisms may not occur in the field. Aspects related to changes in chemical composition of the material and possible temperature effects are not considered in this study.

6.2 Properties of Materials Used

The materials investigated in this study were mixtures of a calcium bentonite, named Calcigel, mined from Southern part of Germany, and quartz sand. Preliminary experiments consisting of basic soil tests and physico-chemical characterisation were performed on both the bentonite and the sand.

6.2.1 Basic Properties

The basic soil tests were performed based on ASTM standards (ASTM, 1997) and DIN standards (DIN, 1987). The tests included the determination of Atterberg limits, specific gravity, and grain-size distribution. The determination of grain-size distribution of the bentonite used was performed using two methods; namely the sedimentation method (ASTM, 1997 and DIN, 1987) and laser particle sizing (LPS) method. The laser particle sizer used in this investigation was a laser particle sizer type LS 230 from Coulter Electronics Inc. (Figure 6.1). The grain-size distribution curves determined for the bentonite (i.e., via the sedimentation method and LPS methods) and for the sand are shown in Figure 6.2. The different curves obtained for the bentonite via different methods indicate dependency of the grain-size distribution of the bentonite on the preparation technique. The oven-dried powder specimen prepared for the grain-size distribution test using the LPS technique is expected to exhibit the least degree of dissociation of clay particles. The specimen used in the sedimentation test was dispersed in a dispersing

solution (i.e., sodium hexametaphosphate) during experiment. Therefore, it exhibited the most dissociated structure.

Figure 6.1 Laser particle sizer type LS 230 from Coulter Electronics Inc.

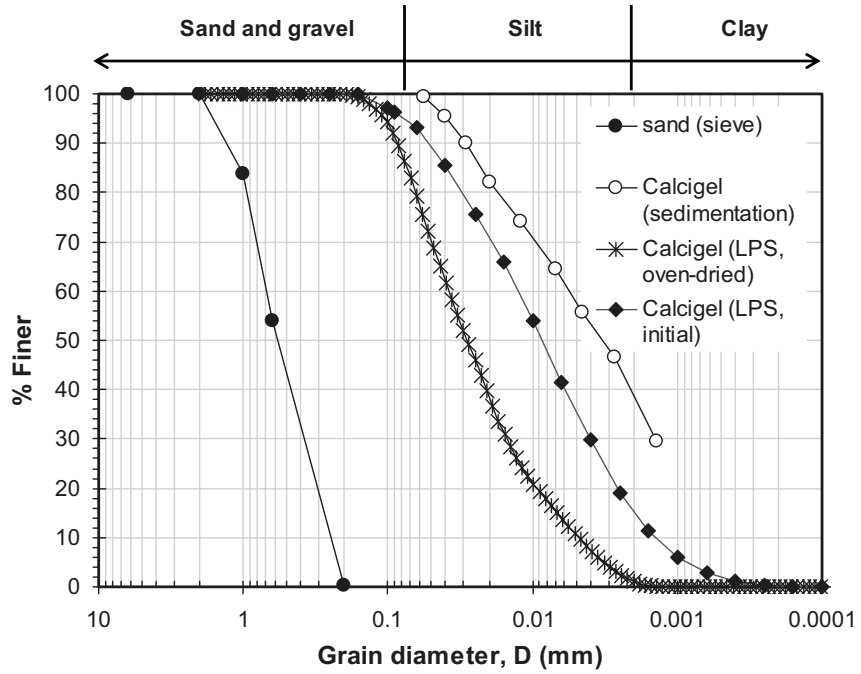

Figure 6.2 Grain-size distribution curves of the bentonite and sand used

6.2.2 Physico-Chemical Characterisation

It is known that the behaviour of clays (i.e., including bentonite-based material) is controlled by physico-chemical properties of the clay minerals. Therefore, physico-chemical characterisation of the bentonite used is important. In this study, the physico-chemical characterisation of bentonite used was performed and included the determination of specific surface area, chemical, and mineralogical compositions.

Complimentarily, similar characterisation was also carried out on the sand. The cation exchange capacity (CEC) of bentonite used was taken from literature.

6.2.2.1 Specific Surface Area

In inert soils such as sands, water is held between or onto surfaces of the soil grains and therefore only external specific surface area is relevant since the external and total specific surface areas of sands are equal. The moisture held in clay soils with expanding minerals are located between the clay clusters (i.e, the inter-cluster or inter-aggregate soil water) as well as within the clay clusters (i.e, the intra-cluster or intra-aggregate clay clusters). In other words, water is bonded to both the external and internal surfaces of the clay clusters. In this case, total specific surface are is more pertinent for describing the capability of this type of soils in retaining water. The external specific surface area of the bentonite and the sand used were measured using the Brunette-Emmett-Teller N_2 Adsorption (BET) method (Brunauer et al., 1938; Chiou et al., 1993; and ASTM, 1997) using BET equipment type SA 3100 S from Coulter Electronics Inc. as shown in Figure 6.3. The external specific surface area of the bentonite used is 69 m^2/g while the external specific surface area of the sand is 0.25 m^2/g. The total specific surface area was determined only for the bentonite using the Ethylene Glycol Monoethyl Ether (EGME) method (Cerato and Lutenegger, 2002) using a setup as shown in Figure 6.4. The total specific surface area of the bentonite used as measured using the EGME method is 651 m^2/g.

Figure 6.3 Equipment for measuring external specific surface area using BET method type SA 3100 S from Coulter Electronics Inc.

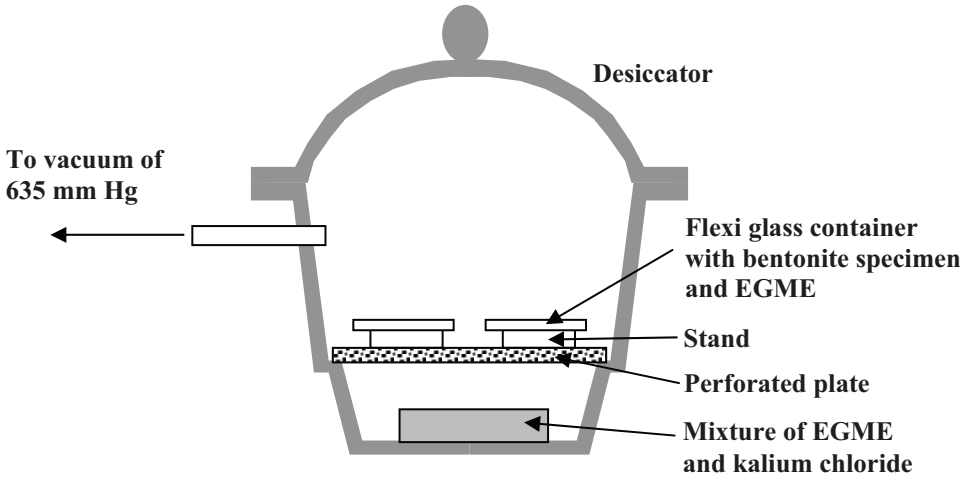

Figure 6.4 Experimental setup for measurement of total specific surface area using EGME method

6.2.2.2 Cation Exchange Capacity (CEC)

The cation exchange capaicity (CEC) of bentonite used was not measured in this study. The CEC value has been reported elsewhere. Herbert and Moog (2002a) measured the CEC of the bentonite used in this study via Ammonium Acetate method and the value is equal to 49 meq/100 g. The main exchangeable cations of bentonite used were reported to be Ca^{2+} and Mg^{2+} (Schmidt et al., 1992). Brenner (1988) reported a higher cation exchange capacity (CEC) of the bentonite compared to the value measured by Herbert and Moog (2002a). The Na^{+} exchangeable cation was 1.8 meq/100 g whereas the Ca^{2+} and Mg^{+} exchangeable cations were 37.6 meq/100 g and 22.4 meq/100 g, respectively. The CEC of the K^{+} was 0.2 meq/100 g. The total CEC of the bentonite was 62 meq/100 g. As a divalent cation-type bentonite it is expected that a fully dispersed single unit layers in the clusters will never be encountered even at very high water contents as a result of the development of a tactoid structures (Iwata et al., 1995). The number of arrangements of unit layers in a clay particle for this type of bentonite ranges from 6 to 16 (Yong, 1999) or even higher (Marcial et al., 2002). It was anticipated that the material would exhibit limited swelling under free swell conditions or a limited swelling pressure development under constrained conditions in distilled water.

6.2.2.3 Mineralogy and Chemical Composition

Müller-Vonmoos and Kahr (1982) investigated the mineralogy of Montigel (i.e., the earlier name of Calcigel) using X-ray diffraction technique and found that the bentonite consisted of 66% montmorillonite, 8.3% quartz, 3.8 % carbonate, 12-15% muscovite, 2-4% feldspat, 2% kaolinite and some other minerals. Quartz sand used mainly consisted of more than 95% quartz.

In this study, mineralogy of the bentonite and sand used were investigated using X-ray diffraction method (Grim, 1968 and Mitchell, 1993). The equipment used was a Roentgen diffractometer type D5000 from Siemens (Figure 6.5). Chemical composition of the bentonite and sand used was determined via emission spectroscopy method (Mitchell, 1993) using an emission spectroscope type ICP-OES Optima 3000 from Perkin-Elmer. The mineralogical composition and the chemical composition of the bentonite and sand used are summarised in Table 6.1 and Table 6.2, respectively.

Figure 6.5 Roentgen diffractometer type D5000 from Siemens

Table 6.1 Mineralogical composition of the bentonite and sand used

Mineral	Content (%)	
	Bentonite	Sand
Calcite	1-5	-
Dolomite	10-15	-
Feldspar	5-8	-
Montmorillonite	50-60	-
Quartz	5-10	94.4
Others	2-29	5.6

Table 6.2 Chemical composition of the bentonite and sand used

Chemical	Content (%)	
	Bentonite	Sand
S_iO_2	53.2	96.7
Al_2O_3	18.4	1.8
Fe_2O_3	5.4	0.1
CaO	3.6	0.0
MgO	3.8	0.0
MnO	0.05	0.0
TiO_2	0.32	0.02
K_2O	1.7	0.87
Na_2O	0.74	0.19
SO_3	0.1	0.0
CO_2	2.78	0.02
P_2O_5	0.13	0.02
Loss of ignition	8.6	0.2

6.2.3 Summary of Basic, Physico-Chemical Characteristics, and Mineralogy of the Bentonite and Sand Used in This Study

Table 6.3 summarises characteristics of the bentonite and sand used in this study. From the table (types of exchangeable cations and montmorillonite content), it is seen that the bentonite used is considered to be a bentonite with a moderate swelling capability as indicated by its 'low' LL value compared with other bentonites such as Kunigel (LL = 474) (Komine and Ogata, 1994) and MX80 (LL = 520) (Marcial et al., 2002) whereas the sand is a poorly graded (uniform) sand.

The mixture 50/50 bentonite-sand (dry mass basis) has an LL of 70, whereas the PL value is 23. Comparing the LL of this mixture with that of the pure bentonite, as given in Table 6.3, suggests the applicability of a linear variation of LL with coarse content (grains coarser than 425 μm) (Srinivasa Murthy et al., 1987). According to the 'clay mixture' theory proposed by Srinivasa Murthy et al. (1987), the LL of 50/50 bentonite-sand mixture used should be 65. The shrinkage limit (SL) of 50/50 bentonite-sand mixture was measured and the value is equal to 9.8%.

Table 6.3 Summary of the material characteristics

Properties	Bentonite	Sand
Specific gravity	2.65	2.65
Liquid limit (%)	130	n.a.
Plastic limit (%)	33	n.a.
Plasticity index (%)	97	n.a.
Clay content (%)	40 *	0
Fine content (%)	100 *	0
D_{10} (mm)	-	0.25
D_{30} (mm)	-	0.40
D_{60} (mm)	-	0.70
USCS classification	CH	SP
External specific surface area (m^2/gm)	69	0.25
Total specific surface area (m^2/gm)	651	0.25
Cation exchange capacity (meq/100 gm)	49 §	n.a.
Main excheangable cations	Ca^{2+}, Mg^{2+}	n.a.
Montmorillonite content (%)	50-60	n.a.

* Obtained from sedimentation test results.
§ Data from Herbert and Moog (2002a), measured using ammonium acetate method.

6.3 Specimen Preparation and Experiments Performed

In the following subchapter, the preparation of specimens and the primary experiments carried out in this study are described. The experiments mainly consisted of suction measurements, wetting and drying tests under unconfined conditions, measurements of swelling pressure and determination of wetting curve under constant volume conditions, one-dimensional compression-rebound tests at saturated and unsaturated states, one-dimensional wetting-drying test under constant load, and measurement of saturated coefficient of permeability. Two types of specimen; namely lightly (or proctor-density) compacted and heavily compacted specimens were used in the tests. The lightly compacted specimens were of four different bentonite contents; namely, 30% bentonite content (i.e., 30/70 bentonite-sand specimens), 50% bentonite content (i.e., 50/50 bentonite-sand specimens), 70% bentonite content (i.e., 70/30 bentonite-sand specimens), and pure bentonite. The suction measurements were performed on the lightly and heavily compacted specimens. Wetting and drying tests under unconfined conditions were carried out only on the heavily compacted specimens. Swelling pressures of both the lightly and heavily compacted specimens were measured whereas the compression and rebound test was only performed on the highly compacted specimens. The one-dimensional wetting-drying test under constant load was performed on the heavily compacted specimens. The following table summarises the main experiments performed in this investigation. The initial conditions of specimens used in each experiment are described in the respective subsections (see Chapter 7). Apart from the main experimental

works tabulated in Table 6.4, additional experiments for investigating uniformity and pore-size distribution of the heavily compacted specimens, microstructure and fabric of the bentonite used were also carried out and are described in this chapter.

Table 6.4 Summary of the main experimental works

	Experiment	Lightly (proctor-density) specimens				Heavily compacted specimens	
		30/70	50/50	70/30	100 *	50/50	100 *
1.	Suction measurement	√	√	√	√	√	-
2.	Unconfined wetting and drying test	-	-	-	-	√	-
3.	Constant volume wetting test	-	-	-	-	√	-
4.	Swelling pressure measurement	√	√	√	√	√	√
5.	1-D compression and rebound test	-	-	-	-	√	-
6.	1-D cyclic wetting-drying test under constant load	-	-	-	-	√	-
7.	Saturated permeability test	√	-	-	-	-	-

* pure bentonite specimens
√ means the experiment was performed; - means the experiment was not performed

Four mixtures were prepared with different bentonite contents (on a dry mass basis); namely 30/70, 50/50, 70/30 bentonite-sand mixtures, with bentonite contents of 30%, 50% and 70%, respectively, and pure bentonite. Quartz sand was first sieved through a 2-mm sieve prior to mixing. The two materials were mixed at initial water content and an adequate amount of water was subsequently added to reach the target water content using a water spray bottle. The mixtures were subsequently cured in a two-layered plastic bag for two weeks to allow for a homogeneous water content distribution.

Proctor compaction curves of the four mixtures of bentonite and sand were first determined. The mixtures were dynamically compacted to obtain two different compaction curves; namely, standard proctor ASTM (ASTM, 1997) with a compaction energy of 600 kN-m/m^3 and enhanced proctor with a compaction energy of 1000 kN-m/m^3. The standard and enhanced compaction curves for the four mixtures are shown in Figure 6.6(a) to Figure 6.6(d). The optimum water contents and the maximum dry densities for the mixtures are listed in Table 6.5. The degrees of saturation corresponding to the optimum water contents or the maximum dry densities are different for different

mixtures. Generally, the higher the bentonite content, the closer optimum conditions are to the zero air void (ZAV) line.

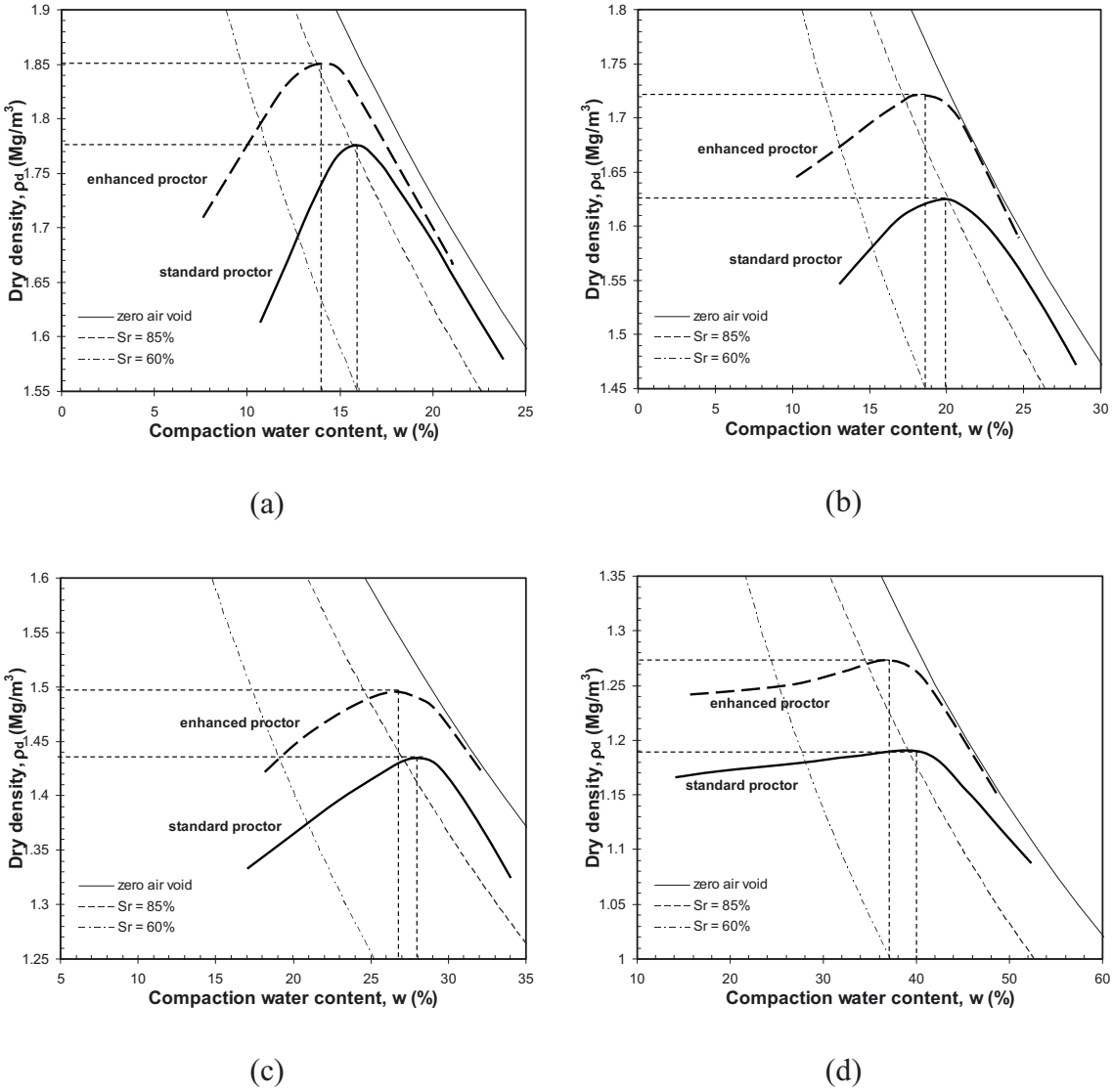

Figure 6.6 Proctor curves of bentonite-sand mixtures (a) 30/70, (b) 50/50, (c) 70/30 and (d) pure bentonite

A number of specimens were prepared for suction and swelling pressure measurements. Several specimens were dynamically compacted in an ASTM standard mold (i.e., 101.6 mm in diameter and 116.4 mm in height) and several others were compacted statically in a small mold measuring 50 mm in diameter and 35 mm in height. Water contents and dry densities of the statically compacted specimens were targeted based on the pre-determined compaction curves. The resulting statically compacted specimens to be used for the suction measurements were 50 mm in diameter and 15 mm in height. The specimens for swelling pressure measurements were 50 mm in diameter and 20 mm in height.

Table 6.5 Optimum water contents and maximum dry densities of the four mixtures

Mixtures	Proctor	Optimum water content, w_{opt} (%)	Maximum dry density, $\rho_{d\ max}$ (Mg/m^3)
30/70 bentonite-sand	Standard	16	1.775
	Enhanced	14	1.850
50/50 bentonite-sand	Standard	20	1.625
	Enhanced	18.6	1.720
70/30 bentonite-sand	Standard	28	1.435
	Enhanced	26.8	1.495
Pure bentonite	Standard	40	1.189
	Enhanced	37	1.275

A number of heavily compacted specimens were also prepared. Conditions (i.e., the water content and density) of the specimens prepared were set to replicate the conditions of brick specimens used in the Sondershausen project (see Chapter 2). The mixture of 50/50 bentonite-sand was compacted in a special compaction cell (i.e., the GRS swelling pressure cell) developed at *Gesellschaft für Anlagen und Reaktorsicherheit* (GRS)*mbH, Braunschweig*. The mixture was initially compacted at 11% average water content to reach an average dry density of 2 Mg/m^3. After delivered to the Laboratory of Soil Mechanics, Bauhaus-University Weimar, the specimens were subsequently allowed to equilibrate with water vapour above an aqueous (or saturated) solution of KCl in a desiccator at 22 ^oC (i.e., corresponding to a total suction of 22700 kPa) for several months. The specimens after equilibration are further named as as-prepared specimens. The as-prepared specimens were expected to exhibit a uniform water content (or suction) distribution or reached the true equilibrium state (see Chapter 3 for the definition). At the end of equilibration stage, specimens with a diameter of 50 mm and a height of 20 mm were produced. The as-prepared specimens had an average water content of 9.07 % and an average dry density of 2.04 Mg/m^3. The statistical distribution of the as-prepared water content and dry density is shown in Figure 6.7 It was found that the heavily compacted specimens had an average initial suction of 22260 kPa (see Chapter 8 for details).

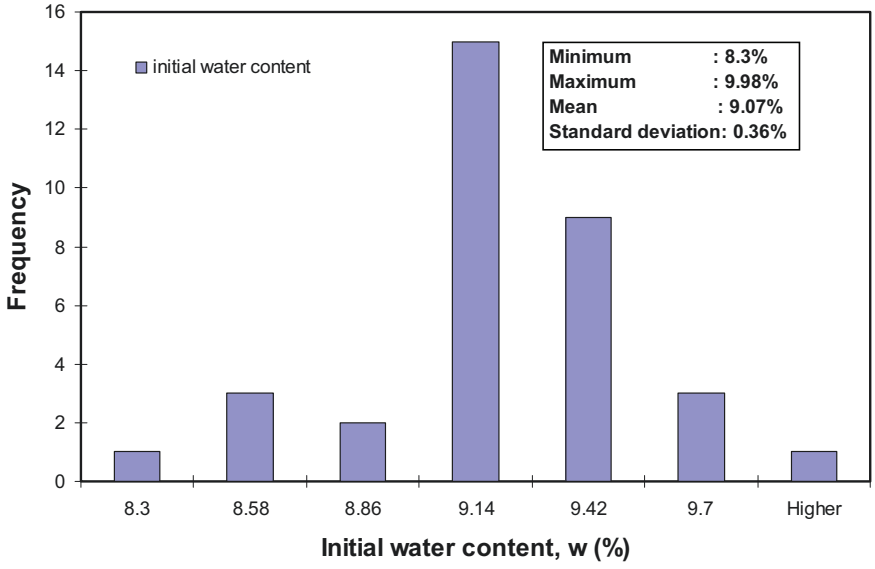

(a)

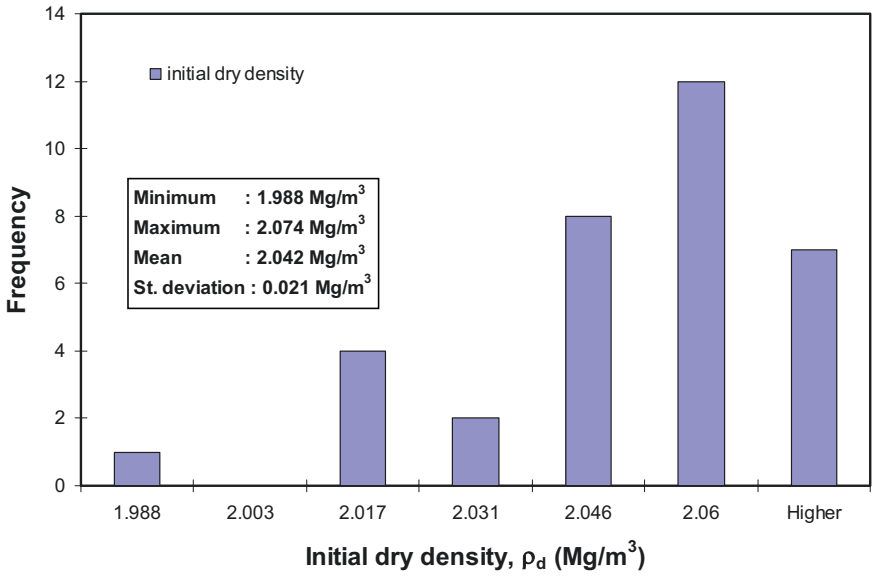

(b)

Figure 6.7 Statistical distribution of the as-prepared specimens: (a) initial water content and (b) initial dry density

6.4 Computer Tomography (CT) Study for Investigating Homogeneity of the As-Prepared Specimen

6.4.1 General

The computer tomography (CT) technique, developed in medical sciences, is a non-destructive technique enabling virtual slicing of opaque objects. The usefulness of CT is that the sample can be laid in the equipment without disturbance. Another usefulness of

the technique in geological research has been demonstrated by many authors (e.g., Wellington and Vinegar, 1987; Orsi et al., 1994; and Duliu, 1999). In this research, computer tomography was used to investigate homogeneity of the heavily compacted specimens with respect to the density.

6.4.2 Experimental Techniques

The computer tomography test was performed on a heavily compacted brick specimen (i.e., similar to those used in the Sondershausen field test) and on a cylindrical form specimen (i.e., the specimen from GRS), both at as-prepared state. The test was carried out using a mobile computer tomography type MCT3 from University of Marburg (Figure 6.8). The cylindrical specimen was placed in a closed constant volume cell for preventing the specimen from changing water during measurement. This was particularly anticipated since the small cylindrical specimen will be affected by room conditions (i.e., relative humidity and temperature) during test. The brick specimen was tested directly without any effort to prevent any change in water content, which was thought to be negligible taking into consideration its much larger size compared to the cylindrical specimen.

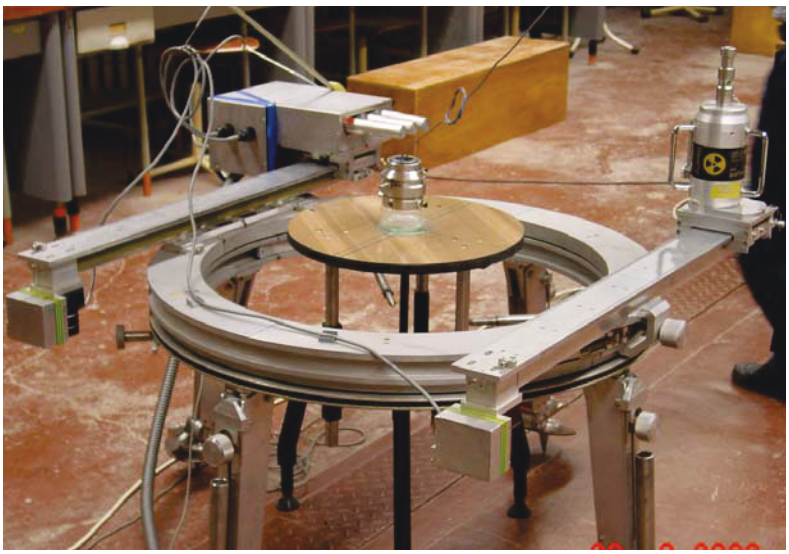

Figure 6.8 Computer tomography test setup

6.4.3 Results and Discussion

Figure 6.9 shows the results of CT test performed on the brick and cylindrical specimens. It is shown that the brick specimen is not uniform with respect to density while a relatively more uniform density distribution is seen in the cylindrical specimen. This fact supports the use of the pre-fabricated cylindrical specimens for the tests in this study. The results also show that the global density of the cylindrical specimen is 2.2 Mg/m^3, which agrees well with the measured value. The distribution of water content in

the both specimens cannot be inferred from the CT test results. However, since the specimens were already at true equilibrium state, water was distributed uniformly and therefore the results of CT test presented indicate the uniformity in the dry density distribution in both the brick and cylindrical specimens.

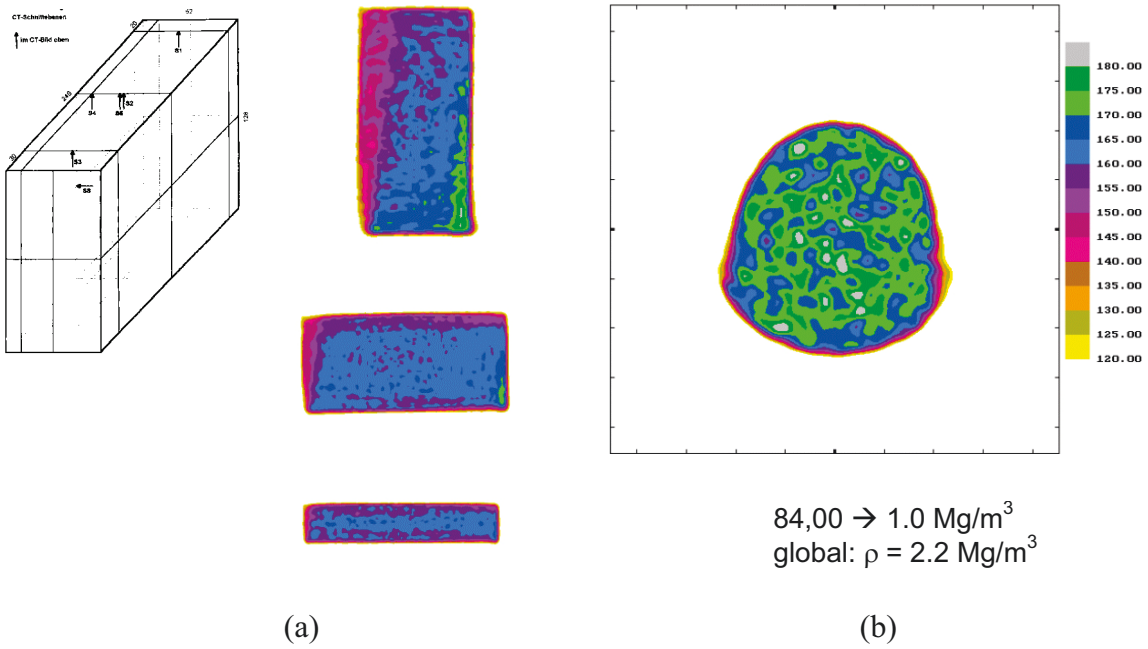

(a) (b)

Figure 6.9 CT test results: (a) brick specimen and (b) cylindrical specimen

6.5 Microstructure and Fabric Investigation by Mercury Intrusion Porosimetry (MIP) Test

6.5.1 General

The pore-size distribution (PSD) of a soil obtained by mercury intrusion porosimetry (MIP) test is an essential fabric element which is related to some soil characteristics such as water, air and heat conductivity, adsorption and desorption isotherms, and volumetric deformation. Some researchers have used the MIP data to study fabric changes of natural clays during consolidation (Griffiths and Joshi, 1995), changes in PSDs due to consolidation of different clay types (Al-Mukhtar, 1995), and prediction of saturated coefficient of permeability (e.g., Garcia et al., 1979 and Romero, 1999). The PSD data was also used to estimate soil-water characteristic curve of expansive soils (e.g., Romero, 1999). Effects of compaction conditions (i.e., dry of optimum and wet of optimum) on the PSD have been reported and discussed in Delage and Graham (1996). In this research, the MIP data was used to obtain information concerning the distribution of pores (i.e., micro-pores and macro-pores) in the heavily compacted specimen at different states. The MIP data are also used for estimating water content versus suction curve and saturated permeability that are known to be a function of pore-size distribution of the soil.

6.5.2 Experimental Techniques

The MIP study was performed using Autopore II 9220 from Micromeritics, Berlin (Figure 2.8). Three heavily compacted specimens at three different states; namely, as-prepared, oven-dried, and swollen states were tested. A small cube specimen was each cut from the as-prepared and oven-dried specimens. The swollen specimen was prepared by first allowing an as-prepared specimen to absorb water under unconfined conditions through vapour diffusion process until the specimen water content reached 19%. This water content corresponds to about 490 kPa suction (see Chapter 7 for details). The initial conditions of the three specimens tested are reported in Table 6.6. All cube specimens were freeze-dried prior to MIP test.

Figure 6.10 Equipment for mercury intrusion test
(Autopore II 9220 from Micromeritics Berlin)

Table 6.6 Initial conditions of the specimens tested in MIP

	Total suction (kPa)		Water content (%)*		Void ratio	
	Initial	Before test	Initial	Before test	Initial	Before test
As-prepared	22700	22700	9.0	9.0	0.299	0.299
Oven-dried	22700	1 000 000*	9.2	0.0	0.330	0.319
Swollen	22700	490§	8.3	19.0	0.281	0.600

* measured using ASTM (1997) oven-dried method (i.e., at 105°C for at least 18 hours)
† suction of oven-dried soil (Croney and Coleman, 1961)
§ inferred from the unconfined wetting curve of the material (see Chapter 9 for details)

6.5.3 Results and Discussion

The results obtained from the MIP test are analysed and some information regarding pore levels can be derived. Several assumptions used in the analyses are also

given herein. The PSD data obtained from the MIP test results are used to estimate hydraulic properties of the specimen tested.

6.5.3.1 Pore-Size Distribution (PSD) of the Heavily Compacted Specimens of 50/50 Bentonite-Sand Mixture

The MIP test results have been interpreted using Washburn method (Washburn, 1921; Sridharan et al., 1971; and Al-Mukhtar, 1995). In the method, the pores in a soil are assumed to be cylindrical. The relationship between the intrusion pressure (p_{int}) and the pore-diameter (D_p) is given in the following equation.

$$p_{\text{int}} = -\frac{4\,T_{HG}\cos\varphi_{HG}}{D_p} \tag{6.1}$$

where T_{HG} is the surface tension of mercury (i.e., 0.484 N/m at 25^{o}C) and φ_{HG} is the contact angle between mercury and the assumed pore surface (i.e., 141.3^{o}).

Figure 6.11 shows the pore-size distribution (PSD) data of the three specimens tested in this study. It is shown that no remarkable changes in PSD of the specimen are noted upon oven-drying. The lower total pore volume of the as-prepared specimen as compared to that of the oven-dried specimen is attributed to the lower initial void ratio of the as-prepared specimen (see Table 6.6). Swelling induces an increase in the pore volume but it narrows the range of PSD of the specimen. It is shown that the PSD of the three specimens is bimodal. The bimodal PSD curves indicate the existence of two level of pores; namely, micro-pores and macro-pores (Delage and Graham, 1996). Romero et al. (2003) observed a trimodal PSD curve of compacted specimens of a 20/80 mixture of sodium bentonite (i.e., Kunigel V1) and silica sand. The bimodal characteristics of the PSD of the three specimens tested in this investigation can be better visualised in the plot of intruded pore volume versus mean pore diameter as shown in Figure 6.12. The apparent transition between micro- and macro-pores is also shown in the figure. The micro-pores represents pores in the clay clusters (or the intra-aggregate pores) while the pores between clay clusters (or the inter-aggregate pores) are considered to be the macro-pores. The non-intruded pores may therefore represent the intra-laminar pores. The existence of bimodal behaviour of the PSD of the specimens tested is consistent with the observation on Jossigny silt reported by Delage et al. (1996) and on a heavily compacted bentonite-sand mixture (i.e., 70/30 Kunigel-Hostun sand mixture) described in Cui et al. (2002a). The manner by which the volumes of three types of pores are determined from the PSD data is given in Figure 6.13.

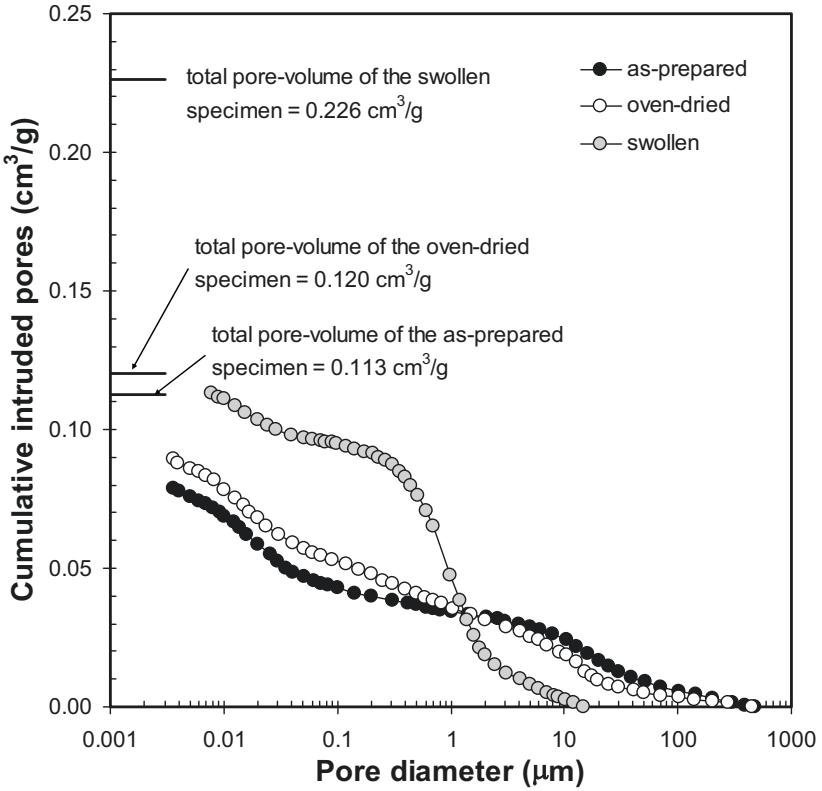

Figure 6.11 Pore-size distribution of the heavily compacted 50/50 bentonite-sand mixture at three different states

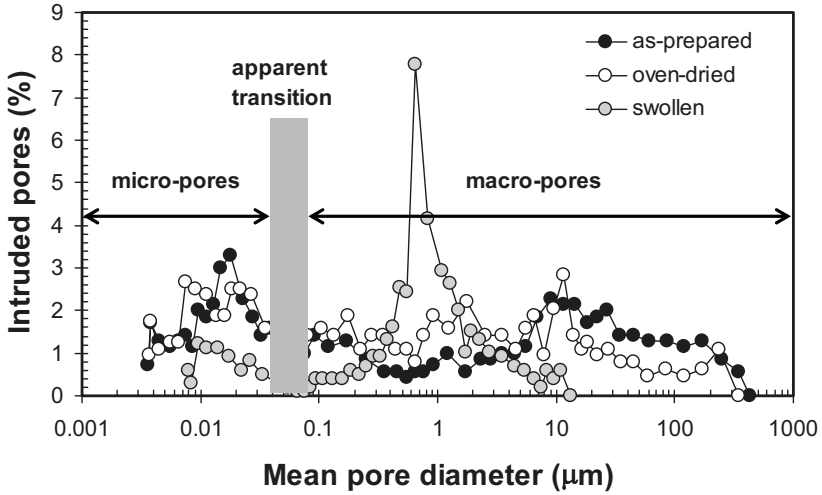

Figure 6.12 Intruded pore volume versus mean pore diameter of the heavily compacted 50/50 bentonite-sand mixture at three different states

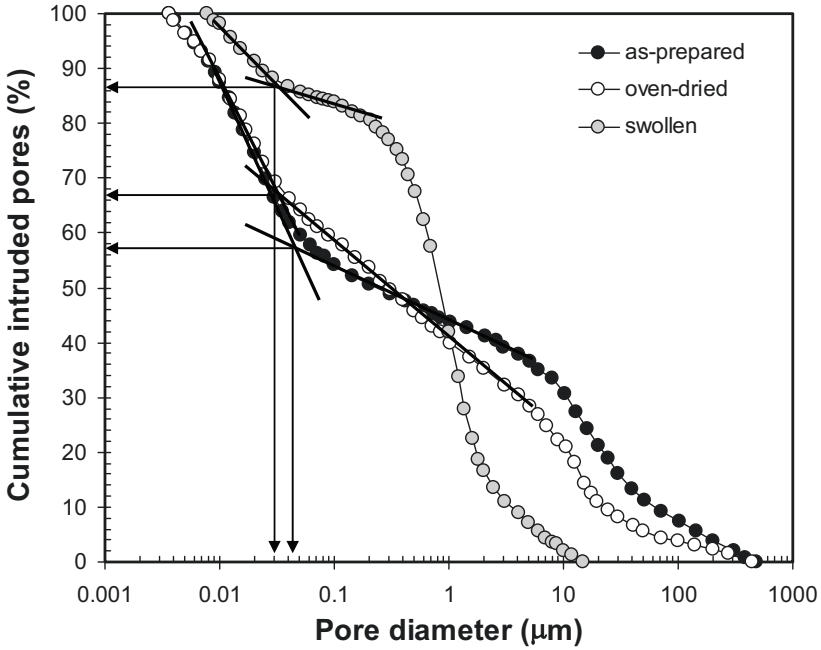

Figure 6.13 Determination of micro- and macropores from the pore-size distribution data

The information of PSD of each specimen that can be derived from the MIP test results are summarised in Table 6.7. The percentage of total intruded pore volume to the theoretical total pore volume reduced as the specimen swelled whereas shrinking had no influence on the percentage of total intruded pore volume. The PSD data may infer that the average diameter of micro-pores decreased due to swelling. The average diameter of micro-pores listed in Table 6.7 does not take into account the micro-pores with diameter smaller than the smallest intruded pore diameter since no information on the PSD below this limit is available. The percentage of volume of the micro-pores to the total pore volume is however similar for the three specimens. Despite the difficulty in assessing the average diameter of the micro-pores, Table 6.7 reveals that there was a significant reduction in the average diameter of macro-pores due to swelling.

The increase in volume of the micro- and macro-pores as the specimen swelled was approximately as much as the increase in total volume of the specimen (i.e., about 100% volumetric strain). By considering that the density of soil water in an expansive soil is equal to unity (Mitchell, 1993), the volumetric strain of the specimen caused by swelling can be assessed and was approximated to be equal to the swelling-induced volumetric strain of water phase in the specimen (Table 6.6). The difference in water content of both specimens (i.e., the as-prepared and swollen specimens) was 10% which corresponds to a 0.1 cm^3/g difference in pore volume. The value is approximately equal to the difference in total volume of both specimens (Table 6.7). According to Table 6.7, the change in volume of the micro-pores due to swelling was only about 0.06 cm^3/g. Since the micro-pores (i.e., the pores located within the clay clusters) are considered to be saturated, this value

corresponds to a 6% increase in water content. This discrepancy may indicate that the absorbed water due to swelling was retained in both the micro- and macro-pores. No conclusion on a possible rearrangement of clay clusters in the specimens can be drawn from the PSD data. An internal rearrangement of clay clusters may occur when the specimen is wetted under constant volume conditions (Delage and Graham, 1996). Cui et al. (2002a) showed that during confined swelling, the size of macro-pores of a swelling soil reduced and diminished at suction close to zero. Cui et al. (2002a) also observed separation of clay sheets in the clusters which led to a more uniform PSD of the specimen.

Table 6.7 Mercury intrusion porosimetry data of the three specimens tested

	As-prepared	Oven-dried	Swollen
Total pore volume, $V_{p\,tot}$ (cm^3/g)	0.113	0.120	0.226
Total intr. pore volume, $V_{p\,int}$ (cm^3/g)	0.079	0.089	0.113
percent of total pore volume (%)	70	74	50
Average diameter, D_{ave} (mm)[*)]	18.8	10.6	1.26
Micro-pores: diameter, $D_{p\,micro}$ (μm)	< 0.05	< 0.02	< 0.02
average diameter, $D_{ave\,micro}$ (μm)[**)]	0.004	0.004	0.01
volume, $V_{p\,micro}$ (cm^3/g)	0.067	0.066	0.129
percent of total pore volume (%)	59	55	57
Macro-pores: diameter, $D_{p\,macro}$ (μm)	0.05 - 500	0.02 - 500	0.02 - 2
average diameter, $D_{ave\,macro}$ (μm)[§)]	19.8	11.2	1.4
volume, $V_{p\,macro}$ (cm^3/g)	0.046	0.054	0.097
percent of total pore volume (%)	41	45	43

[*)] based on weighted average without considering the non-intruded pore volume
[**)] based on weighted average with the smallest intruded pores considered to be the smallest pores
[§)] based on weighted average

The effect of hydraulic cycles (i.e., drying and wetting) on the PSD curve of the bentonite investigated herein is different from that caused by compaction as reported by Sridharan et al. (1971) or consolidation as described in Al-Mukhtar (1995). It was reported that both compaction and consolidation only affected the volume of macro-pores. The study by Al-Mukhtar (1995) also indicated that drying only influenced the macro-pores whereas the micro-pores remained unaffected. This is true since mercury mainly intruded the pores between the clay clusters. The volume of micro-pores in 'non-swelling' clays is insignificant compared to the total pore volume of the soil (Delage and Graham, 1996). In the case of swelling soils such as the bentonite-sand mixture used in this study, the interaction between micro- and macro-pores is more remarkable since the micro-pores constitute more than half the total pore volume.

6.5.3.2 Estimate of Water Content versus Capillary Suction from the MIP Test Results

The process of mercury intrusion during MIP test is similar to intrusion of air to an initially water-saturated soil specimen. In the mercury- and air-filled pore system, mercury acts as the non-wetting phase while air is the wetting phase. On the other hand, water is considered to be the wetting phase whereas air is the non-wetting phase in the water- and air-filled pore system. The following equation is obtained by utilising Equation (6.1) for the water- and air-filled pore system.

$$s_m = \left(u_a - u_w\right) = -\frac{T_w \cos \varphi_w}{T_{HG} \cos \varphi_{HG}} p_{\text{int}} \tag{6.2}$$

where s_m is matric suction, T_w is the surface tension of water (i.e., 0.072 N/m at 25 ^{o}C), and φ_w is the contact angle between water and the assumed pore surface (i.e., assumed to be equal to 180 ^{o}).

Apart from the assumption used in deriving the pore-size distribution curve, it must be noted that matric suction computed using Equation (6.2) does not include the effect of sorptive forces and it is merely the capillary phenomenon. The water content versus matric suction curves for the three specimens tested is shown in Figure 6.14.

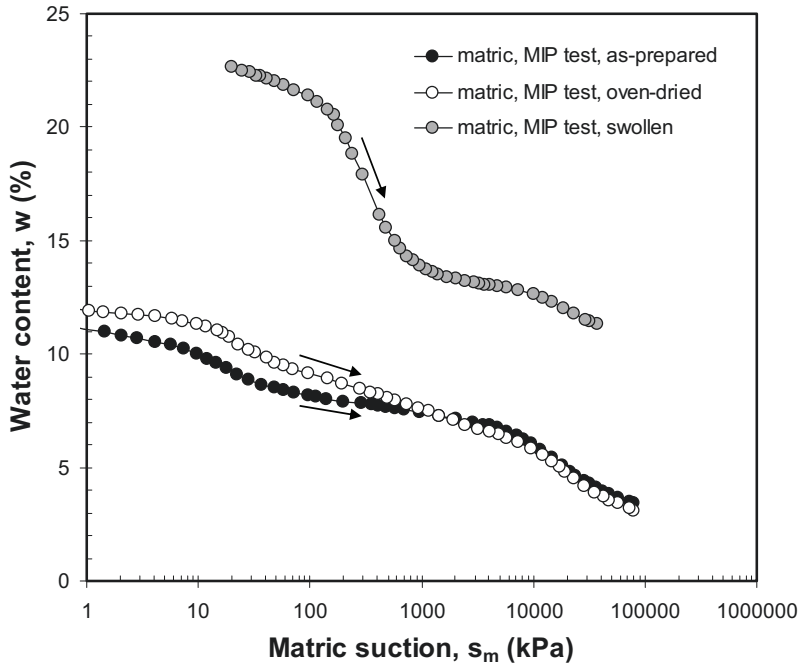

Figure 6.14 Water content versus matric suction curves determined from MIP test results

As expected, the water content versus matric suction curve of the as-prepared specimen is almost similar to that of the oven-dried specimen since their PSDs are almost

similar. Comparison of the water content versus matric suction curve with that directly measured is given in Chapter 8. It will later be shown that the water content versus suction curve shown in Figure 6.14 can be used as a preliminary estimate in the absence of measured data.

6.5.3.3 Estimate of Permeability from the MIP Test Results

In the earlier subchapter, the estimate of soil-water characteristic curve from the PSD data has been presented. Hydraulic properties of a soil consist mainly of soil-water characteristic curve and coefficient of permeability. It has been shown that the latter may also be estimated from the PSD data (Romero et al., 1999). The computation of coefficient of permeability from the PSD data involves an integration of the PSD curve. Since water located in the micro-pores is essentially immobile (Pusch, 2001), the integration is only performed on the PSD of the macro-pores. The equation used to compute saturated coefficient of permeability (k_s) from the PSD data has been given in Chapter 4. The equation is re-written herein for clarity.

$$k_s = \frac{\rho_w g}{32\mu_w} \frac{{n_M}^2}{m^2} \sum_{i=1}^{m} (2i-1) D_{pi}^2 \tag{6.3}$$

where ρ_w is the density of water, μ_w is the absolute viscosity of water, g is the gravitational acceleration, n_M is the soil macro-porosity, m is the number of pore classes, and D_{pi} is the mean diameter of pores of class i. The diameter smallest pore is represented by D_{pn}.

The integration performed using the above formula gives a saturated coefficient of permeability of 1.74×10^{-6} m/s for the as-prepared specimen. The saturated coefficient of permeability of the oven-dried and swollen specimens estimated from the PSD data is 1.27×10^{-6} m/s and 2.38×10^{-8} m/s, respectively. The values are much higher than the measured values (see Chapter 8 for the discussion).

6.6 Study of Fabric of the Bentonite Used by Environmental Scanning Electron Microscopy (ESEM) Test

6.6.1 General

The environmental scanning electron microscope (ESEM) is a relatively new scanning electron microscopy (SEM) technique for qualitative assessment of microstructure of soil (Doehne and Stulik, 1990 and Williams and Miknis, 1997). The ESEM coupled with a digital image analysis (DIA) has also been used to estimate the swelling-shrinkage potential of soils at aggregate scale (Montes, 2004). The primary advantage of ESEM over the conventional SEM technique is that the ESEM does not require the test sample to be under high vacuum. Thus, wet, oily, dirty, or non conductive

samples can be examined in their natural state without modification or special preparation (Williams and Miknis, 1997). The sample environment can be varied through a range of pressures, temperatures, gas composition, and humidity. The reason of using ESEM in this research is because the technique also enables the study of swelling phenomena at microscopic scale to be performed. The technique is used to gain information about fabric of the bentonite used. The MIP data only provides information regarding the existence of micro- and macro-pores in the bentonite and the PSD distribution. However, the fabric of bentonite as affected; for instance, by water content and density cannot be inferred directly from the MIP test results.

6.6.2 Experimental Techniques

ESEM photos of the bentonite and the 50/50 bentonite-sand mixture at different states were taken in this study. The ESEM photos were taken using an environmental scanning electron microscope type XL 30 from Philips (Figure 6.15). Two pure bentonite; one at dried powder state (oven-dried) and one at slurried state, were first investigated. The observation was meant to study fabric of the bentonite as influenced by water content variation. Some compacted specimens of pure bentonite and 50/50 bentonite-sand mixture at Proctor densities were also studied. Additionally, the ESEM photos were also taken on the heavily compacted 50/50 bentonite-sand specimens at as-prepared as well as swollen states. The ESEM photos taken on the specimens with different densities were aimed at investigating the effect of density on the fabric of bentonite.

Figure 6.15 Environmental scanning electron microscope type XL 30 from Philips

A simulation of swelling was also performed on a heavily compacted specimen where the relative humidity (*RH*) of the specimen in the ESEM chamber was increased progressively. The ESEM photos of the specimen during simulation were taken. The following table summarises the conditions of the specimens used in the ESEM investigation.

Table 6.8 Initial conditions of the specimens used in the ESEM investigation

Specimen code	Water content, w (%)	Dry density, ρ_d (Mg/m^3)	Remarks
ESEM-1	0	-	Pure bentonite, powder, oven-dried
ESEM-2	272	-	Pure bentonite, slurried
ESEM-3	18	1.17	Pure bentonite, compacted, dry side
ESEM-4	48	1.13	Pure bentonite, compacted, wet side
ESEM-5	18	1.62	50/50 bentonite-sand, compacted, dry side
ESEM-6	25	1.55	50/50 bentonite-sand, compacted, wet side
ESEM-7	9	2.03	50/50 bentonite-sand, heavily compacted, as-prepared
ESEM-8*	19	1.65	50/50 bentonite-sand, heavily compacted, swollen
ESEM-9	9	2.03	50/50 bentonite -sand, heavily compacted, for swelling simulation

* cut from the same specimen used in the MIP investigation

6.6.3 Results and Discussion

In this subchapter, qualitative analyses of the ESEM photos taken are given with respect to the effects of water content, density, and swelling on fabric of the bentonite used in this investigation.

6.6.3.1 Effect of Water Content on Fabric of the Bentonite

Figure 6.16(a) and Figure 6.16(b) show the ESEM photos of pure bentonite at powder (oven-dried) form and slurried form (i.e., specimens ESEM-1 and ESEM-2), respectively. It is depicted in the figure that even at a very loose state (Figure 6.16(a)), aggregation (or clustering) occurs. The size of clay clusters is seen to be inhomogeneous apparently with a diameter of as large as 15 μm to as small as 2 μm. At high water content, the expandable clay minerals expand and form a 'wavy flake-like' structure consisting of clay platelets with different orientations. It indicates the existence of edge-to-face layer aggregations that possibly competes favourably with face-to-face layer aggregations. The separation of clay sheets from the clusters in the slurried specimen is depicted in the figure, which is in agreement to what was observed by Cui et al. (2002a) for Kunigel-Hostun sand mixture. The existence of clay clusters is not apparent in the slurried specimen (Figure 6.16(b)).

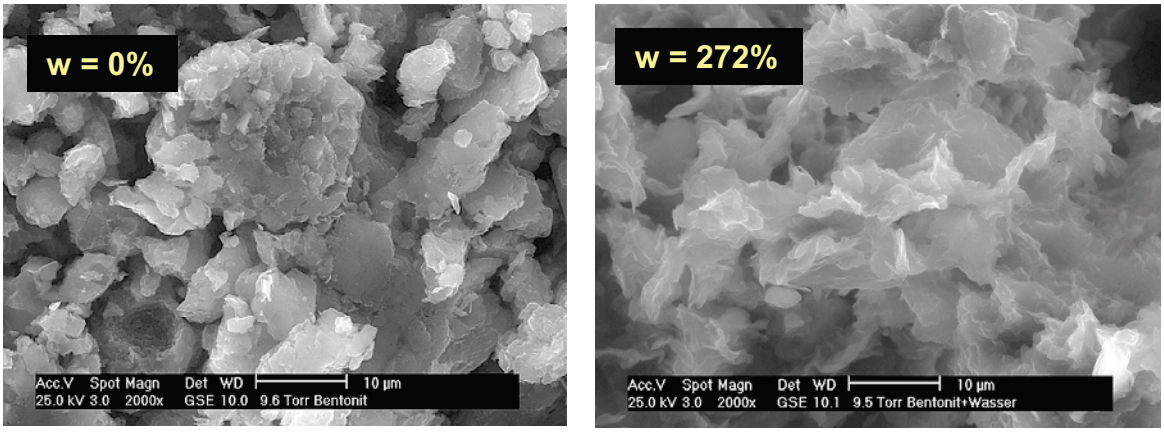

(a) (b)

Figure 6.16 ESEM photo of the pure bentonite specimens: (a) specimen ESEM-1 (powder form, oven-dried) and (b) specimen ESEM-2 (slurried form) (magnification: 2000X)

6.6.3.2 Effect of Density on Fabric of the Bentonite

Figure 6.17(a) and Figure 6.17(b) show the ESEM photos of pure bentonite compacted at Proctor densities on dry and wet side (i.e., specimens ESEM-3 and ESEM-4), respectively. Comparison of Figure 6.16 with Figure 6.17 indicates that, essentially, compaction of pure bentonite from loose state to a Proctor density, either on dry or wet side, induces no significant change in the fabric of bentonite. The size of clay clusters of the specimen compacted on dry side of optimum (Figure 6.17(a)) is essentially similar to that observed in the powder specimen (Figure 6.16(a)). Compaction only reduces the volume of macro-pores (or inter-aggregate pores) while the intra-aggregate pores remain unaffected. It is illustrated in Figure 6.17(b) that although the specimen was at compacted state with a significantly lower water content compared to that of Specimen ESEM-2, the bentonite (in the compacted specimen) still exhibits the 'wavy flake-like' structure. The existence of clay clusters depicted in Figure 6.17(b) (i.e., specimen ESEM-4) is more obvious than that observed in Figure 6.16(b) (i.e., specimen ESEM-2).

Figure 6.18(a) and Figure 6.18(b) show the ESEM photos of 50/50 bentonite-sand mixture compacted at Proctor densities on dry and wet side (i.e., specimen ESEM-5 and specimen ESEM-6), respectively. Instead of the 2000X magnification as used in Figure 6.16 and Figure 6.17, in order to show the sand grains in the specimen more clearly, the magnification used in the presentation of ESEM photos of specimens ESEM-5 and ESEM-6 is 500X. It is depicted in Figure 6.18(a) that sand grains in the compacted mixture are surrounded by clay clusters of different sizes. The 'wavy flake-like' structure of clay is also seen in the specimen with higher water content (i.e., specimen ESEM-6) (Figure 6.18(b)).

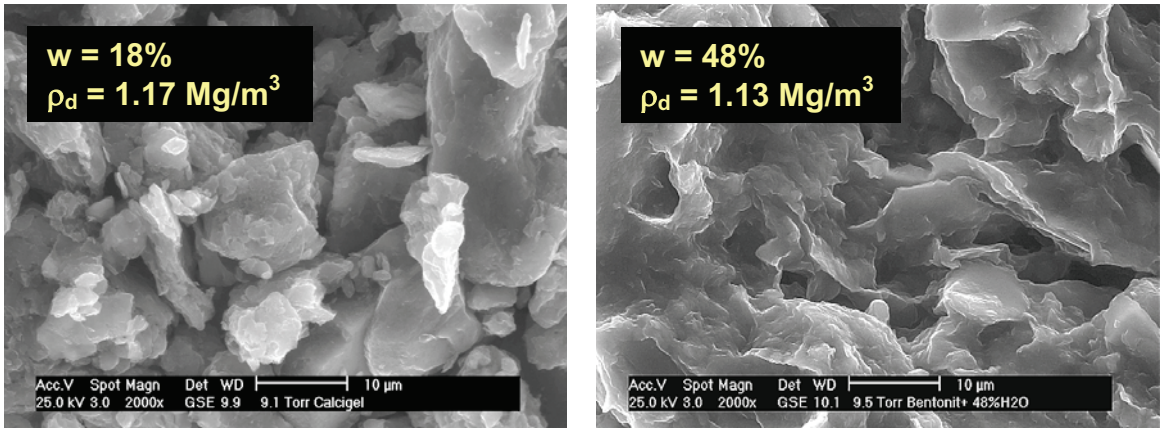

(a) (b)

Figure 6.17 ESEM photo of compacted pure bentonite at Proctor density: (a) specimen ESEM-3 (dry side) and (b) specimen ESEM-4 (wet side) (magnification: 2000X)

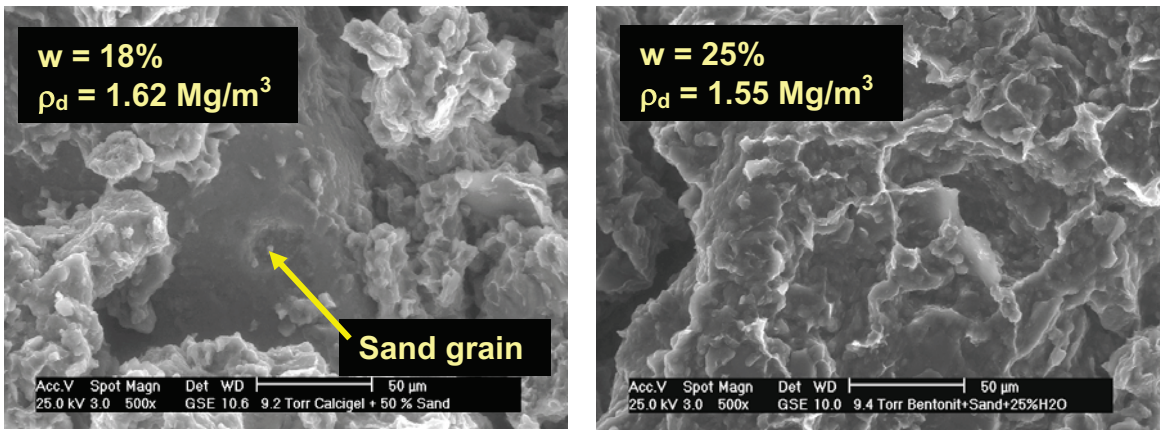

(a) (b)

Figure 6.18 ESEM photo of compacted 50/50 bentonite-sand mixture at Proctor density: (a) specimen ESEM-5 (dry side) and (b) specimen ESEM-6 (wet side) (magnification: 500X)

6.6.3.3 Effect of Swelling on Fabric of the Bentonite

Figure 6.19(a) shows the ESEM photo of the heavily compacted specimen of 50/50 Calcigel-sand mixture at its as-prepared state. The ESEM photo of the swollen specimen is shown in Figure 6.19(b). Clay clusters with a 'wavy flake-like' structure was not developed after the as-prepared specimen (w = 8.3%) was allowed to absorb water until it reached a water content of 19%. The figure also depicts no apparent disintegration of clay clusters due to wetting under unconfined conditions. This observation supports the hypothesis drawn earlier that during swelling water was absorbed in both the micro- and macro-pores of the specimen resulting in an increase in the size and a separation of the clay clusters. If the swollen specimen is at a hydraulic equilibrium, the water potential (or total suction) has the same value for the micro- and macro-pores in the specimen.

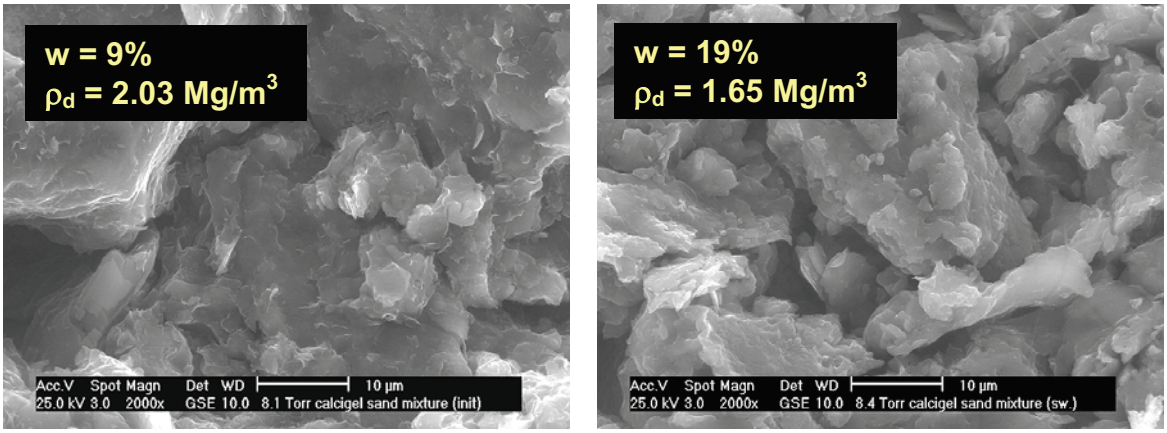

(a) (b)

Figure 6.19 ESEM photo of heavily compacted 50/50 bentonite-sand mixture: (a) specimen ESEM-7 (as-prepared state) and (b) specimen ESEM-8 (swollen state) (magnification: 2000X)

The fabric of swollen specimen (i.e., specimen ESEM-6 as shown in Figure 6.19 (b)) seems to be similar to that of specimen ESEM-3 (Figure 6.17(a)). By considering that the water content and the dry density of both specimens are almost the same, it is concluded that the development of 'wavy flake-like' structure is solely affected by water content and no significant influence of dry density (of the bentonite) appears to play a role. No discernible limit of water content which marks the development of such a fabric has been determined for the bentonite.

Figure 6.20(a) to Figure 6.20(d) shows ESEM photos of the heavily compacted specimen of 50/50 bentonite-sand mixture taken during swelling simulation. The magnification used (i.e., 5000X) was higher than those used in the earlier ESEM photos shown to enable a clearer view of micro-structures of the bentonite. The figure shows a progressive development of the 'wavy flake-like' clay structure as relative humidity of the chamber where the specimen was contained was increased (i.e., wetting process). This was not observed at a lower microscope magnification (i.e., 2000X) (e.g., Figure 6.19). The size of clay clusters is observed to have increased during wetting. However, the photos also indicate insignificant volumetric strain developed (qualitatively) during wetting from 20% *RH* to 81% *RH* (Figure 6.20(a) to Figure 6.20(d)) while one could anticipate more drastic changes.

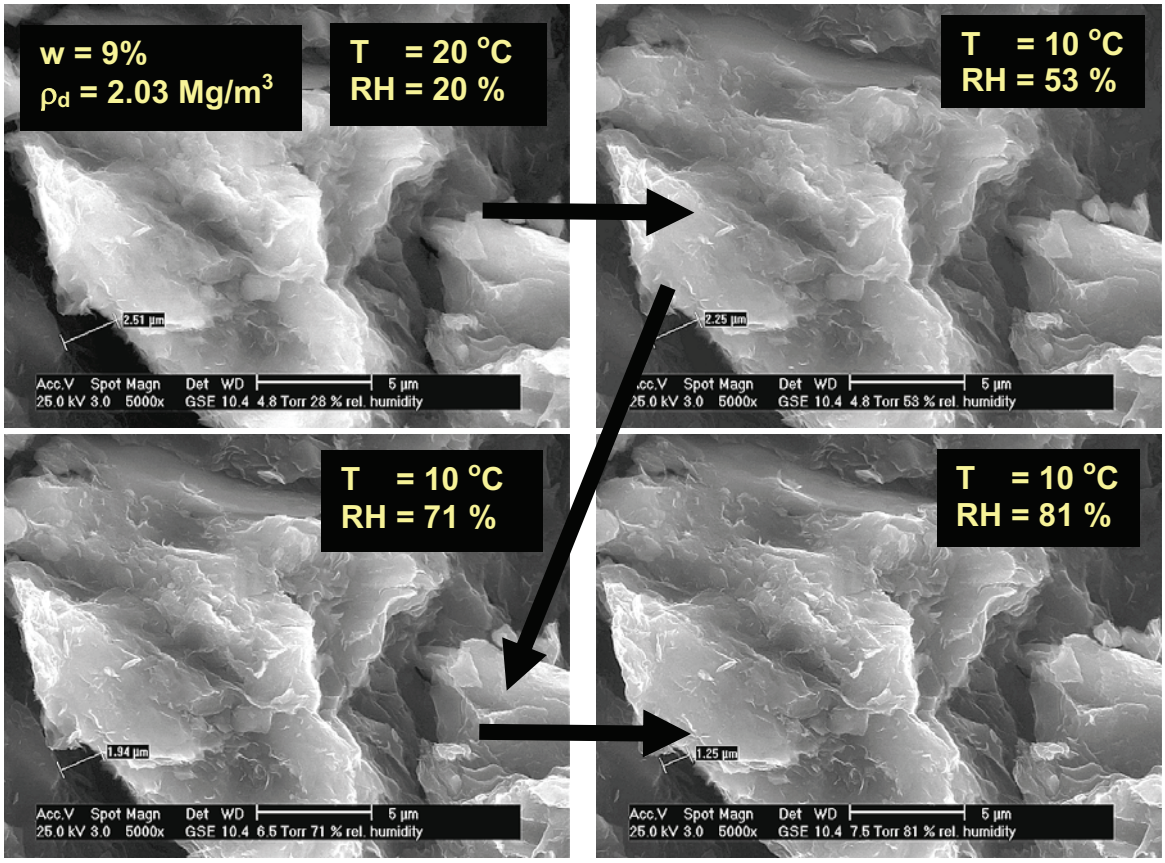

Figure 6.20 ESEM photos taken during simulation of swelling of a heavily compacted 50/50 bentonite-sand mixture (specimen ESEM-9) (magnification: 5000X)

6.7 Summary of Characteristics of the Material Used

The followings can be summarised from the material characterisation tests and specimen preparation carried out in this investigation of which the results are presented and discussed in the earlier subchapters.

1. The bentonite used (i.e., Calcigel) is a Calcium-type bentonite with a moderate swelling potential.

2. The as-prepared compacted specimen of 50/50 bentonite-sand mixture is microscopically uniform with an average initial water content of 9.07 % and an initial dry density of 2.04 Mg/m^3. The average initial total suction of the as-prepared specimen was 22700 kPa.

3. The as-prepared compacted specimen of 50/50 bentonite-sand mixture exhibits a bimodal pore-size distribution curve indicating the presence of a double porosity structure. The bimodal characteristic of the PSD is preserved even after the as-prepared specimen undergoes drying or wetting. Micro-pores constitute more than half the total pore volume of the as-prepared specimen. Hydraulic cycles (i.e.,

wetting and drying) affects the volume of both micro- and macro-pores whereas the percentage of each pores essentially remains constant.

4. During wetting under unconfined conditions, water is absorbed in the micro- as well as macro-pores resulting in an increase in the size of clay clusters and separation between clay clusters.

5. The as-prepared compacted specimen of 50/50 bentonite-sand mixture consists of an arrangement of clay clusters each made of several 'wavy flake-like' clay sheets oriented randomly in the clusters.

CHAPTER 7

EXPERIMENTAL TECHNIQUES AND PROCEDURES

7.1 General

This chapter describes experimental techniques and procedures that were adopted in this study. The experiments described herein consisted of measurement of matric and total suctions using several different techniques, unconfined wetting and drying tests, swelling pressure measurements and wetting test under constant volume conditions, one-dimensional compression-rebound test, one-dimensional cyclic wetting-drying test under constant load, and saturated permeability tests. Results of the experiments are presented and discussed in Chapter 8.

7.2 Suction Measurements

The suction measurements performed in this study were in-contact and non-contact filter paper methods for measuring matric and total suction, respectively, psychrometer, relative humidity (RH) sensor, and chilled-mirror hygrometer techniques for measuring total suction. Figure 7.1 shows data points corresponding to the specimens used for suction measurements.

7.2.1 Filter Paper Method

In this study, the filter paper suction measurements were performed using Whatman No. 42 filter paper disks. The measurements of matric and total suction using the filter paper technique commenced with the determination of calibration curve for matric and total suction.

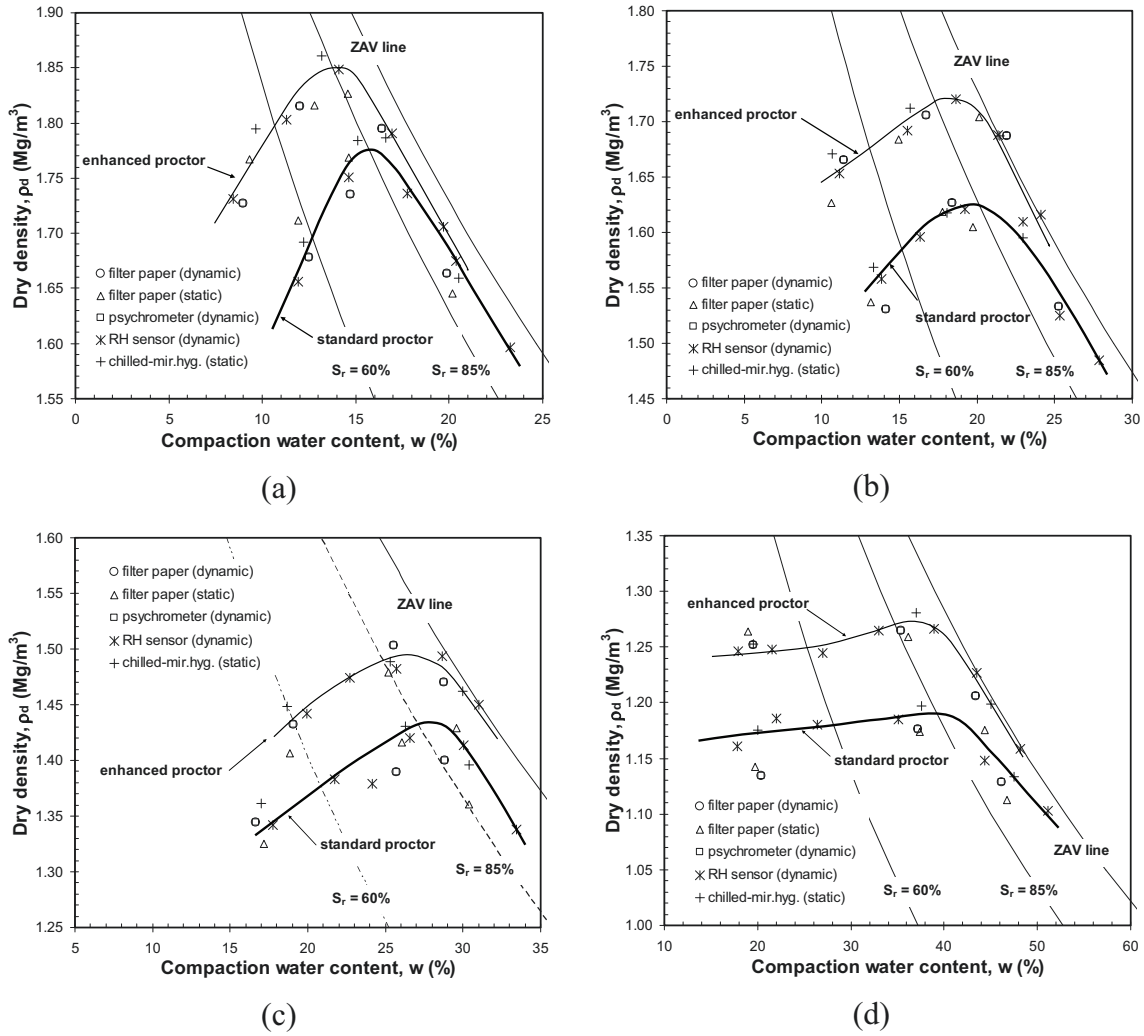

Figure 7.1 Data points corresponding to the specimens used in suction measurements: (a) 30/70 bentonite-sand mixture; (b) 50/50 bentonite-sand mixture; (c) 70/30 bentonite-sand mixture; and (d) pure bentonite (Note: 'dynamic' refers to the dynamically compacted specimens and 'static' refers to the statically compacted specimens)

7.2.1.1 Calibration

Although many calibration curves for the Whatman No. 42 filter paper are available in literatures (e.g., Fawcett and Collis-George, 1967; Al-Khafaf and Hanks, 1974; Hamblin, 1981; Chandler and Gutierrez, 1986; Greacen et al., 1987; Chandler et al., 1992; Deka et al., 1995; ASTM D 5298-94, ASTM, 1997; Leong et al., 2002 and many others), it is desirable to have a calibration curve for each study involving different filter paper lots (Deka et al., 1995). The calibration curve of the Whatman No. 42 filter paper was established using a pressure plate apparatus or axis-translation technique (ATT) for suction less than 1500 kPa and using a desiccator or vapour equilibrium technique (VET) for suction higher than 2000 kPa.

Two filter papers with different sizes; namely, a standard-sized (i.e., 55-mm diameter) filter paper and a small-sized (i.e., 25-mm diameter) filter paper that was cut from the standard-sized filter paper were used in the determination of each calibration point. The filter papers were not pre-treated against bacterial, algal, and fungus growth prior to the calibration. Chandler and Gutierrez (1986) stated that the pre-treatment of the filter papers against the growth of bacterial, algal, and fungus was not required. Chandler et al. (1992) used a soil with known suction induced in a pressure plate for calibrating filter papers with respect to matric suction. Leong et al. (2002) plotted the calibration curves for the filter papers that were obtained in a similar manner to that carried out by Chandler et al. (1992). It was found that the data exhibited a large scatters which were attributed to the uncertainty in the matric suction of the soil specimens used. In this study, the matric suction calibration for the filter papers was not performed using soils with known values of matric suction. To maintain good contact between the filter paper and the ceramic disk in the pressure plate during matric suction equalisation, a dead weight was placed on each filter paper resulting in a vertical pressure of about 7 kPa being applied. It was anticipated that the dead weight might compress the filter paper resulting in slightly lower filter paper water contents, especially at low matric suctions. A three-week equilibration time was used in the calibration. The filter paper calibration curve obtained is referred to as the in-contact (or matric suction) filter paper calibration curve.

For suction greater than 2000 kPa, the two filter papers were placed on a glass stand in a glass container about half filled with salt solution. Several aqueous salt solutions and several molal NaCl solutions were used in the non-contact filter paper calibration. Each salt solution produces water vapour corresponding to a certain relative humidity or total suction (see Chapter 5 for details on the VET). Since the VET is sensitive to temperature fluctuation, extensive cares were taken when measuring the total suction calibration curve of the filter paper used. The vapour equilibrium calibration of the filter paper was carried out in a thermally-insulated box (i.e., a water bath), with a constant temperature (i.e., 22 ± 0.2^{o}C). The filter papers were equilibrated to a constant relative humidity (*RH*) in five weeks duration. The corresponding calibration curve obtained is referred to as the non-contact (or total suction) filter paper calibration curve. The in-contact and non-contact calibration curves for the Whatman No. 42 filter paper used are shown in Figure 7.2 together with the calibration curve published in the standard ASTM D 5298-94 (ASTM, 1997) for comparison. Equation (7.1) and Equation (7.2) are presented in a similar form to that used by Leong et al. (2002) and represents the matric and total suction calibration curve for the Whatman No. 42 filter paper, respectively, as measured in this study. The equation form is based on the equation proposed for the soil-water characteristic curve for soils by Fredlund and Xing (1994).

$$s_m = 93.82\left[\exp\left(\frac{299.93}{w_{fp}}\right)^{0.148} - \exp(1)\right]^{5.235} \quad (7.1)$$

$$s_t = 2223\left[\exp\left(\frac{235.57}{w_{fp}}\right)^{0.129} - \exp(1)\right]^{3.822} \quad (7.2)$$

where s_m and s_t is matric and total suction, respectively, in kPa and w_{fp} is filter paper water content in percent.

Equation (7.1) has a coefficient of determination (r^2) of 0.99 with a standard error of estimate (*SEE*) of 29.5 kPa while Equation (7.2) has an r^2 value of 0.904 with an *SEE* value of 860 kPa for low total suction range (i.e., lower than 10000 kPa) and 7000 kPa for high total suction range (i.e., higher than 10000 kPa). All the calibration data fall within 95% confidence intervals.

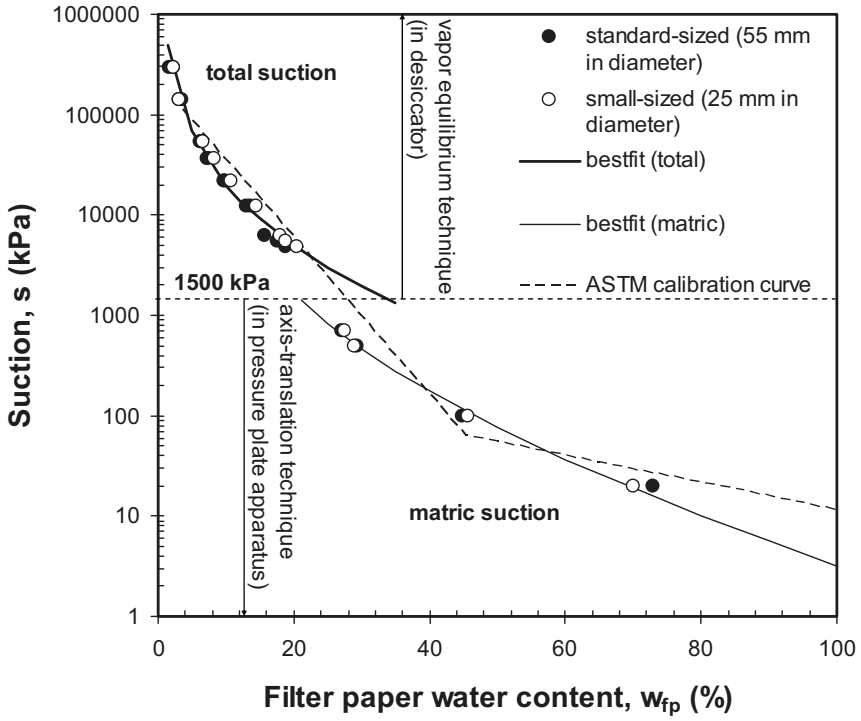

Figure 7.2 Matric and total suction calibration curves of the Whatman No. 42 filter paper

7.2.1.2 Experimental Procedures

Two 2-cm thick slices of soil were carefully cut from the standard-sized dynamically compacted specimens using a sharp blade. A standard-sized (i.e., 55 mm in diameter) filter paper was sandwiched between two protective filter papers (also Whatman No. 42) with a larger diameter and was placed between the two slices of

specimen to measure matric suction. The gap between the two slices of specimen was sealed using a plastic seal to prevent moisture loss. For total suction measurements, a 55-mm diameter filter paper was mounted on a stainless steel wire mesh, placed directly on the upper surface of the specimen. A protective filter paper with a larger diameter was also placed on the measuring filter paper to avoid direct contact between the measuring filter paper and the container lid. The entire specimen was subsequently placed in a sealed air-tight container that was almost the same size as the specimen. The container was immersed in the water bath at constant temperature (i.e., 22 ± 0.2^{o}C) for five weeks similar to that of the calibration process. The experimental setup of the filter paper suction measurements performed in this investigation is shown in Figure 7.3.

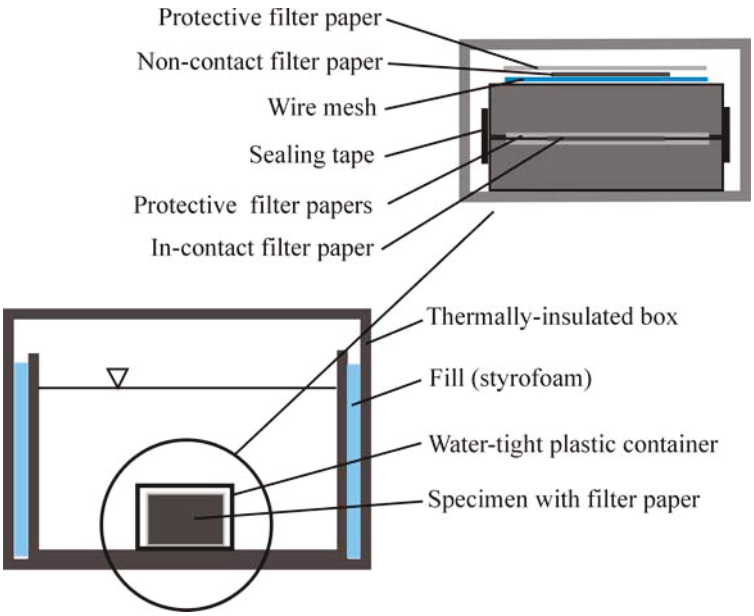

Figure 7.3 Experimental setup for the filter paper matric and total suction measurements

It was found that good contact between the filter paper and the soil in the matric suction measurement was not attained in the dynamically compacted specimens. Some specimens even showed leakage through the sealing. Hence, a slightly different approach was adopted for the statically compacted specimens. The mixtures were statically compacted in two layers in a stainless steel ring with a diameter of 50 mm. The targeted dry densities were based on the predetermined compaction curves. After the first layer was compacted, a 25-mm diameter filter paper sandwiched between two larger-diameter filter papers (i.e., 35-mm diameter) was placed on the specimen for matric suction measurement. The second layer was subsequently compacted such that specimens with a height of 15 mm were produced. Procedures similar to that implemented in the case of the dynamically compacted specimens were also adopted for placing the second filter paper used for the total suction measurement. The statically compacted specimens are smaller than the dynamically compacted specimens and accordingly, a smaller air-tight container was used with a better sealing. Similarly, the entire setup was placed in the water bath to

maintain constant temperature during measurement. In this case, a five-week equilibration time was also used. This period was much longer than the two-week minimum equilibration time specified in ASTM D 5298-94 (ASTM, 1997). The water contents of the two measuring filter papers were determined and suctions were calculated using Equations (7.1) and (7.2). The water content of each specimen was also measured as it might differ from the compaction water content. No significant differences in water content were observed in the specimens.

7.2.2 Psychrometer Technique

The psychrometers used in this study were thermocouple psychrometers type PCT-55 from Wescor Inc. with a ceramic screen at the tip. The psychrometer set (Figure 7.4) consisted of ten PCT-55 thermocouple psychrometers, a reading device (i.e., a micro-voltmeter) type HR-33T, and a reading switch type PS-10, both also from Wescor Inc.

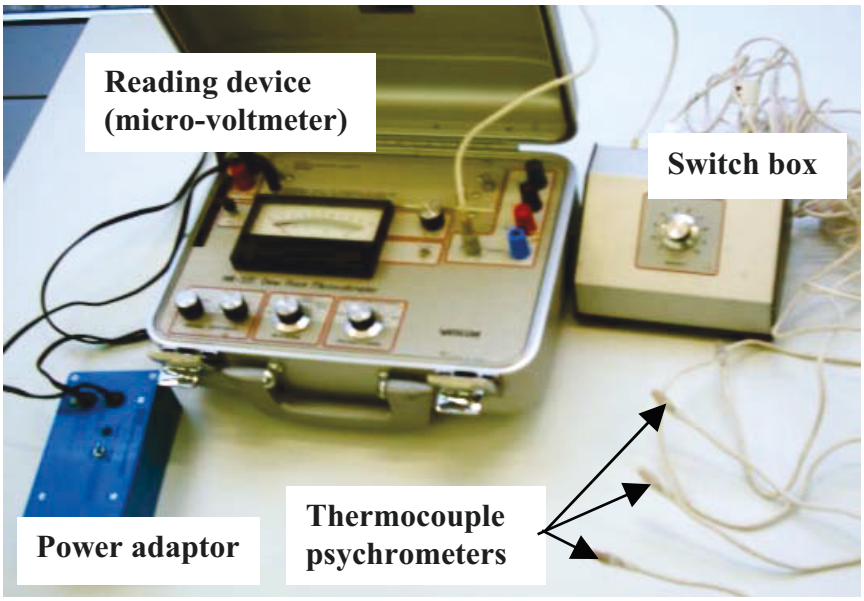

Figure 7.4 Psychrometer set used in this study

7.2.2.1 Calibration

The psychrometric measurement of total suction started with individual calibration of the psychrometers using salt solutions (i.e., the VET). The ten psychrometers were suspended over the salt solution in a desiccator for one day. Suspending the psychrometer above salt solution was found to be less destructive than submerging it in the salt solution (Tang et al., 1997). Total suction less than about 8500 kPa was generated in this method for the calibration (Fredlund and Rahardjo, 1993; and Ridley and Wray, 1996). The calibration of psychrometers was performed by measuring the electromotive force generated which corresponded to the total suction induced by the salt solution in the desiccator. Two modes of measurement; namely, dew point and psychrometer modes can

be done in the psychrometer technique. In the dew point mode, the signal (i.e., the electromotive force) generated converges to a value corresponding to the dew point of the vapour space in the specimen. In the psychrometer mode, a 'plateau' signal is obtained before the electromotive force decreases rapidly towards a zero value. In the psychrometer mode, there is a need to correct the readings to the actual temperature, whereas in the dew point mode, the effect of temperature on the psychrometer readings is accounted for by setting the psychrometer cooling coefficient prior to measurement. The corrected reading ($R_{corrected}$) in the psychrometer mode as affected by temperature can be computed using the following equation (Wescor, 1986).

$$R_{corrected} = \frac{R_{psy}}{\left(0.325 + 0.027\,T\right)} \tag{7.3}$$

where R_{psy} and $R_{corrected}$ are in kPa and T is the temperature in ^{o}C.

The calibration curves for the ten psychrometers used generally showed an intercept indicating that the electromotive force at zero total suction was not equal to zero similar to that found by Tang et al. (1997). The slopes of calibration curves for the ten psychrometers used were found to be less than those described in the specification (i.e., 0.75 μV/bar for dew point mode and 0.47 μV/bar for psychrometer mode) (Wescor, 1986). Table 7.1 shows statistics of the thermocouple psychrometer calibration curves obtained. Generally, all calibration data fall within 95% confidence intervals.

Table 7.1 Statistics of the thermocouple psychrometer calibration curves

Psych. No.	Dew point mode			Psychrometer mode		
	Zero offset, c (μV)	Slope, m (μV/bar)	r^2	Zero offset, c (μV)	Slope, m (μV/bar)	r^2
1	4.195	0.556	0.985	0.901	0.340	0.998
2	1.861	0.628	0.991	2.077	0.348	0.989
3	0.457	0.641	0.989	1.881	0.329	0.992
4	1.233	0.626	0.994	0.499	0.388	0.983
5	4.18	0.516	0.981	1.875	0.333	0.981
6	Not functioning					
7	1.671	0.606	0.978	0.390	0.389	0.975
8	1.258	0.602	0.978	1.783	0.319	0.987
9	1.704	0.597	0.982	0.389	0.363	0.975
10	0.810	0.620	0.989	1.881	0.329	0.992

7.2.2.2 Experimental Procedures

Two holes were drilled in each dynamically compacted mixture to bury two psychrometers. The compacted mixture with the psychrometers was subsequently wrapped with plastic and aluminium foil to avert moisture loss. To attain constant temperature during measurement, the wrapped compacted sample was placed in a water-tight container and the container was immersed in the water bath. An additional temperature sensor was placed over the water surface in the water bath to ensure temperature equilibrium between the water bath and the specimen. The experimental setup for the total suction measurement using psychrometers is shown in Figure 7.5. Sufficient time is required to isothermally equilibrate the psychrometers with the mixture. The higher is the measured total suction; the longer will be the required equilibration period.

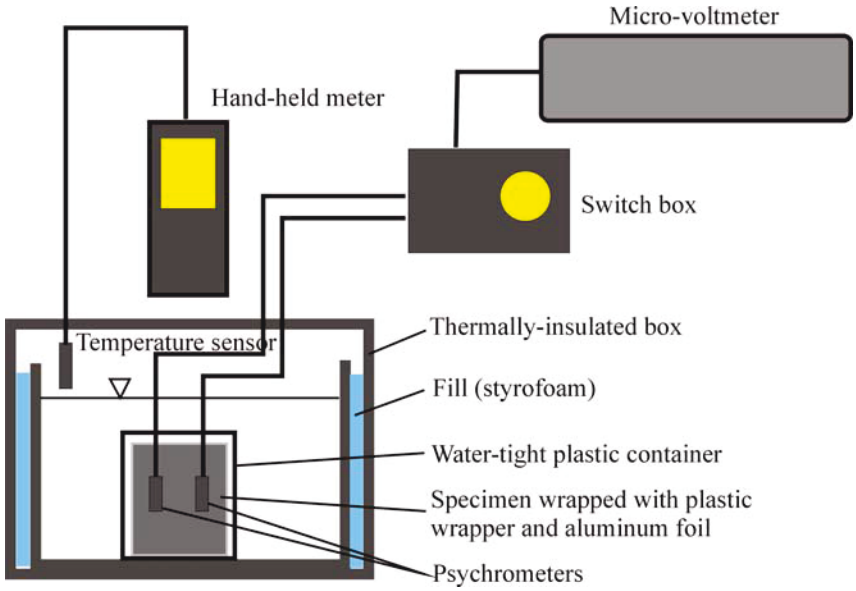

Figure 7.5 Experimental setup for the psychrometer total suction measurement

The measurement was performed when the temperature of the system was about the same as the temperature of specimen which was measured by the psychrometers. The internal temperature equilibrium in the psychrometers was observed through the individual zero offset. A value of zero offset greater than 1 μV indicated that the difference in temperature between the measuring and reference junctions was excessive (Wescor, 1986). The time required for establishing a thermal and vapour equilibrium between the psychrometer, the soil specimen, and the vapour space (i.e., the water vapour in the holes) depends on the magnitude of total suction being measured. Generally, a longer equilibration period is required when measuring higher total suction. A one-day equilibration period was used throughout the study and no attempts were made to determine the optimum equilibration period for the material tested. The measurement was performed by cooling down the measuring junction in the psychrometer for an adequate

cooling time which is also a function of total suction being measured (Wescor, 1986). After the cooling stage, the condensed water in the measuring junction (depending on the total suction measured in the junction) evaporated and caused a drop in the temperature of the junction. The electromotive force due to the reduction of temperature of the measuring junction was measured using a micro-voltmeter. The calibration curves previously obtained for the psychrometers were used to convert the measured electromotive force to total suction. The typical psychrometer reading for the dew point and psychrometer modes is shown in Figure 7.6(a) and Figure 7.6(b), respectively.

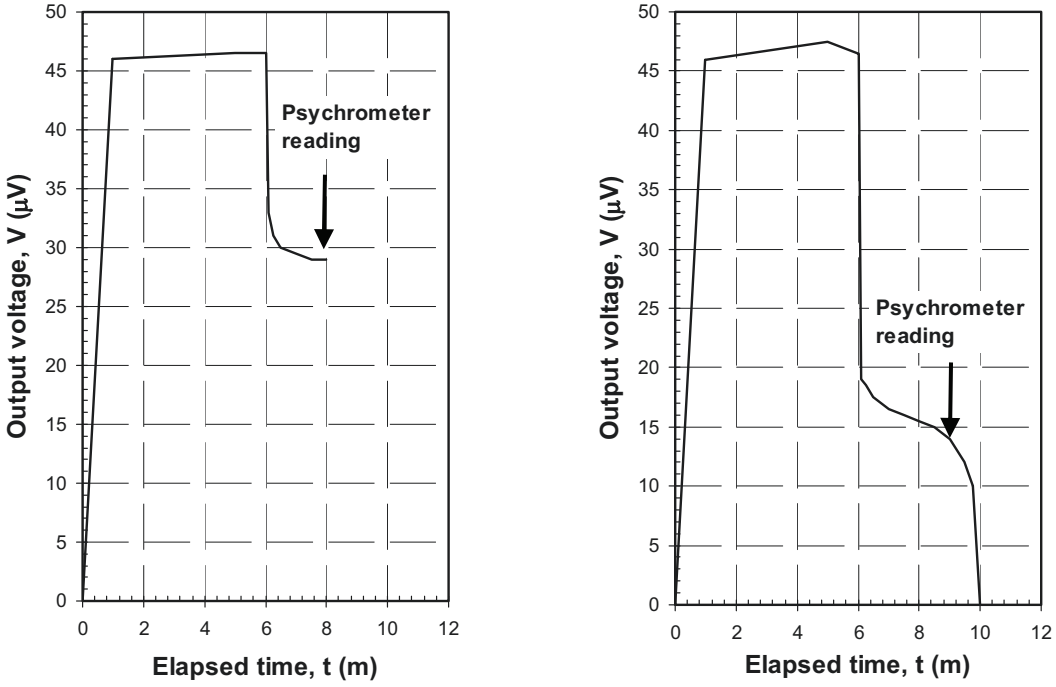

Figure 7.6 Typical psychrometer reading: (a) dew point mode and (b) psychrometer mode

7.2.3 Relative Humidity (RH) Sensor

The relative humidity (RH) sensor together with its accompanying temperature sensor used in this study has been intensively adopted in meteorological applications for measuring dew point of air where temperature and relative humidity fluctuate rapidly. The RH and temperature sensor used was a capacitance sensor Humicap® HMP 243 and a T temperature sensor, respectively, both from Vaisala Oyj (Figure 7.7). Dueck and Börgesson (2001) used a similar sensor to monitor total suction of a swelling clay specimen wetted under constant volume conditions. The RH sensor measures relative humidity (*RH*) of vapour space in the specimen, which is then converted to suction using Kelvin's equation (Equation (5.1) in Chapter 5).

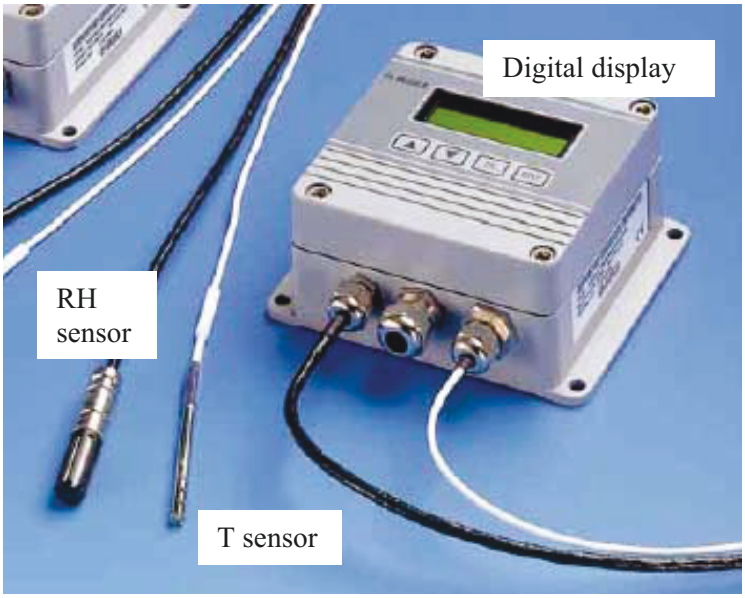

Figure 7.7 RH and T sensors used in this study

The warming function keeps the RH sensor head dry when excessive condensation is detected, thus it can measure low total suctions (or high *RH* values). For sensors without warming function, condensation may occur when measuring high *RH* (i.e., above 95%). The condensation causes erroneous readings since the measurements show too high *RH* values. The RH sensor used had a diameter of 8 mm and a length of 60 mm with a sintered stainless steel cap. The temperature sensor used had a diameter of 5 mm and a length of 60 mm. The head of the RH sensor comes with a stainless steel sintered filter. Readings are shown on a digital display and automatic data collection can be done through a personal computer.

7.2.3.1 Verification

The RH sensor was first checked for its response to several known *RH* values generated by salt solutions. It was found that the sensor responded accurately to the generated relative humidities and exhibited insignificant hysteresis. The verification results have been reported in Agus and Schanz (2003b). The following figure shows the response of RH sensor to several known *RH* values and typical readings of the sensor.

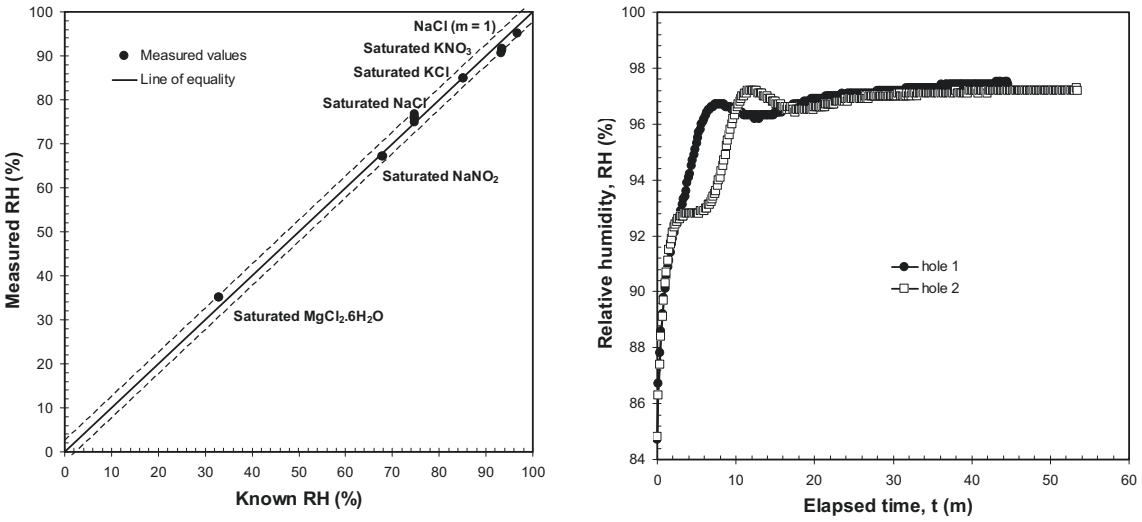

(a) (b)

Figure 7.8 (a) Response of the RH sensor to several known RH values and (b) typical readings of the RH sensor (Agus and Schanz, 2003b)

7.2.3.2 Experimental Procedures

Two holes, one 20-mm diameter and one 10-mm diameter both 80 mm deep were drilled in each dynamically compacted specimen at an arbitrary distance of 40 mm for the insertion of both sensors. The larger diameter hole was for the RH sensor while the smaller one was for embedding the temperature sensor. The clearance between the two sensors must be sufficient to prevent the temperature sensor from being heated by the warming function in the RH sensor during measurement. A perforated PVC pipe was inserted into the larger diameter hole to accommodate the RH sensor and to avoid direct contact between the sensor and the compacted mixture. Procedures similar to those used in the psychrometer technique were adopted to prevent moisture loss and to maintain constant temperature during measurement. The experimental setup for the total suction measurement using the RH sensor is shown in Figure 7.9. The measurement of RH was carried out immediately after compaction and terminated after stable *RH* and temperature readings were attained. Typically, 20 to 30 minutes were required to measure total suction in the compacted bentonite-sand mixtures (Figure 7.8).

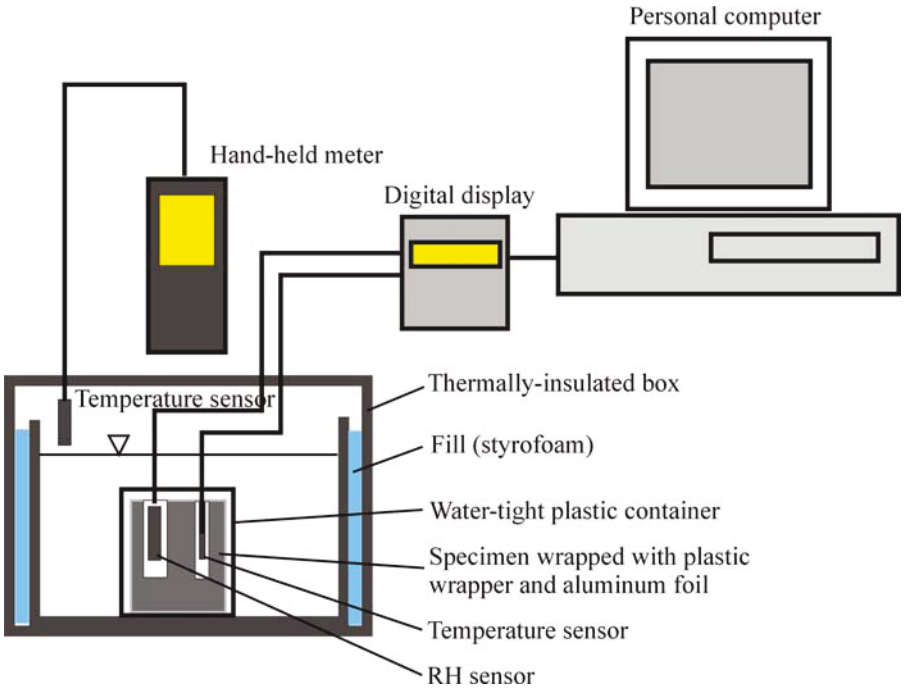

Figure 7.9 Experimental setup for total suction measurement using dew point sensor

7.2.4 Chilled-Mirror Hygrometer Technique

The chilled-mirror hygrometer used in this study was a water activity meter type 3TE produced by Decagon Devices Inc. (Figure 7.10). The equipment has a special specimen closed chamber of about 12 cc in volume, where the soil specimen is contained.

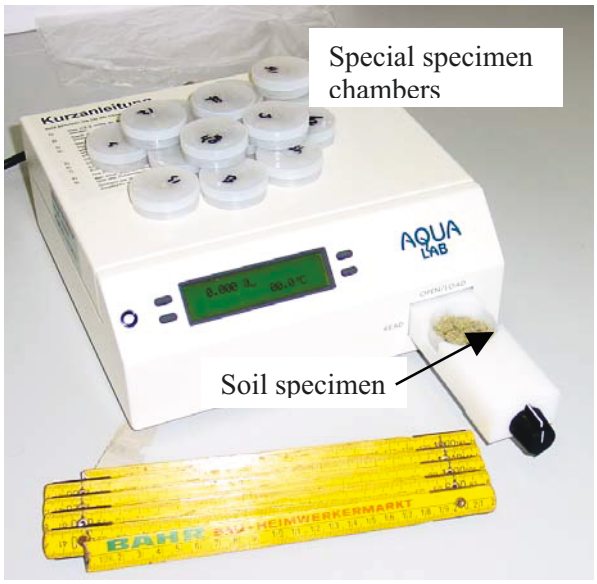

Figure 7.10 The chilled-mirror hygrometer used in this study

7.2.4.1 Verification

Prior to use, the chilled-mirror hygrometer was verified for its performance in measuring total suction. The verification was carried out using standard salt solutions provided by the manufacturer. The readings obtained for the standard salt solutions were found to vary less than 0.2% *RH* with a response time of no longer than 3 minutes. The quick measurement time of the device enabled a lot of total suction measurements to be conducted in a quite short time duration.

7.2.4.2 Experimental Procedures

The measurement of total suction using this technique was started by placing the chamber with the soil specimen into the device. In the case of compacted specimens, small pieces of specimen were cut from the statically compacted specimen at the as-compacted conditions and were placed in the sealed chamber (also about half capacity). Extra care was taken when cutting the compacted specimens with high sand content as the cutting might introduce structural disturbance to the specimens. There was concern that disturbance might affect the capillary component of suction. The soil in the specimen chamber in the device was allowed to reach isothermal equilibrium which was defined as the difference between temperature of the vapour space and the specimen. The device showed the difference in temperature between the headspace and the mirror. It is suggested that the mirror temperature be set to a slightly higher value than the temperature of the vapour space, particularly when measuring high relative humidities (or low total suctions) as condensation may occur on the mirror. The chamber was subsequently closed and after reaching equilibrium, the relative humidity and the temperature of the vapour space were displayed. An average equilibration time of 3 minutes was required for the total suction measurement of the materials used in this study. Additional total suction measurements were also carried out on loose specimen (i.e., in powder form) to study the effect of density on total suction. For loose soil specimens, the special measuring chamber was filled up to half capacity with the cured mixture which was previously prepared (see Chapter 6).

7.3 Wetting and Drying Tests under Unconfined Conditions

The wetting and drying tests under unconfined conditions were performed on several heavily compacted specimens of 50/50 bentonite-sand mixture (i.e., those prepared by GRS Braunschweig). In this sub-chapter, procedures adopted in the determination of wetting and drying curves of the heavily compacted specimens are described. The tests performed involved tests using the axis-translation technique (ATT) in the pressure plate apparatus and those using the vapour equilibrium technique (VET) by means of desiccator tests. Table 7.2 summarises the initial conditions of specimens

used while Figure 7.11 shows suction paths followed by each specimen in the unconfined wetting and drying tests.

Table 7.2 Initial conditions of the specimens used in the wetting and drying tests under unconfined conditions

Specimen code	Initial conditions		
	Water content (%)	Void ratio	Suction (kPa)
UC-1	9.14	0.300	22700*
UC-2	8.88	0.282	22700*
UC-3	8.52	0.286	22700*
UC-4	8.69	0.281	22700*
UC-5	8.31	0.282	22700*
UC-6	9.00	0.292	22700*
UC-7	9.19	0.284	22700*
UC-8	9.20	0.289	22700*
UC-9	8.90	0.293	22700*
UC-10	9.60	0.299	22700*
UC-11	9.18	0.318	22700*
UC-12	9.13	0.292	22700*

* the as-prepared suction

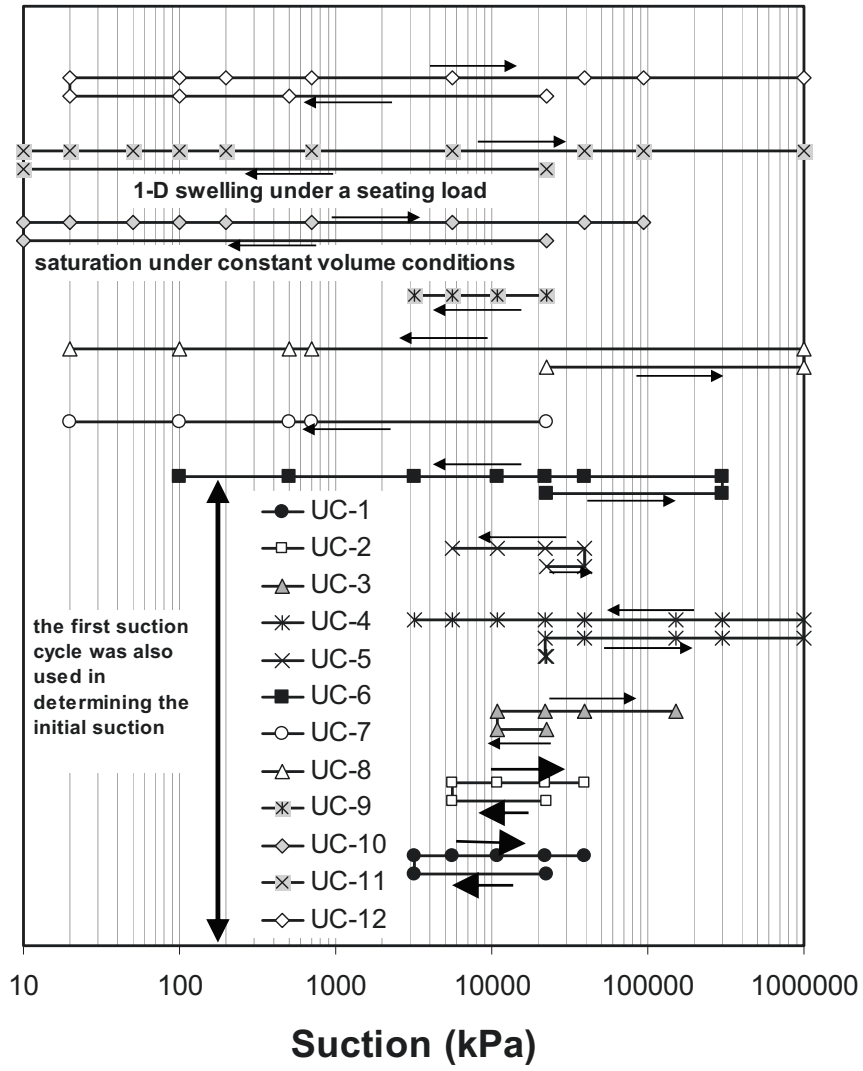

Figure 7.11 Suction paths followed in the unconfined wetting and drying tests

7.3.1 Experimental Techniques and Procedures

7.3.1.1 Axis-Translation Technique using Pressure Plate Apparatus

The technique was adopted to determine unconfined wetting and drying curves in the low suction range (i.e., less than 1500 kPa). In the technique, matric suction is applied. Descriptions of the applicability and problems related to this technique have been described in Chapter 5. A pressure plate apparatus from Soilmoisture (Figure 7.12) was used in this experiment. The main part of the pressure plate apparatus is the high-air entry ceramic plate. Three ceramic plates with different air entry values; namely, 100 kPa, 500 kPa and 1500 kPa were used in the investigation depending on the applied matric suction. The use of ceramic plate with a high air entry value is not desirable when much lower matric suction is to be applied. This is due to the fact that the coefficient of permeability

of the ceramic plate with a higher air entry value is lower than that of the ceramic plate with a lower air entry value. Therefore, the test can run for long time duration.

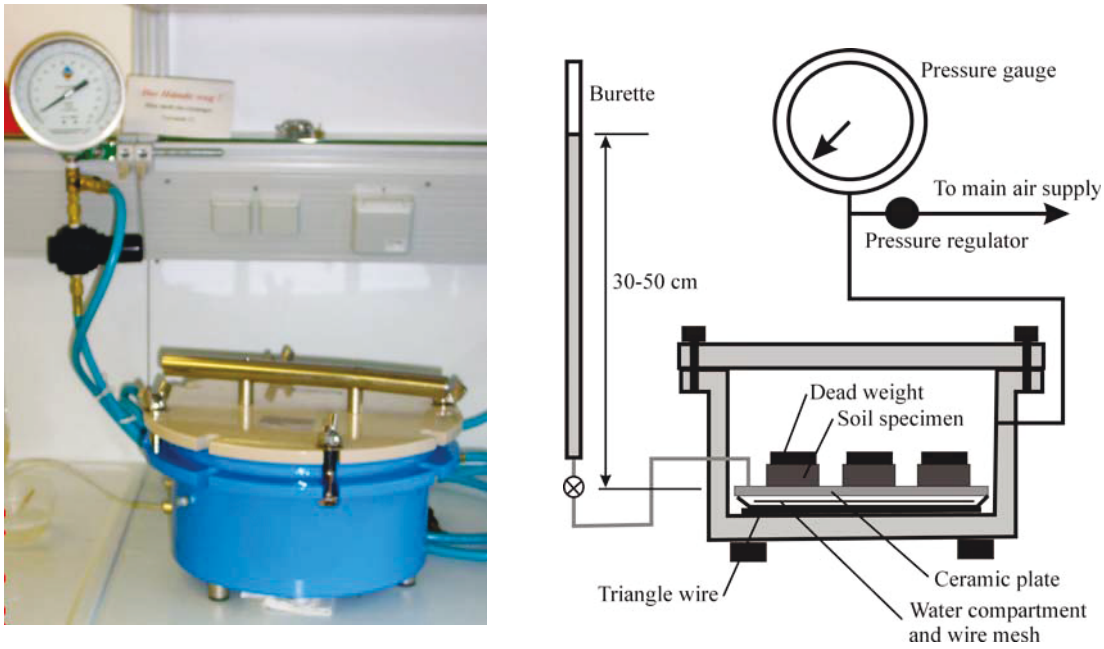

Figure 7.12 Pressure plate apparatus setup

The water outlet in the pressure plate apparatus was connected to a burette for flushing purpose. The test started with saturating the ceramic plate with distilled deaired water. The water compartment located between the ceramic plate and the rubber membrane was filled with distilled deaired water. Water will come out of the ceramic plate when the water compartment is fully filled with distilled deaired water. An amount of distilled deaired water was subsequently poured on the ceramic plate surface. An air pressure of about 100 kPa was applied to pressurise water on the ceramic plate for several hours. The pressurisation was stopped when no air bubbles were observed to come out of the compartment and flowed towards the burette. Diffused air bubbles collected beneath the ceramic plate was flushed using water in the burette. A sufficient amount of water was supplied to the water compartment through the burette. The water outlet valve was closed and a small air pressure was applied and held for approximately 5 minutes. The water outlet valve was opened and the air pressure was slowly incrementally increased to about 100 kPa. Air bubbles will be flushed and come out of the water compartment and flow to the burette. It was found that no air bubbles were observed after the second flushing process.

The saturation of the ceramic plate was confirmed by verifying the air-entry value of the ceramic plate. The water left on the ceramic plate was wiped off and an air pressure as high as the air entry value of the ceramic plate was applied. The water level in the burette was monitored. Initially, there was a small increase in burette water level. The

water level in the burette stopped increasing indicating that there was no air flowed across the ceramic plate.

The highly compacted bentonite-sand specimen was placed on the ceramic plate. A dead weight of about 50 g was placed on the specimen to maintain a good contact between the specimen and the ceramic plate. An air pressure was slowly and step-wisely applied to reach the target matric suction by also considering the water column in the burette. The flushing of water compartment was performed regularly to remove the diffused air bubbles collected beneath the ceramic disk. It is important to note that the existence of diffused air bubbles in the water compartment results in the discontinuity between the water phase in the specimen and the source of water. The water phase continuity has to be established through out the experiment as to warrant liquid transfer of water into and out of the specimen.

The change in mass and dimensions (i.e., the diameter and height) of the specimen were monitored. A precision weighing balance with an accuracy of 0.01 g was used to weigh the specimen. The dimensions of the specimen were monitored using a digital calliper that could measure to the nearest 0.01 mm. At low matric suction (i.e., below 50 kPa), the measurement of dimensions of the soil specimen was only performed after the specimen had reached equilibrium based on the water content versus time plot. At matric suction below 50 kPa, the specimen was soft enough such that the dimension measurement using the digital calliper could introduce disturbance along the circumference of the specimen. After each suction equilibration, the ceramic disk was resaturated. Both water content and void ratio of the specimen were used to judge the equilibrium conditions before applying the next matric suction increment or decrement.

7.3.1.2 Vapour Equilibrium Technique or Desiccator Tests

The vapour equilibrium technique (VET) was used to determine wetting and drying curves in the high total suction range (i.e., greater than 2000 kPa). Descriptions of the applicability and problems related to this technique have been described in Subchapter 5.3.2. In this study, two types of desiccator; namely, the large desiccator for testing up to six specimens simultaneously (Figure 7.13) and the small desiccator (i.e., glass container) that could only accommodate one specimen, were used. Several aqueous and molal salt solutions were used to induce total suction to the specimen by changing the relative humidity of the vapour space in the desiccator.

The specimen was placed in the glass container similar to that used in the calibration of non-contact filter paper. The glass container was one-half filled with the salt solution. The entire setup was placed in the thermally-insulated chamber (i.e., water bath) similar to that used inn the non-contact filter paper calibration. The large desiccator with the specimens was not placed in the water bath. A piece of Whatman No. 42 filter

paper was placed in the large desiccator to measure the actual total suction applied to the specimens. The experiment was conducted in a temperature-controlled room that could maintain a constant temperature of 22°C ± 0.5°C. Procedures similar to those used in the axis-translation technique to determine the changes in water content void ratio were adopted. At the end of the test, water content of the filter paper was measured and the filter paper calibration curve shown in Figure 7.2 was used to compute the actual total suction applied to the specimens. It was found that the actual total suctions were not far different from the targeted values.

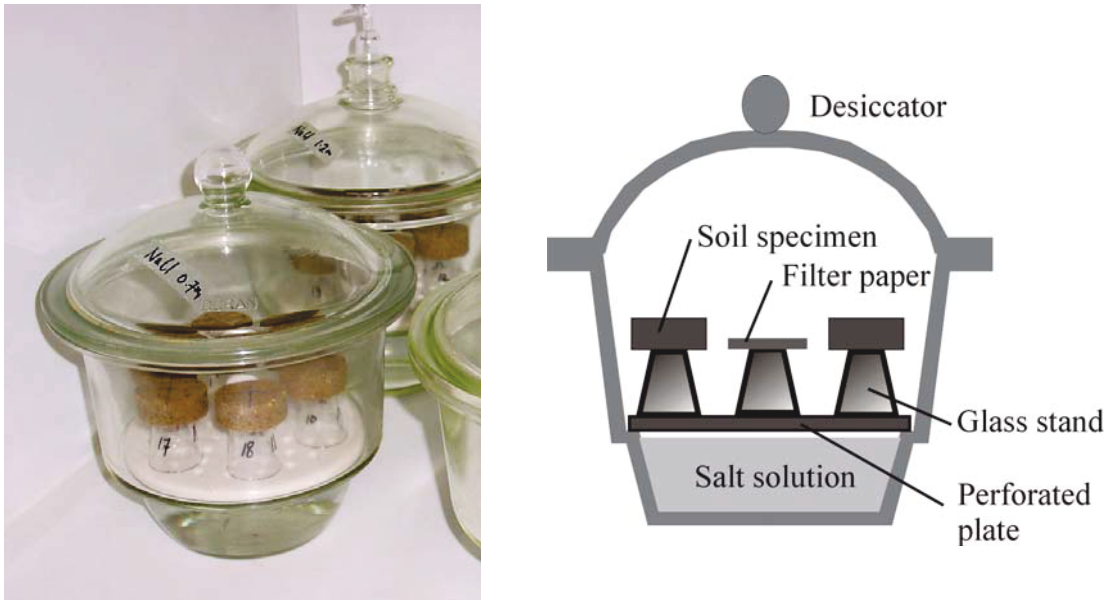

Figure 7.13 Large desiccator test setup

7.4 Swelling Pressure Tests and Determination of Wetting Curve under Constant Volume Conditions

The measurement of swelling pressure was performed on the lightly and heavily compacted bentonite-sand mixture specimens. Three types of test; namely, constant volume including one-step and multi-step tests, swell-under-load test, and swell-load test were carried out. In this sub-chapter, procedures adopted in the swelling pressure measurement are outlined. The equipment used for the swelling pressure measurements is described. The swelling pressure were determined for the lightly (or proctor density) compacted specimens as well as for the heavily compacted specimens. The tests involved the one-step measurement of swelling pressure using the water circulation method. The axis-translation technique (ATT) and the vapour equilibrium technique (VET) were used in the multi-step swelling pressure measurement. The multi-step swelling pressure tests were also meant for measuring wetting characteristics of the specimen under constant volume conditions.

The initial conditions (i.e., water content and void ratio) of the lightly compacted specimens tested are shown in Figure 7.14 while Table 7.3 summarises the initial conditions of the heavily compacted specimens tested.

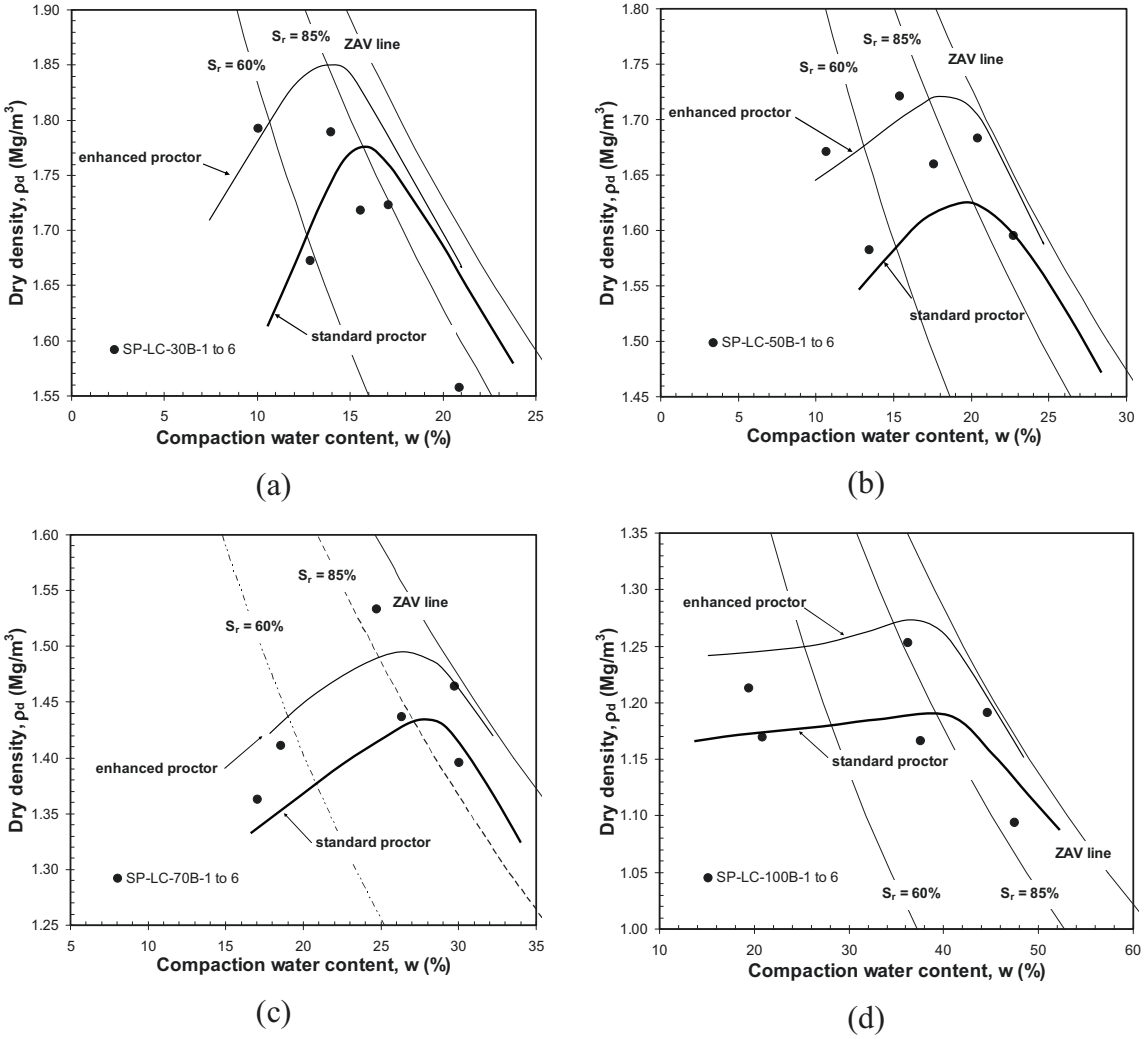

Figure 7.14 Data points corresponding to the specimens used in one-step constant volume swelling pressure tests: (a) 30/70 bentonite-sand mixture; (b) 50/50 bentonite-sand mixture; (c) 70/30 bentonite-sand mixture; and (d) pure bentonite

Table 7.3 Initial conditions of the heavily compacted specimens used in the swelling pressure tests

Specimen code*	Initial conditions				Remarks
	Bentonite content (%)	Water content (%)	Void ratio	Suction (kPa)	
SP-HC-50B-1	50	9.98	0.310	22700§	One-step
SP-HC-50B-2	50	9.00	0.320	22700§	One-step
SP-HC-50B-3	50	9.04	0.287	22700§	Multi-step, VET
SP-HC-50B-4	50	9.29	0.298	22700§	Multi-step, ATT
SP-HC-50B-5	50	9.05	0.295	22700§	Multi-step, VET
SP-HC-50B-6	50	9.25	0.319	22700§	Multi-step, VET
SP-HC-50B-7	50	9.10	0.289	22700§	Multi-step, ATT
SP-HC-50B-8	50	9.50	0.290	22700§	1-D swell, One-step
SP-HC-50B-9	50	9.42	0.285	22700§	1-D swell, One-step
SP-HC-50B-10	50	9.37	0.281	22700§	1-D swell, One-step
SP-HC-100B-1	100	21.05	0.672	15243‡	Multi-step, VET
SP-HC-100B-2	100	19.89	0.687	20508‡	Multi-step, ATT
SP-HC-100B-3	100	21.05	0.672	15243‡	Oven-dried, Multi-step, VET

* LC means lightly compacted specimen and HC means heavily compacted specimen
§ the as-prepared suction
‡ computed from the total suction versus bentonite water content relationship (see Chapter 8)

The suction path followed by specimens SP-LC-30B-1 to 6, SP-LC-50B-1 to 6, SP-LC-70B-1 to 6, SP-LC-100B-1 to 6, and SP-HC-50B 1 to 2 was simple and only involved one-step saturation (i.e., the one-step constant volume swelling pressure tests). The following figure shows the suction paths planned for the test on specimens SP-HC-50B-3 to 10 and SP-HC-100B-1 to 3.

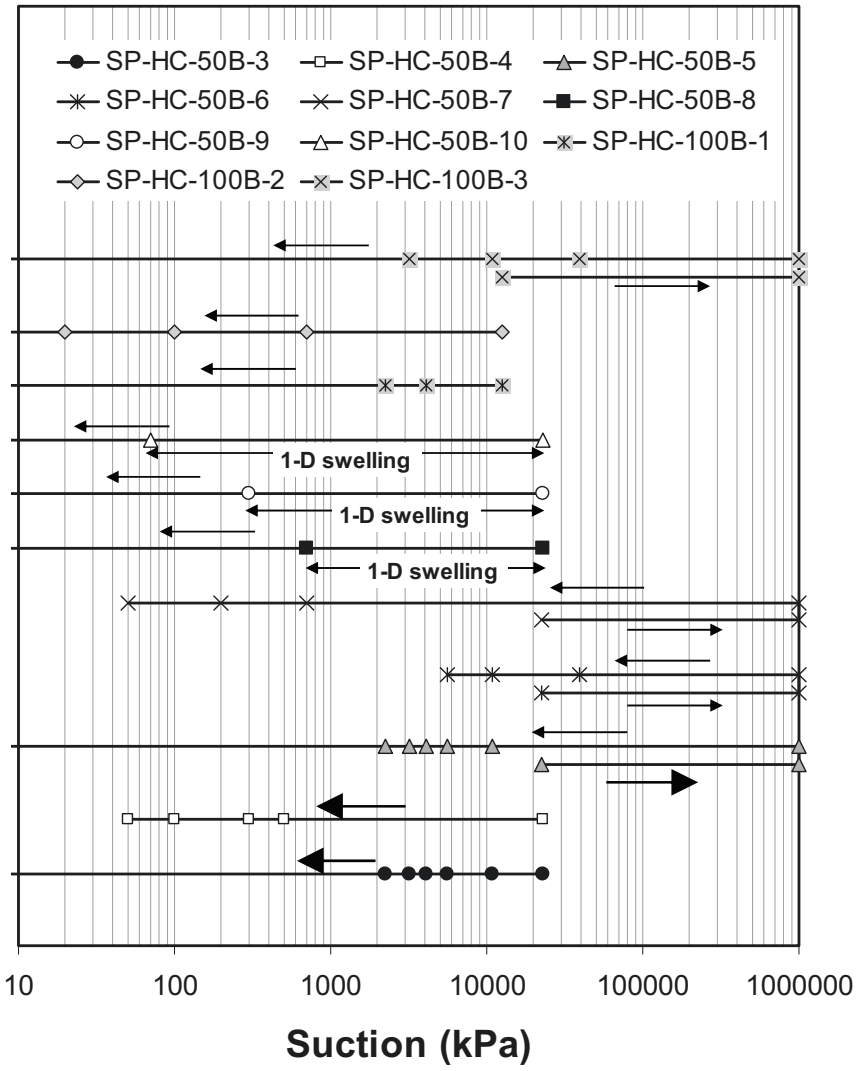

Figure 7.15 Suction paths planned for the swelling pressure test on specimens SP-HC-50B-3 to 10 and SP-HC-100B-1 to 3

7.4.1 Description of the Equipment Used

The one-step swelling pressure test was conducted using the Barcelona constant volume cell (Figure 7.16) that was developed at the Technical University of Barcelona (or UPC) Spain. The equipment mainly consists of a pedestal, a threaded top part with a top cap and a load cell. The pedestal is exchangeable that makes it possible to perform tests using the water circulation, axis-translation, and vapour equilibrium techniques. The pedestal used for the ATT was designed to have a grooved water compartment where a high-air entry ceramic disk is seated flushed and glued. The grooves are 3-mm wide and 1.5-mm deep and form a spiral. The ceramic disk used has an air entry value of 1500 kPa. The top cap has a corrosion resistant metal porous disk. The cell is equipped with an

Erlenmeyer flask and an air pump to circulate water vapour through the specimen bottom and top boundaries.

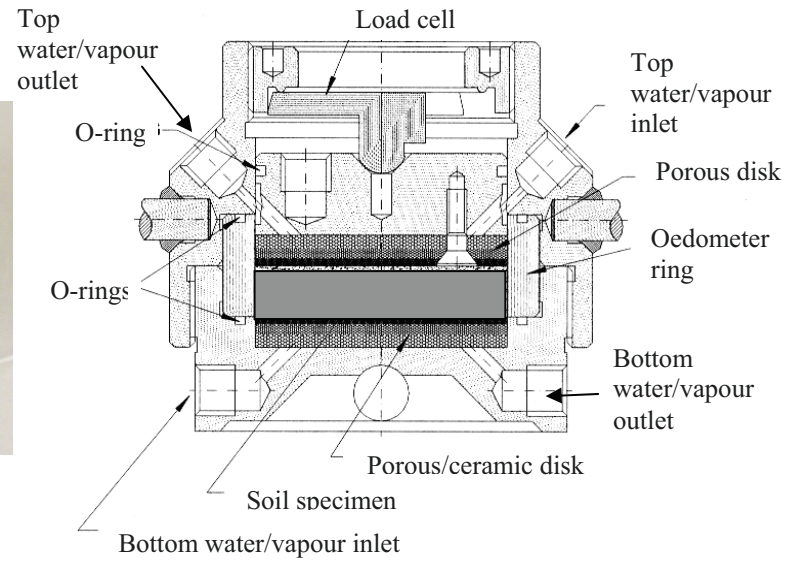

(a) (b)

(c)

Figure 7.16 The UPC Barcelona constant volume cell: (a) photo, (b) schematic drawing, and (c) components of the cell

The swelling pressure was measured using a load cell which consists of four strain gauges (full bridge configuration) attached to a steel plate. The readings were taken using a precision voltmeter (type 189 from Fluke) that measures excitation voltage resulting from small deformations of the strain gauges. The equipment used in the swell-under-load (SUL) and swell-load (SL) tests was a pneumatic oedometer and description of the equipment is given in Subchapter 7.5.

7.4.2 Verification of the Equipment Used

Four constant volume cells were used in this study. Prior to experiment, the deformability of four cells used was examined by pressurising the cells (with the load cells installed) with air. The cells were subjected to increasing and decreasing air pressures while the deformations were recorded using linear vertical displacement transducers (LVDT). The following figure shows vertical deformation of the cells as a function of applied air pressure.

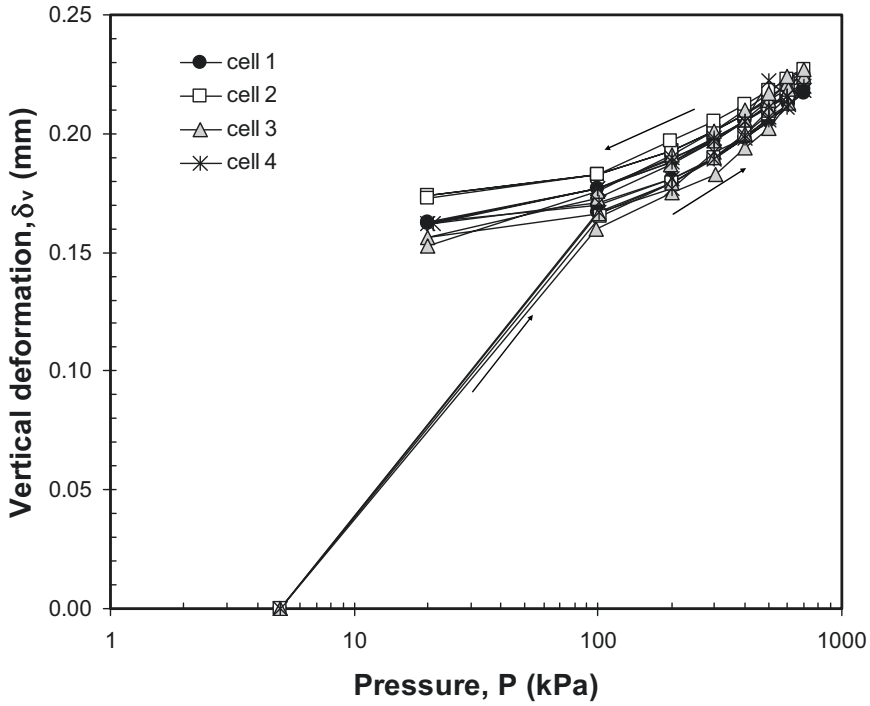

Figure 7.17 Deformation of the four UPC Barcelona constant volume cells as a function of applied air pressure

The calibration constant of each load cell was also checked regularly. It was foreseen that the load cells might deteriorate with time. In some cases, it was found that the calibration constants of the load cells changed significantly, particularly after the cells were used to measure swelling pressures greater than 2000 kPa. One of the load cells (i.e., that in Cell 4) was found to break down. The load cell was replaced with a new load cell with the same configuration and recalibration was carried out.

7.4.3 Experimental Techniques and Procedures

7.4.3.1 One-Step Constant Volume Swelling Pressure Test using Water Circulation Method

The test started by placing the specimen in the cell. The inner wall of the specimen ring was lubricated to minimise ring friction. The ring friction effects are thought to be pronounced in bentonites (or clay soils) due to the exerted swelling pressures. Olson (1986) suggested that the ring friction effects could be estimated by taking an assumption that the wall friction angle was equal to 90% of the drained friction angle of the specimen. The magnitude of the ring friction also depends on the height to diameter ratio of the specimen tested (or the specimen's ring used). The load cell was fixed such that the top porous disk was just in contact with the specimen without inducing significant pressure to the specimen. In the water circulation method, the total suction of the specimen was reduced in one step from its initial value to zero. Distilled deaired water was circulated through the bottom and top boundaries of the specimen. The arrangement of the water saturation method is shown in Figure 7.18. The bottom water outlet was connected to the top water inlet using a nylon tube. The top water outlet was connected with a two-way valve for flushing purpose. Distilled deaired water flowed from the bottom water inlet where it was supplied through the nylon tube and finally came out of the cell via the top water outlet. The procedures flushed the air bubbles that came out of the specimen as a result of internal swelling of the specimen (i.e., self-sealing effect). The flushing was performed regularly. The porous disk was ensured to be always fully filled with water by observing the water outflow during flushing. The porous disk was assumed to be free of air bubbles when no air bubbles were observed to come out of the top water outlet during flushing.

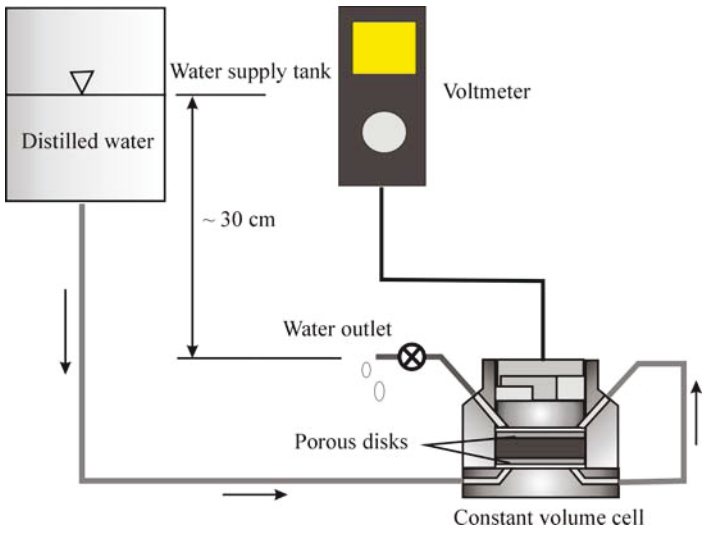

Figure 7.18 Schematic drawing of experimental setup for the one-step swelling pressure measurement using water circulation method

The specimen tested absorbed water as a result of water potential gradient induced by the total suction of the specimen tested. Swelling pressure reading was taken during flushing to minimise the effect of additional pressure caused by the water column. The entire cell was weighed after each swelling pressure reading. The weight of the entire cell was measured using a precision weighing balance to the nearest 0.01 g. The equilibrium was deemed based on the development of swelling pressure and the amount of absorbed water with time.

The final water content of the specimen was measured to determine the degree of saturation of the specimen at the end of test. It is important to remove water in the porous disk before dismantling the specimen. The release of swelling pressure during dismantling decreases water potential of the specimen. The water potential of the specimen will have a value which is lower than that of the distilled water. Accordingly, there will be a rapid water movement from the wet porous disk to the specimen during the dismantling process. Water was first removed from the porous disk by blowing it with fresh air. A correction to account for water in the porous disk is required in the computation of the absorbed water versus time curve. The final mass of the specimen together with the mass of empty cell and the final mass of the entire cell (i.e., the cell together with the specimen before dismantling) were used to compute the correction factor for the absorbed water.

7.4.3.2 Multi-Step Swelling Pressure Test using Axis-Translation Technique

The axis-translation technique (ATT) was used to investigate the change in swelling pressure with decreasing matric suction. For this purpose, the pedestal with a high air-entry ceramic disk was used. The bottom water inlet was connected to a water supply at a constant height of 30 cm to the bottom water outlet. Therefore, a constant water pressure of 3 kPa was maintained throughout the experiment. The bottom water outlet is connected to a two-way valve for flushing purpose. The 3-kPa constant water pressure was used to flush the water compartment. Air pressure was applied using an air pressure controller (i.e., a stepper motor) that could deliver a constant air pressure with 1 kPa accuracy.

Procedures similar to those adopted in the water saturation technique were used for placing the specimen in the cell. Specimens SP-HC-50B- 7 and SP-HC-100B-3 had a diameter less than the ring diameter since they were oven-dried prior to multi-step swelling pressure test. A stiff plastic sheet was used to fill the gap between the specimen and the ring such that no or minimum radial expansion of the specimen could be expected. The stiff plastic sheet in contact with the specimen was lubricated to minimise friction between the specimen and the plastic sheet. The water compartment was filled with water prior to experiment. Air pressure was applied to the specimen through the top air pressure inlet (i.e., the top water/vapour pressure inlet Figure 7.16(b)). Flushing was performed regularly to remove air bubbles that were collected in the water compartment as a result of air diffusion through the soil specimen and the saturated ceramic disk. The

measurement of swelling pressure and the weight of the specimen were performed according to the procedures similar to those adopted in the one-step swelling pressure test. Water content of each specimen after the test was also measured and the amount of absorbed water for each suction decrement was back-calculated.

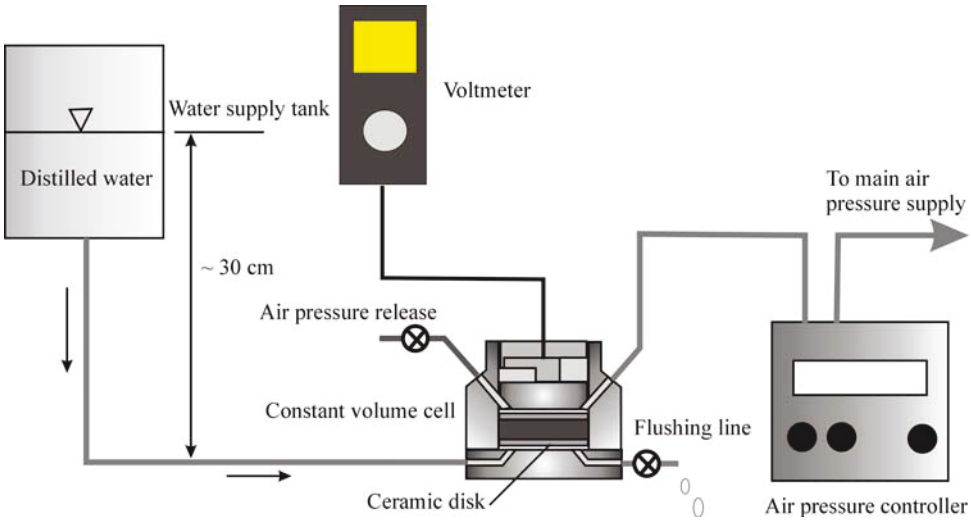

Figure 7.19 Schematic drawing of experimental setup for the multi-step swelling pressure test using axis-translation technique

7.4.3.3 Multi-Step Swelling Pressure Test using Vapour Equilibrium Technique

The vapour equilibrium technique (VET) was used in the multi-step swelling pressure test where total suction of the specimen tested was reduced by changing the relative humidity of the specimen's pore space. The use of VET in the swelling pressure test was limited to a total suction value of 2000 kPa. The multi-step swelling pressure test using VET was performed in the styrofoam box that could maintain a constant temperature of 22^{o}C ± 0.5^{o}C (Figure 7.20). The test commenced with preparing salt solution. Only sodium chloride (NaCl) solution was used in the test. The salt solution was prepared one day before each test. The salt solution in the Erlenmeyer flask was thermally equilibrated in the styrofoam box in order to have a thermal stability. The specimen was subsequently placed in the cell with the same procedures as in the one-step swelling pressure test. Vapour above the salt solution in the Erlenmeyer flask was circulated through the bottom and top boundaries of the specimen using an air pump. Specimens SP-HC-50B-5 and 6 which were oven-dried prior to test were placed in the swelling pressure cells in a similar way to specimens SP-HC-50B-7 and SP-HC-100B-3 that were tested using the ATT from the oven-dried conditions.

The pedestal with porous disk was used which was similar to that used in the one-step swelling pressure test. Measurement of swelling pressure was performed using the precise voltmeter. The tubes connecting the constant volume cell with the pump and the Erlenmeyer flask were disconnected before taking the mass of entire cell (i.e., the cell

with the specimen). The temperature sensor hung in the styrofoam box was meant for observing possible fluctuations in room temperature where the test was conducted. Severe fluctuations of room temperature may induce excessive water vapour condensation on the specimen since the styrofoam box used was not really a thermally-insulated box. The influence of excessive condensation on the development of swelling pressure has been reported in Agus and Schanz (2004).

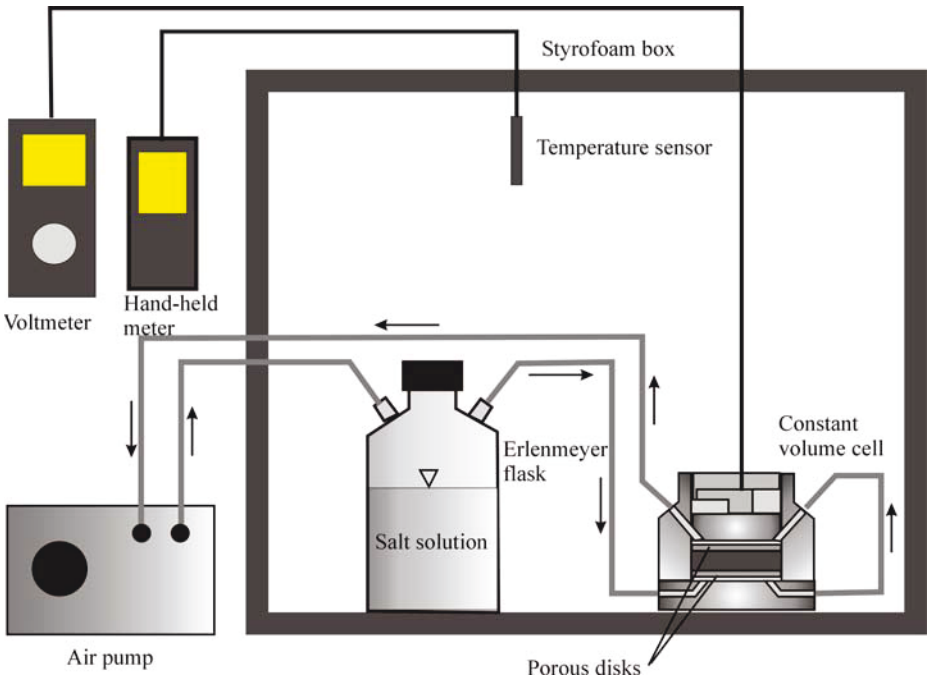

Figure 7.20 Schematic drawing of experimental setup for the multi-step swelling pressure test using vapour equilibrium technique

7.4.3.4 One-Step Swelling Pressure Test by Means of Swelling-Under-Load Test

A series swell-under-load (SUL) tests for swelling pressure measurement were performed using a UPC Barcelona pneumatic oedometer system (see Subchapter 7.5) for the description). Several heavily compacted 50/50 bentonite-sand mixture specimens at the as-prepared state were subjected to different net vertical stresses in the oedometer cell. Distilled deaired water was introduced to the specimens by circulating it through the bottom and top boundaries of the specimens (i.e., the water circulation method). The specimens swelled depending on the magnitude of net vertical stress applied. The deformation of the specimens was measured using a dial gauge with a least count of 0.001 mm until reaching equilibrium.

7.4.3.5 One-Step Swelling Pressure Test by Means of Swell-Load Test

The swell-load (SL) test was performed on an as-prepared specimen (i.e., specimen SL-1) using the UPC Barcelona pneumatic oedometer system. The test was performed

only on one specimen. The test was conducted by first allowing the specimen to swell when it was in contact with distilled water under a 50 kPa net vertical stress. Distilled water was circulated through the bottom and top boundaries of the specimen (i.e., the water circulation method). The specimen was subsequently loaded in a similar manner to the conventional oedometer test procedures. The deformation of the specimen during experiment was measured periodically using a dial gauge with a least count of 0.001 mm until no significant deformation was observed.

7.5 One-Dimensional Compression-Rebound, and One-Dimensional Cyclic Wetting-Drying Tests

The compression and rebound tests were performed on several heavily compacted 50/50 bentonite-sand mixture specimens. The following table summarises the initial conditions of specimens used.

Table 7.4 Initial conditions of the heavily compacted specimens used in the one-dimensional compression-rebound and one-dimensional cyclic wetting-drying tests

Specimen code*	Initial conditions				Remarks
	Bentonite content (%)	Water content (%)	Void ratio	Suction (kPa)	
SL-1	50	9.51	0.283	22700§	SL test
SUL-1	50	9.51	0.283	22700§	SUL test
SUL-2	50	8.50	0.287	22700§	SUL test
SUL-3	50	8.60	0.275	22700§	SUL test
SUL-4	50	9.01	0.299	22700§	SUL test
SUL-5	50	9.36	0.288	22700§	SUL test
SUL-6	50	8.90	0.305	22700§	SUL test
CR-1	50	9.11	0.288	22700§	Saturated CR test, high vertical stresses
CR-2	50	9.14	0.292	22700§	Unsaturated CR test, high vertical stresses
CR-3	50	8.90	0.288	22700§	Unsaturated CR test, high vertical stresses
Cyclic-1	50	8.85	0.301	22700§	1-D cyclic DW test, low vertical stresses
Cyclic-2	50	9.00	0.305	22700§	1-D cyclic DW test, low vertical stresses

* 'SL' means swell-load test, 'SUL' means swell-under-load test, 'CR' means compression-rebound test, 'Cyclic' means one-dimensional cyclic wetting-drying test

§ the as-prepared suction

7.5.1 Description of the Equipments Used

The one-dimensional compression-rebound tests in the low range of net vertical stresses and cyclic wetting drying tests were conducted using a pneumatic oedometer system (Figure 7.21) that was developed at the Technical University of Barcelona (or UPC), Spain. The equipment mainly consists of a pedestal screwed to a bottom part, a middle and a top part, a rubber membrane with a screwed top cap, and a dial gauge with a least count of 0.001 mm. The pedestal and top cap each has a corrosion resistant metal porous disk. The top cap has a doubling system which enables the pneumatically applied vertical load to be doubled. This is because the cross-sectional area of part of the top cap in contact with the rubber membrane is double of that in contact with the soil specimen. The cell is also equipped with an Erlenmeyer flask and an air pump to circulate water vapour through the bottom and top boundaries of the specimen. The system can be used to test soil specimens with a diameter of 50 mm and a varying height between 10 mm and 20 mm.

The compression-rebound tests in the high net vertical stress range were performed using a Weimar high pressure oedometer cell (Figure 7.22) (Schanz and Tripathy, 2003). The cell consists of a bottom part with a stainless steel porous disk, a middle part, and a top part where a load cell and a top cap with a stainless steel porous disk are attached. The load cell is capable of measuring 50 kN load which is equivalent to a pressure of 25000 kPa (the diameter of specimen tested is 50 mm). The load cell is equipped with a hand-held digital display for vertical pressure reading. The cell is instrumented with a dial gauge with a least count of 0.001 mm which is attached to the loading rod of the cell.

7.5.2 Verification of the Equipments Used

Prior to use, deformability of both the UPC Barcelona pneumatic oedometer system and the Weimar high pressure oedometer system during loading and unloading were verified. Correction to account for the oedometer system deformability is required for stiff soils (Fredlund and Rahardjo, 1993) such as the compacted bentonite-sand specimens tested in this investigation. The verification was carried out using a dummy stainless steel specimen. The stainless steel specimen was placed in the oedometer cells with two dry filter papers (i.e., each on the top and bottom of the dummy specimen). When a real soil specimen is saturated, the filter papers used will be wet and therefore dummy tests were also performed with wet filter papers. The dummy stainless steel specimen with the filter papers was subjected to increasing and decreasing vertical pressure in the oedometer test system. Figure 7.23(a) and Figure 7.23(b) shows the deformation characteristic of the UPC pneumatic oedometer system and the Weimar high pressure oedometer system, respectively. The deformation characteristic of the systems was used to give correction to the compression-rebound and 1-D cyclic wetting-drying test results.

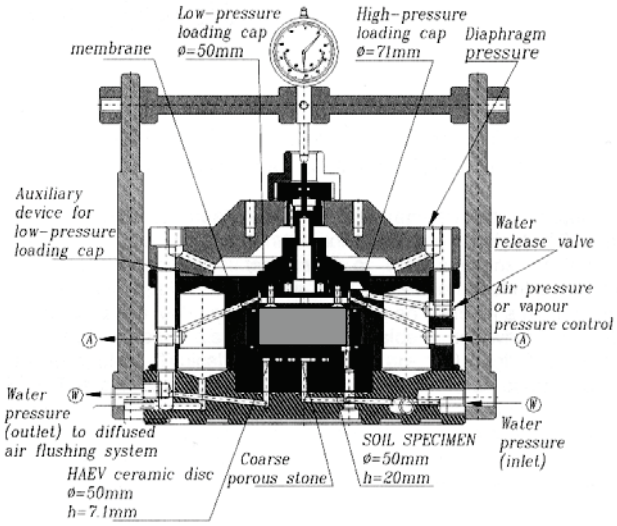

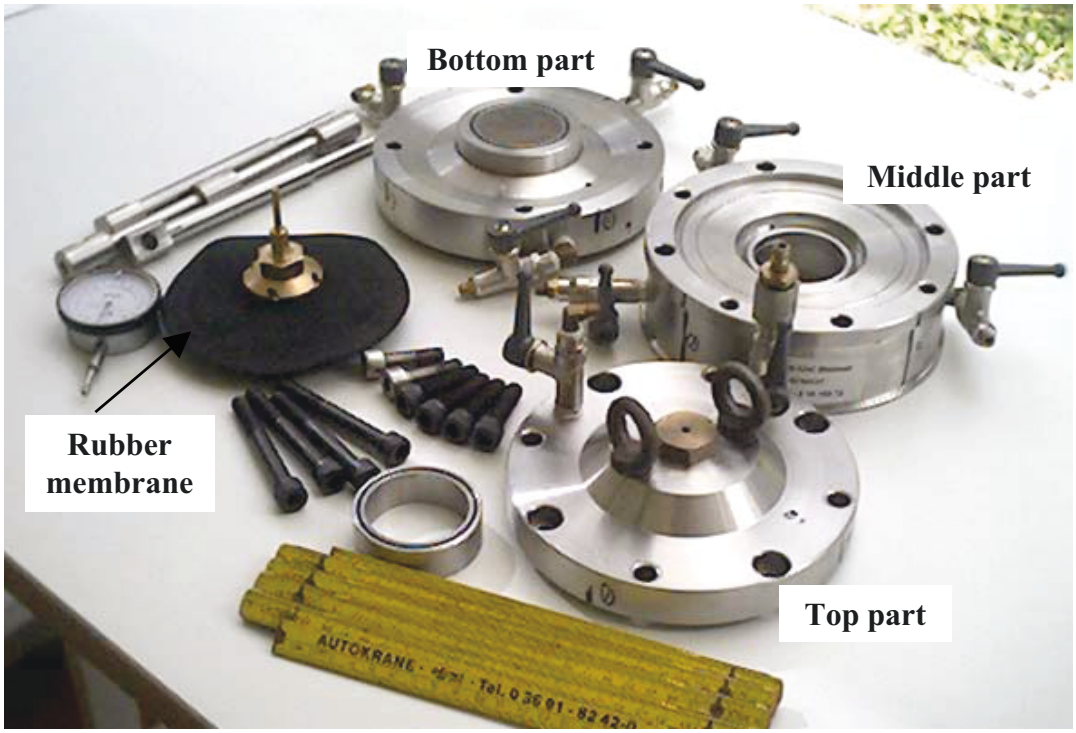

Figure 7.21 The UPC Barcelona pneumatic oedometer cell: (a) photo, (b) schematic drawing, and (c) components of the cell

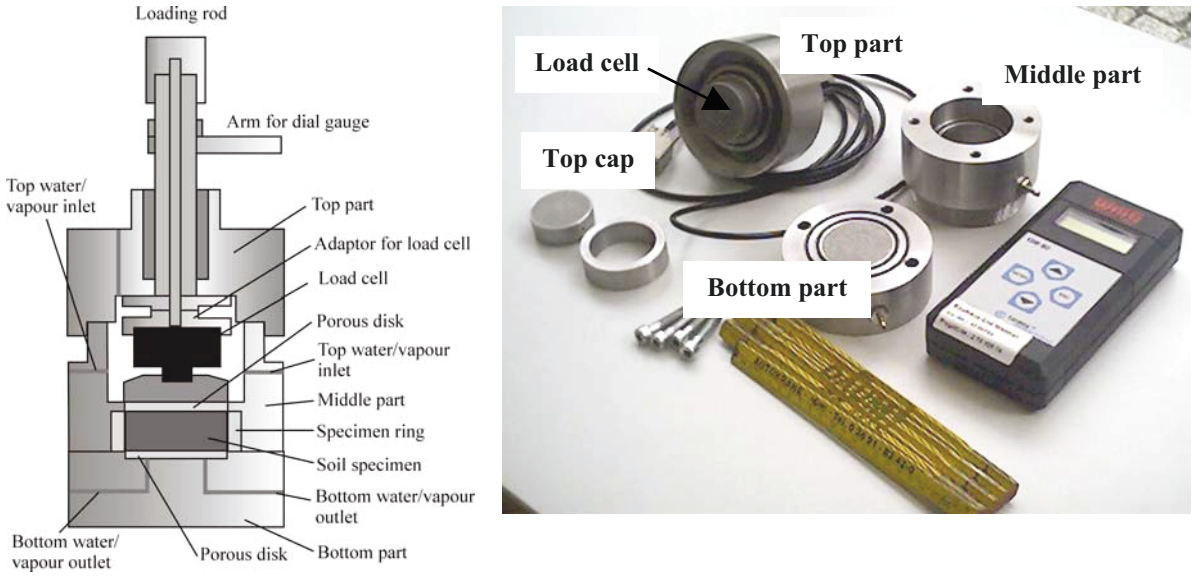

Figure 7.22 The Weimar high pressure oedometer cell (Schanz and Tripathy, 2003): (a) schematic drawing and (b) components of the cell

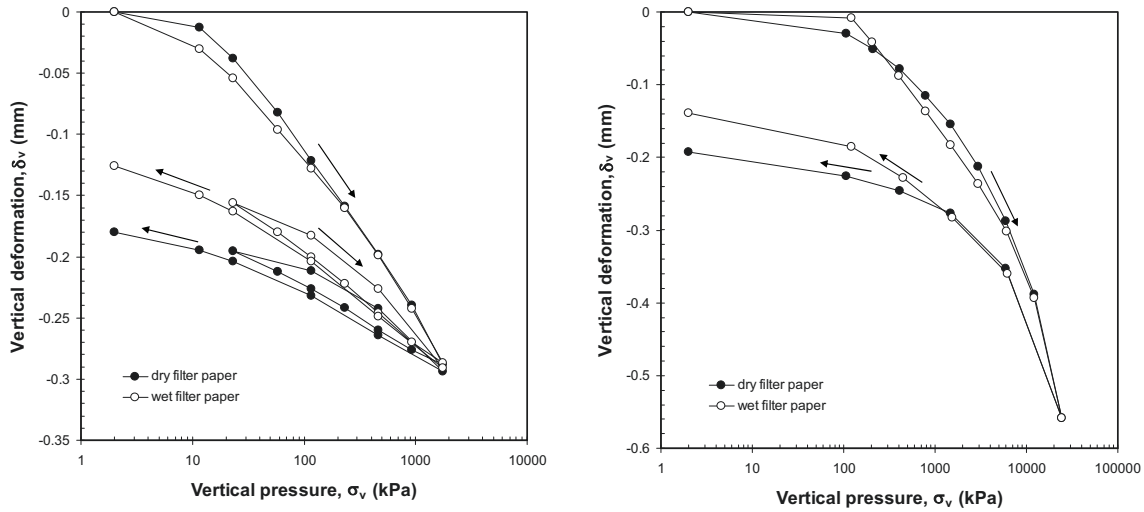

Figure 7.23 Deformability of: (a) the UPC Barcelona pneumatic oedometer system and (b) the Weimar high pressure oedometer system

7.5.3 Experimental Techniques and Procedures

7.5.3.1 Saturated Compression-Rebound Tests for Low Range of Net Vertical Stresses

The saturated compression-rebound tests described in this subchapter include the swell-under-load (SUL) and swell-load (SL) tests meant for measuring swelling pressure of the as-prepared specimen. Procedures adopted in the SUL and SL tests have been

described in Subchapter 7.4.3.4 and 7.4.3.5, respectively. In the SL test, only one specimen was tested (i.e., denoted as specimen SL-1 in Table 7.4) while six specimens were used in the SUL test (i.e., denoted as specimen SUL-1 to SUL-6 in Table 7.4). The stress and suction paths followed in the tests on specimens SL-1 and SUL-1 to SUL-6 are shown in Figure 7.24 and Figure 7.25, respectively.

The soil specimen (with filter papers) was placed in the UPC pneumatic oedometer system and the oedometer system was arranged in accordance with the arrangement shown in Figure 7.26. To minimise ring friction, the inner wall of the specimen ring was lubricated. Distilled deaired water was supplied to the bottom boundary of the soil specimen and was circulated through the bottom and top boundaries of the specimen. Vertical stress was applied to the specimen through an air pressure controller. The magnitude of air pressure used was half the targeted vertical pressure since the system has a pressure doubling system. Flushing in a similar way to that adopted in the one-step constant volume swelling pressure tests was performed in a regular basis. Readings were taken regularly until no significant change in deformation of the specimen was noted.

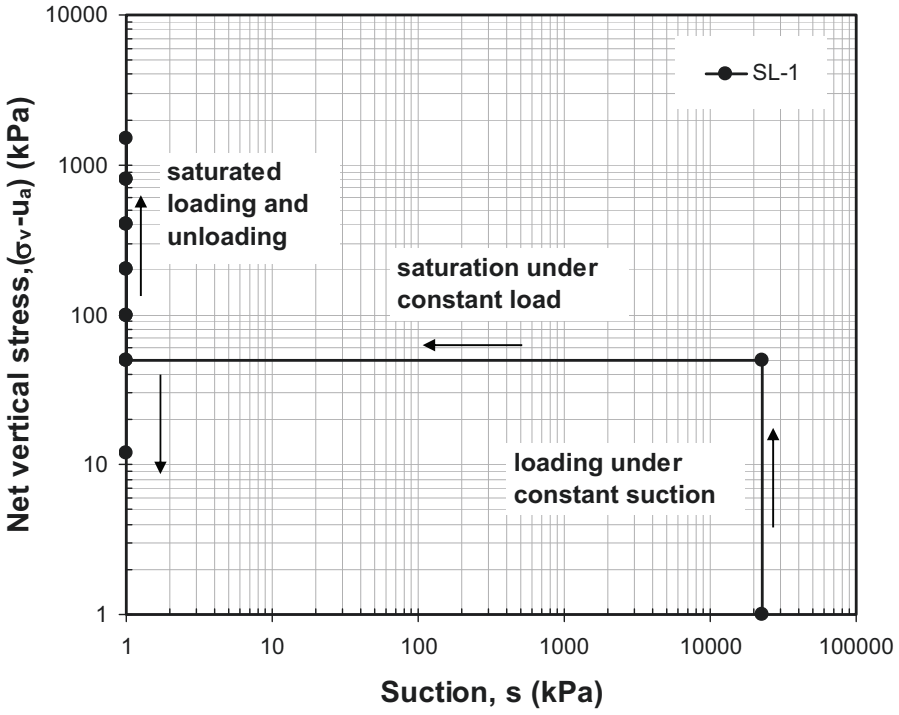

Figure 7.24 Stress and suction paths planned for the tests on specimen SL-1

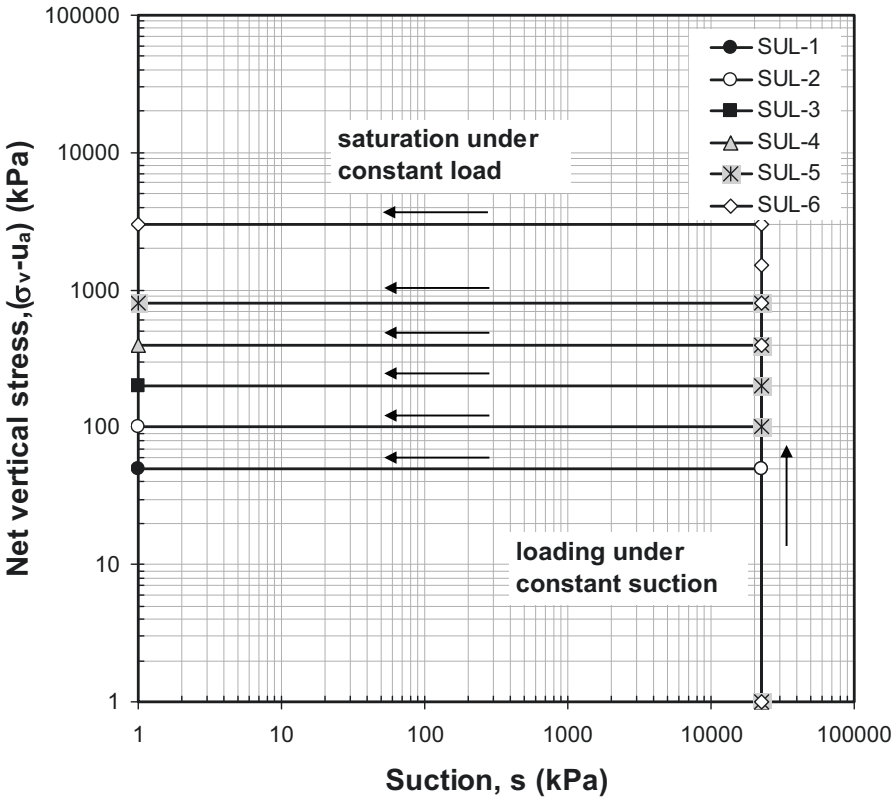

Figure 7.25 Stress and suction paths planned for the tests on specimens SUL-1 to SUL-6

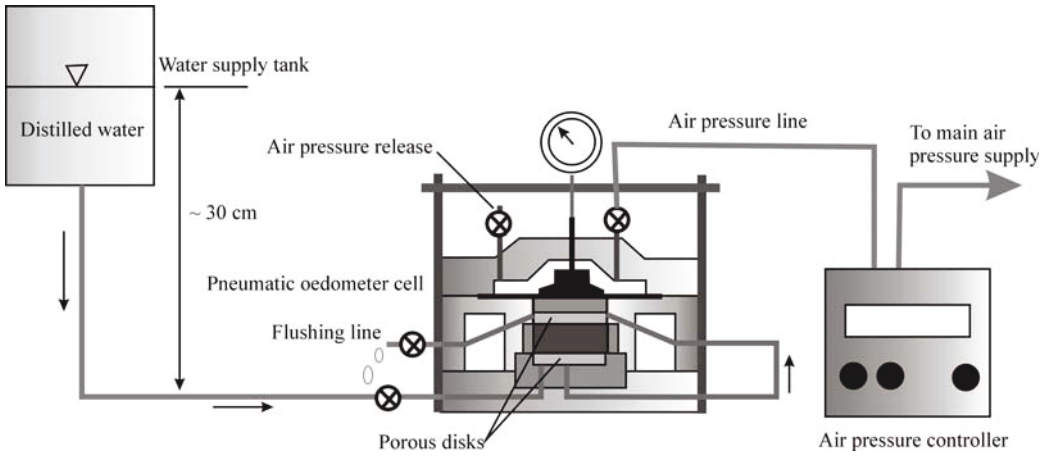

Figure 7.26 Schematic drawing of experimental setup of the saturated compression and rebound test for low range of net vertical stresses

7.5.3.2 Compression-Rebound Tests for High Range of Net Vertical Stresses

Procedures of placing specimen in the compression-rebound test for high range of vertical stresses were basically similar to those used in the test in the low range of vertical stresses. The difference lies on the way vertical stress was applied. In the test using the Weimar high pressure oedometer system, loading was applied to the specimen

mechanically through a loading frame (Figure 7.27). The loading frame was capable of delivering loads up to 100 kN. The loading system was controlled through a personal computer. Three specimens (i.e., specimens CR-1 to CR-3 in Table 7.4) were tested for the compression-rebound characteristics in the high vertical stress range using the Weimar high pressure oedometer system. Figure 7.28 shows the stress and suction paths planned in the tests.

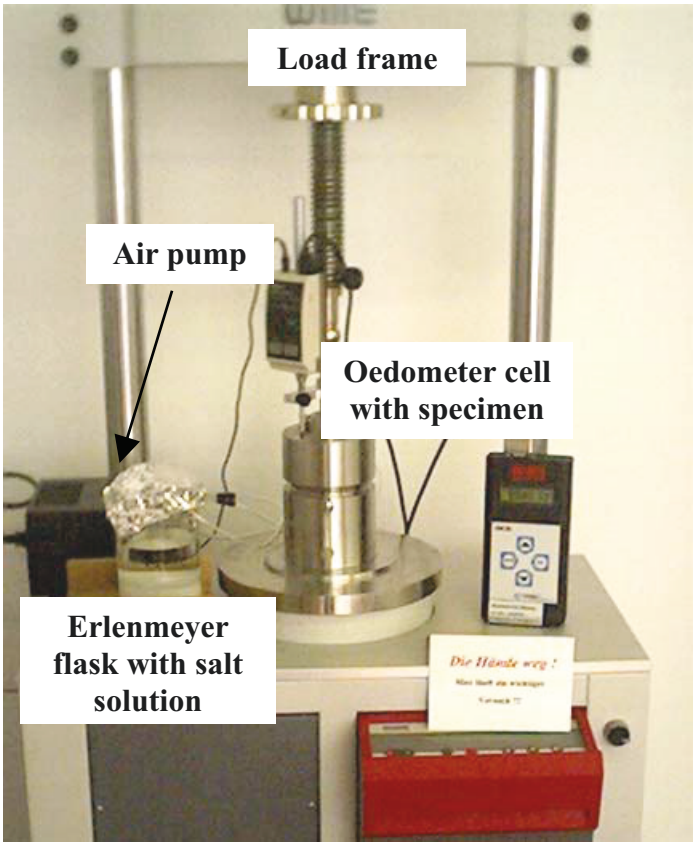

Figure 7.27 Arrangement of the compression and rebound test for high range of net vertical stresses

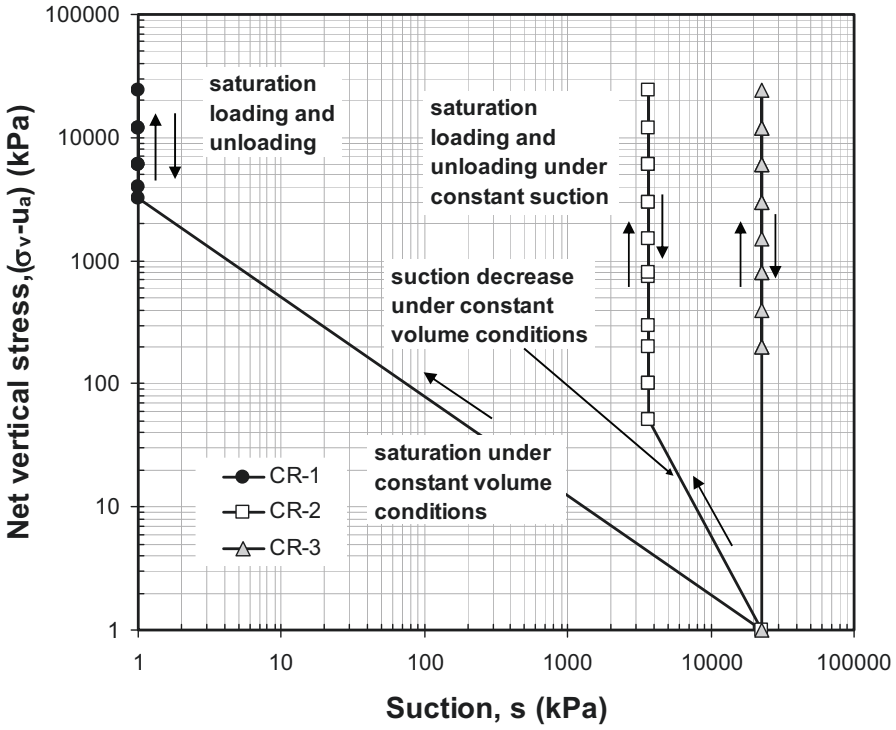

Figure 7.28 Stress and suction paths planned for the test on specimens CR-1 to CR-3

The specimen (with filter papers) was placed in the cell. The inner wall of the specimen ring was lubricated to minimise the ring friction effects. The cell (with the specimen and filter papers) was subsequently set in the loading frame. Specimen CR-1 was loaded after it was saturated with distilled deaired water under constant volume conditions (i.e., swelling pressure test) and therefore the test is referred to as swelling-pressure-compression-rebound test. The test on specimen CR-2 can also be called the swelling-pressure-compression-rebound test since the specimen was equilibrated to 3700 kPa total suction, which was lower than the initial total suction of the specimen, using saturated K_2SO_4 solution (i.e., VET) under constant volume conditions. The compression and rebound test on specimen CR-3 was performed under as-prepared conditions. The results of three tests performed will be used in the subsequent chapters to discuss the alteration of material behaviour from elastic to plastic behaviour. It was already anticipated that the transition might occur at a particular suction by which the axis-translation technique (ATT) should be used (i.e., lower than 1500 kPa). However, at its present form, the Weimar high pressure oedometer cell is not capable to be used for tests using the ATT.

In the test on specimen CR-1, the water circulation method in the same way as used in the one-step constant volume swelling pressure test was adopted. After swelling pressure was fully developed, the compression-rebound test was started. In the test on

specimen CR-2, water vapour above saturated K_2SO_4 solution in a flask was circulated through the bottom and top boundaries of the specimen.

7.5.3.3 One-Dimensional Cyclic Wetting-Drying Tests under Low Net Vertical Stresses

The one-dimensional (1-D) cyclic wetting-drying tests under low net vertical stresses were carried out on two heavily compacted 50/50 bentonite-sand mixture specimens (i.e., specimens Cyclic-1 and Cyclic-2 in Table 7.4). The tests were performed in the UPC pneumatic oedometer system. The experimental setup is schematically shown in Figure 7.29. The procedures of placing the specimen in the oedometer cell were similar to those used in the saturated compression-rebound tests. The test on specimen Cyclic-1 was performed under a targeted net vertical stress of 200 kPa while the test on specimen Cyclic-2 was carried out under a targeted net vertical stress of 1500 kPa. Figure 7.30(a) and Figure 7.30(b) shows the stress and suction paths planned for the test on specimen Cylic-1 and Cyclic-2, respectively.

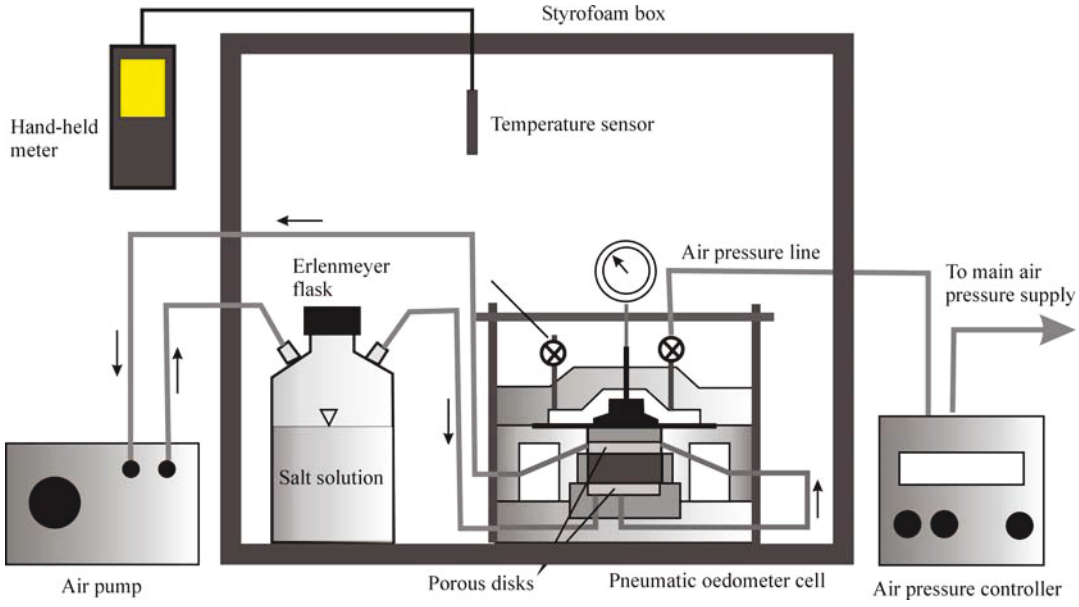

Figure 7.29 Schematic drawing of experimental setup for the cyclic wetting and drying test under low net vertical stress

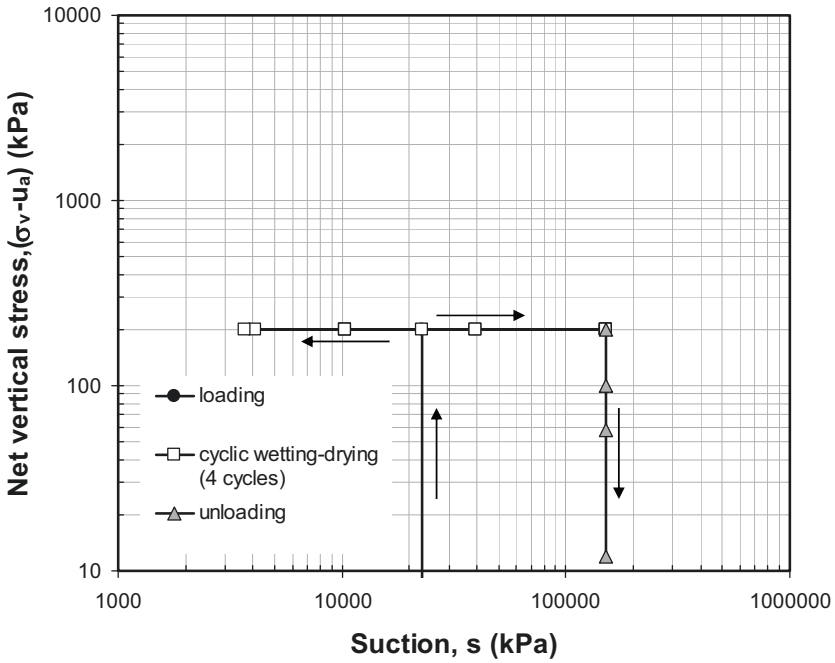

(a)

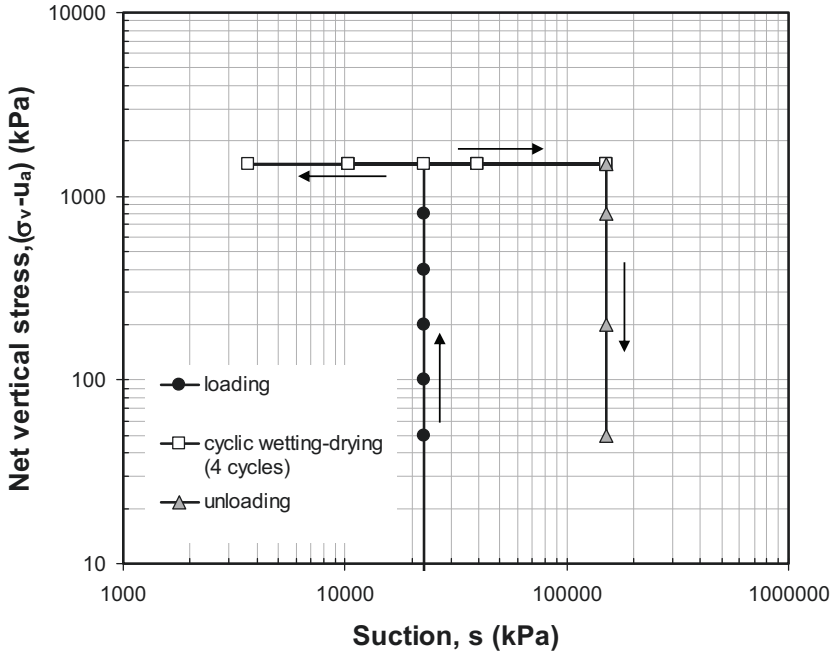

(b)

Figure 7.30 Stress and suction paths planned for the test on: (a) specimen Cyclic-1 (200 kPa net vertical stress) and (b) specimen Cyclic-2 (1500 kPa net vertical stress)

Total suction was control during wetting and drying under constant net vertical stress using salt solution (i.e., VET). Water vapour above salt solution in an Erlenmeyer flask was circulated through the bottom and top boundaries of the specimen using an air

pump in a similar manner to the procedures adopted in the multi-step swelling pressure test using the VET. Vertical stress was delivered to the specimen through an air pressure controller. The styrofoam box was also used to minimise room temperature fluctuations that might occur during experiment. The temperature sensor placed in the styrofoam box served the same function as that in the multi-step swelling pressure test using the VET. The equilibrium conditions of each suction increment or decrement were judged based on the dial gauge readings.

7.6 Saturated Permeability Test

The saturated permeability test was performed only on five compacted specimens of 30/70 bentonite-sand mixture. The specimens used in the test were basically specimens SP-LC-30B-1 to 5 that were also tested in the one-step swelling pressure tests. The test was performed in accordance with the rigid-walled constant-head method (DIN, 1987 and ASTM, 1997). At the end of swelling pressure test on each specimen, the specimen (still in the UPC constant volume cell) was subjected to a maximum pressure gradient as high as the measured swelling pressure of the specimen in order to avoid side-wall leakage. Water inflow and outflow were monitored using a burette attached to the influent and effluent ends of the specimen. The test was terminated after steady-state flow occurred indicated when the water inflow rate was equal to the water outflow rate.

CHAPTER 8

SUCTION MEASUREMENT RESULTS

8.1 General

In this chapter, results of suction measurements that were performed using four different techniques are presented and discussed. The discussion brought out in this chapter includes comparison of the results from different techniques used, error in the measurements, effect of density, and comparison between matric and total suction measured for the compacted specimens.

8.2 Comparison of the Different Techniques Used for Measuring Total Suction

Figure 8.1(a) to Figure 8.1(d) show a comparison of results of the four different techniques adopted in this study for measuring total suction. The filter paper measurement data were computed from the filter paper water content using Equation (7.2). The total suction data obtained using the filter paper technique in the low total suction range (i.e., below 2000 kPa) were computed by extrapolating the filter paper total suction calibration curve (shown in Figure 7.2) to the lower total suction range using Equation (7.2). The psychrometer measurement data were computed from the measurement of electromotive force using the calibration data as tabulated in Table 7.1.

The data points obtained for the standard proctor densities are not distinguishable from those obtained for the enhanced proctor specimens. The fact signifies the insignificant influence of compaction on the magnitude of total suction of the compacted bentonite-sand mixtures investigated. It is also depicted in the figures (Figure 8.1(b) to Figure 8.1(d)) that the filter paper total suction measurement results of the dynamically compacted specimens are essentially the same as those of the statically compacted specimens. It will later be shown that even total suction of a loose specimen of a mixture largely has the same magnitude as that of a compacted specimen of the same mixture provided both have the same water content. The best-fit curve for each technique has been obtained by fitting Equation (8.1) to the corresponding experimental data. The equation has a similar form to that used in the filter paper calibration curves (see Chapter 7) and is based on the Fredlund and Xing (1994) SWCC equation for soils.

$$s_t = a\left[\exp\left(\frac{b}{w}\right)^c - \exp(1)\right]^d \qquad (8.1)$$

where s_t is total suction, w is the compaction water content, and a (kPa), b (%), c, and d are the fitting parameters.

The value of a, b, c, and d for each technique and each mixture and the goodness of fitting parameters (i.e., the coefficient of determination and the standard error of estimate) are summarised in Table 8.1.

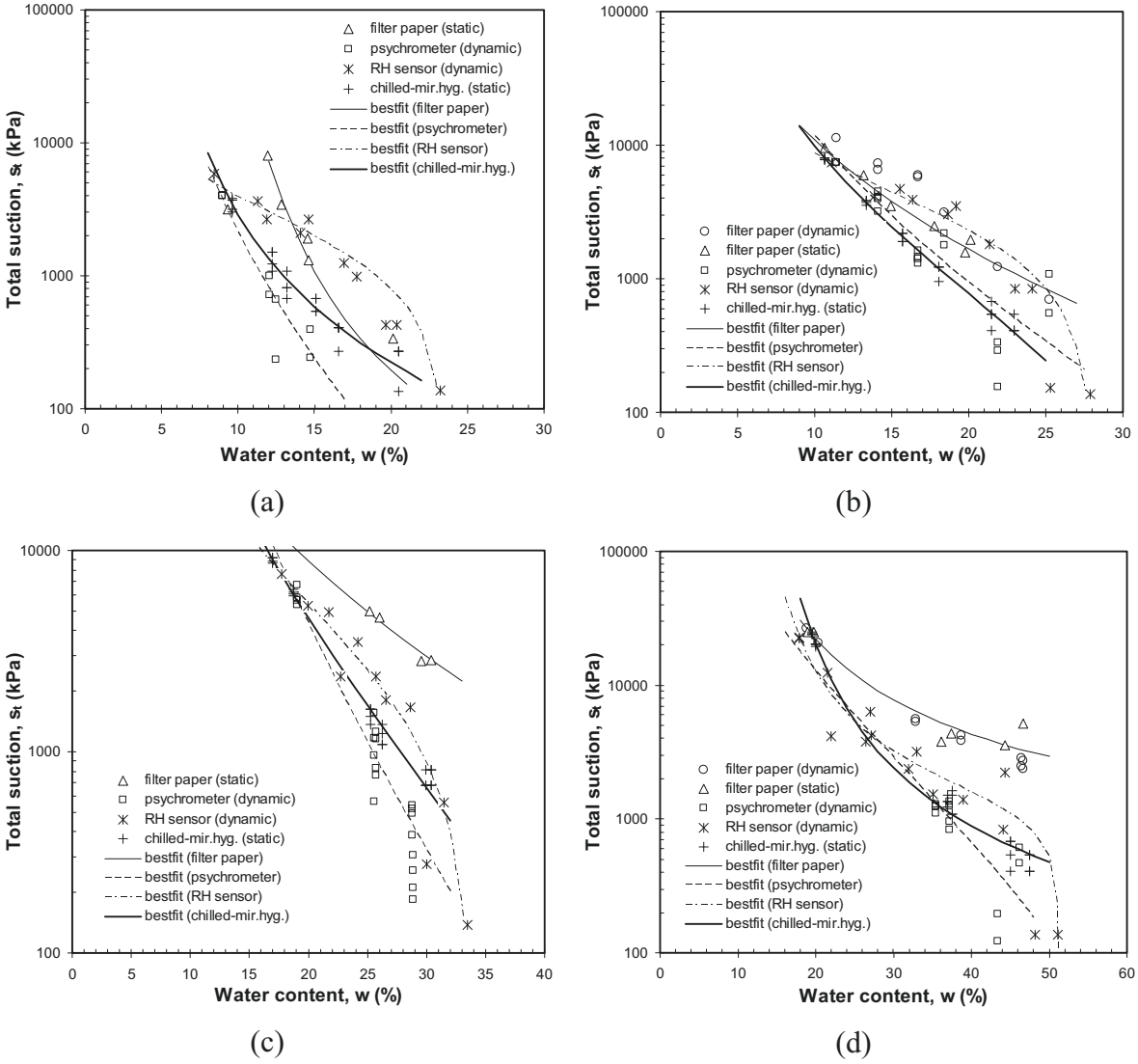

Figure 8.1 Comparison of the results obtained from the four different techniques used for measuring total suction of compacted specimens of: (a) 30/70; (b) 50/50; (c) 70/30 bentonite-sand mixtures; and (d) pure bentonite

The psychrometer method seems to exhibit the largest scatter particularly in the low total suction range. The possible causes of this are the insensitivity of psychrometers due to temperature effect when used for measuring low total suctions (Ridley and Wray, 1996), the accuracy of reading device used (i.e., HR-33T), and sensor-to-sensor differences. Further analyses of Table 8.1 indicate that the chilled-mirror hygrometer

technique, in most cases, has the highest coefficient of determination (r^2) with the lowest value of standard error of estimate (*SEE*). The facts support the earlier hypothesis that the equipment possesses the best accuracy among the four techniques used (see Chapter 7). Therefore, the chilled-mirror hygrometer technique is further used as benchmark to assess the performance of three other techniques adopted in the investigation for measuring total suction of the bentonite-sand mixtures.

Table 8.1 Fitting and goodness of fitting parameters of the four total suction measurement techniques

Mixture*	Technique§	Fitting parameter				Statistics‡	
		a (kPa)	*b* (%)	*c*	*d*	r^2	*SEE*
30B/70S	FP	12	80.00	1.280	0.550	0.983	789
	PSY	327	292.51	0.090	12.743	0.997	136
	RH	2717	23.47	0.449	1.000	0.972	368
	CMH	14	61.63	0.790	1.281	0.971	203
50B/50S	FP	2641	228.85	0.105	5.528	0.990	496
	PSY	31897	91.86	0.107	5.513	0.947	583
	RH	3351	27.86	0.568	0.802	0.944	644
	CMH	457	36.85	0.544	1.929	0.998	130
70B/30S	FP	7160	253.20	0.111	4.786	0.998	266
	PSY	141225	117.02	0.111	8.326	0.978	351
	RH	2598	33.74	0.884	0.941	0.945	662
	CMH	413	52.18	0.575	0.225	0.997	187
100B	FP	353	344.61	0.790	0.535	0.980	2384
	PSY	347142	77.83	0.098	3.765	0.761	273
	RH	1152	51.16	1.934	0.389	0.952	1838
	CMH	141	92.04	1.377	0.608	0.999	363

* 'B' refers to bentonite and 'S' refers to sand
§ 'FP' means filter paper method, 'PSY' means psychrometer technique, 'RH" means RH sensor, and 'CMH' means chilled-mirror hygrometer technique
‡ r^2 is the coefficient of determination and *SEE* is the standard error of estimate

Figure 8.1 indicates that except in the case of compacted specimens of 50/50 bentonite-sand mixture, the psychrometer technique consistently measured lower total suction compared to the chilled-mirror hygrometer. By excluding the potential equipment errors causing the scatter in psychrometer technique, the lower psychrometer results may be due to possible excessive condensation of water vapour on the measuring junction of the psychrometers (Ridley and Wray, 1996). Theoretically, a dissipation of condensed water takes place when the psychrometer is heated prior to measurement. However, the condensed water may not be fully dissipated into the soil specimen tested. Therefore, re-condensation may still take place on the thermocouple mount or on the inner wall of the psychrometer cup. The amount of undissipated condensed water vapour is a function of relative humidity (*RH*) of the vapour space in the soil specimen (or measured total suction) and the equilibration period of psychrometer.

It is also depicted in the figure that the total suction measurement results obtained by the RH sensor exhibits a different trend. In the low total suction range, measured total suction decreased rapidly with increasing water content. The activated warming function of the RH sensor heated the vapour space in the specimen generating a temperature gradient between the vapour space where the measurement was conducted and the pore space in the soil. This occurred when measuring high *RH* values or low total suctions.

8.3 Error of the Total Suction Measurements

Errors of total suction measurements can generally be divided into three categories:

1. Errors which are induced by inaccuracy of the equipment (or sensor) used. This type of error can mostly be found in the filter paper and psychrometer techniques.

2. Errors due to an isothermal non-equilibrium between the vapour space, the soil, and the sensor used. This type of error can be found in the filter paper (when the size of vapour space is not minimised) and in the total suction measurement using the RH sensor.

3. Errors due to an excessive condensation of water vapour on the measuring device as a result of rapid temperature fluctuations. The excessive condensation causes a drop in the temperature of water vapour in the vapour space and therefore this type of error can also be regarded as an isothermal non-equilibrium in the measuring system. This type of error can be found in the psychrometer technique.

The temperature gradient existed in the total suction measurements via psychrometer and RH sensor can be estimated by taking the chilled-mirror hygrometer reading as benchmark. The estimated temperature gradients that existed in the total suction measurements using the psychrometer and RH sensor are shown in Figure 8.2(a) and Figure 8.2(b), respectively. The estimated temperature gradients in the psychrometer total suction measurement are negative in the low total suction range indicating possible excessive water vapour condensations. On the other hand, the estimated temperature gradients that existed when measuring total suction using the RH sensor are positive almost in the whole range of total suction measured.

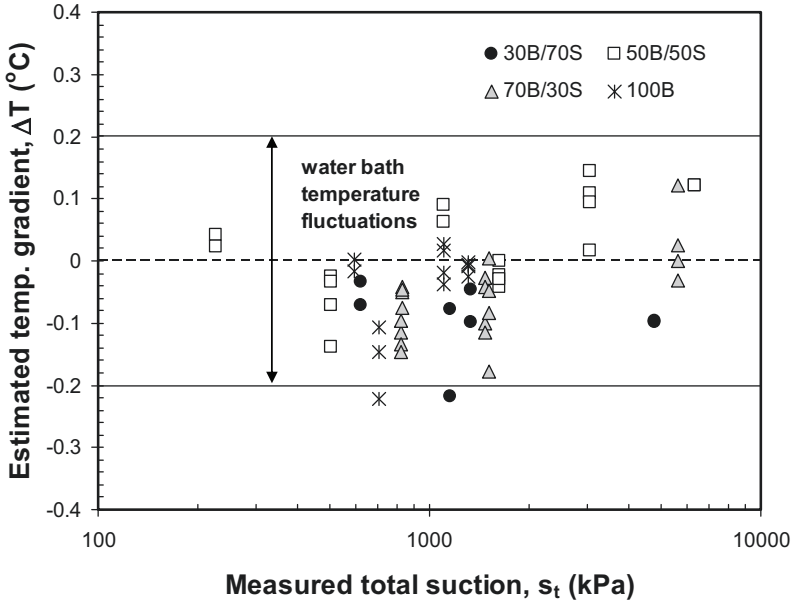

(a)

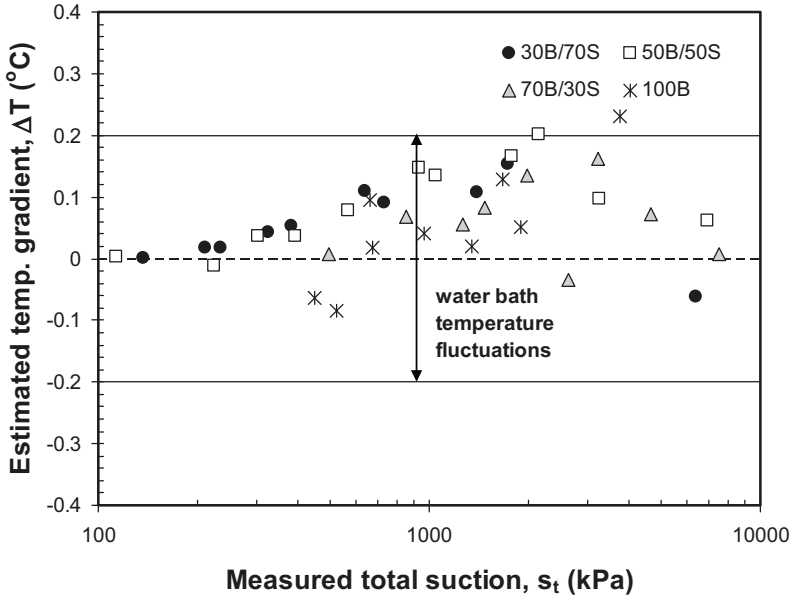

(b)

Figure 8.2 Estimated temperature gradient in total suction measurements using: (a) psychrometer technique and (b) RH sensor

The suction measurement error can be inferred from the estimated temperature gradient using Equation (5.2). The inferred total suction error is shown in Figure 8.3(a) and Figure 8.3(b) for the psychrometer technique and RH sensor, respectively. The psychrometer technique seems to exhibit lower errors in the measurement compared to the RH sensor. Despite the more obvious scatter in the psychrometer measurement

results, the technique offers better accuracies mainly in the low total suction range (i.e., below 1000 kPa).

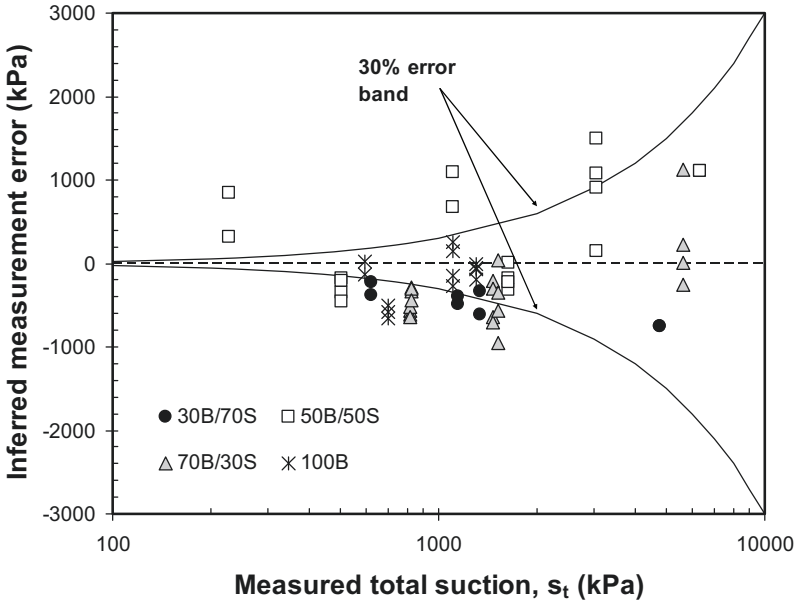

(a)

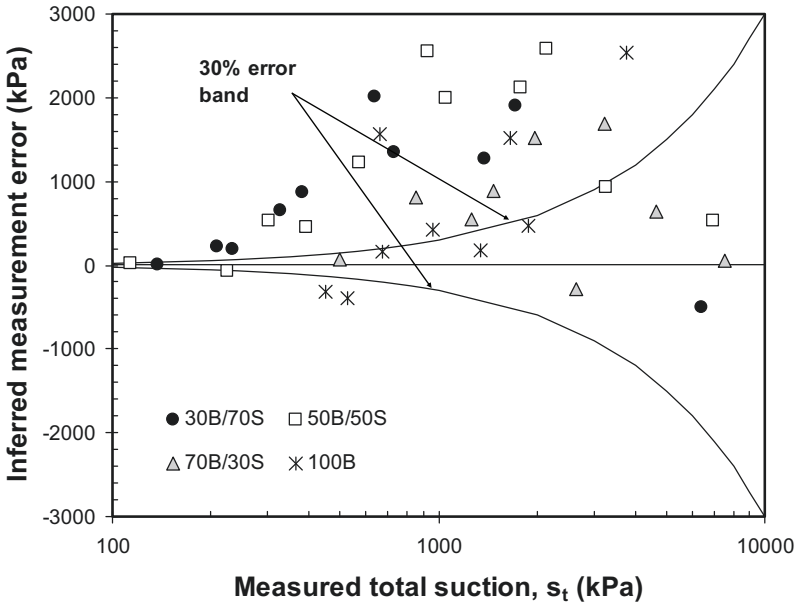

(b)

Figure 8.3 Inferred total suction measurement error: (a) psychrometer technique and (b) RH sensor

8.4 Hydration Effect on the Total Suction Measurement

Figure 8.4(a) to Figure 8.4(d) shows a comparison between total suction measured by the filter paper method and that measured by the chilled-mirror hygrometer technique.

The results obtained clearly indicate a systematic difference with higher total suctions being determined by the filter paper method. It is believed that the accuracy the two methods is comparable since the filter paper was equilibrated in a narrow vapour space above the soil specimen and the fluctuation in temperature was minimised by immersion in the water bath. The difference in results obtained by the two techniques is ascribed to hydration effect due to the difference in age of the specimens used in the filter paper method to those used in the chilled-mirror hygrometer technique. The hydration (or apparent aging) effect is due to internal redistribution of water (between the inter-layer, intra-, and inter-aggregate pores) and is thought to be significant in soils with double porosity structure such as expansive soils.

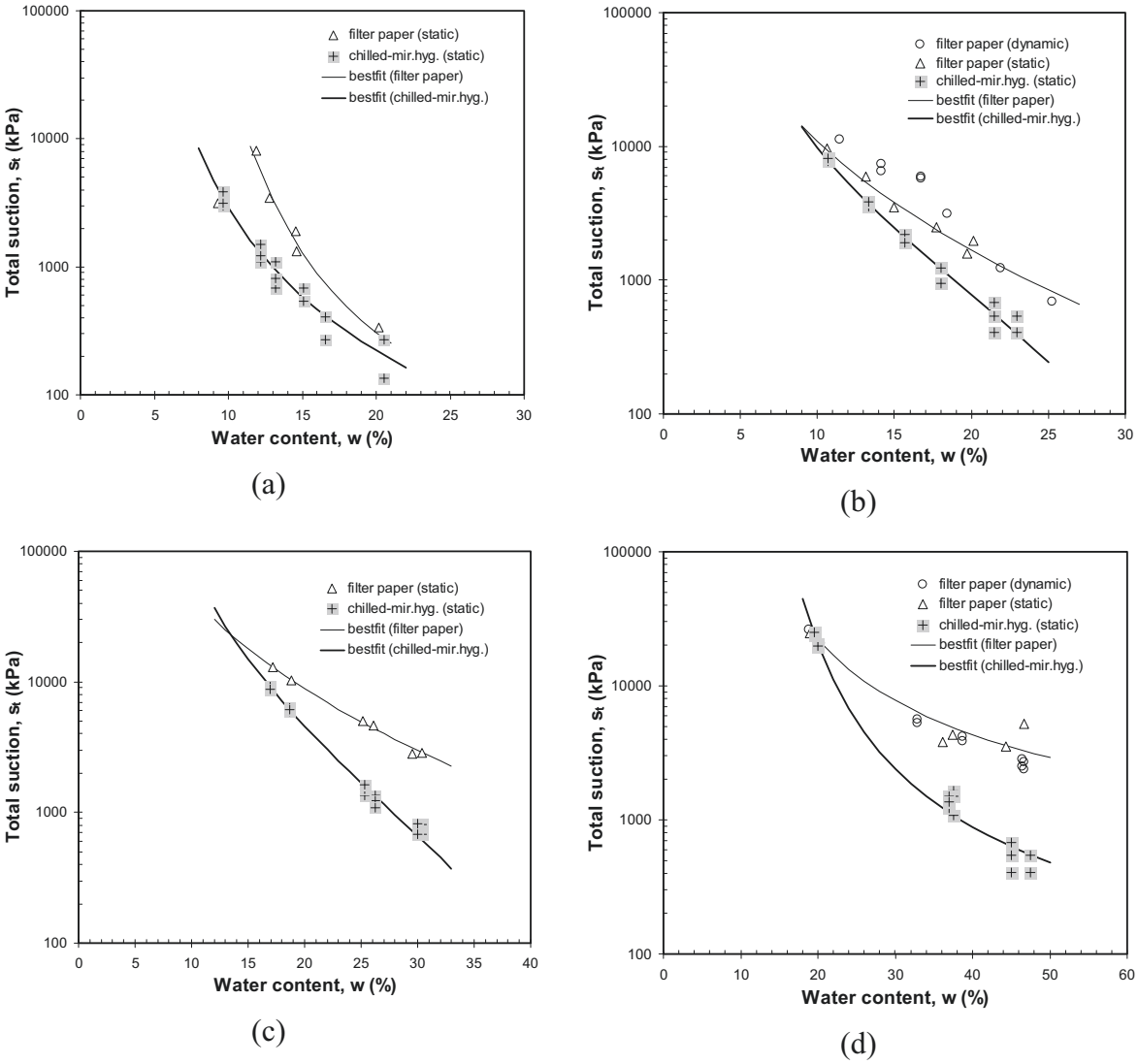

Figure 8.4 Comparison of the results of filter paper and chilled-mirror hygrometer total suction measurements of compacted specimens of: (a) 30/70; (b) 50/50; (c) 70/30 bentonite-sand mixtures; and (d) pure bentonite

Several additional tests were performed on several compacted specimens of 30/70 bentonite-sand mixture using the chilled-mirror hygrometer. The compacted specimens were first stored in air-tight containers for five weeks. Attempts in maintaining a constant temperature were made using the water bath in a similar manner to the filter paper total suction measurement procedures. It was expected that the specimens were subjected to the same conditions to those used in the filter paper total suction measurement with respect to their internal water content distribution. Figure 8.5 depicts the results of additional tests performed and it is shown that the results from both methods agree fairly well one to the other. It indicates that the difference in water content versus total suction curves of the specimens at two different conditions (i.e., the as-compacted and 'aged' conditions) was not due to different accuracies associated with the two methods. The difference can be ascribed to the internal redistribution of pore-water. The total suction measured by the chilled-mirror hygrometer (i.e., the as-compacted total suction) represents the total suction at a transient state. The internal redistribution of pore-water is believed to occur with time as a result of a difference in total suction (or total water potential) between the inter-aggregate, intra-aggregate, and intra-laminar pores at this state. The in-contact filter paper technique measures total suction at a quasi-equilibrium state after the internal redistribution of pore-water takes place.

The effects of aging on the behaviour of clay soils have also been studied with respect to swelling potential and swelling pressure (e.g., Subba Rao and Tripathy, 2003). The aging effects were found to decrease swelling potential and swelling pressure of clay and were more remarkable in the specimens with high water contents (Subba Rao and Tripathy, 2003). In the aging process, the fabrics of a clay specimen changes due to rearrangement of clay particles. During the internal water redistribution process (under constant void ratio and water content), there is an increase in intra-aggregate (or micro) void ratio while the inter-aggregate void ratio decreases. Since the total void ratio and water content of the specimen remain constant, the swelling pressure and swelling potential of the specimen are similar to that of the as-compacted specimen. The aging effects (i.e., due to the clay particle rearrangement and fabric changes) is thought to proceed after the internal water redistribution process.

The unbalanced force (or the non-uniform total suction distribution) between the inter-aggregate pores and the intra-aggregate and intra-laminar pores for each mixture can be inferred from Figure 8.4 using the best-fit equation (Equation (8.1)) with the fitting parameters as listed in Table 8.1. The inferred total suction difference between the as-compacted and quasi-equilibrium total suctions of the four mixtures is shown in Figure 8.6.

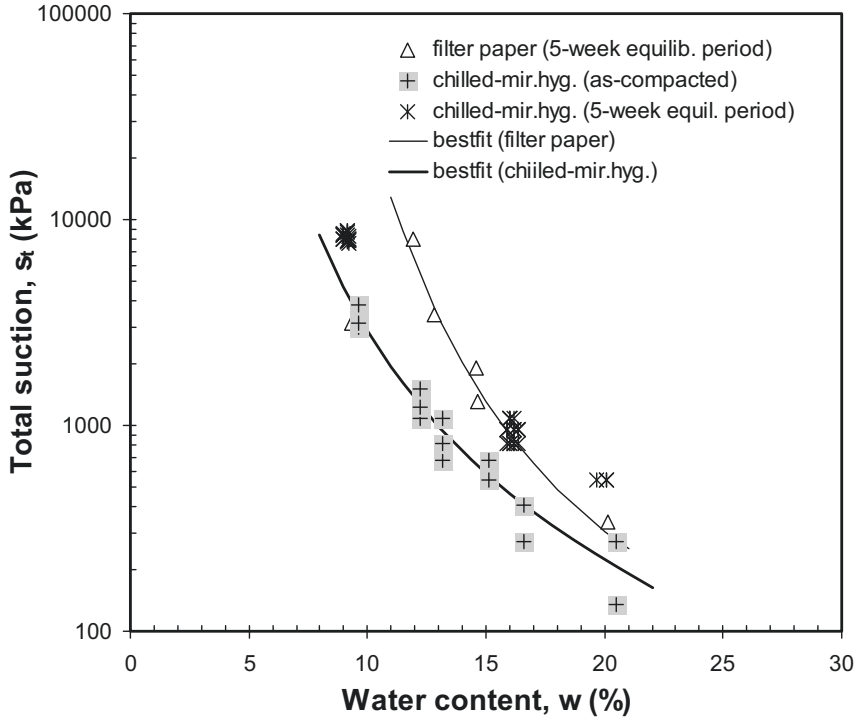

Figure 8.5 Comparison of total suction measurements on the as-compacted and 5-week aged compacted specimens of 30/70 bentonite-sand mixture

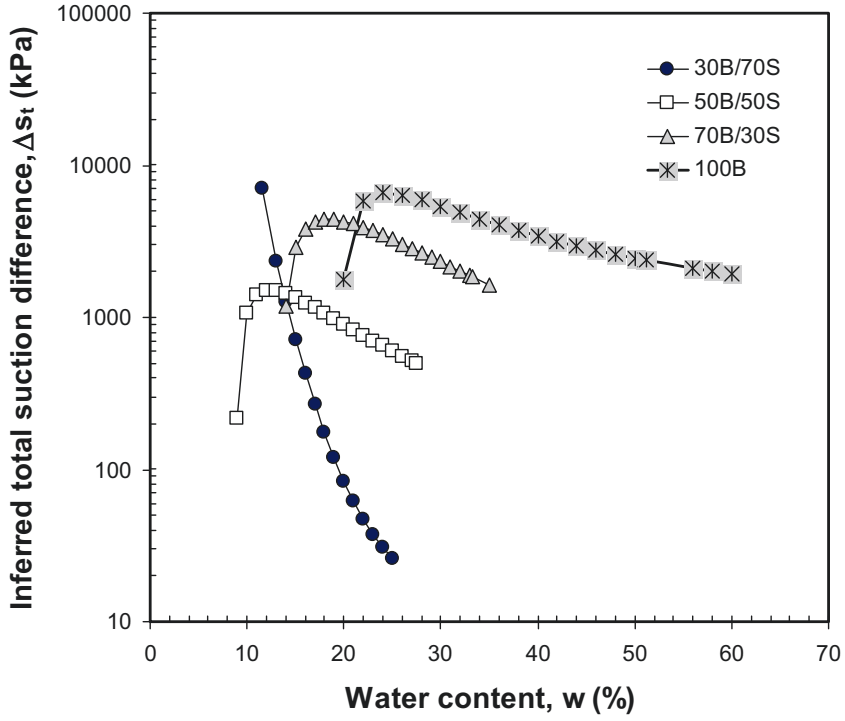

Figure 8.6 Inferred total suction difference due to the unbalance total suction (or total water potential) distribution in the different levels of pores

8.5 Total Suction of the Loose and Compacted Specimens

Figure 8.7 depicts a comparison between total suctions measured using the chilled-mirror hygrometer technique for the small-sized statically compacted specimens and those for the loose specimens (powder form) for the four bentonite-sand mixtures tested. The measurements of total suction on both the compacted and loose specimens were conducted at almost the same time. No effect of internal pore-water redistribution is thought to play a role. The figure shows that no significant impact of compaction is noted in the total suction versus water content curves obtained for the compacted and loose specimens. The results for a particular mixture essentially fall on a single curve. Total suction is shown to be primarily a function of water content and bentonite content. The higher the percentage of bentonite in the mixture, the higher will be the total suction for the same water content. The reason for this is that the bentonite minerals possess surface electric charges and at the same water content, a mixture with a higher percentage of bentonite has a greater osmotic and sorptive forces which are governed by the properties of bentonite. The consequence of this fact is that there appears to be an insignificant contribution of capillary action in the magnitude of total suction.

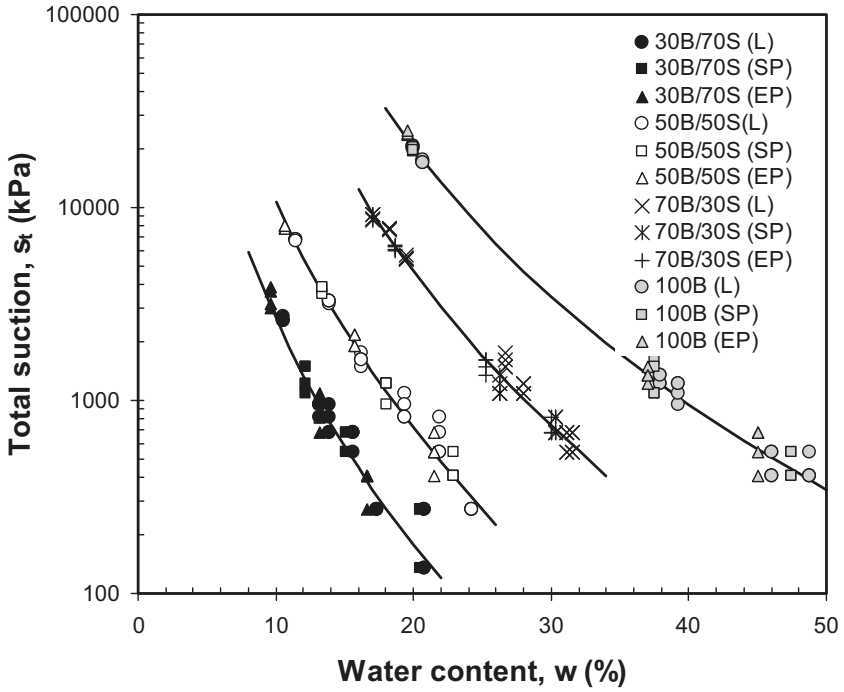

Figure 8.7 Total suction versus water content of the four mixtures at different states (Note: 'L' means loose state, 'SP' means compacted to standard proctor density, and 'EP' means compacted to enhanced proctor density)

Due to the much larger specific surface area of the bentonite compared to that of the sand, the amount of water required to cover the area a unit dry mass of bentonite is much

higher than that required to cover the area of a unit dry mass of sand. Thus, the added water during mixture preparation will mostly be absorbed by the bentonite even for mixtures with a small percentage of bentonite. Therefore, it is reasonable to assume that water is only absorbed by the bentonite and the mixture void ratio can be regarded to belong to bentonite or considered to be bentonite void ratio. Based on this assumption, the bentonite water content, w_b (%) can be computed according to Equation (8.2) with w_m (%) is the mixture water content and B (%) is the bentonite content in the mixture. The corresponding bentonite dry density, ρ_{db} (Mg/m^3) can be computed using Equation (8.3) with ρ_m (Mg/m^3) and G_{ss} is the mixture density and the specific gravity of the sand, respectively.

$$w_b = \frac{100\, w_m}{B} \tag{8.2}$$

$$\rho_{db} = \frac{(B/100)\, \rho_m G_{ss}}{G_{ss}(1 + w_m/100) - \rho_m(1 - B/100)} \tag{8.3}$$

The semi-logarithmic plot of total suction versus bentonite water content for the four bentonite-sand mixtures at the three different conditions (i.e., loose, standard proctor compacted, and enhanced proctor compacted states) is shown in Figure 8.8. The plot indicates that the suction versus water content curves for the four different mixtures as shown in Figure 8.7 appear to merge into a single curve. These results support the suggestion that total suction is strongly controlled by the mixture water content and the mixture bentonite content, or collectively is a function of bentonite water content.

The suction and water potential concepts, and the micro-structural view of suction as described in Chapter 3 provide explanations how the presence of bentonite can increase total suction (or total water potential) of the mixtures. The difference in the total suction for different mixtures (or bentonite contents) at the same mixture water content is believed to be due to the difference in the sum of osmotic suction and sorptive forces, whereas surface tension or capillary action has an insignificant influence.

Re-examination of Figure 3.6 shows that when the bentonite-sand mixture at a certain water content is compacted to a higher density, its degree of saturation increases. The increase in degree of saturation is caused by a reduction in the amount of air in the inter-aggregate pores. This phenomenon has also been found by Sridharan et al. (1971), Al-Mukhtar (1995), and recently by Romero et al. (1999). Compaction reduces the size of inter-aggregate pores, whereas the cation concentration of water in these pores remains unchanged. The unapparent change in total suction due to compaction indicates the insignificant contribution of capillary action in controlling the magnitude of total suction. Only if the specimen is further compressed so that some pore water gets squeezed out, will there possibly be apparent change in total suction due to a change in osmotic suction.

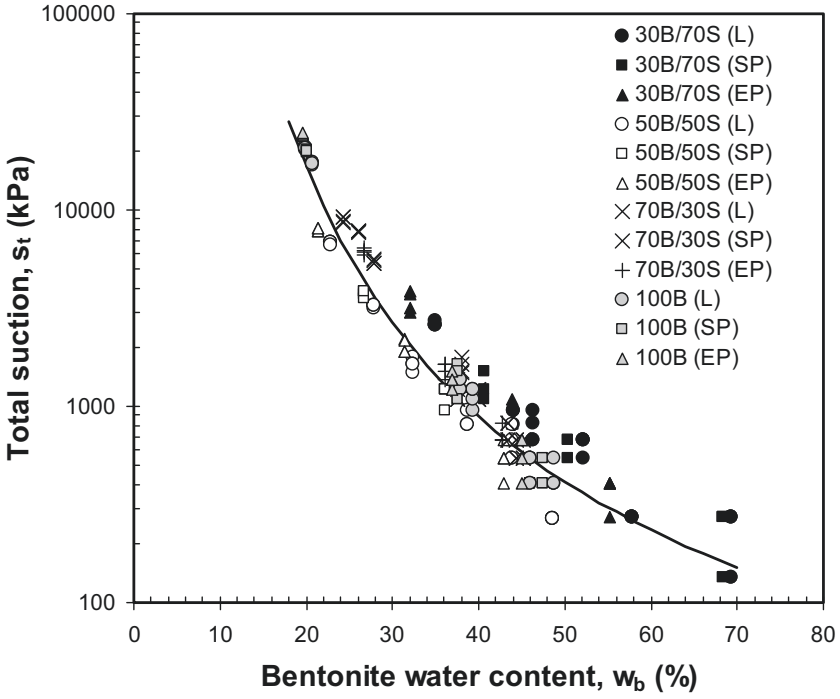

Figure 8.8 Total suction versus bentonite water content of the four mixtures at different states (Note: 'L' means loose state, 'SP' means compacted to standard proctor density, and 'EP' means compacted to enhanced proctor density)

The following best-fit equation can be used to express the relationship between bentonite water content in percent and total suction in kPa for the bentonite-sand mixtures tested. The equation has a coefficient of determination (r^2) of 0.952 with a standard error of estimate (*SEE*) of 142 kPa for total suction less than 1000 kPa and 1694 kPa for total suction higher than 1000 kPa.

$$s_t = 0.31\left[\exp\left(\frac{6508}{w_b}\right)^{0.478} - \exp(1)\right]^{0.697} \tag{8.4}$$

8.6 Total Suction versus Degree of Saturation

Based on Equation (8.2) and Equation (8.3), it can be easily proved that the bentonite degree of saturation is essentially the same as degree of saturation of the compacted mixture. Semi-logarithmic plots of total suction versus bentonite degree of saturation for the four mixtures are shown in Figure 8.9(a) to Figure 8.9(d). Points corresponding to the optimum water contents and the maximum dry densities for the standard proctor and the enhanced proctor curves are also marked in each figure for clarity. The plots indicate a non-uniqueness of the total suction versus degree of saturation relationship for the compacted mixtures while the total suction versus water

content relationship of each mixture with different compaction efforts is shown to be unique.

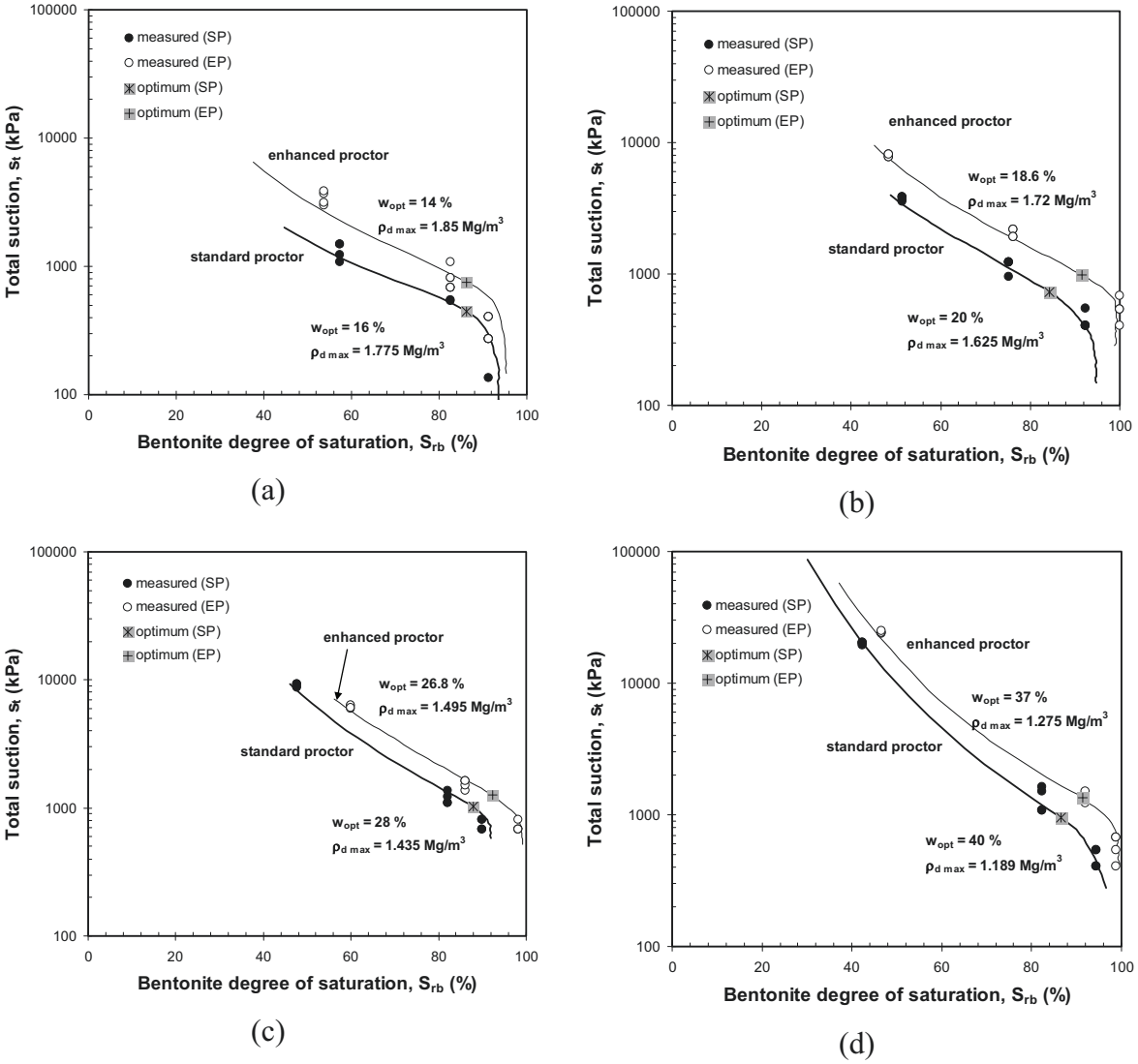

Figure 8.9 Total suction measured by the chilled-mirror hygrometer versus bentonite degree of saturation for compacted specimens of: (a) 30/70; (b) 50/50; (c) 70/30 bentonite-sand mixtures; and (d) pure bentonite

For the specimens compacted wet of optimum with a certain compaction effort, the change in total suction (with compaction water content) at a relatively constant degree of saturation indicates discontinuity of the air phase. It is reflected in a drop in dry density with compaction water content. The increase in amount of absorbed water (or compaction water content) decreases the total suction and dry density.

The total suction is related to the compressibility of the inter-aggregate fluids where air remains entrapped. Higher compaction energy of the specimens reduces the size of entrapped air bubbles. The increase in degree of saturation at a constant total suction

occurs due to the initially high compressibility of the air bubbles. The air bubbles are completely dissolved and the specimens will never reach complete saturation. This is due to a drop in the compressibility of inter-aggregate pore fluids. Consequently, the pore-water pressure that develops after compaction increases the water potential in the inter-aggregate pores. It is a part of the potential gradient besides the internal water potential gradient by which the internal redistribution of pore-water is controlled.

The rate of internal pore-water redistribution is controlled by the sum of the pore-water pressure developed in the inter-aggregate pores and the magnitude of total suction in the intra-aggregate and intra-laminar pores (or the unbalanced forces). When specimens are compacted dry of optimum, the air phase is continuous. In this case, the rate of internal redistribution of pore-water water is controlled only by the difference in water potential (or total suction) between the inter-aggregate, intra-aggregate, and inter-laminar pores without significant influence of pore-water pressure development. Therefore, the difference between total suction of the as-prepared specimens with that of the aged specimens increases with increasing compaction water content to reach a maximum value. Subsequently, the value decreases with increasing compaction water content since the unbalanced forces decreases as a result of a decrease in the total suction.

8.7 Matric and Total Suction of the Compacted Mixtures

Figure 8.10(a) to Figure 8.10(d) show semi-logarithmic plots of matric and total suctions versus water content for the compacted mixtures obtained via the filter paper method. The matric suction data were computed from the filter paper water content using Equation (7.1) whereas the total suction data were computed using Equation (7.2). Since the calibration data for the matric suction filter paper measurement are only available for matric suctions below 1500 kPa, the calibration curve (i.e., Figure 7.2) was extrapolated for the higher range of matric suction. Similarly, for the total suction filter paper measurement data, the extrapolation was also done for the lower total suction range (i.e., below 2000 kPa). The total suction minus matric suction curve was computed from the best-fit curves (i.e., the total and matric suction curves shown in Figure 8.10). The matric suctions of the compacted 30/70 bentonite-sand mixture specimens are essentially constant up to certain water content and then tends to cross the corresponding total suction curve in the high water content range. The results indicate that there might be a significant contribution of matric suction to the total suction magnitude of the 30/70 bentonite-sand mixtures at high water contents. The geometry of pores influences the magnitude of total suction more dominantly than the properties of the clay minerals. The curve should, however, remain below the total suction curve as matric suction is always less than total suction. On the other hand, the other three compacted mixtures generally show that the total suction minus matric suction curves follow closely the shape of the total suction curves indicating an insignificant contribution of matric suction.

Filter paper is not a true semi-permeable membrane and therefore the effect of cations in the pore-water is by-passed in the measurement of matric suction. The results are believed to provide the values of the capillary component. Hence, the total suction minus matric suction as shown in the figure represents the magnitude of sum of the osmotic suction and contribution due to sorptive forces. The decrease in total suction with increasing water content occurs largely as a result of the decrease in both the osmotic suction and the sorptive forces that are induced by the addition of water.

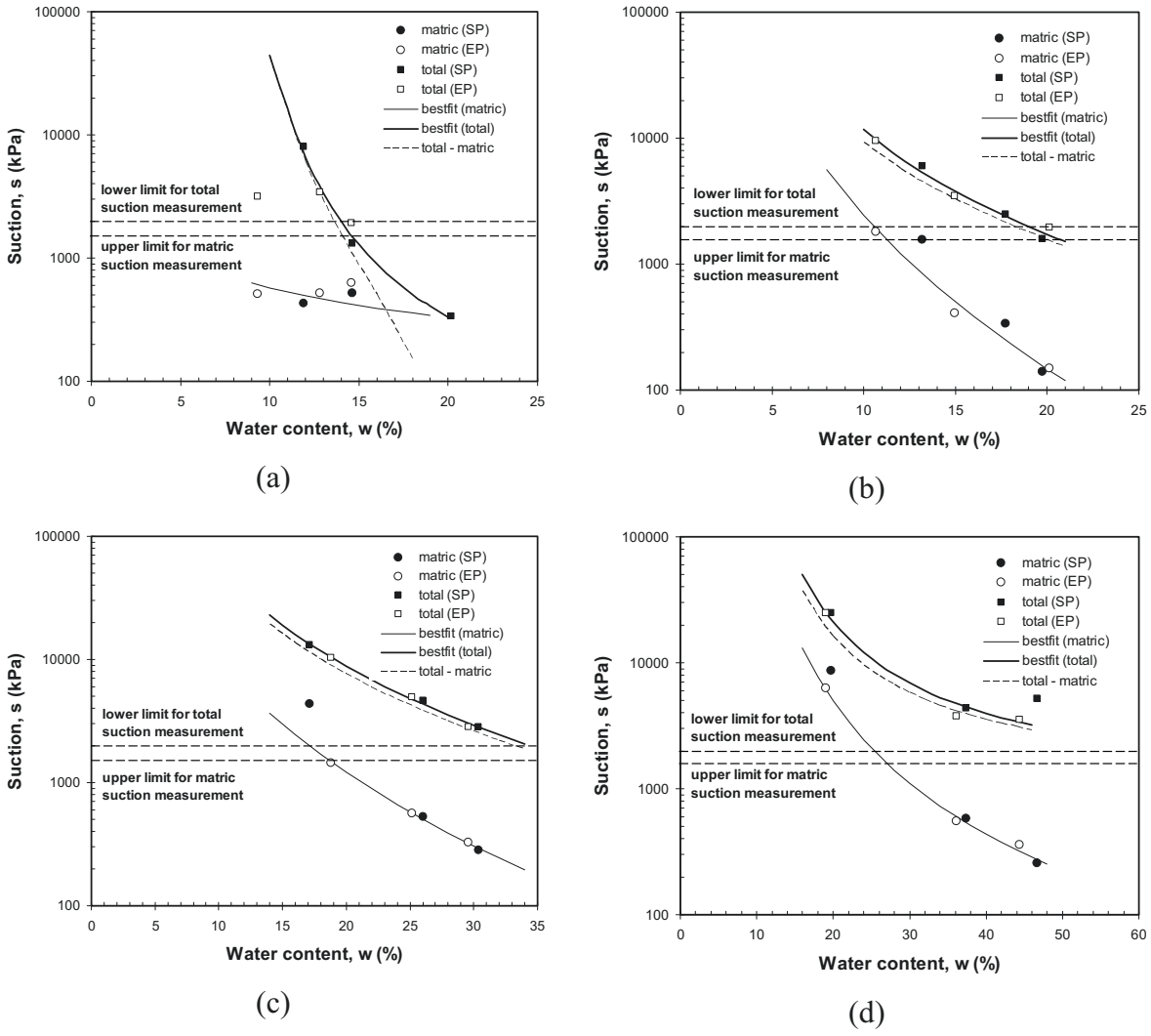

Figure 8.10 Total suction and matric suction measured by the filter paper method versus water content for compacted specimens of: (a) 30/70; (b) 50/50; (c) 70/30 bentonite-sand mixtures; and (d) pure bentonite

8.8 Summary of the Suction Measurement Results

The following conclusions can be drawn based on the results of suction measurements on four bentonite-sand mixtures at loose and compacted states.

1. The chilled-mirror hygrometer technique possesses the best accuracy among the four total suction measurements assessed in this study. It is recommended that the technique be used for measuring total suction of expansive soils and can be used as benchmark for assessing other available techniques.

2. The non-contact filter paper technique measures total suction at a quasi-equilibrium state. Internal redistribution of water occurs in the compacted specimens as time elapses due to unbalance force or unbalance distribution of total suction (or total water potential) in the specimens (i.e., the hydration effects).

3. The in-contact filter paper technique measures the capillary component of suction. The difference in suction between the values obtained via the non-contact filter paper technique and that obtained via the in-contact filter paper technique provides the magnitude of sum of the osmotic and sorptive forces.

4. Total suction of the bentonite-sand mixtures studied is a function of mixture water content and mixture bentonite content or collectively a function of bentonite water content. No significant influence of compaction (or dry density) and fabric is observed in the magnitude of total suction.

5. The total suction versus bentonite water content is a unique function while the uniqueness is not observed in the total suction versus bentonite degree of saturation.

CHAPTER 9

UNCONFINED AND CONSTANT LOAD CYCLIC WETTING AND DRYING BEHAVIOUR

9.1 General

In this chapter, results of the unconfined wetting and drying test and cyclic wetting and drying test under constant vertical load are presented and discussed. Although the use of axis-translation technique (ATT) by means of pressure plate tests results in matric suction being applied whereas the vapour equilibrium technique (VET) imposes total suction, both are considered to bring the same effects to the specimens tested. This is particularly true when no dilution of ions is assumed to occur during test using the ATT. Thus, the results of both techniques can be combined to establish continuous relationships between aspects under consideration (i.e., water content, void ratio, and degree of saturation) with suction.

9.2 Unconfined Wetting and Drying Behaviour

9.2.1 Initial Total Suction

Figure 9.1 shows a semi-logarithmic plot of water content and volumetric water content versus suction of specimens UC-1 to UC-6 in which the first applied suction was used for determining the average initial total suction of the specimens. The method is analogue to the measurement of swelling pressure using swell-under-load method. The specimens, which were subjected to total suctions less than the initial total suction, swelled and absorbed water. The specimens subjected to total suctions higher than the initial total suction shrunk and release water. Lines of average initial water content and initial volumetric water content are drawn in the figure. The average initial total suction was indicated by the intersection between water content and volumetric water content curves and the corresponding initial values (i.e., 8.8% and 18%, respectively). The average initial total suction based on the average initial water content of the specimens was 15400 kPa while the value inferred based on the average volumetric water content was 17000 kPa. A separate measurement of total suction made on the as-prepared specimen using the chilled-mirror hygrometer gave an initial total suction of 25980 kPa. The total suction induced by the aqueous KCl solution which was used in the equilibration (i.e., 22700 kPa) is considered to be the average initial total suction of the as-prepared compacted specimens and further used in the data analyses.

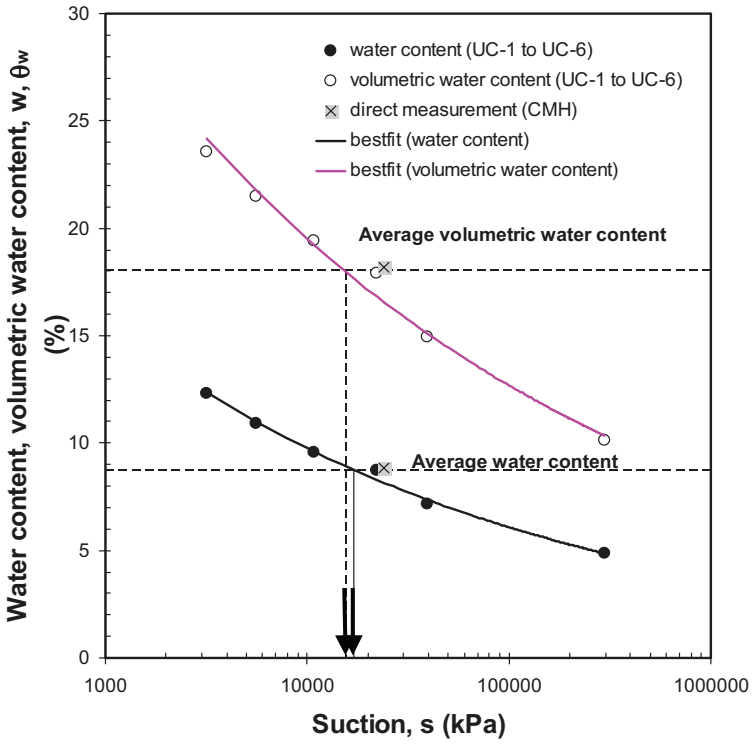

Figure 9.1 Equilibrium water content and volumetric water content versus suction for specimens UC-1 to UC-6 (first suction cycle)

9.2.2 Main Drying and Wetting Curves

The main drying and wetting curves represent the most attainable states of a soil subjected to drying and/or wetting cycles under unconfined conditions. The main drying curve of a clay soil is usually obtained from unconfined drying test of a slurried clay specimen with initial water content higher than its liquid limit (Al-Mukhtar et al., 1999; Marcial et al., 2002; and Fleureau et al., 2002). However, the main drying curve for water content versus suction relationship is shown to be unique and independent of the specimen initial conditions (Fleureau et al., 2002).

In this study, the main drying and wetting curves were obtained from the test results of specimens UC-4, 8, 10, 7, and 9 since they constitute the most attainable states (i.e., the main drying and wetting curves) at least for the specimens tested in this study. Figure 9.2(a) to Figure 9.2(c) shows; respectively, water content, void ratio, and degree of saturation versus suction of several specimens (i.e., specimens UC-4, 8, 10, 7, and 9) wetted under unconfined conditions. Figure 9.2(a) indicates that the curve of water content versus suction for specimens UC-10 (i.e., the specimen which was initially saturated under constant volume (CV) conditions before test) form the most part of the main drying curve.

The main wetting curve of the material is constituted by the data obtained for specimens UC-4 and UC-8. The void ratio versus suction relationships of the five specimens presented in Figure 9.2 show a different characteristic. The data of specimen UC-10 cross the void ratio versus suction curves of the four other specimens. Apparently, there are no main drying and main wetting curves that can be obtained from the void ratio versus suction relationship. It will later be shown that the void ratio versus suction curve is dependent on the initial conditions of the specimen.

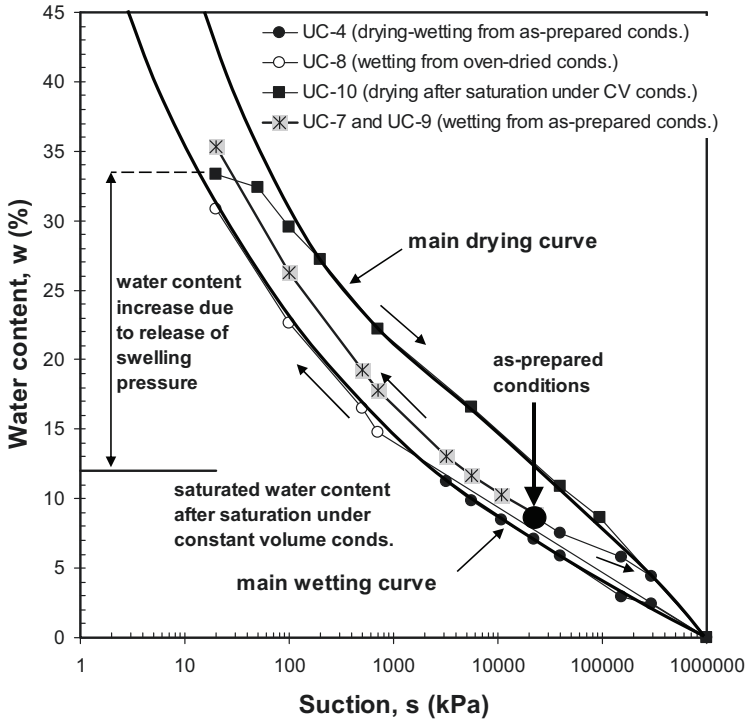

(a)

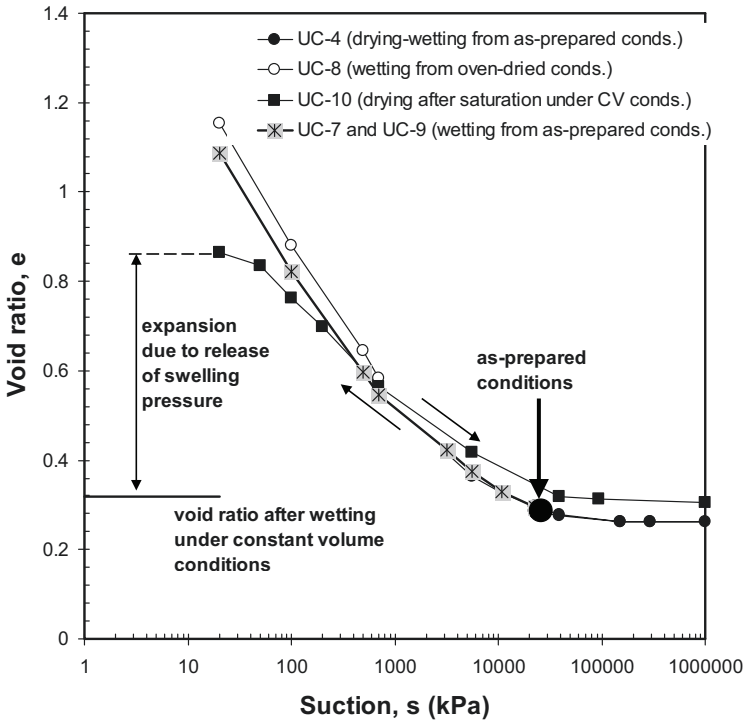

(b)

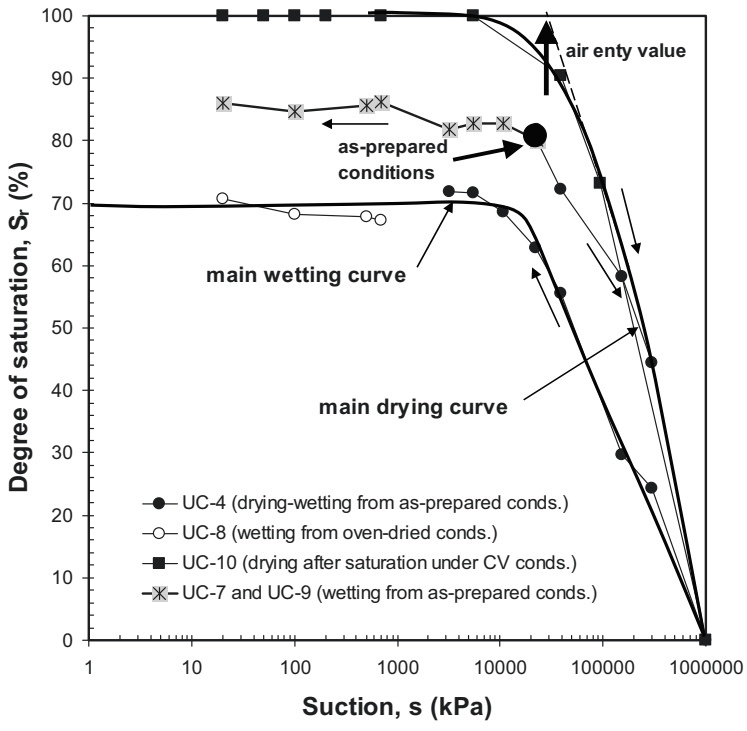

(c)

Figure 9.2 Possible main wetting curves: (a) water content versus suction; (b) void ratio versus suction; and (c) degree of saturation versus suction

The degree of saturation of specimens UC-7 and UC-9 show largely no change with decreasing suction on wetting (Figure 9.2(c)). The degree of saturation versus suction curve of specimen UC-10 also forms the main drying path of the material. The air entry value of this particular specimen that can be inferred from the figure as the point where the degree of saturation starts to drop from the saturation value is about 25000 kPa, which is almost similar to the initial total suction of the as-prepared specimens.

Similar to the water content versus suction curve, the main wetting curve of the material is composed by the experimental data of specimens UC-4 and UC-8. However, the data indicate that there is a limiting suction below which further wetting (or decrease in suction) does not induce significant increase in the degree of saturation.

According to Figure 9.2(c), the value of such a limiting suction is close to the initial total suction of the as-prepared specimens. The limiting value of degree of saturation that can be reached during wetting is a function of suction at which the wetting path begins or in other words is a function of the highest total suction that is ever experienced by the specimen. The higher the suction at which wetting is started; the lower will be the limiting degree of saturation of the specimen. The different main paths obtained for the drying and wetting curves of water content and degree of saturation versus suction relationships signify hysteresis in the hydraulic behaviour of the specimens.

This finding is in contradiction with the observation made by Fleureau et al. (2002) on different clay specimens. In their observation, the clay specimens reached a complete saturation on wetting from a high suction value. Fleureau et al. (2002) used a non-wetting liquid (i.e., kerdane) for measuring void ratio of the specimens. The non-wetting liquid intruded small cracks (and probably also some of the large continuous air-filled pores) in the specimen which developed due to the previous drying cycle. Therefore, the cracks and some of the large continuous air-filled pores were accounted for in the computation of degree of saturation.

9.2.3 Reversible Drying-Wetting Behaviour

Figure 9.3(a) show water content versus suction of several specimens that underwent wetting-drying cycles (i.e., specimens UC-1, 2, 3, 5, 6 and 12). The figure indicates that as long as the drying and wetting paths do not ever touch the two boundaries (i.e., the main drying and wetting curves), the response of specimens to hydraulic processes (i.e., drying or wetting) is reversible. A similar behaviour is also seen in the case of void ratio and degree of saturation versus suction relationships as shown in Figure 9.3(b) and Figure 9.3(c), respectively.

The reversible drying and wetting behaviour was also observed by Cui et al. (2002b) on FoCa7 clay specimens, which were subjected to cyclic drying and wetting

under unconfined conditions (suction range between 200 kPa and 300 000 kPa). No information was given regarding the main drying and wetting curves of the specimens.

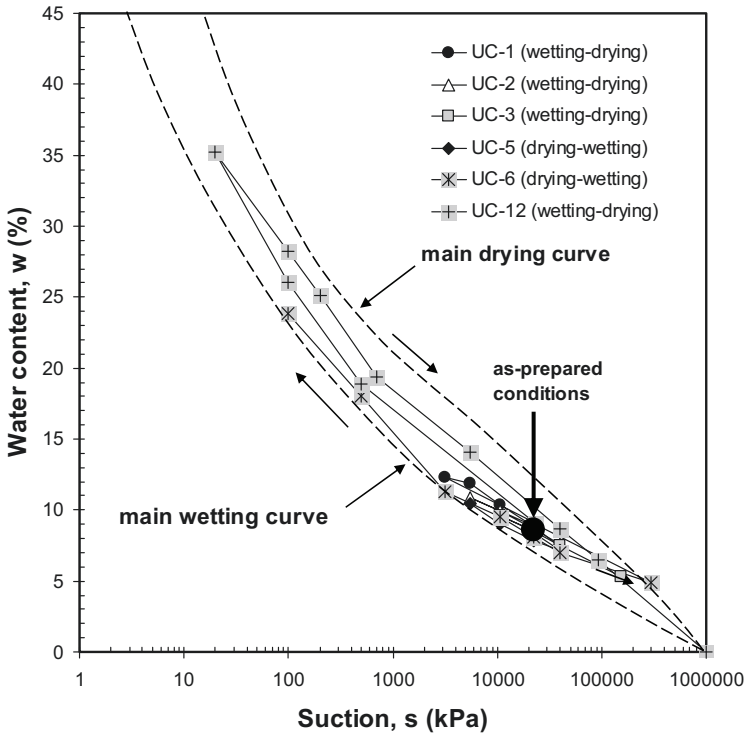

(a)

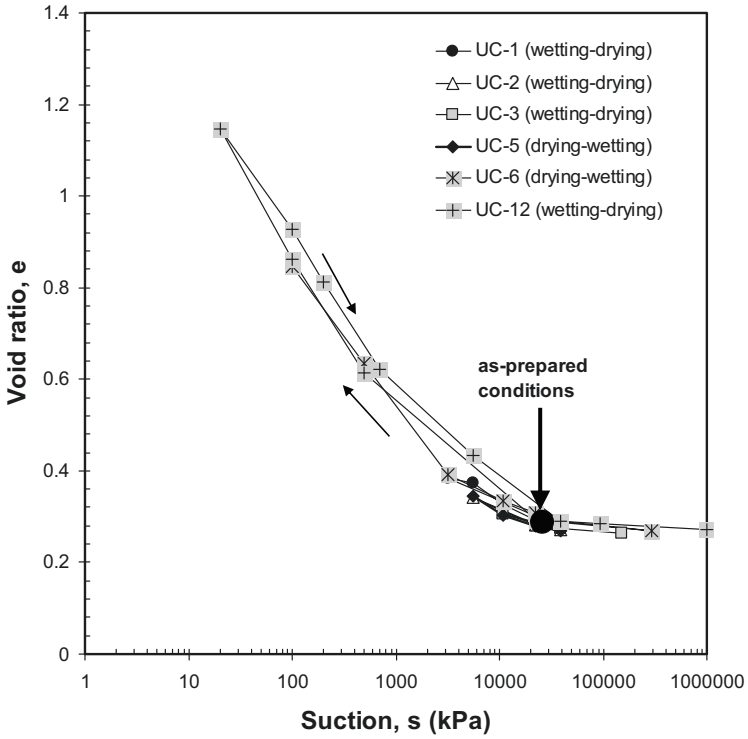

(b)

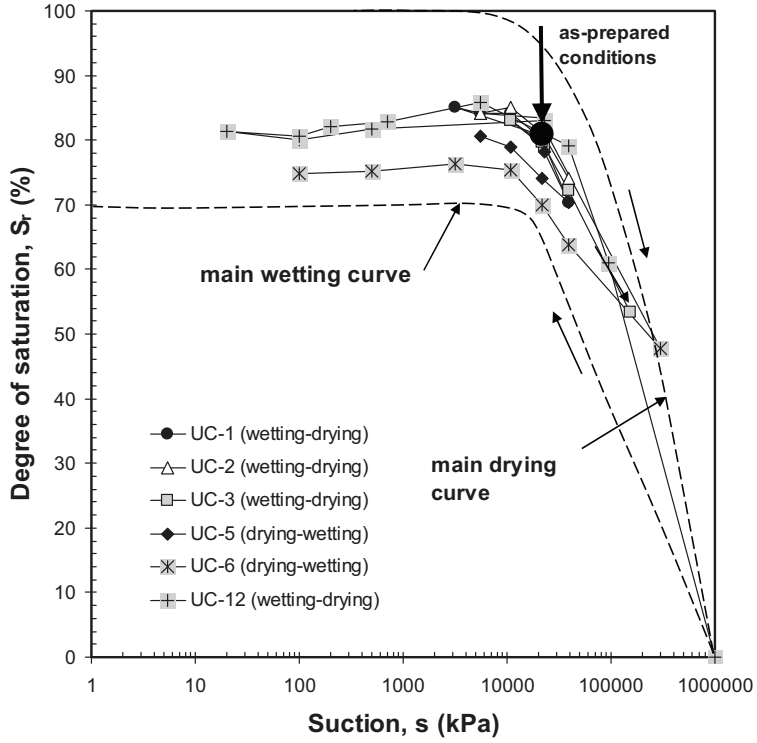

(c)

Figure 9.3 Wetting and drying behaviour of several specimens: (a) water content versus suction; (b) void ratio versus suction; and (c) degree of saturation versus suction

9.2.4 Observation of Cracks during Drying

Figure 9.4 shows water content versus suction curve of specimens UC-10 in comparison with that of specimen UC-11. The drying curve of specimen UC-11 contradictorily goes much below the apparent main wetting curve. At high suction, the curve even appears to follow the main wetting path. The reason for this discrepancy may be the cracks which developed during drying of specimen UC-11. Crack development is one of the major concerns regarding the use of this material as sealing and buffer material for nuclear waste repository. The presence of cracks significantly increases the intrinsic permeability of the material.

The influence of cracks is clearly seen in the degree of saturation versus suction curve (Figure 9.5). The degree of saturation of specimen UC-11 dropped much lower than that of specimen UC-10 at the same suction. Although both specimens were at saturation before the commencement of drying process, due to the cracks that were not taken into account, the computed degree of saturation (i.e., based on mass and dimension of the specimen) of specimen UC-11 was much less than 100% even at low values of suction. However, it is thought that the intact block of specimen UC-11 might be at saturation and the degree of saturation versus suction curve should have followed that of specimen UC-10 (i.e., the apparent main drying path).

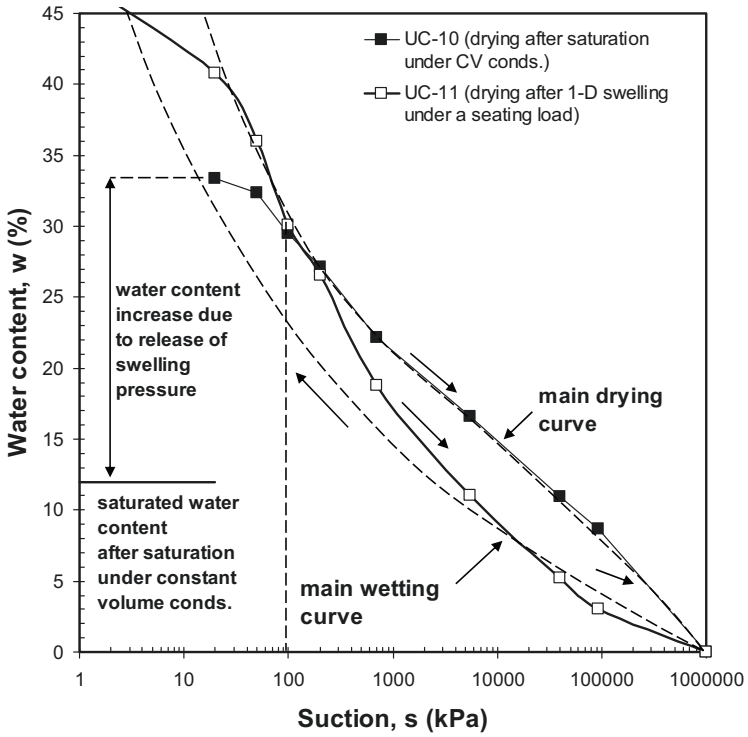

Figure 9.4 Water content versus suction for specimens UC-10 and UC-11

By assuming that the air-entry value of specimen UC-11 is equal to that of specimen UC-10 and no change in volume of the specimen took place upon drying beyond the air-entry value, a corrected drying curve for cracked specimen can be obtained. The drying curve of the cracked specimen (i.e., specimen UC-11) is also plotted in Figure 9.5.

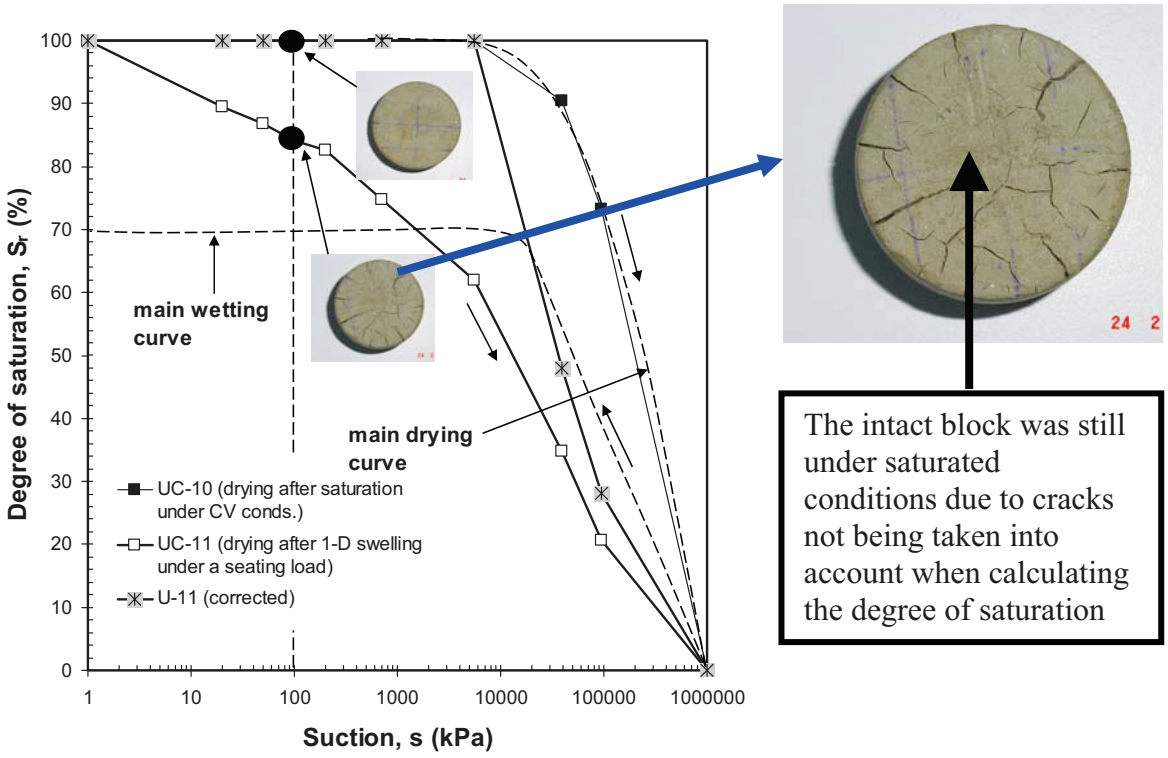

Figure 9.5 Degree of saturation versus suction for specimens UC-10 and UC-11 and digital photo of specimen UC-11 at 100 kPa suction

Figure 9.6 illustrates the evolution of soil structure of specimen UC-10 during wetting and drying cycles which has been postulated based on the data presented so far. After wetting under constant volume conditions, homogenisation of soil structure occurred and the specimen was at saturation (i.e., State 2 in the figure) (Delage et al., 1996). There was a little increase in void ratio of the specimen due to the deformability of constant volume cell used. Release of swelling pressure induced an increase in water content and void ratio whereas the specimen remained saturated and structurally homogeneous (i.e., State 3 in the figure). At an intermediate suction on drying (i.e., State 4 in the figure), the specimen shrunk while maintaining its structural homogeneity. Only at a very high suction value, the specimen became inhomogeneous following further shrinking (i.e., State 5 in the figure). At this state, visible cracks were seen in the specimen. However, the intact blocks of the specimen were most probably close to saturation. In this case, air was located in the large pores (i.e., the cracks) or in the case when the intact blocks were not at saturation, air might also exist within the blocks. Therefore, the intact blocks DO NOT represent the clay clusters but they are a combination of clay clusters with inter-aggregate pores in between. It should be noted that the void ratio and degree of saturation at State 5 are only the apparent values based on the mass and dimension measurements.

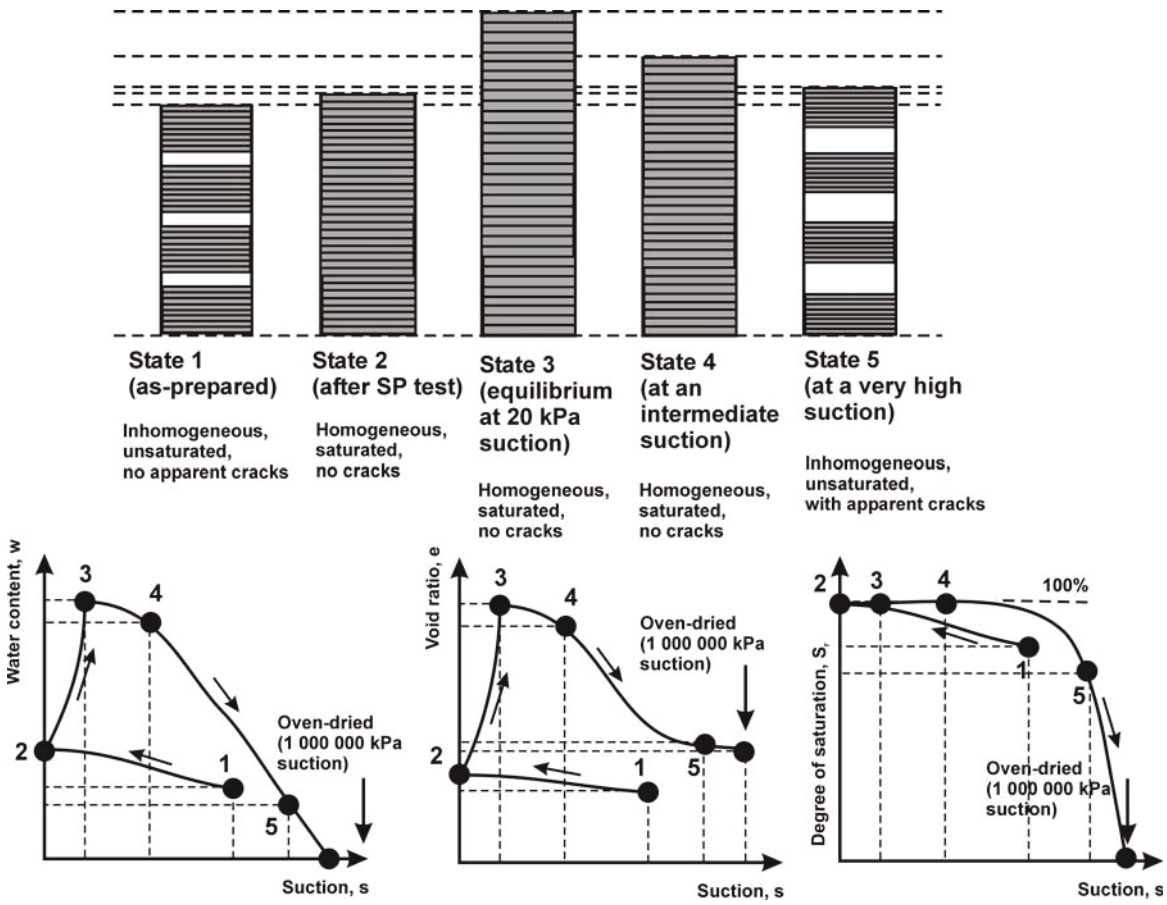

Figure 9.6 Evolution of the structure of specimen UC-10 during wetting and drying cycles

A similar illustration can also be made for specimen UC-11 (Figure 9.7). In this case, the one-dimensional swelling at a seating load of the initially structurally inhomogeneous specimen on wetting led to a more inhomogeneous specimen even the degree of saturation at the end of swelling was 100% (i.e., State 2 in the figure). At this point, a non-uniform distribution of water potential (or suction) between the inter- and intra-aggregate pore-water might exist in the specimen although its (macroscopic) swelling was completed. Oppositely, a uniform suction distribution in the specimen was also possible. In the former case, water in the inter-aggregate pores drained out first when suction was increased to 20 kPa (i.e., State 3 in the figure) whereas the intact blocks between cracks were still at saturation. Simultaneously, internal redistribution of water occurred. In the latter case, no internal redistribution of water took place within the specimen and the cracks were caused by a difference in response of the clay clusters to deform as a result of water being drained out and the movement of inter-aggregate pore-water during drying. The mechanisms that occurred at State 4 and State 5 are thought to be similar to that at State 3 where the specimen became more structurally inhomogeneous and severe cracks developed at the end.

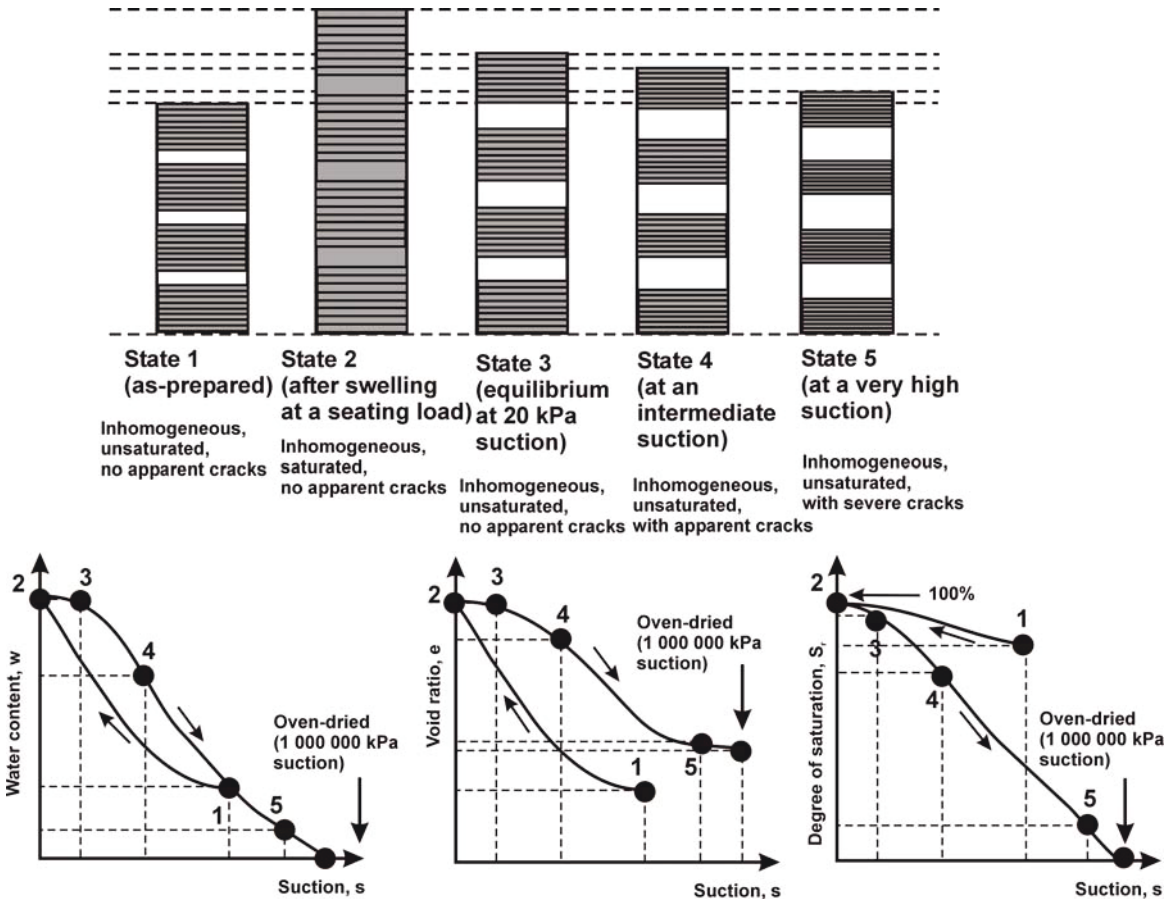

Figure 9.7 Evolution of the structure of specimen UC-11 during wetting and drying cycles

9.2.5 Influence of Initial Conditions before Drying or Wetting on the Final Void Ratio

Figure 9.8 depicts the void ratio versus water content curves of the drying paths (or the shrinkage curve) of several specimens tested in the study. It is shown that the final void ratio (i.e., at zero water content) appears to depend on the specimen conditions (i.e., the water content and void ratio) at which drying is first started. Specimens UC-10 and UC-11 had the same suction before drying (i.e., zero equilibrium suction); however, they had different final void ratios at zero water content. Since the end values of the void ratio are only the apparent values (i.e., without accounting for the cracks), a unique value of final void ratio should have been obtained for several specimens on step-wised drying to oven-dried conditions (i.e., by means of multi-step suction increase) although the specimens have different initial conditions before drying.

The intersection point between two linear parts of the shrinkage curve of each specimen, which lies between 8% and 10%, agrees well with the measured shrinkage limit of the material (i.e., 9.8%) (Figure 9.8). The shrinkage limit of a clay soil is usually

obtained from drying of a specimen with a high initial water content (i.e., higher than its liquid limit) or from a slurried specimen (Sridharan and Prakash, 2000).

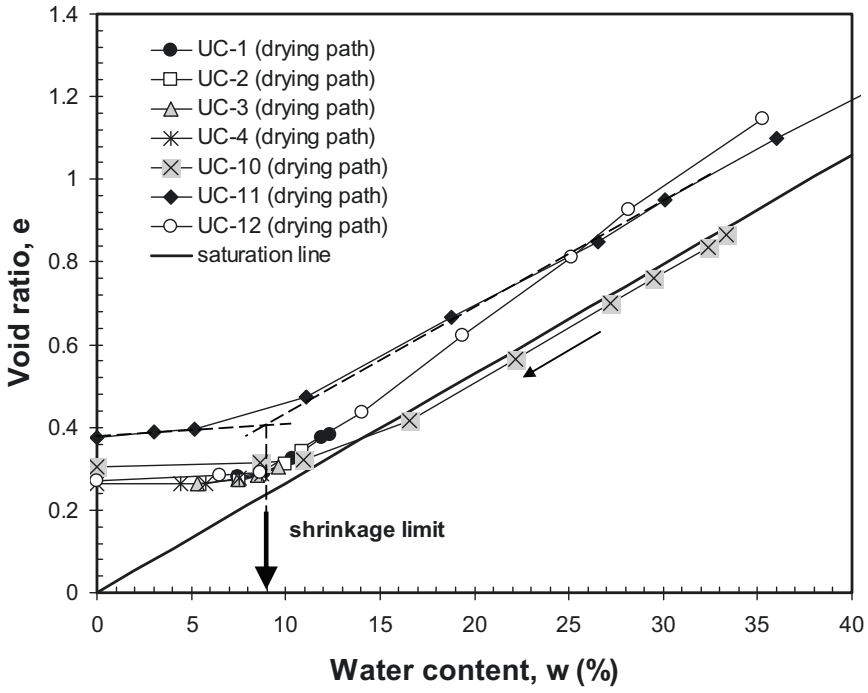

Figure 9.8 Shrinkage curves of several specimens tested

A similar plot can also be made for the void ratio versus water content wetting curves (or the swelling curves) (Figure 9.9). Similarly, a 9-% average shrinkage limit of the material can also be depicted in the figure in similar way to how the value has been obtained for the drying case. The void ratio at intermediate water content (e.g., at 30% water content) can be considered as a reference to assess the swelling curves. It appears that the void ratio at the reference water content is a function of water content corresponding to the suction at which wetting is started. The higher is the specimen water content when wetting is first started; the higher will be the specimen void ratio at the reference water content. The void ratio of specimen UC-8 at the reference water content was the highest compared to the void ratio of specimens UC-6 and UC-7 at the same water content. This is reasonable since the water content of specimen UC-8 when wetting started was the lowest among the three specimens considered (i.e., 0%). This phenomenon signifies the fact that the equilibrium void ratio after swelling depends on the initial water content before swelling takes place (Holtz and Gibbs, 1956). It was reported that the magnitude of swelling potential (i.e., swelling under a seating load) depends on the initial water content of specimen tested with insignificant influence of the initial specimen void ratio (or dry density). With the data presented in this subchapter, the dependency of equilibrium void ratio upon wetting is also shown to be valid for the case of swelling due to a finite decrease in suction.

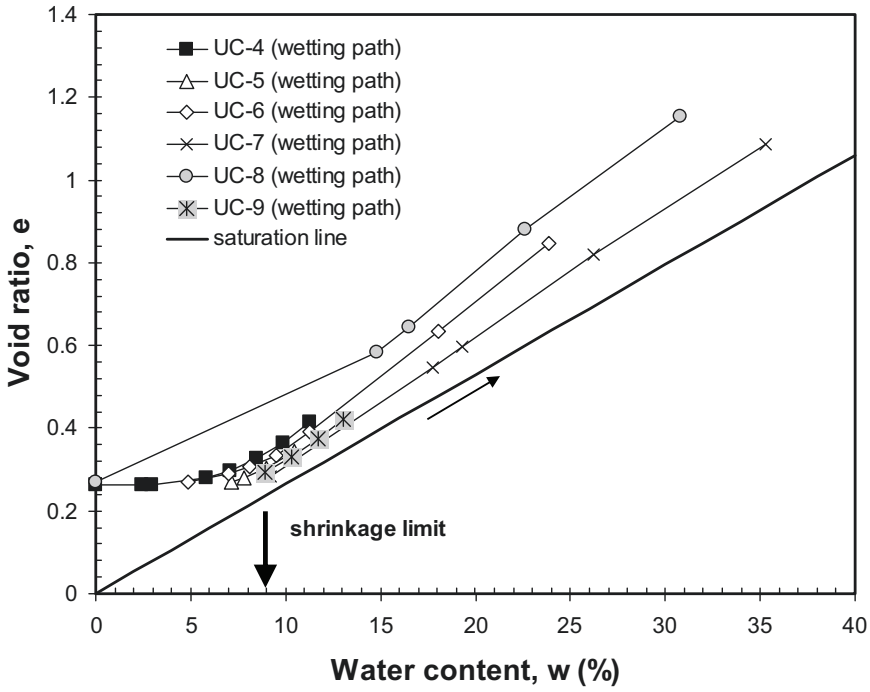

Figure 9.9 Swelling curves of several specimens tested

9.2.6 Anisotropy

Figure 9.10(a) shows the radial strain versus suction curve for specimens UC-4, 8, 10, and UC-7 and UC-9 while Figure 9.10(b) shows the corresponding plot of the vertical strain versus suction. Specimen UC-10 shows the largest anisotropy with respect to radial and vertical strain. The anisotropy with respect to the radial and vertical strain following unconfined wetting is possibly due to inherent structural anisotropy of the specimens caused by static compaction during preparation. However, the stress dissipation during equilibration of the specimen to reach the 22700 kPa initial suction might have significantly reduced the degree of structural anisotropy of the specimens. Except in the case of specimen UC-10, the ratio of radial to vertical strain of the specimens is about 0.6 in the low suction range. The anisotropy tends to decrease with increasing suction.

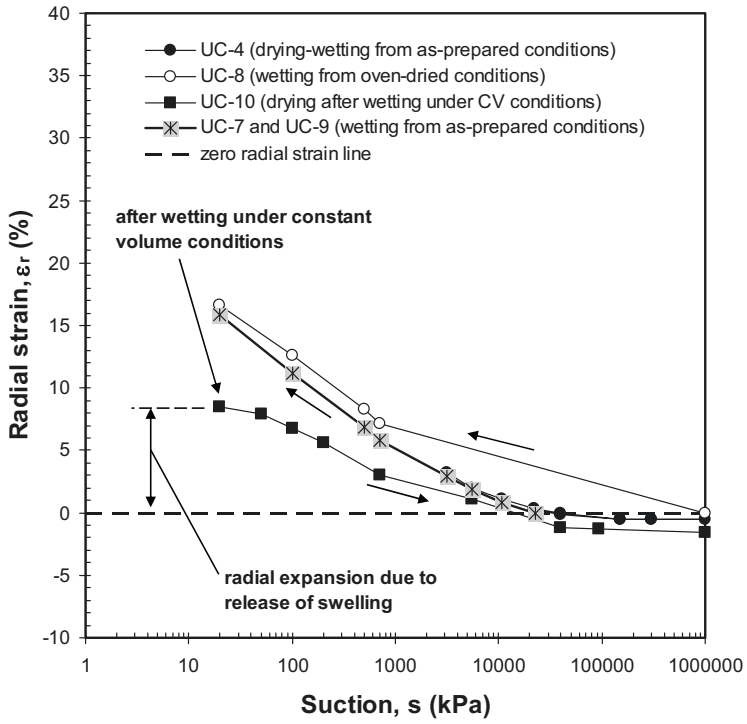

(a)

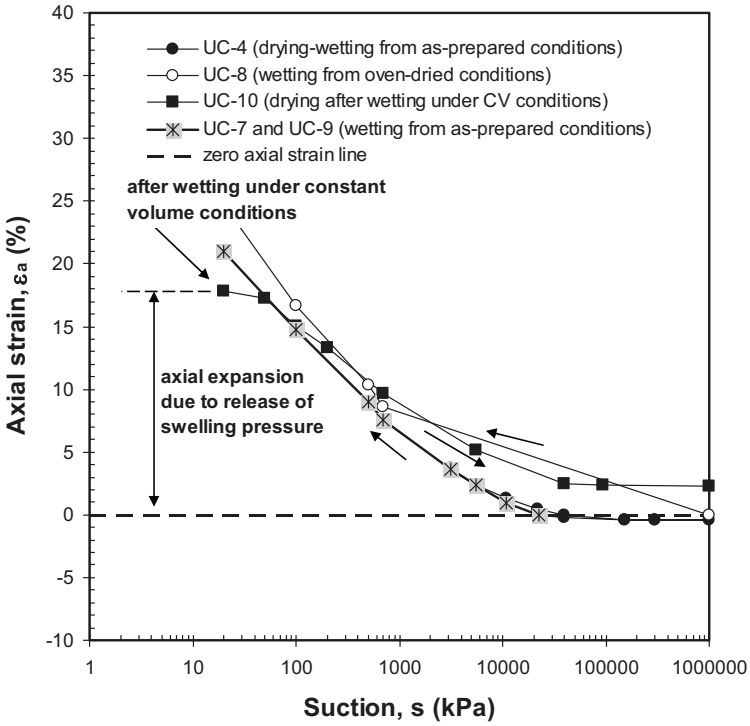

(b)

Figure 9.10 (a) Radial strain and (b) axial strain versus suction for several specimens tested

9.2.7 Comparison of Wetting Curve with the Curve of Water Content versus Suction

Figure 9.11 show a comparison between the water content versus suction curve (or wetting curve) of the as-prepared specimen and the water content versus suction characteristic curve (or the suction characteristic curve) for the as-compacted specimens of 50/50 bentonite-sand mixture measured using the chilled-mirror hygrometer (see Chapter 8). The plot indicates that at any suction, the suction characteristic curve lies above the wetting curve. Since the effect of dry density (and fabric) on the suction characteristic curve is insignificant, it is expected that suction of the as-compacted specimen delivered by GRS (i.e., with an average water content of 11%) was initially located on the suction characteristic curve. The suction equilibration with the water vapour above KCL aqueous solution prior to experiment increased the total suction while at the same time an internal redistribution of water in the specimen took place.

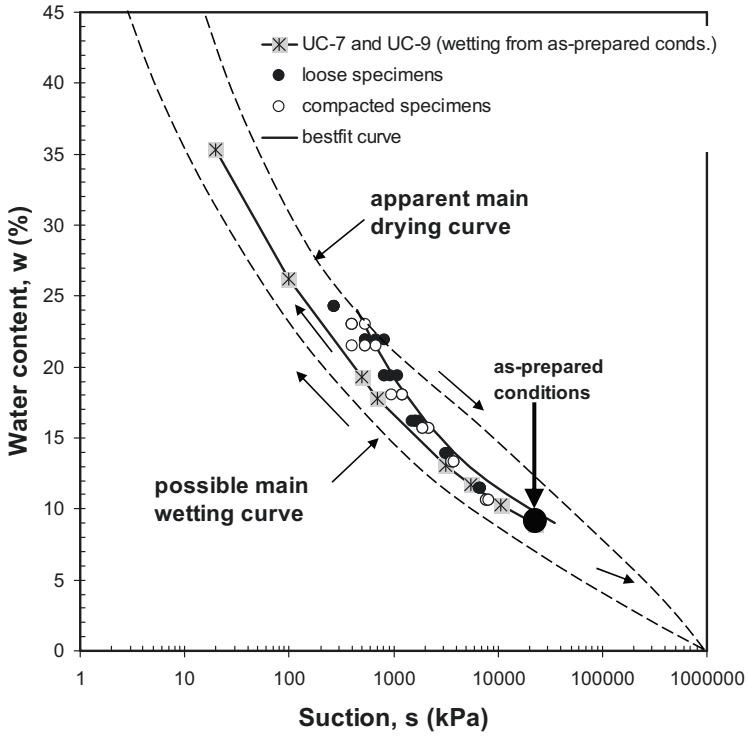

Figure 9.11 Wetting curve versus water content-suction characteristic curve

The difference between the wetting and suction characteristic curve might be due a difference in the structure and fabric of the specimens. Consider two specimens with the same final water content, one is brought to that water content by progressively wetting it by means of suction reduction and the other is directly prepared at that water content and is subsequently statically compacted. The two specimens will have different suctions and void ratios (or dry densities). However, the differences (i.e., the suction and void ratio differences) in this case are not related one to the other. Based on this, it is thought that

the difference is solely due to a fabric difference between the two specimens. The fabric of the first specimen at as-compacted state was preserved after wetting whereas the second specimen has a different fabric as they both have been prepared at different water contents.

9.2.8 Unconfined Wetting and Drying Characteristics Based on the Experimental Results

Figure 9.12 presents an illustration of possible unconfined wetting and drying characteristics postulated based on the experimental data presented herein. The main drying and wetting curves (i.e., the water content and degree of saturation versus suction curves) obtained using the experimental are called as the apparent main drying and possible main wetting curves, respectively. The reason is that the 'true' drying curve of an expansive soil should be obtained from a drying test on a slurried specimen. Hysteresis is seen in the water content versus suction curve. The void ratio versus suction curve shows insignificant hysteresis in response to suction increase and decrease. However, the degree of saturation versus suction characteristic indicates the most obvious hysteretic behaviour. The as-prepared suction appears to be a threshold suction beyond which a rapid change in the degree of saturation occurs with increasing suction.

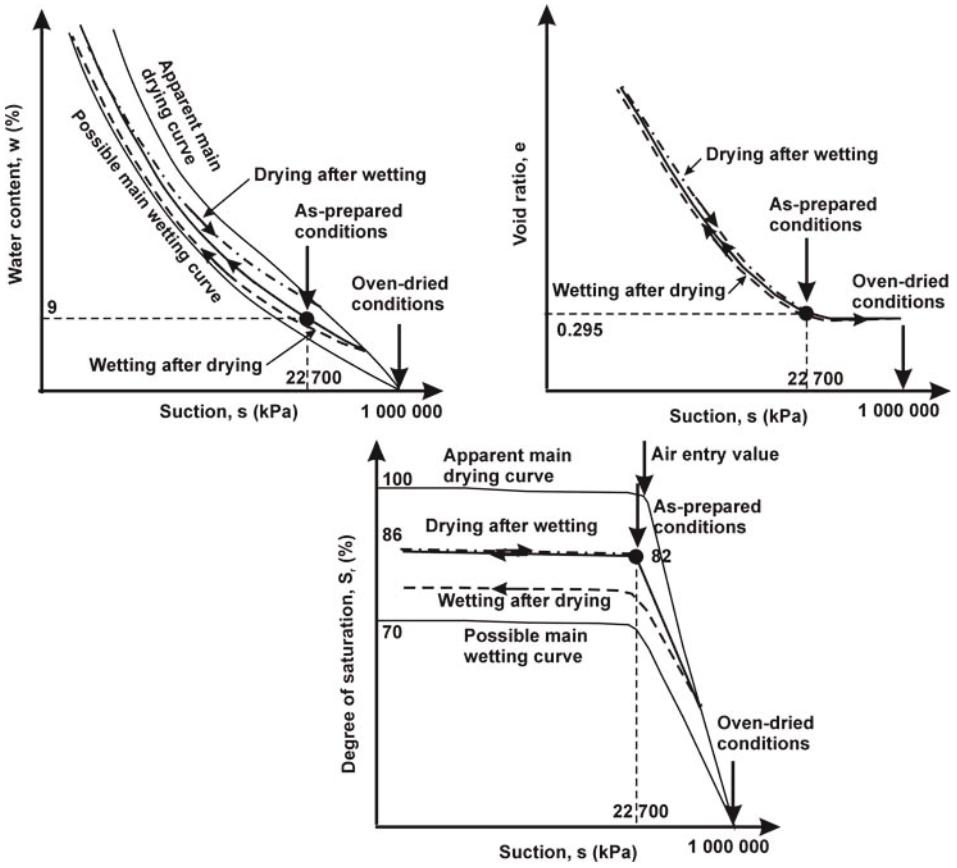

Figure 9.12 Possible unconfined wetting and drying characteristics of the as-prepared specimen

9.3 One-Dimensional Cyclic Wetting-Drying Behaviour under Constant Load Conditions

Figure 9.13 and Figure 9.14 show evolution of void ratio with suction decrease and increase during one-dimensional cyclic wetting-drying test on the as-prepared specimen under 200 kPa and 1500 kPa net vertical stress (i.e., specimens Cyclic-1 and Cyclic-2), respectively. The void ratio changes were computed from the vertical deformation of the specimen as measured by the dial gauge assuming that the K_o-conditions hold. The deformation of the oedometer system used (i.e., the UPC pneumatic oedometer cell) was considered in the data analysis.

The initial deformation of both specimens was induced by the increase in net vertical stress prior to wetting-drying cycles. It is observed from the figures that the subsequent drying after the first wetting on specimen Cyclic-2 induced a larger decrease in void ratio compared to that observed on specimen Cyclic-1. The fact signifies micro- and macro-structural level of deformation as described by Alonso et al. (1999) that more shrinkage of soil specimen on drying is observed at high stress level.

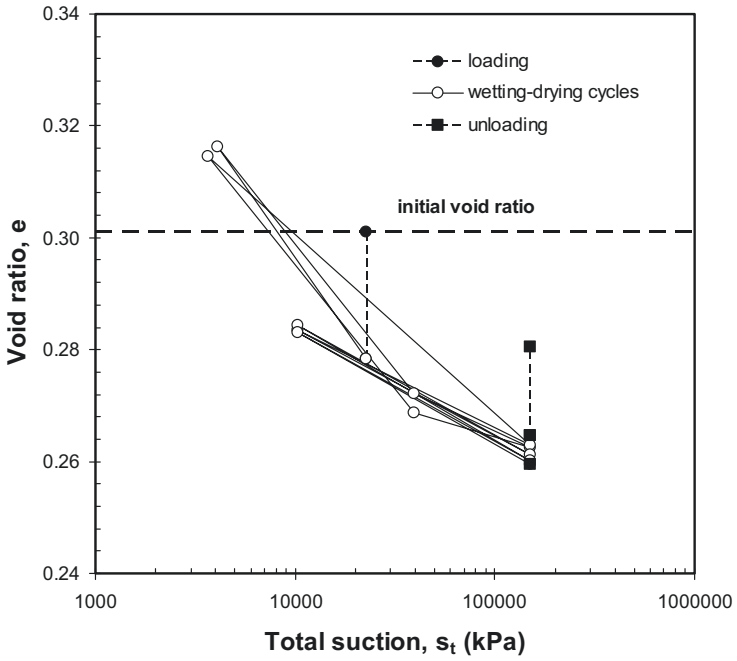

Figure 9.13 Void ratio versus total suction of specimen Cyclic-1 (the one-dimensional cyclic wetting-drying test under 200 kPa net vertical stress)

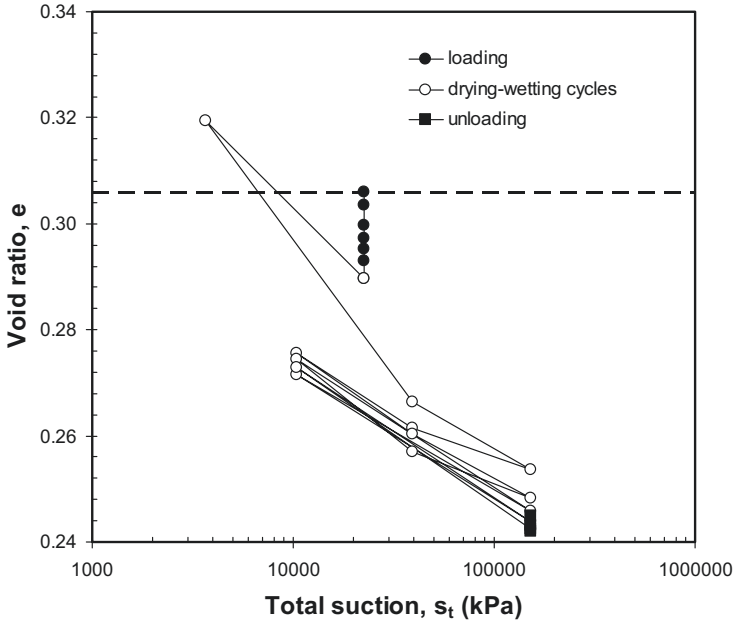

Figure 9.14 Void ratio versus total suction of specimen Cyclic-2 (the one-dimensional cyclic wetting-drying test under 1500 kPa net vertical stress)

The results of one-dimensional wetting-drying tests under constant net vertical stress presented in Figure 9.13 and Figure 9.14 can also be plotted as a relationship between changes in volumetric strain versus suction cycle. Figure 9.14 and Figure 9.15 show such a plot for specimen Cyclic-1 and Cyclic-2, respectively. In the plot, the negative volumetric strain indicates volume reduction. After the first cycle of wetting and drying, specimen Cyclic-1 exhibited a positive volumetric strain change indicating a net swelling of the specimen. In specimen Cyclic-2, a net shrinkage was observed after the first wetting-drying cycle. However, both specimens showed a zero net volumetric strain change at the end of wetting-drying cycles. The response of both specimens to suction increase and decrease after the fourth cycle of wetting-drying is elastic and reversible.

This observation is in agreement with the experimental results of heavily compacted 80/20 bentonite-sand specimens presented by Alonso et al. (2001). Initially, a significant part of the swelling is irrecoverable indicating the significant portion of the macro-structural plastic volumetric strain (Gens and Alonso, 1992). The macro-structural plastic strain decreases with increasing net vertical stress indicating the less pronounced effects of micro-structural elastic deformation on the macro-structural plastic deformation (Alonso et al., 1999). Based on the experimental data presented in this subchapter, the effect of net vertical stress on the accumulated total volumetric strain is found to be unobvious. The results of both tests (i.e., Cyclic-1 and Cylic-2) showed an almost similar final accumulated volumetric strain (i.e., about -2%). The effects of net vertical stress are only pronounced in the ratio of plastic to elastic volumetric strain (see Chapter 11).

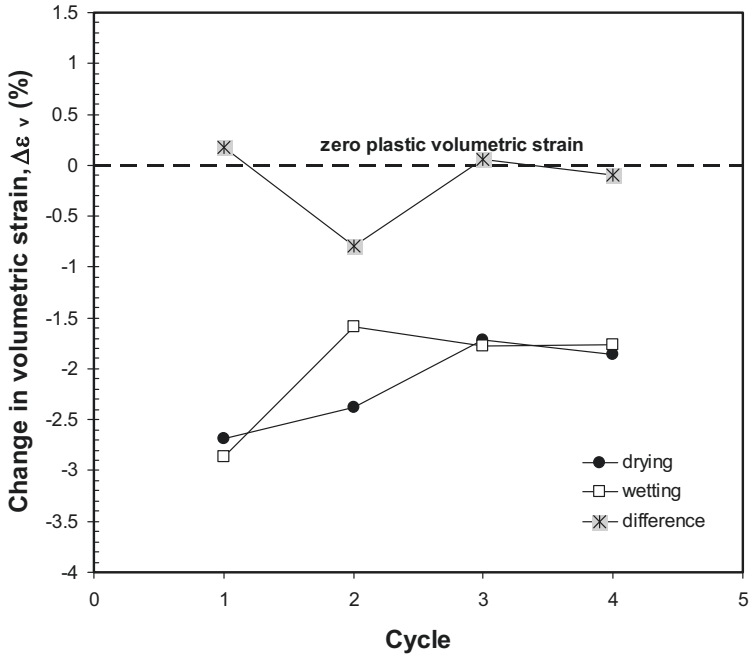

Figure 9.15 Change in volumetric strain for specimen Cyclic-1 (the cyclic wetting-drying test under 200 kPa net vertical stress)

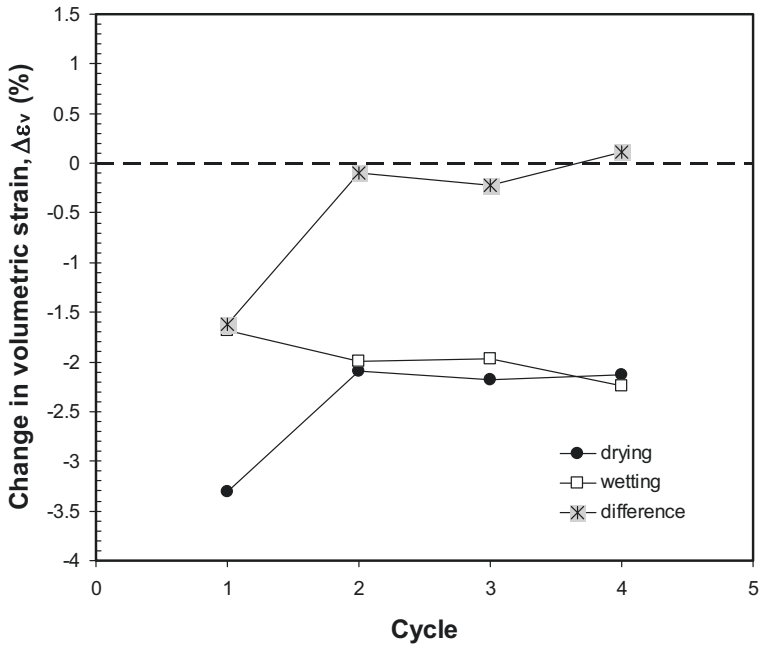

Figure 9.16 Change in volumetric strain for specimen Cyclic-2 (the cyclic wetting-drying test under 1500 kPa net vertical stress)

9.4 Summary of Unconfined and Constant Load Cyclic Wetting and Drying Behaviour

The following conclusions can be drawn based on the results of unconfined and cyclic constant load wetting and drying tests.

1. No general main drying curves (i.e., the water content, void ratio, and degree of saturation versus suction curves) can be defined from the experimental results. The curves that can be considered to be the main wetting and apparent main drying curves in the case of water content and degree of saturation versus suction curves cannot be taken to represent the main wetting and main drying curves for the void ratio versus suction relationship.

2. The as-prepared suction is a limiting suction below which further reduction in suction does not induce any significant increase in the specimen degree of saturation. The limiting degree of saturation is a function of the highest suction that is ever experienced by the specimen before wetting starts.

3. The as-prepared material shows insignificant hysteresis in the void ratio versus suction relationships. The significant hysteretic behaviour is seen in the water content degree of saturation versus suction relationships.

4. The in-homogeneity of water content distribution in the as-prepared specimen after wetting under a low vertical pressure induces cracks when the specimen is subjected to a drying process even at a relatively low suction. The suction at which cracks start to develop appears to be a function of stress level under which the as-prepared specimen is saturated prior to drying.

5. During cyclic wetting and drying under constant load conditions, the specimen with a higher stress level exhibited a higher shrinkage on drying. After the fourth cycle of wetting and drying, the response of the heavily compacted bentonite-sand specimen was elastic with respect to suction decrease and increase.

CHAPTER 10

SWELLING PRESSURE, CONSTANT VOLUME WETTING, AND ONE-DIMENSIONAL COMPRESSION AND REBOUND BEHAVIOUR

10.1 General

This chapter discusses results of the swelling pressure measurement and one-dimensional constant suction compression and rebound test. In the light of thermodynamic concepts of water potential and suction, suction at equilibrium (i.e., the combination of its matric and osmotic components) may not be the same for different types of test. However, it is merely the equilibrium suction which is considered in the discussion but not the actual suction which exists in the specimen. For example, at the end of constant volume swelling pressure test (with distilled deaired water), the swelling pressure developed balances the water deficiency or water potential which exists in the soil specimen such that the total water potential (i.e., the equilibrium suction) will have the same value as that of the distilled deaired water. This equilibrium conditions induce no further water absorption by the specimen. Thus, it is said, in this case, that the equilibrium suction at the end of the test is ZERO. The swelling pressure which develops during the swelling pressure test or the net vertical stress which acts in the one-dimensional compression-rebound test represents the net repulsive force of the specimen as a result of physico-chemical interactions between the specimen and water (Bolt, 1956).

10.2 Swelling Pressure and Constant Volume Wetting Behaviour

The swelling pressure test results presented herein were analysed by taking into account deformability of the swelling pressure measurement systems used (i.e., the UPC constant volume and oedometer cells and the Weimar high pressure oedometer system). Other factors that might influence the results such as specimen-ring friction were not taken into account since the lubrication is assumed to be sufficient in minimising the ring friction effects.

10.2.1 Compatibility of the UPC Constant Volume Cell and the Weimar High Pressure Oedometer System

Figure 10.1 shows a comparison between swelling pressure measured using the UPC constant volume cell (i.e., specimen SP-HC-50B-3) and that measured using the

Weimar high pressure oedometer system (i.e., specimen CR-1). The two specimens were chosen to make the comparison as both had almost the same final void ratio (or final dry density). The final void ratio is considered instead of the initial one as the deformability characteristics of both system are different (see Chapter 7). In spite of a slight difference in the final swelling pressures measured using the two different swelling pressure measurement systems, the development of swelling pressures (i.e., the swelling pressure versus elapsed time curves) of both specimens are fairly similar. It indicates that both cells are comparable.

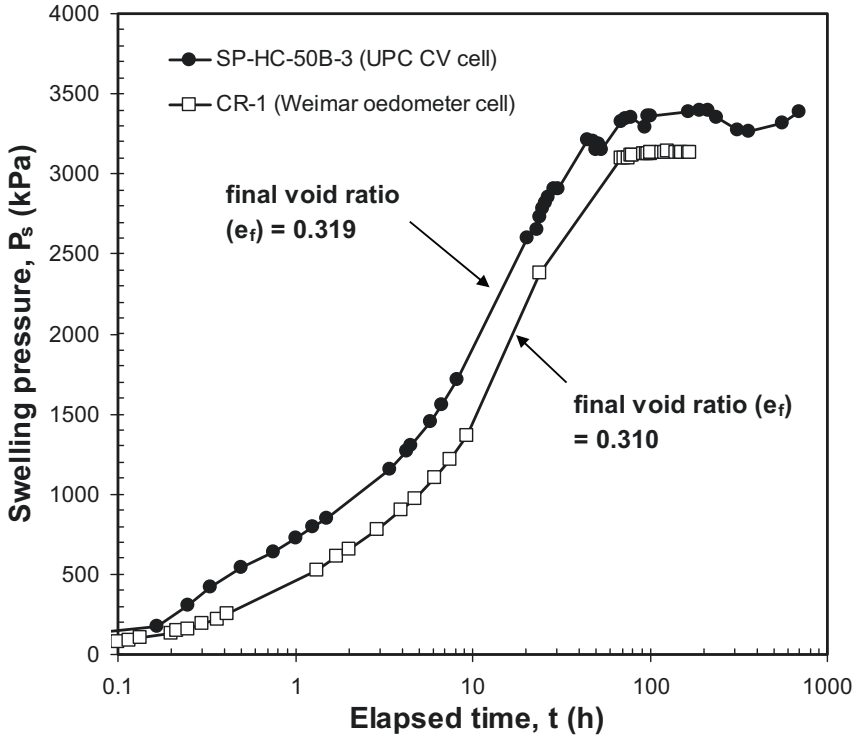

Figure 10.1 Results of tests on specimens SP-HC-50B-3 and CR-1 indicating the compatibility of UPC constant volume cell and Weimar high pressure oedometer cell

10.2.2 Swelling Pressures from the Different Methods of Test

Figure 10.2 show a comparison between three different methods (i.e., the swell-load, swell-under-load, and constant volume tests) carried out for measuring swelling pressure of the heavily compacted 50/50 bentonite-sand mixture. The results of test on specimen SL-1 (i.e., the swell-load test) are extrapolated to define the void ratio corresponding to the initial void ratio of the specimen. The swelling pressure determined by the constant volume test was taken as an average value of five swelling pressures among them four were measured in the UPC constant volume swelling pressure cell (i.e., specimens SP-HC-50B-1, 2, 3, and 5) whereas the other swelling pressure data was obtained from test on specimen CR-1 (i.e., the swelling-pressure-compression-rebound test) using the Weimar high pressure oedometer cell.

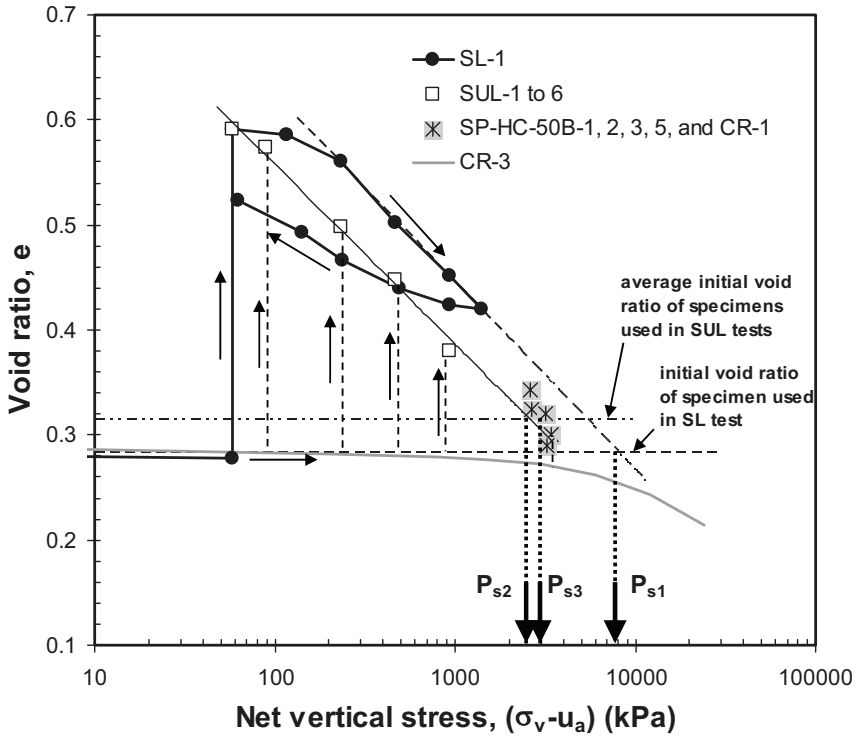

Figure 10.2 Swelling pressure of the heavily compacted 50/50 bentonite-sand mixture measured using three different types of test

The swelling pressures obtained using the three different methods used are summarised in Table 10.1. The different values of swelling pressure measured by different methods indicate the stress- and suction-path dependency of swelling pressure. The swelling pressure value measured by the constant volume method may be deemed to be the most accurate value as it involves less stress and suction paths as compared to the other two methods (Sridharan et al., 1986). The swell-under-load method may give the least accuracy due to possible variability of the specimens used.

Table 10.1 Summary of the results of three swelling pressure test methods

Test	Specimens used	Swelling pressure (kPa)		Remarks
Swell-load	SL-1	P_{s1}	8100	Maximum
Swell-under-load	SUL-1 to 6	P_{s2}	2575	Minimum
Constant volume	SP-HC-50B-1, 2, 3, 5, and CR-1	P_{s3}	3022	Middle value

10.2.3 Swelling Pressure of the Compacted Bentonite-Sand Mixtures

Figure 10.3 shows the relationship between swelling pressure versus mixture dry density of the compacted specimens of four bentonite-sand mixtures used in this study.

The dry density of compacted mixtures considered herein is the corrected dry density by accounting for the deformation of UPC Barcelona constant volume cells as presented in Chapter 7. As specified before, the lightly compacted specimens with 30% bentonite content are denoted in the figure as SP-LC-30B-1 to 6 and similarly other specimens with different bentonite contents are also denoted this way. As expected, swelling pressure of each compacted bentonite-sand mixture is a function of mixture dry density. The swelling pressure of a specimen with higher bentonite content is higher compared to another specimen with lower bentonite content at the same mixture dry density. By utilising Equation (8.3), the bentonite dry density (ρ_{db}) of each specimen can be computed and the relationship between swelling pressure and bentonite dry density for the four bentonite-sand mixtures is shown in Figure 10.4. The data of swelling pressure measurements on the heavily compacted specimens (SP-HC-50B-1, 3, 5, 8 to 10 and SP-HC-100B-1 to 3) are also plotted in the figure. Similar to the relationship between total suction and bentonite water content, the swelling pressure versus bentonite dry density data obtained for the four mixtures fall in a single curve indicating that swelling pressure is collectively a function of bentonite dry density.

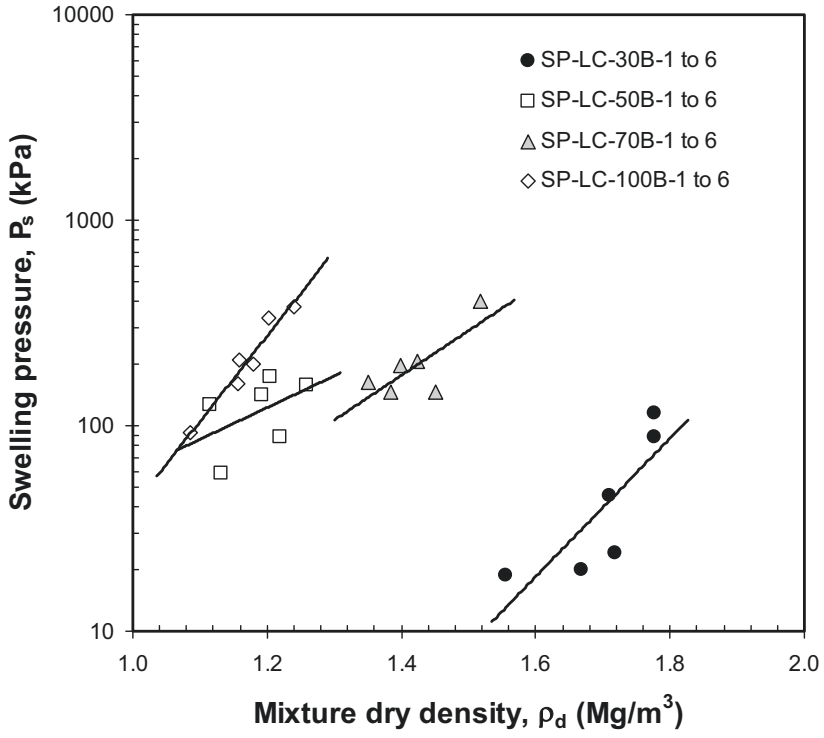

Figure 10.3 Swelling pressure versus mixture dry density of the compacted bentonite-sand mixtures tested

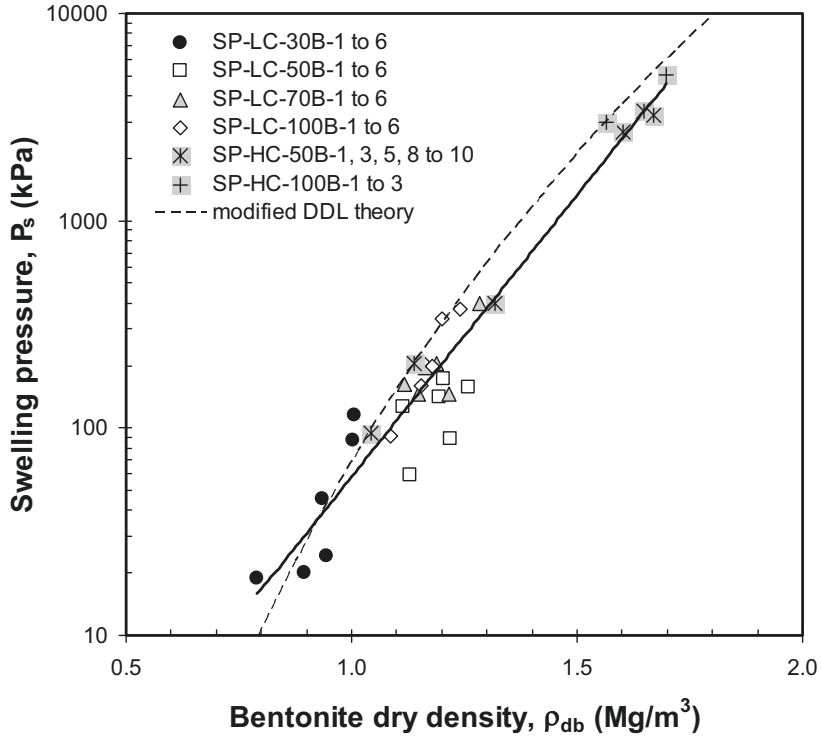

Figure 10.4 Swelling pressure versus bentonite dry density of the compacted bentonite-sand mixtures tested

The following equation can be used to best-fit the experimental data with an r^2 value of 0.931 and an *SEE* of 52 kPa. In the equation, swelling pressure (P_s) is in kPa and bentonite dry density (ρ_{db}) is in Mg/m^3.

$$P_s = 0.1116 \exp\left(6.26\rho_{db}\right) \tag{10.1}$$

The theoretical curve as computed from the modified DDL theory (Tripathy et al., 2004) for Montigel bentonite (i.e., the earlier name of Calcigel) is also given in the figure for comparison. The theoretical curve shows a good agreement with the experimental data indicating the capability of the method to empirically account for some factors that are not accounted for in the original DDL theory.

Figure 10.5 show a semi-logarithmic plot of net vertical stress or swelling pressure of the compacted specimens (i.e., both the lightly and heavily compacted specimens) obtained from the constant volume (CV) and swell-under-load (SUL) tests presented as a relationship between bentonite void ratio versus net vertical stress or swelling pressure. The use of bentonite void ratio instead of mixture void ratio enables the test results of different mixtures to be compared. The bentonite void ratio of the specimens was calculated from the corresponding bentonite dry density (Equation (8.3)). The results show that the SUL test data tend to flatten at low net vertical stress.

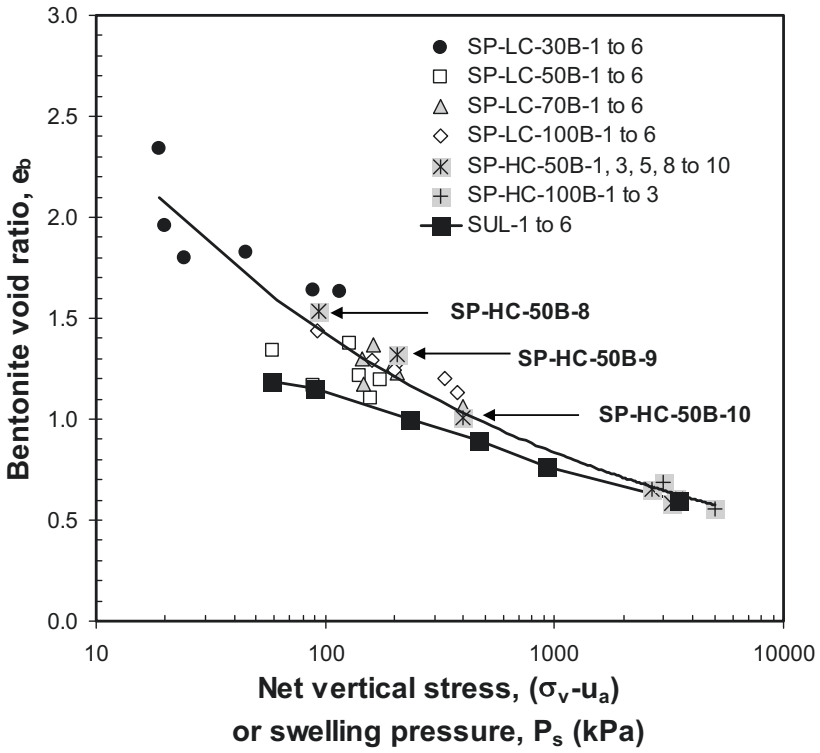

Figure 10.5 Bentonite void ratio versus vertical stress or swelling pressure obtained from constant volume swelling pressure tests

According to the figure, the equilibrium void ratio obtained from the SUL test hardly reaches the corresponding value for the swelling pressure curve at low net vertical stresses. The retarded swelling in the SUL test might be due to difference in structure of the specimens used in the test compared to that of the specimens used in the CV tests at the equilibrium void ratio. The difference in initial conditions (i.e., initial water content and initial void ratio) of the specimens appears to have insignificant impact. Consider specimens SP-HC-50B-8 to 10 (i.e., marked in the figure) which had 'similar' initial conditions to specimens SUL-1 to 6. If the initial conditions played a role, the points would have been located close to the SUL test results.

The difference in structure of the specimens used in the CV tests compared to those used in the SUL tests at the equilibrium void ratio is related to the difference in size of the clay clusters whereas the size and volume of inter-aggregate pores of the specimens might not differ significantly (Nagaraj and Miura, 2001). An as prepared specimen which is loaded and subsequently allowed to imbibe water until reaching equilibrium would have clay clusters with a smaller size compared to a similar specimen which is first wetted to an intermediate suction and subsequently tested in the constant volume cell. The fact is true provided that the net vertical stress under which the former has reached its equilibrium is of the same magnitude as the swelling pressure of the latter specimen. It appears that the change in cluster size during wetting depends on the applied net vertical

stress under which the specimen is wetted. During CV test, swelling pressure develops gradually thus allowing expansion of the clay clusters until the swelling pressure development vanishes whereas the applied net vertical stress retards the expansion of clay clusters from the beginning of wetting process. Since both specimens have the same equilibrium suction at the end of test (i.e, zero equilibrium suction), the difference in size of the clay clusters reflect the difference in arrangement of clay particles in the clusters.

10.2.4 Rates of Swelling Pressure Development and Water Sorption

Figure 10.6(a) and Figure 10.6(b) shows, respectively, typical curves of swelling pressure and absorbed water versus elapsed time plotted in semi-logarithmic scales. The increase in both the swelling pressure and amount of absorbed water with time was rapid at the earlier stage of tests (i.e., up to 50 hours). The rate of both swelling pressure development and amount of absorbed water asymptotically decreases beyond a point which marks the end of primary swelling pressure development. The test results performed by Gattermann (1998) showed that swelling pressure was constant with time after the maximum value was reached. Alonso et al. (1999) showed that swelling pressure may also decrease as a result of collapse of the clay macro-structure. According to Figure 10.6(a), after the maximum primary swelling pressure is reached, swelling pressure might increase, stay constant, or decrease with time. However, the rate of swelling pressure development generally decreased with time after the maximum swelling pressure was attained.

The rate of swelling of several expansive soils tested in oedometer was reported by Sridharan and Gurtug (2004), where the percent swell versus time curve was approximated using a rectangular hyperbola equation. Sridharan et al. (1986) showed that the swelling pressure versus time curve for several clays could also be approximated using the rectangular hyperbola equation. In case of the swelling pressure development and the amount of absorbed water of the compacted specimens used in this study, the rectangular hyperbola equation is found to be unable to give a satisfactory fit to the experimental data of either the swelling pressure development or the amount of absorbed water with time. The experimental data show that a linear relationship is obtained between the normalised swelling pressure ($P_s/P_{s\ max}$) and the square root of elapsed time at earlier stage of the swelling pressure development (i.e., mostly up to 60% of the maximum swelling pressure). Thus:

$$\frac{P_s}{P_{s\,\max}} = c_P\, t^{0.5} \tag{10.2}$$

where c_P is the slope of $P_s/P_{s\ max}$ versus $t^{0.5}$ at the earlier swelling pressure development which represents the rate of swelling pressure development, $P_{s\ max}$ is the maximum swelling pressure (kPa), and t is elapsed time (hours).

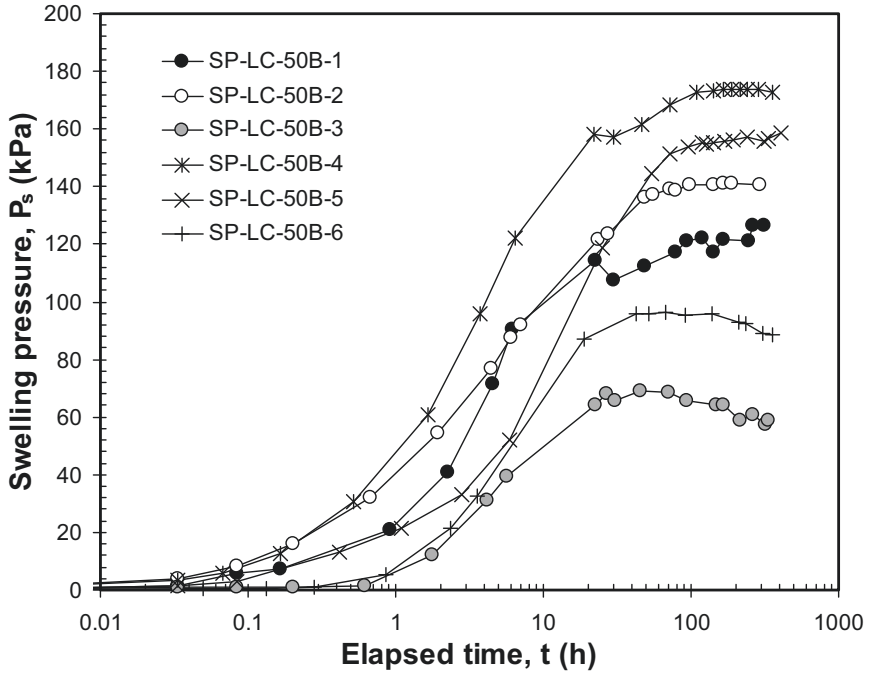

(a)

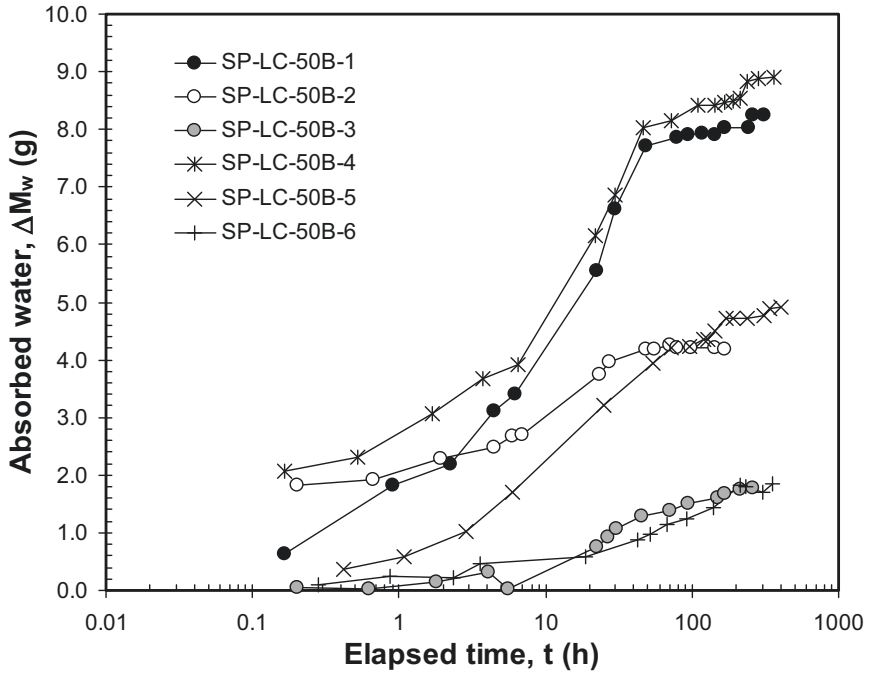

(b)

Figure 10.6 (a) Typical results of the one-step constant volume swelling pressure test (a) swelling pressure and (b) absorbed water versus elapsed time

Figure 10.7(a) depicts the swelling pressure development plotted against $t^{0.5}$ for two compacted specimens (i.e., SP-LC-30B-4 and SP-LC-70B-5). Specimen SP-LC-30B-4 had a higher initial bentonite water content (i.e., 31%) thus a higher total suction compared to specimen SP-LC-70B-5 which had an initial bentonite water content of 36%. It is shown in the figure that the slope of P_s versus $t^{0.5}$ curve of specimen SP-LC-70B-5 is higher than that of specimen SP-LC-30B-4. However, the normalised curve shows that the slope of P_s versus $t^{0.5}$ curve (i.e., the c_P value) of specimen SP-LC-30B-4 is higher than that of specimen SP-LC-70B-5 (Figure 10.7(b)). In a similar way, the following equation is used to fit the experimental absorbed water versus time data at the earlier stage of test.

$$\frac{\Delta M_w}{\Delta M_{w\max}} = c_M \, t^{0.5} \tag{10.3}$$

where c_M is a constant representing the rate of absorbed water, ΔM_w is the absorbed water (g), and $\Delta M_{w\,max}$ is the maximum value of absorbed water (g).

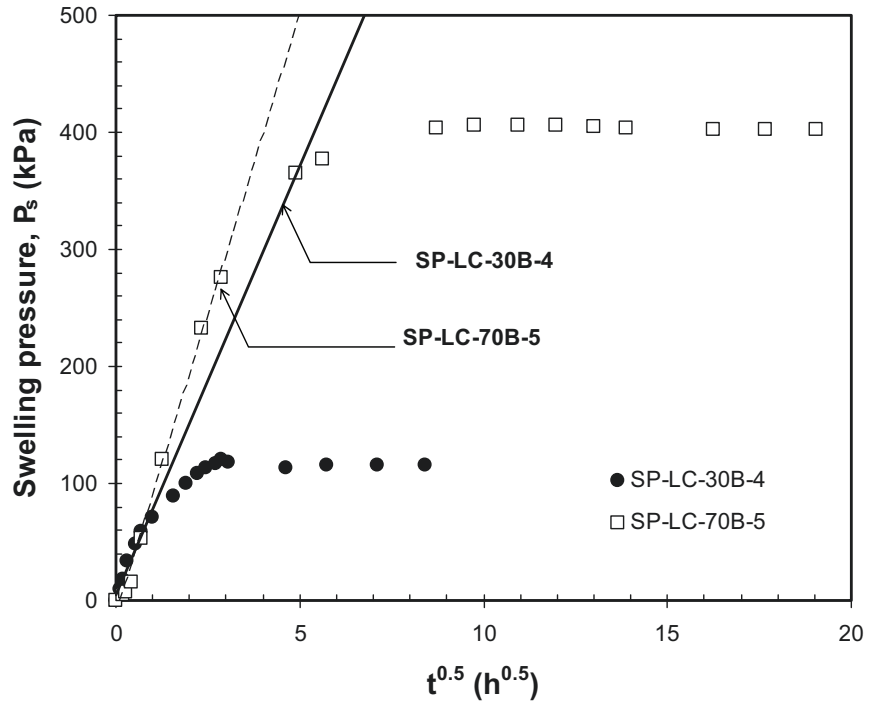

(a)

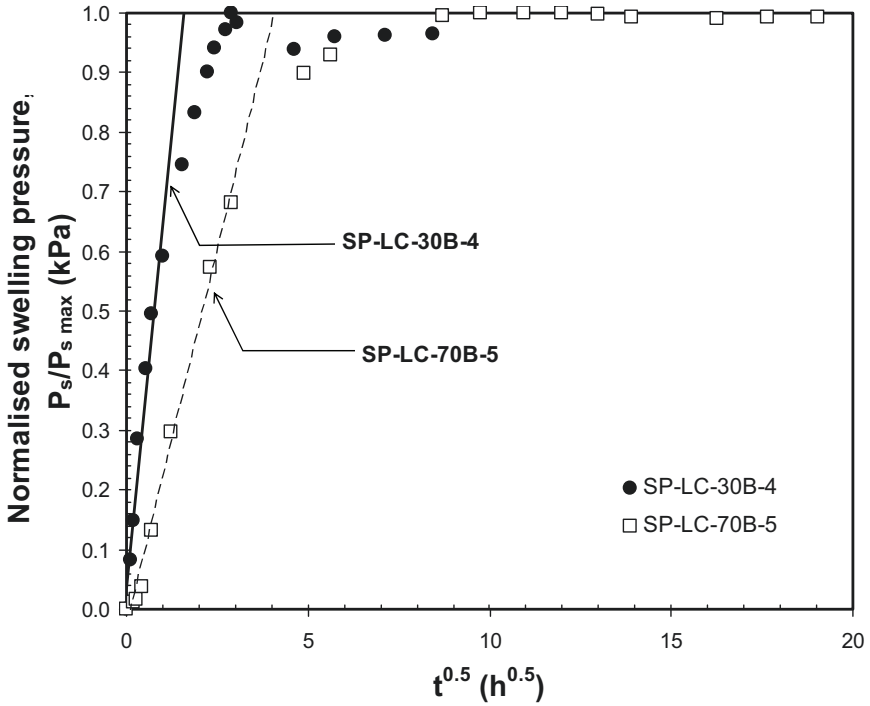

(b)

Figure 10.7 (a) Swelling pressure versus square root of time and (b) normalised swelling pressure versus square root of time of two compacted specimens

The c_P and c_M values were thought to be related to the initial total suction of the specimen. The initial total suction of each specimen was approximated using Equation (8.5) and the plot of c_P and c_M values versus initial suction of the specimens is shown in Figure 10.8 and Figure 10.9, respectively. It is depicted in Figure 10.8 that the c_P value increases with increasing specimen initial total suction for specimens SP-LC-50B-1 to 6, SP-LC-70B-1 to 6, and SP-LC-100B-1 to 6 with 50%, 70%, and 100% bentonite content, repsectively. However, the relationship does not hold for specimens SP-LC-30B-1 to 6 and the heavily compacted specimens (i.e., specimens SP-HC-50B-1, 3, 5, 8 to 10 and SP-HC-100B-1 to 3). The relationship between c_P and initial total suction shows an opposite trend. The reason for this appears to be the more pronounced effect of bentonite density for the specimens with 'very high' and 'very low' bentonite void ratio. No discernible trends are seen in the c_M versus initial total suction relationship (Figure 10.9). This might be due to the presence of air bubbles in the porous disk of the constant volume cells used at the earlier stage of swelling pressure tests.

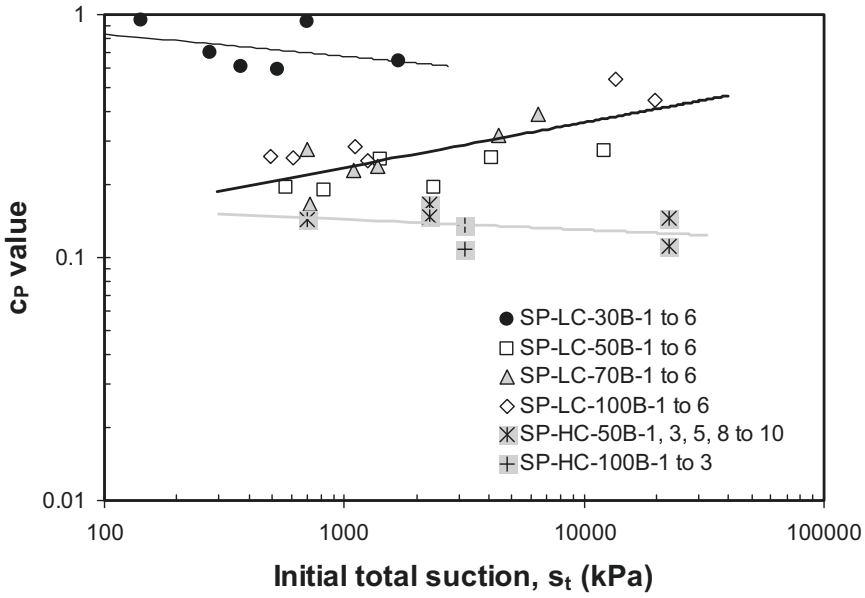

Figure 10.8 c_P value versus initial total suction

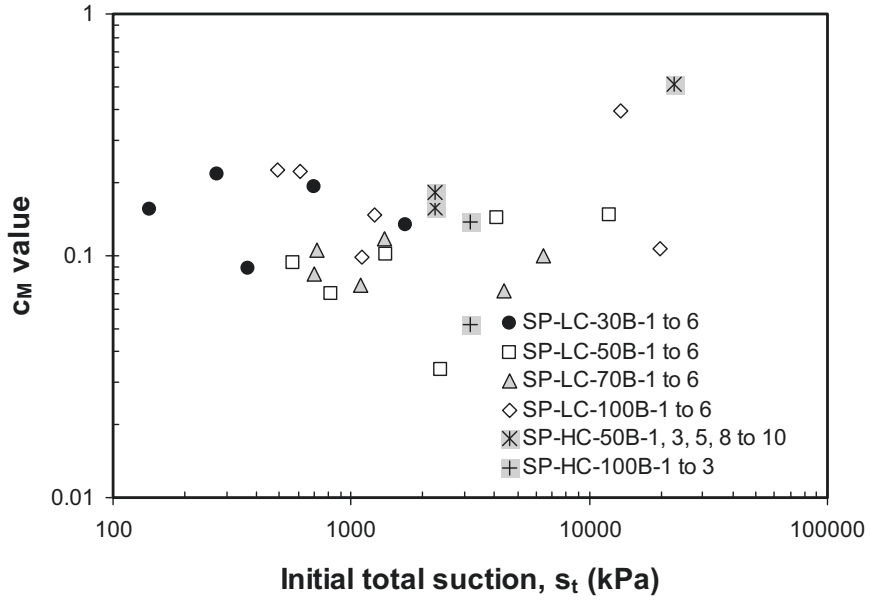

Figure 10.9 c_M value versus initial total suction

10.2.5 Swelling Pressure Development with Decreasing Suction and Wetting Behaviour under Constant Volume Conditions

Figure 10.10 shows swelling pressure development with decreasing suction for the as-prepared compacted specimen of 50/50 bentonite-sand mixture (i.e., specimens SP-HC-50B-3 and 4). It is shown that there was practically no development of swelling pressure upon wetting from the as-prepared suction to about 2000 kPa suction. A rapid development of swelling pressure occurred afterward. The migration of water during wetting from the as-prepared suction to about 2000 kPa suction mainly occurred in vapour form since the vapour equilibrium technique (VET) was used for applying suction within this range. In this mechanism, water molecules first migrate into the open voids in the soil specimen and are further absorbed as soon as they are in contact with the exposed surfaces of clay clusters (Pusch, 2001). The mechanism of water movement from the exposed surfaces of clay clusters to the intra-cluster (or intra-aggregate) pores is driven by a water potential (or suction) gradient that exists between the inter-aggregate and intra-aggregate pore-water (i.e., the internal water redistribution process) and the mixture permeability at micro and macro scales. The water absorption by the clay clusters and that occurs in the inter-aggregate pores take place simultaneously since a suction gradient also exists between the inter-aggregate pore-water and the external source of water (i.e., the circulated water vapour).

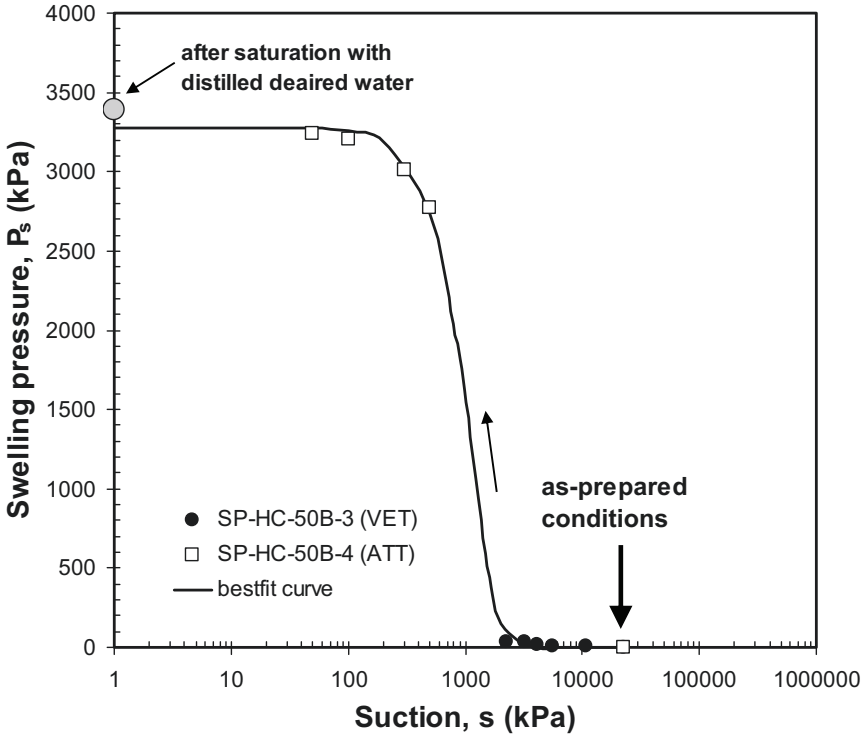

Figure 10.10 Swelling pressure development with decreasing suction for as-compacted specimens (SP-HC-50B-3 and 4)

By considering the abovementioned water transport mechanisms, the insignificant swelling pressure development during wetting up to 2000 kPa suction might be due to a delayed 'true' equilibrium in the specimen. Although the swelling pressure developed and the amount of water absorbed during each suction decrement appeared to cease, an internal redistribution of water might still occur within the specimen. At an apparent equilibrium state for each suction decrement, the water potential (or suction) of the inter-aggregate pore-water might have the same value as the suction induced by the circulated water vapour. Further water absorption and swelling pressure increase would continue as soon as the equilibrium between inter- and intra-aggregate pore-water was attained. However, the rate of water movement from the inter-aggregate to intra-aggregate pores might be very low. Therefore, the 'true' equilibrium might be attained after long test duration.

The water transport during suction reduction below 2000 kPa occurred in the liquid form since the test in this suction range was performed using the axis-translation technique (ATT). As the clay clusters expanded, the inter-aggregate pores were closed and the effects of internal water redistribution became less obvious (Alonso, 1998).

The following equation gives the best-fit to the experimental data and can be used to express the development of swelling pressure with decreasing suction for the as-

prepared specimen with both P_s and s are in kPa. The equation gives a coefficient of determination (r^2) of 0.999 and a standard error of estimate (*SEE*) of 54 kPa.

$$P_s = \frac{3279}{\left\{\ln\left[\exp(1)+\left(\frac{s}{10375}\right)^{2.05}\right]\right\}^{248}} \tag{10.4}$$

Figure 10.11(a) and Figure 10.11(b) show the corresponding constant volume wetting characteristics of the as-prepared compacted specimen of 50/50 bentonite-sand mixture. By comparing Figure 10.11(a) with Figure 10.10, it is shown that the development of about 80% of the maximum swelling pressure resulted from a moisture intake of only 50% of that required to saturate the specimen. Similarly, a rapid increase in the degree of saturation occurred upon wetting until the degree of saturation of specimen reached 100% at a suction of about 100 kPa. Equation (10.5) and Equation (10.6); respectively, can be used to express the increase in water content (w) and degree of saturation (S_r) with decreasing suction (s) with w and S_r are in percent and s is in kPa. Similar to Equation (10.4), the equations has a similar form to the Fredlund and Xing (1994) SWCC equation.

$$w = \frac{15.37}{\left\{\ln\left[\exp(1)+\left(\frac{s}{2.63}\right)^{0.397}\right]\right\}^{0.409}} \tag{10.5}$$

$$S_r = \frac{100}{\left\{\ln\left[\exp(1)+\left(\frac{s}{202}\right)^{1.147}\right]\right\}^{0.106}} \tag{10.6}$$

Equation (10.5) has an r^2 value of 0.990 with an *SEE* of 0.18% whereas Equation (10.6) has an r^2 value of 0.988 with an *SEE* of 0.78%.

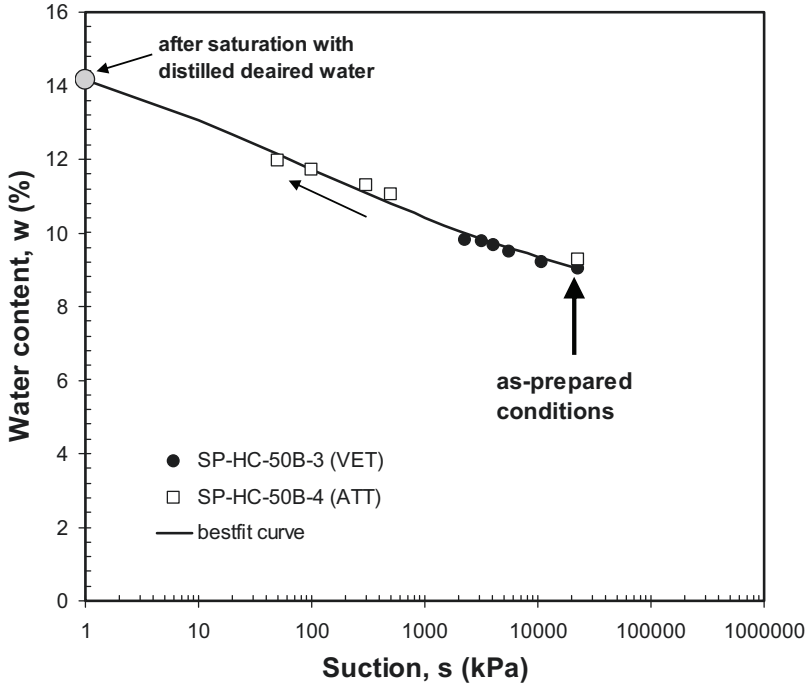

(a)

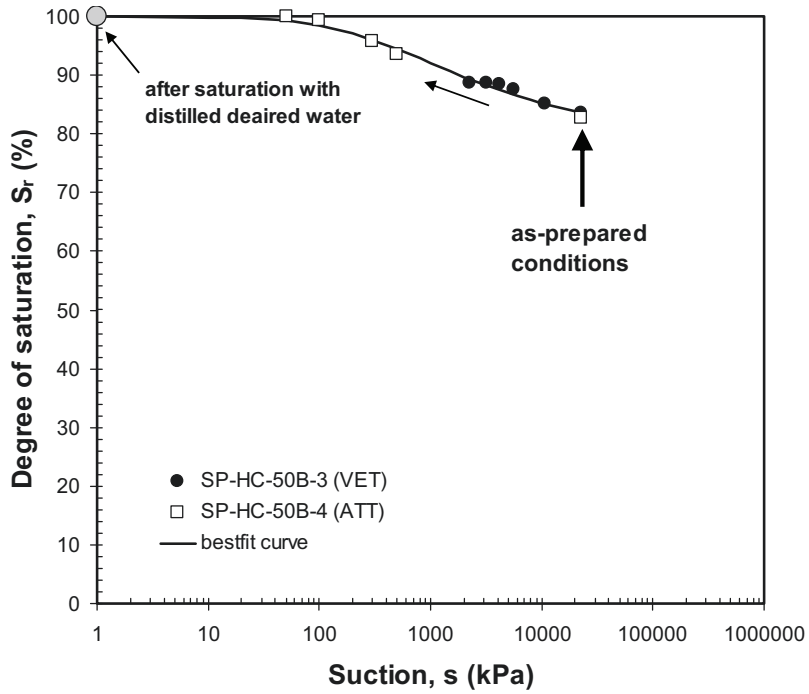

(b)

Figure 10.11 Constant volume wetting characteristics of the as-compacted specimens (SP-HC-50B-3 and 4): (a) water content versus suction and (b) degree of saturation versus suction

10.2.6 Comparison of Unconfined and Constant Volume Wetting Curves and Estimated Wetting Curve from the PSD Data

Figure 10.12(a) and Figure 10.12(b) present a comparison between the measured water content versus suction curve and that estimated from the MIP test results for the as-prepared and oven-dried specimens, respectively. It is shown that for both the as-prepared specimen (Figure 10.12(a)) and the oven-dried specimen (Figure 10.12(b)), the water content versus matric suction curve estimated from the MIP test results is close to that obtained from the wetting test under constant volume conditions. It is plausible since during mercury intrusion the volume of specimen was essentially constant (Sridharan et al., 1971). The differences in both curves can be attributed to the possible differences in drying and wetting behaviour or hysteresis and the effects of osmotic and sorptive forces that are not accounted for in the computation of water content versus suction curve based on the Washburn equation (see Chapter 6).

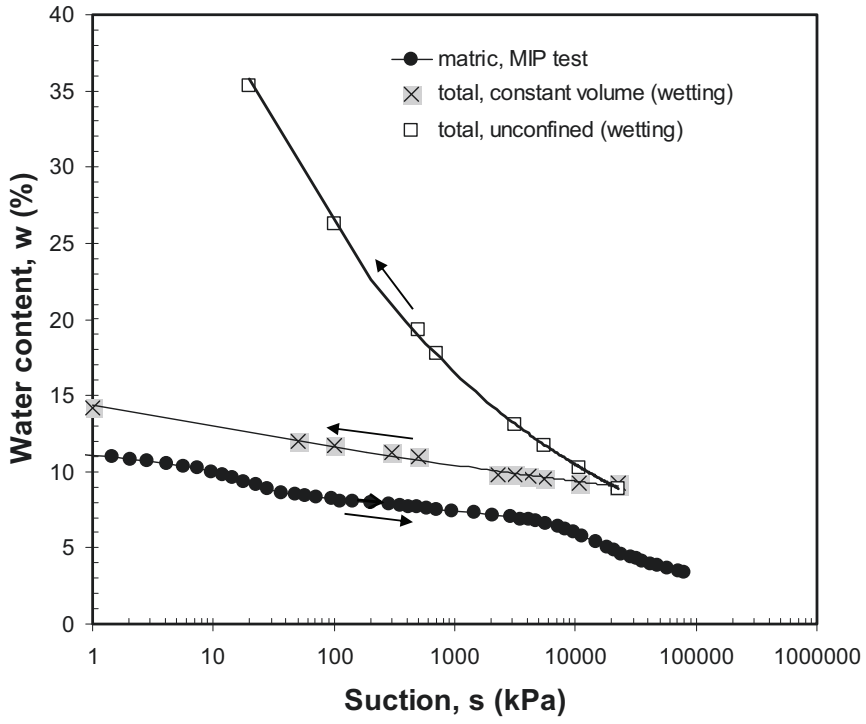

(a)

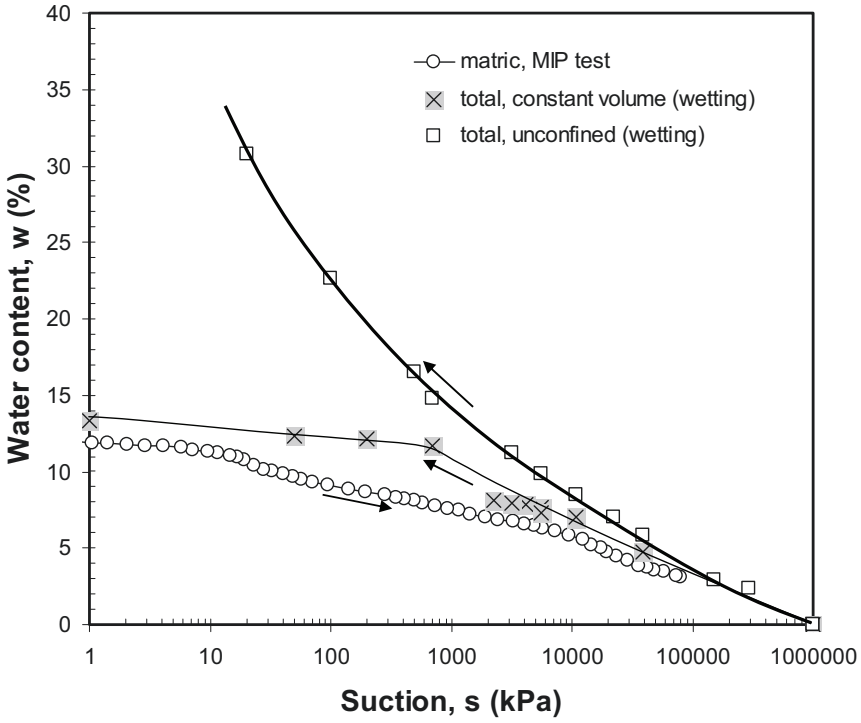

(b)

Figure 10.12 Comparison between the measured water content versus suction curve and that estimated from the MIP test data for: (a) as-prepared specimen and (b) oven-dried specimen

10.2.7 Swelling Pressure as a Function of Initial Suction

The results of one-step constant volume swelling pressure test on specimens SP-HC-50B-3, 5, and 8 to 10 are presented on a logarithmic plot of swelling pressure versus initial suction in Figure 10.13. Specimens SP-HC-50B-8 to 10 were equilibrated to different suction values (in the pressure plate) and allowed to swell until reaching an equilibrium void ratio prior to swelling pressure test. It is shown by the trend-line given in the figure that in the low suction range (approximately below 220 kPa), the measured swelling pressure is approximately of the same magnitude as the specimen's initial suction.

Since the three specimens were equilibrated to different suctions in the pressure plate, it is interpreted that the equilibrium suction was the matric component provided that the soil pore-water had the same compositions as the supplied water at the equilibrium. However, a partial dilution of ions that occurred during equilibration did not allow a full equalisation of ion concentration between the soil pore-water and supplied water. The osmotic and sorptive forces that were not fully dissipated at equilibrium were balanced by the capillary effect (i.e., u_a - u_w) and the self weight of the specimen.

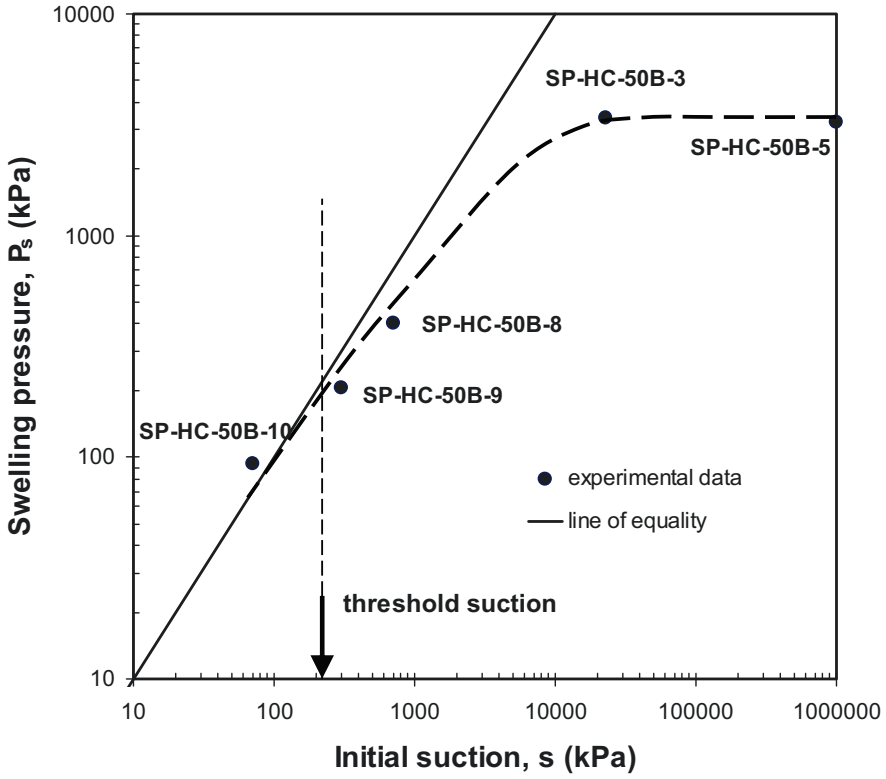

Figure 10.13 Swelling pressure as a function of initial suction for the heavily compacted 50/50 bentonite-sand mixture

Specimen SP-HC-50B-8 was allowed to equilibrate one-dimensionally to a suction of 700 kPa (in the pressure plate) before tested for its swelling pressure with distilled deaired water. Therefore, the specimen underwent a net suction decrement of 700 kPa. Another assessment can also be made by calculating the ratio of swelling pressure increase (ΔP_s) to suction decrease (Δs) for the result of a multi-step swelling pressure test presented in Figure 10.10. The ratio of swelling pressure increase to suction decrement (α_p) is computed using the following equation.

$$\alpha_p = \frac{\Delta P_s}{\Delta s} \tag{10.7}$$

The computed α_p value is plotted against the average (logarithmic) suction and shown in Figure 10.14. The threshold suction is defined as an average suction below which the α_p value is equal to unity. The value of threshold suction for the multi-step swelling pressure test from as-prepared suction (specimens SP-HC-50B-3 and 4) is about 400 kPa, which is fairly in good agreement with the threshold suction presented in Figure 10.13. A similar finding was reported by Kassiff and Ben Shalom (1971) who observed a threshold suction of 200 kPa for a montmorillonitic clay which was tested following the multi-step constant volume swelling pressure test.

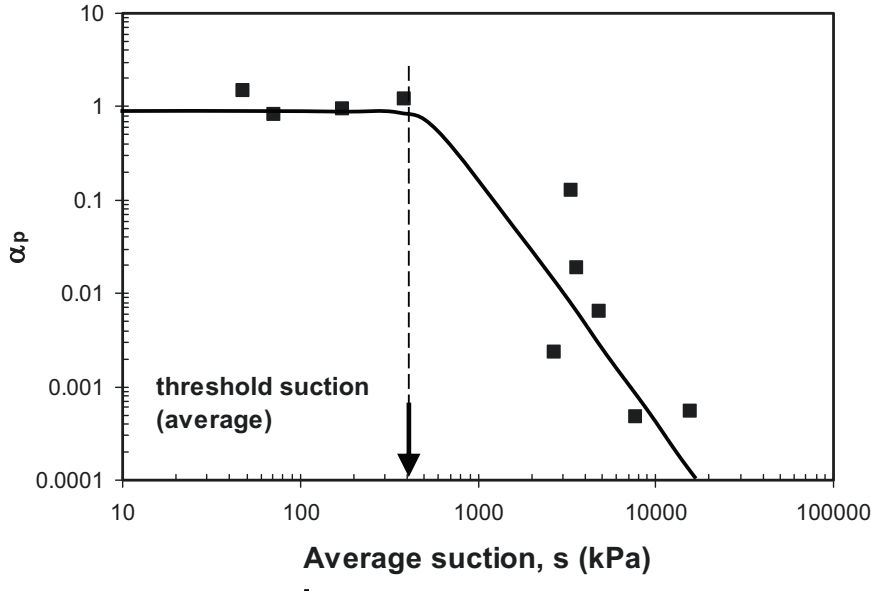

Figure 10.14 α_p value versus average suction for the multi-step swelling pressure test from the as-prepared suction (specimens SP-HC-50B-3 and 4)

If swelling pressure is regarded as effective stress (or net stress), below the threshold value, a decrease in suction will be accompanied by an increase in effective stress of the same magnitude. This fact is in favour with the concept of effective stress for unsaturated soils (see Chapter 3). However, the degree of saturation corresponding to the suction threshold as shown in Figure 10.14 is about 100%. This indicates that the micro-structural effective stress concept as formulated in Chapter 4 (i.e., Equation (4.2)) is also valid at macroscopic level provided that the soil is saturated or very close to saturation.

10.2.8 Three-Dimensional Visualisation of the Swelling Pressure Tests

Figure 10.15 shows a three-dimensional plot of swelling pressure tests; namely, swell-load (SL) test (i.e., specimen SL-1), swell-under-load (SUL) test (i.e., specimen SUL-1 to 6), multi-step swelling pressure test (i.e., specimens SP-HC-50B-3 and 4), and one-step swelling pressure test after 1-D wetting (i.e., specimens 3, 5, and 8 to 10). The three-dimensional plot presented shows a consequence of the two stress state variables approach in representing the different methods of the swelling pressure tests, which clearly visualises how the different methods adopted measured different values of swelling pressure. However, it should be noted that a simplification has been made in representing net vertical stress (σ_v - u_a) and suction (s) together on one plot. The natures of the two stress variables are different; net vertical stress is one-dimensional whereas suction is isotropic in nature.

The constitutive surface for unloading case is formed by the one-dimensional swelling curve on the *e-s* plane (i.e., for one-dimensional case only) and the rebound

curve from a sufficiently high net vertical stress (i.e., an approximated curve based on the saturated compression-rebound tests). The paths of constant volume swelling pressure tests lie outside the constitutive surface in the e-(σ_v - u_a)-s space. The paths appear to compose the loading constitutive surface instead of the unloading one. The figure implies that the convergence void ratio for the unloading constitutive surface may be close to 0.8.

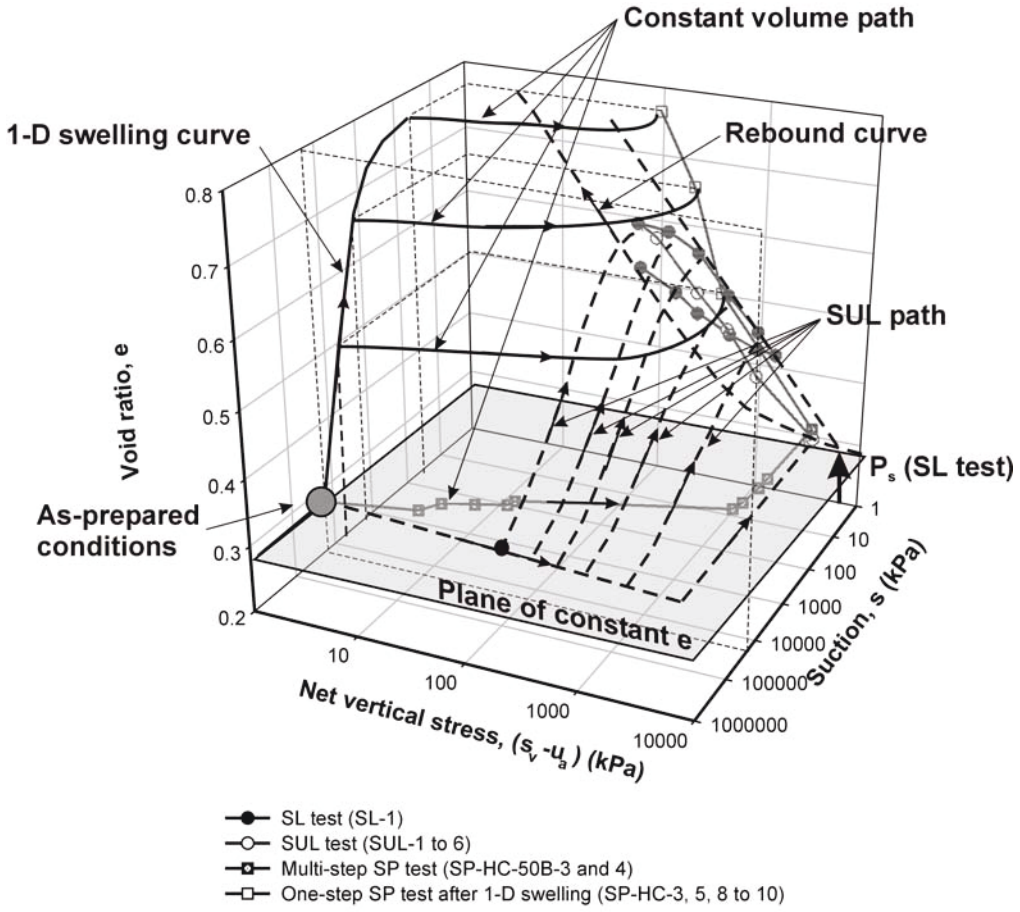

Figure 10.15 Three-dimensional visualisation of different swelling pressure tests

10.2.9 Influence of Initial Conditions and Bentonite Content on the Swelling Pressure Development and Unconfined Wetting Characteristics

The development of swelling pressure with decreasing suction for the specimens that were wetted from different initial conditions and bentonite contents are shown in Figure 10.16. Swelling pressure did not increase with suction reduction above 2000 kPa suction for the specimens with 50% bentonite content irrespective of the initial suction of the specimens. The pure bentonite specimen, which was tested from about 20% water content (i.e., referred to as the 'wet' specimens), shows a similar behaviour. Swelling pressure developed rapidly following suction reduction in the specimen of pure bentonite tested from oven-dried conditions. Having considered the factors influencing the insignificant swelling pressure development of the as-prepared 50/50 compacted

bentonite-sand specimen at high suctions as described before, it is understood that the delayed 'true' equilibrium in the specimen with 50% bentonite content is mainly due to the low permeability of the specimen. The presence of sand reduced the average flow of water (i.e., in liquid and/or vapour forms) per unit area of the specimen with 50% bentonite content in comparison with the pure bentonite specimen. The delayed 'true' equilibrium of the 'wet' pure bentonite specimen appears to be caused by the 'low' water potential gradient. This specimen had an average initial suction of about 18000 kPa which was much lower than the initial suction of the oven-dried pure bentonite specimen with an initial suction of 1 000 000 kPa which corresponds to the suction at oven-dried conditions (Croney and Coleman, 1961).

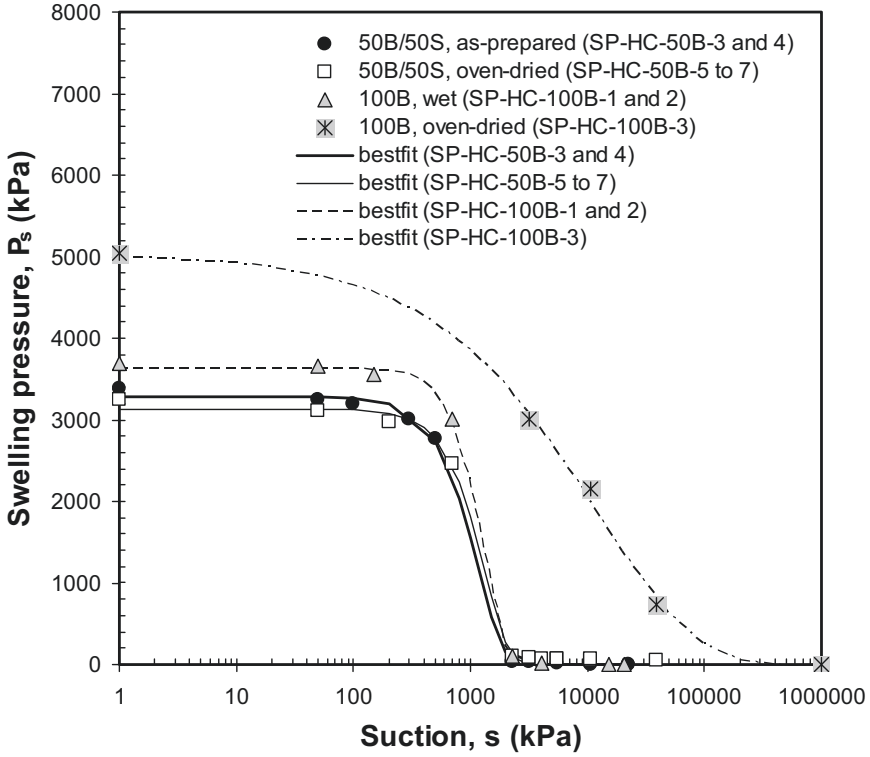

Figure 10.16 Swelling pressure development with decreasing suction for specimen with different initial conditions and bentonite content

Figure 10.17(a) and Figure 10.17(b) show, respectively, water content and degree of saturation versus suction plot of the specimens with different initial conditions and bentonite contents. A rapid increase in water content with decreasing suction was observed in the oven-dried specimens. The specimens wetted from 'wet' conditions generally show an insignificant increase in water content up to 2000 kPa suction. A rapid increase in the water content was observed afterward. The characteristic of degree of saturation versus suction generally shows a similar behaviour.

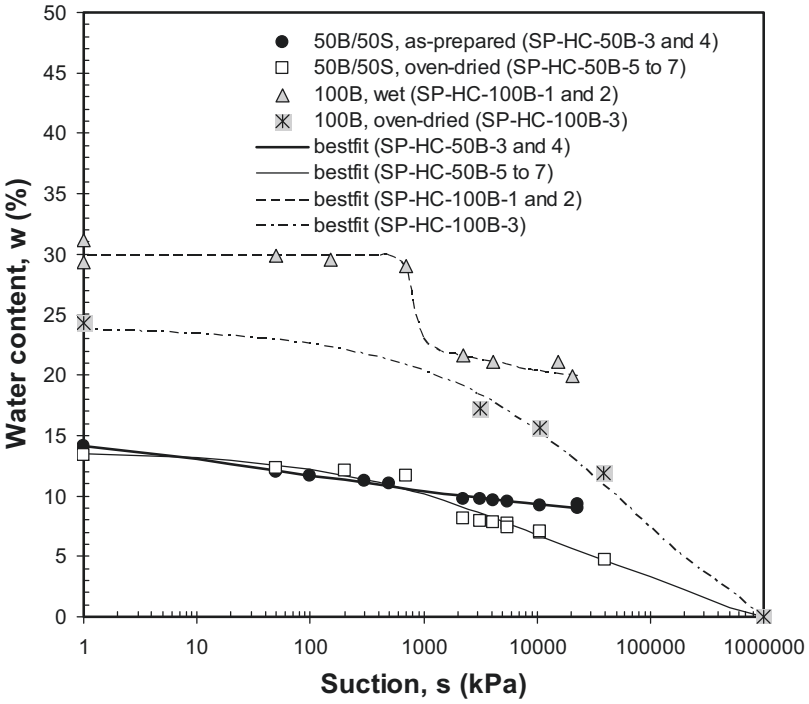

(a)

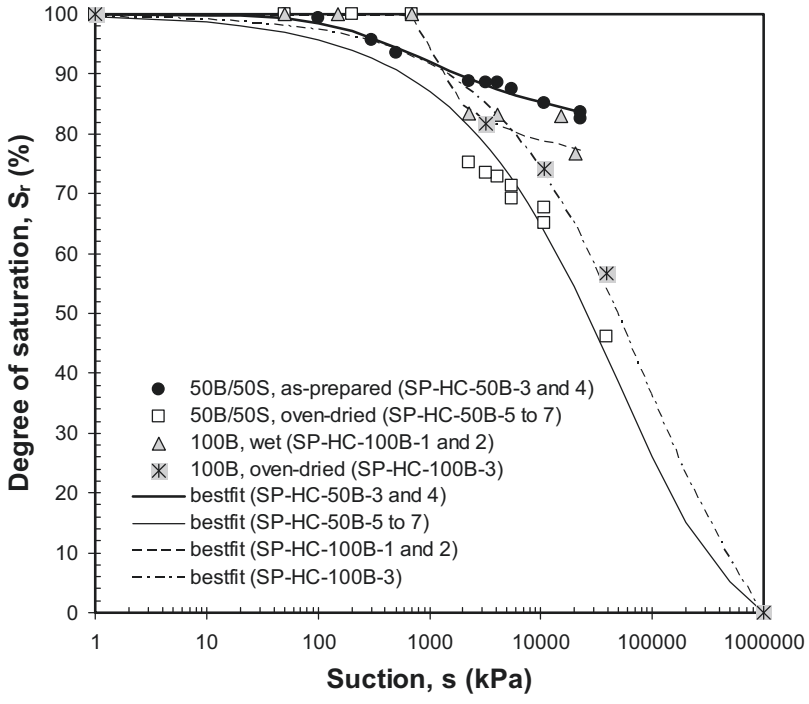

(b)

Figure 10.17 Constant volume wetting characteristics of the specimens with different initial conditions and bentonite contents: (a) water content versus suction and (b) degree of saturation versus suction

The α_p value for each test can also be computed in a similar manner to the data for the as-compacted specimen. Figure 10.18 shows a variation of α_p value versus average (logarithmic) suction. The figure indicates that the threshold suction depends on the bentonite content without any apparent effects of initial suction (or initial water content). For specimen with the same bentonite content, the α_p value before reaching unity is a function of specimen's initial suction (or initial water content).

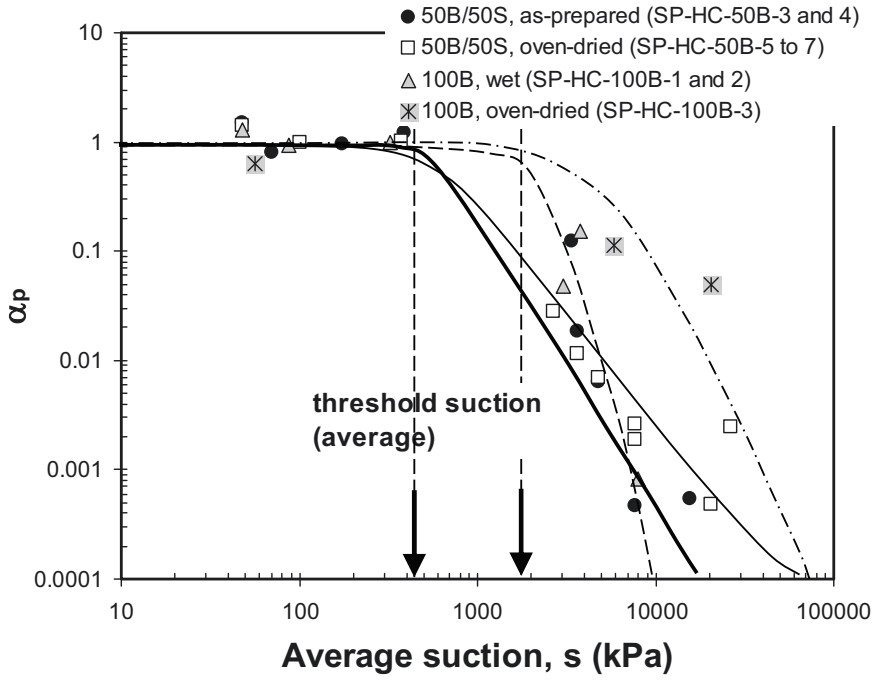

Figure 10.18 α_p value versus average suction for the specimens with different initial conditions and bentonite contents

To investigate the increase of swelling pressure with increasing water content during unconfined wetting, a plot of swelling pressure versus water content for the specimens with different initial conditions and bentonite contents was produced and shown in Figure 10.19. The specimens with the same bentonite content appear to behave similarly irrespective of the initial suction (or initial water content). Both cases (i.e., the specimens with 50% bentonite content and pure bentonite) show a threshold water content beyond which a small increase in water content results in a significant increase in swelling pressure.

The threshold water content of the 50/50 bentonite-sand specimens (i.e., the as-prepared and oven-dried specimens) and the oven-dried pure bentonite specimen is between 8% and 10%, whereas the threshold water content of the 'wet' pure bentonite specimen is about 21% (i.e., close to its initial water content). No conclusion can be drawn from Figure 10.19 regarding factors controlling the magnitude of threshold water

content. However, it seems that the rate of swelling pressure increase with respect to water content increase is a function of bentonite content.

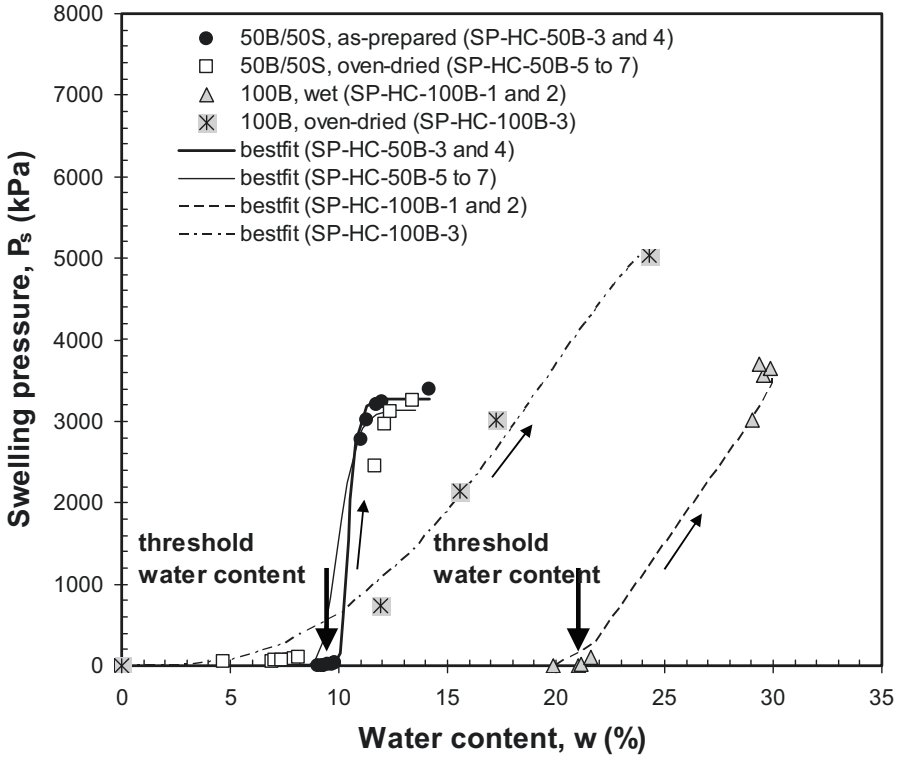

Figure 10.19 Swelling pressure as a function of water content during suction reduction for the specimens with different initial conditions and bentonite contents

10.2.10 Summary of the Swelling Pressure Test Results

The following conclusions can be drawn from the swelling pressure test results:

1. The three different types of one-step swelling pressure measurement techniques used (i.e., the swell-load, swell-under-load, and constant volume swelling pressure tests) measured three different values of swelling pressure. It indicates the stress- and suction-path dependency of swelling pressure (Sridharan et al., 1986).

2. Swelling pressure of the bentonite-sand mixtures studied is a function of mixture dry density and mixture bentonite content or is collectively a function of bentonite dry density.

3. The rate of swelling pressure development in the one-step constant volume swelling pressure test appears to be a function of initial total suction of the specimen. The effect of density plays a role in the specimens with ‘very high’ or ‘very low’ bentonite dry density.

4. The swelling pressure development with decreasing suction in the as-prepared specimen was insignificant up to 2000 kPa suction. This might be due to a delayed 'true' equilibrium state of the specimen which is influenced by the water potential (or suction) gradient between the inter- and intra-aggregate pore-water and the mixture permeability at micro and macro scales.

5. There is a threshold suction below which a decrease in suction causes an increase in swelling pressure of the same magnitude. The threshold suction of the as-prepared specimen ranges from 200 to 400 kPa. The existence of the threshold suction is supported by the findings of Kassiff and Ben Shalom (1971). The similarity between the decrease in suction and the increase in swelling pressure indicates the possible applicability of the effective stress concept which incorporates suction in the formulation (Gens and Alonso, 1992). However, this is limited to conditions very close to saturation. The magnitude of threshold suction is generally a function of bentonite content without significant effects of initial conditions.

6. There exists a threshold water content beyond which a further increase in water content results in a significant increase in swelling pressure. The magnitude of threshold water content appears to be also a function of bentonite content.

10.3 One-Dimensional Compression and Rebound Behaviour

10.3.1 Influence of Stiffness of the Oedometer System and Correction Used in the Analysis of the Experimental Data

The as-prepared 50/50 bentonite-sand mixture specimens tested in this investigation were considered to be stiff soils and therefore correction with respect to the oedomoter system stiffness (or deformability) is necessary for analysing the compression-rebound test results (Fredlund and Rahardjo, 1993). Additionally, the applied net vertical stress should also be corrected to account for efficiency of the oedometer test system in delivering pressure to the specimen. This is especially true in the UPC pneumatic oedometer system and is not that significant in the Weimar high pressure oedometer test system. Romero (2003) described that the actual net vertical pressure $(\sigma_v - u_a)_{actual}$ which acts on the specimen when an air pressure of u_a is applied on the rubber membrane with doubling system can be computed as:

$$\left(\sigma_v - u_a\right)_{actual} = 2.329\, u_a \tag{10.8}$$

Figure 10.20 show the uncorrected and corrected data of the compression-rebound test on an as-prepared specimen (i.e., specimen CR-3). The correction with respect to oedometer stiffness significantly affects the test result.

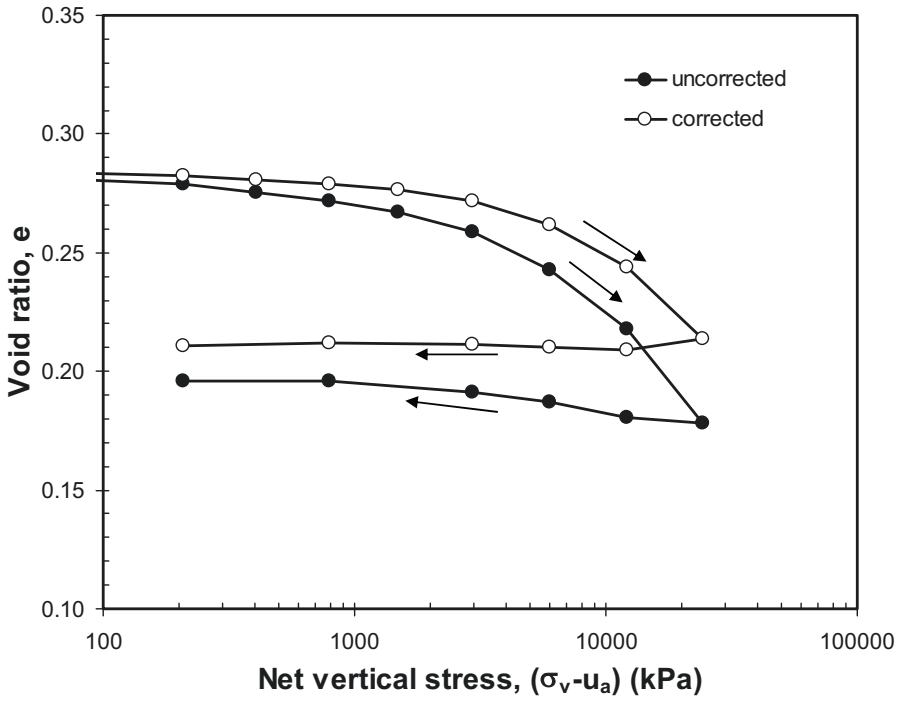

Figure 10.20 Uncorrected and corrected compression and rebound curves of specimen CR-3

10.3.2 One-Dimensional Saturated Compression and Rebound Curves at Low and High Net Vertical Stresses

Figure 10.21 shows a plot of void ratio versus net vertical stress obtained from the saturated compression-rebound tests in the low and high ranges of net vertical stresses (i.e., specimen SL-1 and CR-1). In the low range of void ratio (i.e., apparently below 0.3), the response of specimen to increasing and decreasing net vertical pressure is essentially elastic (i.e., path BG in the figure). The plastic behaviour appears to play a role at higher void ratio (i.e., path AFE in the figure). The plastic behaviour at low void ratio was also observed in unsaturated FoCa7 clay specimens reported by Cui et al. (2002b).

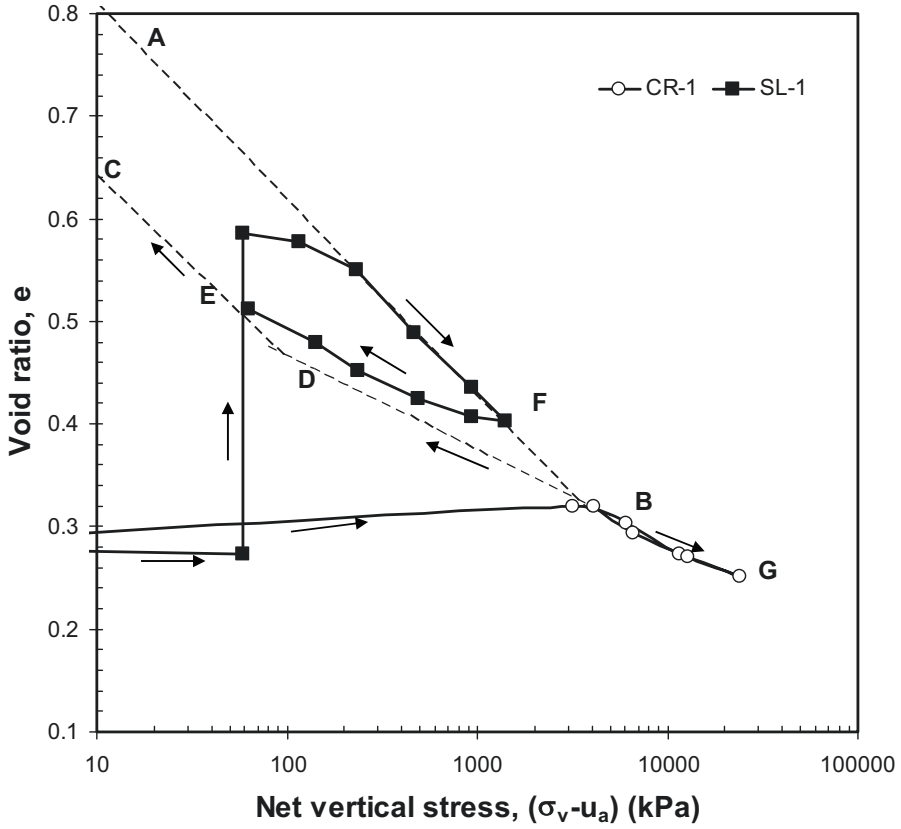

Figure 10.21 Characteristics of saturated compression and rebound curves

The elastic behaviour of the saturated specimen at low void ratio may be attributed to two factors:

1. More parallel clay particle arrangements. The amount of water, which was high enough to saturate the specimen, induced a possibility for the more parallel clay particles arrangement in the clay clusters when subjected to high net vertical stresses under oedometric conditions. The elastic behaviour of the material vanishes with increasing suction (or decreasing amount of water in the specimen) since less parallel orientation of the clay particles in the cluster is expected due to insufficient water present in the specimen. For the elastic behaviour to occur, the stress level should also be high enough (or the void ratio should be low enough) for the clay clusters to be compressed during loading.

2. Elastic compression and rebound of the sand particles in the specimen. At high net vertical stresses, elastic compression of the sand particles might occur. During swelling pressure development when water was introduced to the specimen, the clay particles (or clay clusters) invade the macro-pores resulting in a 'homogeneous' clay-sand system. The high density of the specimen made it possible for a collective compression of the clay clusters and the sand particles

when the specimen is compressed after completion of the development of swelling pressure. The elastic behaviour induced by the elastic behaviour of the sand particles is expected to decrease with increasing suction. This is related to the existence of air phase in the specimen. At unsaturated state, loading first reduces the volume of pore-air in the specimen. The volume of pore-air is not fully recovered when the specimen is unloaded.

10.3.3 Saturated Coefficient of Permeability Computed from the One-Dimensional Saturated Compression-Rebound Test Results

The results of oedometer test on saturated specimens (i.e., specimens SL-1 and CR-1) can be used to compute the saturated coefficient of permeability as a function of void ratio. The computation was performed by assuming the applicability of Terzaghi's theory of consolidation (Terzaghi, 1925). The following equation can be used to relate saturated coefficient of permeability with void ratio during compression and rebound of a saturated soil specimen.

$$k_s = \rho_w \, g \, c_v \frac{\Delta e}{\left(1+e_o\right)\Delta\sigma_v} \tag{10.9}$$

The coefficient of consolidation (c_v) was calculated from the deformation versus time curve of each increment of vertical stress (σ_v) using rectangular hyperbola method (Sridharan et al., 1987). The experimental deformation versus time curve was best-fitted using the following equation.

$$\frac{t}{\delta_v} = c_{RH} + m_{RH} t \tag{10.10}$$

The coefficient of consolidation (c_v) was calculated from the intercept of the linear part of the (t/δ_v) versus t curve (c_{RH}) and its slope (m_{RH}) using the following equation with H is the length of drainage path (Sridharan et al., 1987).

$$c_v = 0.24 \frac{m_{RH} H^2}{c_{RH}} \tag{10.11}$$

The saturated coefficient of permeability computed from the one-dimensional saturated compression-rebound test results are plotted in Figure 10.22 together with the measured data (i.e., specimens SP-LC-30B-1 to 5) and several other data available in Sitz (1997). The data are presented as a relationship between saturated coefficient of permeability and bentonite dry density. The use of bentonite dry density allows the results of specimens with different bentonite content to be compared.

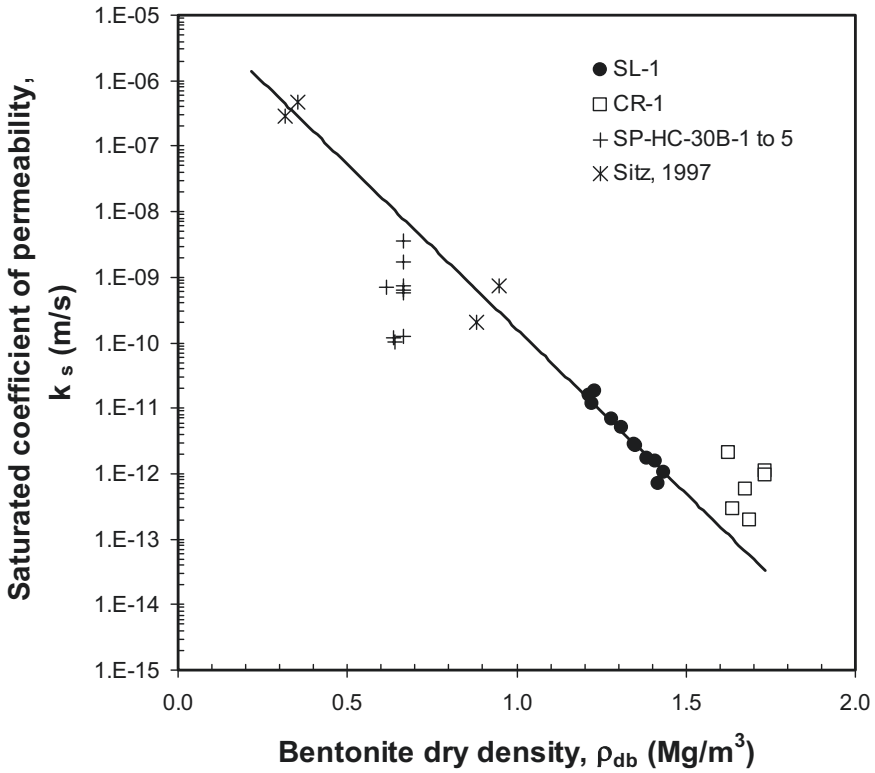

Figure 10.22 Saturated coefficient of permeability versus bentonite dry density

The following equation best-fits the saturated coefficient of permeability (in m/s) versus bentonite dry density (in Mg/m^3) data presented in Figure 10.22 with a coefficient of determination (r^2) of 0.987.

$$k_s = 1.72\times10^{-5}\exp\left(-0.12\rho_{db}\right) \tag{10.12}$$

10.3.4 Suction-Induced Change in the Compression and Rebound Behaviour

Figure 10.23 depicts the compression and rebound curves of three as-prepared specimens after being subjected to different values of suction (i.e., specimens CR-1 to CR-3). The apparent pre-consolidation pressure of the specimens (P_o) generally increases with increasing suction indicating that the material hardened as suction increased. The compression and rebound curves of specimen CR-2 are almost similar to those of specimen CR-3), which indicates a diminishing influence of suction in the high suction range. The plastic behaviour is seen more apparent in both specimens as they were unsaturated.

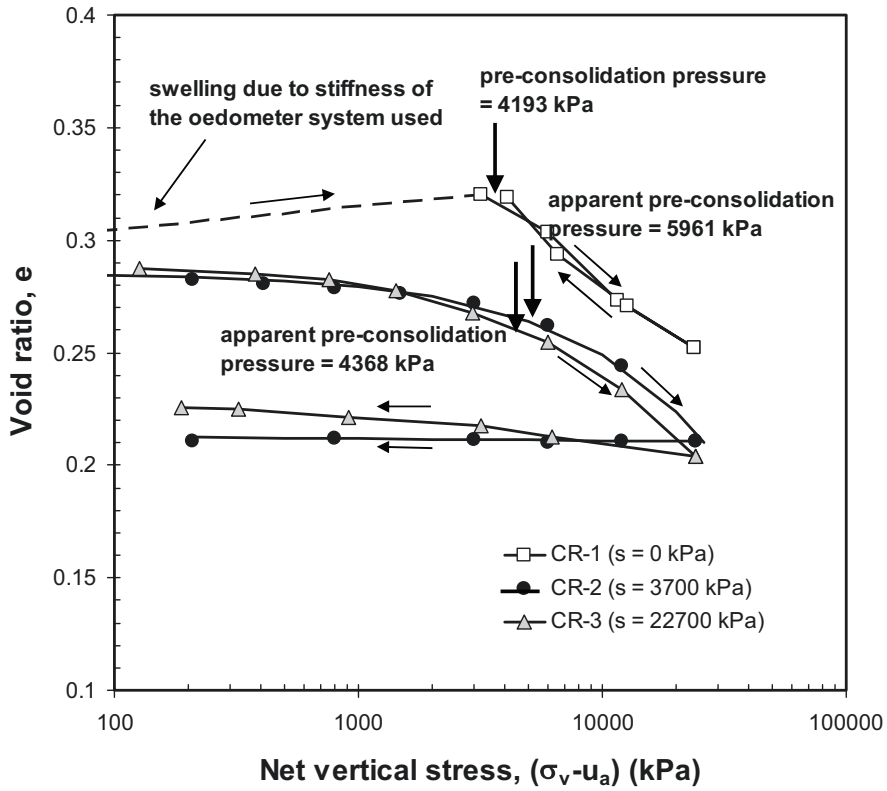

Figure 10.23 Compression and rebound curves of specimens CR-1, CR-2, and CR-3

10.3.5 Summary of the One-Dimensional Compression and Rebound Behaviour

The following conclusions can be drawn from the compression-rebound test results:

1. The saturated compression and rebound curves shows an elastic behaviour at high net vertical stress (or low void ratio). The behaviour is not seen in the low range of net vertical stress.

2. The apparent pre-consolidation pressure increases with increasing suction. The elastic behaviour as seen in the saturated compression and rebound behaviour at high net vertical stress is not found in the unsaturated specimens.

CHAPTER 11

DERIVATION OF MODELLING PARAMETERS

11.1 General

In this chapter, some parameters that can be used in the constitutive modelling, which have been derived based on the experimental data described in the preceding chapter, are presented. The experimental data were analysed according to an elasto-plastic model for unsaturated expansive soils (Barcelona Expansive Model or BExM) and a non-linear elastic volume change model based on the soil phase continuity requirements. The relationship between saturated permeability and void ratio for the material is derived based on the classical Kozeny-Carman model (Kozeny, 1927 and Carman, 1938) and cluster model (Olsen, 1962). The unsaturated permeability function for the material is computed using the van Genuchten-Mualem (van Genuchten, 1980 and Mualem, 1976) and Fredlund and Xing-Mualem (Fredlund and Xing, 1994 and Mualem, 1976) statistical models.

11.2 Parameters for Constitutive Modelling I: An Elasto-Plastic Model for Unsaturated Expansive Soils (Barcelona Expansive Model or BExM)

Parameters used in the constitutive modelling based on the Barcelona Basic Model (BBM) and Barcelona Expansive Model (BExM) consist of elastic parameters for the micro- and macro-structural deformation and plastic parameters. The parameters derived using the BExM are the micro-structural compressive index (κ_m) and the micro- and macro-structural interaction functions. Since the model was originally developed based on isotropic loading case, a simplification is made to enable derivation of the parameters from the oedometer test data. The simplification is that net vertical stress (σ_v - u_a) can be substituted for net mean stress (p) (Alonso et al., 2001). This brings a consequence that the K_o value is considered to be constant with net vertical stress and suction.

11.2.1 Elastic Parameters

The elastic parameter controlling micro-structural deformation is κ_m which is the micro-structural compressive index. The value was computed from the change in void ratio with increasing suction from the last drying of the cyclic wetting-drying test. As mentioned Chapter 8, the response of the material to suction changes after several wetting- drying cycles is generally elastic (or reversible). The κ_m value for specimen

Cyclic-1 (i.e., the specimen tested under 200 kPa net vertical stress) is 0.0087 and the value for specimen Cyclic-2 (i.e., the specimen tested under 1500 kPa net vertical stress) is 0.0117. Therefore, the following equation is formulated to express the change in κ_m value with net vertical stress (in kPa).

$$\kappa_m\left(\sigma_v - u_a\right) = 0.0008 + 0.0015\ln\left(\sigma_v - u_a\right) \tag{11.1}$$

Based on the saturated one-dimensional compression-rebound test, the following simplified curve is considered to give a relationship between void ratio and net vertical stress.

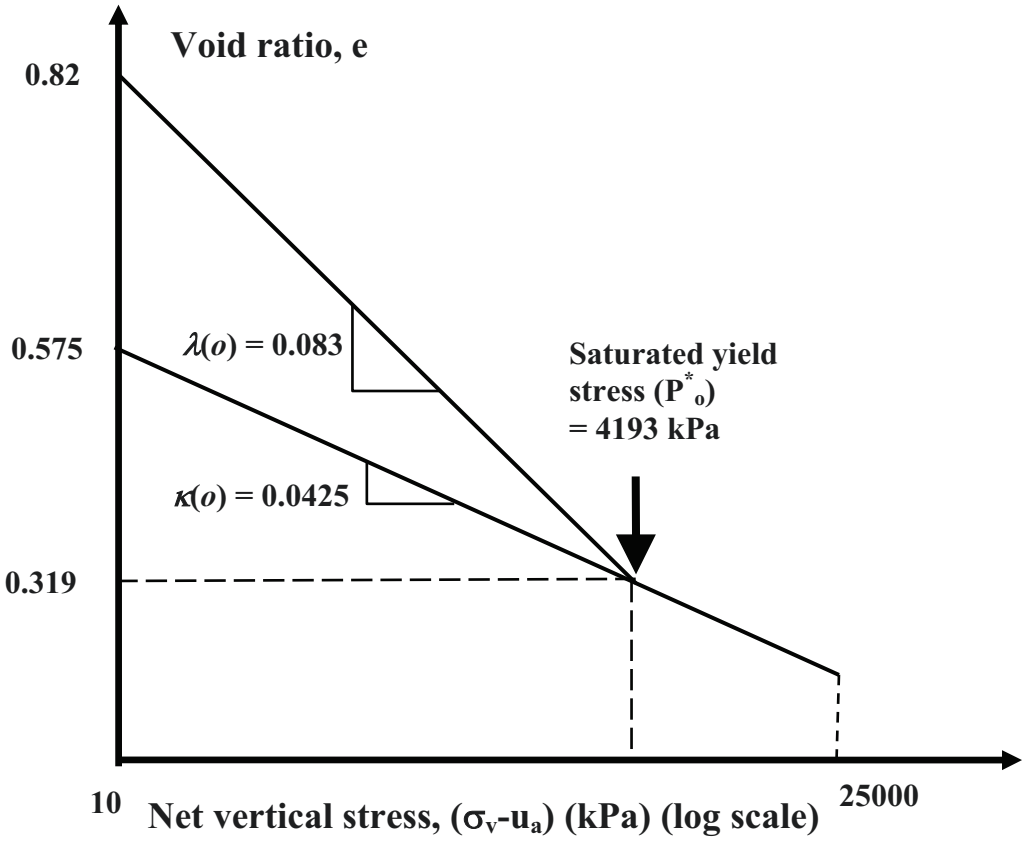

Figure 11.1 Simplified saturated compression and rebound curves

Based on Figure 11.1, the slope of saturated rebound (and recompression) curve ($\kappa(o)$) is equal to 0.0425. For unsaturated case, the $\kappa(s)$ value can also be computed and the value for 3700 kPa and 22700 kPa suction is 0.0028 and 0.0025, respectively. The following equation can be used to formulate the variation of κ value with suction where s is also in kPa.

$$\kappa\left(s\right) = 0.0425\left[0.059 + 0.941\exp\left(-0.00134\, s\right)\right] \tag{11.2}$$

The compressive index with respect to changes in suction (κ_s) is obtained from the unconfined wetting and drying curves (i.e., isotropic case at zero net mean stress) and the value follows the following relationship with suction is in kPa.

$$\kappa_s(s) = 0.1426\exp\left(-1.128\times10^{-4}s\right) \tag{11.3}$$

11.2.2 Plastic Parameters and Loading-Collapse (LC) Yield Curve

The plastic parameters consist of the compressive index with respect to changes in net mean stress (or in this case net vertical stress) for the virgin states of the soil (λ) and the compressive index with respect to changes in suction for the virgin states of the soil (λ_s). According to Figure 11.1, the $\lambda(o)$ value is equal to 0.083. Similarly the $\lambda(s)$ value can also be computed for unsaturated case and the value is equal to 0.0431 for 3700 kPa suction and 0.0429 for 22700 kPa suction. The following table summarises the λ and κ values for different values of suction obtained from the experimental data.

Table 11.1 Parameters λ and κ for different values of suction

Suction	0 kPa	3700 kPa	22700 kPa
λ value	0.083	0.0431	0.0429
κ value	0.0425	0.0028	0.0025

The following equation can be used to express the relationship between λ value and suction based on Equation (4.7) the data presented in Table 11.1 with s is in kPa.

$$\lambda(s) = 0.083\left[0.517 + 0.483\exp\left(-0.00137\,s\right)\right] \tag{11.4}$$

Figure 11.2 shows the variation of λ and κ values with suction for the material tested in this investigation.

The loading-collapse (LC) yield curve of the material (Figure 11.3) is obtained by making use of the variation of κ and λ values with suction, the saturated pre-consolidation pressure (or yield stress) (P_o^*), and the variation of pre-consolidation pressure (P_o) with suction. The apparent pre-consolidation pressure of the specimen with 3700 kPa suction (i.e., specimen CR-2) is 4368 kPa and that of the specimen with 22700 kPa suction (i.e., specimen CR-3) is 5961 kPa. The following figure shows the plot of LC curve of the material. The result of multi-step constant volume swelling pressure test of the specimens from as-prepared state (i.e., specimens SP-HC-50B-3 and 4) are also drawn in the figure for comparison. The swelling pressure of the specimen at zero suction lies closely to the saturated pre-consolidation pressure. In absence of the saturated compression and rebound data, the value can be taken as a first estimate of P_o^* (Alonso et al., 2001).

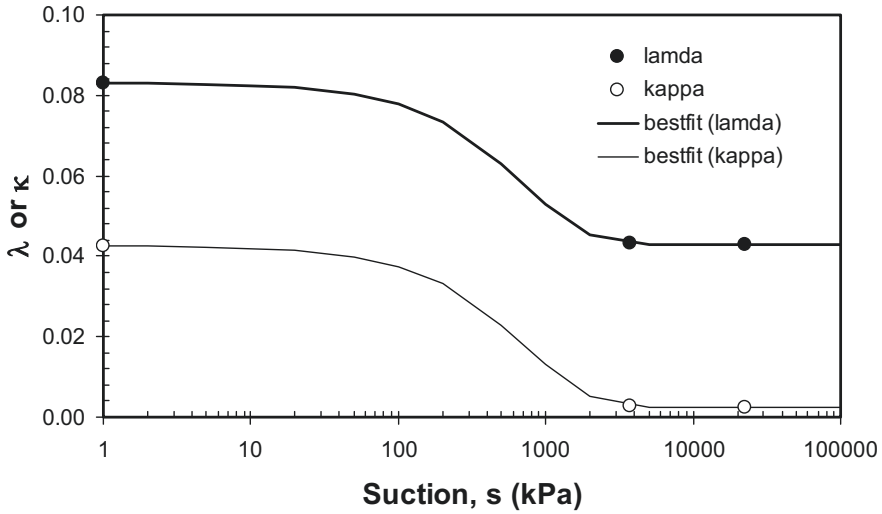

Figure 11.2 Variation of λ and κ values with suction

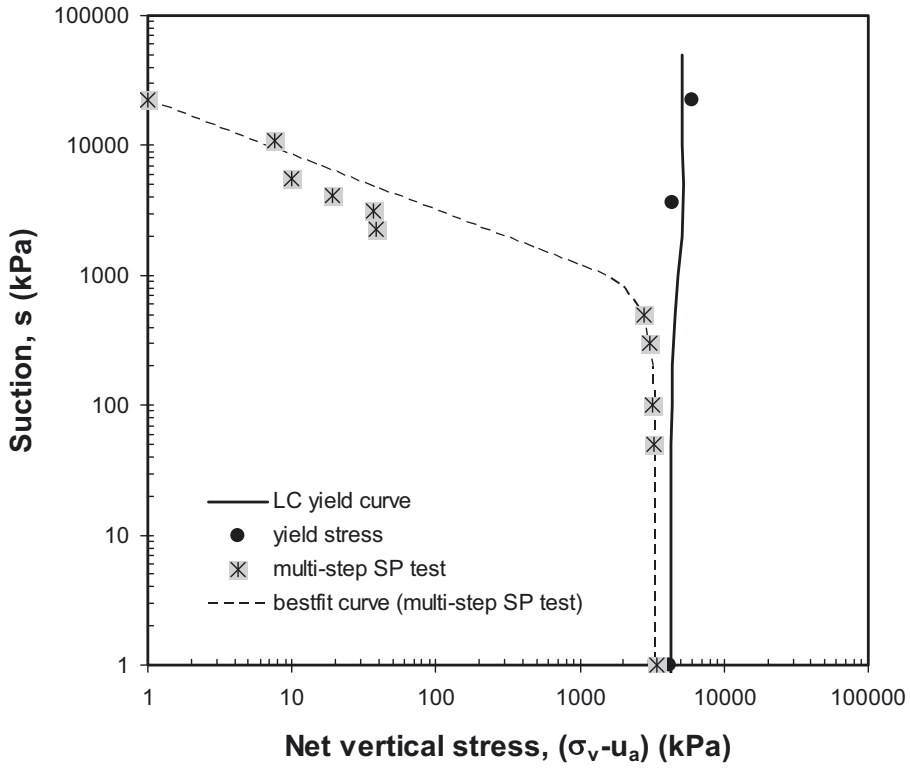

Figure 11.3 LC yield curve of the as-prepared specimen

The equation of LC yield curve based on Equation (4.6) is given in Equation (11.5) where P_o is in kPa. It can be inferred from Equation (11.5) that the reference pressure (or net vertical stress) is 3389 kPa.

$$p_o = 3389 \times 1.237^{\left[\frac{0.083-\kappa(s)}{\lambda(s)-\kappa(s)}\right]} \tag{11.5}$$

11.2.3 Verification of Macroscopic Response during One-Dimensional Compression-Rebound Test

To verify the mechanical parameters that have been derived, a simulation was performed using CODE_BRIGHT to model mechanical response of the as-prepared specimen during one-dimensional compression-rebound test (i.e., specimen CR-3). The following mechanical parameters are required for the modelling (Table 11.2 and Table 11.3).

Table 11.2 Elastic parameters

No.	Parameter	Symbol	Value
1	Saturated compressive index with respect to changes in net mean stress	$\kappa(o)$	0.0029*
2	Compressive index with respect to changes in suction at zero net mean stress and zero suction	$\kappa_s(o)$	0.1426
3	Minimum bulk modulus (MPa)	K_{min}	10
4	Poisson's ratio	υ	0.3§
5	Parameter expressing changes in κ_s with suction‡	α_{ss}	-0.1128
6	Parameter expressing changes in κ with suction‡	α_i	-0.006
7	Parameter expressing changes in κ_s with net mean stress‡	α_{sp}	-0.3
8	Reference stress (MPa)	p_{ref}	0.75

* the value is defined such a way to give κ equal to 0.0028 and 0.0025 at suction of 3700 kPa and 22700 kPa, respectively when used in conjunction with α_i

§ reported in IfB (2001)

‡ see the equations below for the relationships (CODE_BRIGHT, 2003)

$$\kappa_s\left(p', s\right) = \kappa_s\left(o\right)\left[1 + \alpha_{sp} \ln\left(\frac{p}{p_{ref}}\right)\right]\exp\left(\alpha_{ss}\, s\right) \tag{11.6}$$

$$\kappa\left(s\right) = \kappa(o)\left(1 + \alpha_i\, s\right) \tag{11.7}$$

Table 11.3 Plastic parameters

No.	Parameter	Symbol	Value
1	Saturated virgin compressive index with respect to changes in net mean stress	$\lambda(o)$	0.083
2	First parameter describing changes in λ with suction*	r	0.517
3	Second parameter describing changes in λ with suction (/MPa)*	β	1.372
4	Parameter which takes into account decrease in tensile strength with increasing temperature (/°C)§	ρ	0.2 (assumed)
5	Parameter which takes into account increase in tensile strength with increasing suction (/MPa)§	k	0.1 (assumed)
6	Reference pressure (MPa)	p_c	3.39
7	Critical state line parameter§	M	1.412
8	Non-associativity parameter	α	0.75 (assumed)
9	Initial void ratio	e_o	0.288
10	Initial saturated pre-consolidation pressure (MPa)	p_o*	4.193

* see Equation (11.4) for the relationship
§ see the equations below for the relationship (Alonso et al., 1999 and CODE_BRIGHT, 2003)

$$t_s = -\rho T + ks \tag{11.8}$$

$$q^2 - M^2 \left(p + t_s \right)\left(p_o - p \right) = 0 \tag{11.9}$$

$$K_o = \frac{\upsilon}{1-\upsilon} = \frac{6-2M}{6+M} \tag{11.10}$$

where t_s is the tensile strength, T is temperature, q is the deviator stress, K_o is the coefficient of earth pressure at rest, and υ is the Poisson's ratio.

Note: In CODE_BRIGHT, pressures and suction are in MPa. Therefore, some constants have been redefined by best-fitting the experimental data with the constitutive laws available in the code.

Figure 11.4 shows a comparison between the experimental data and the modelling results of the compression-rebound test on the as-prepared specimen (i.e., specimen CR-3). The good agreement between the modelling results and the experimental data indicates that the parameters obtained can be used to give quite satisfactory prediction of void ratio changes during compression and rebound. The mechanical parameters used in the modelling were mainly obtained from the one-dimensional tests although the model itself was developed for isotropic case.

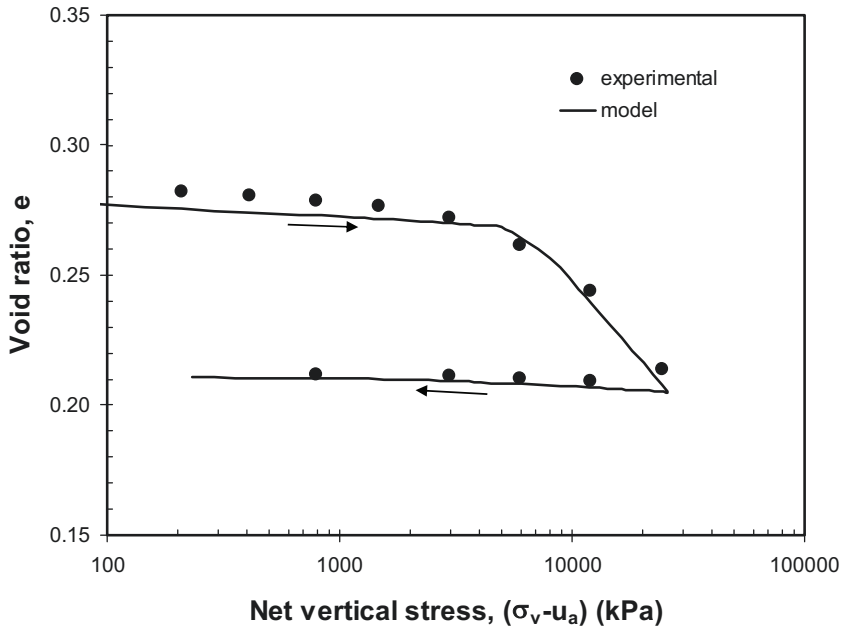

Figure 11.4 Comparison between the experimental data and the modeling results of the compression-rebound test on the as-prepared specimen (specimen CR-3)

The evolution of K_o value during compression and rebound as obtained from the modelling is shown in Figure 11.5. It was shown that K_o is not a constant but it is a function of stress level and suction (Vu and Fredlund, 2004). Initially, the K_o value is high (possibly close to unity). During elastic compression, the value decreases and tends to reach the elastic K_o value (i.e., that computed using Equation (11.10)). The value increases slightly after the specimen reaches its yield point and is constant (i.e., equal to 0.53) during plastic compression. During rebound, the K_o value increases rapidly and is even greater than unity at low net vertical stresses.

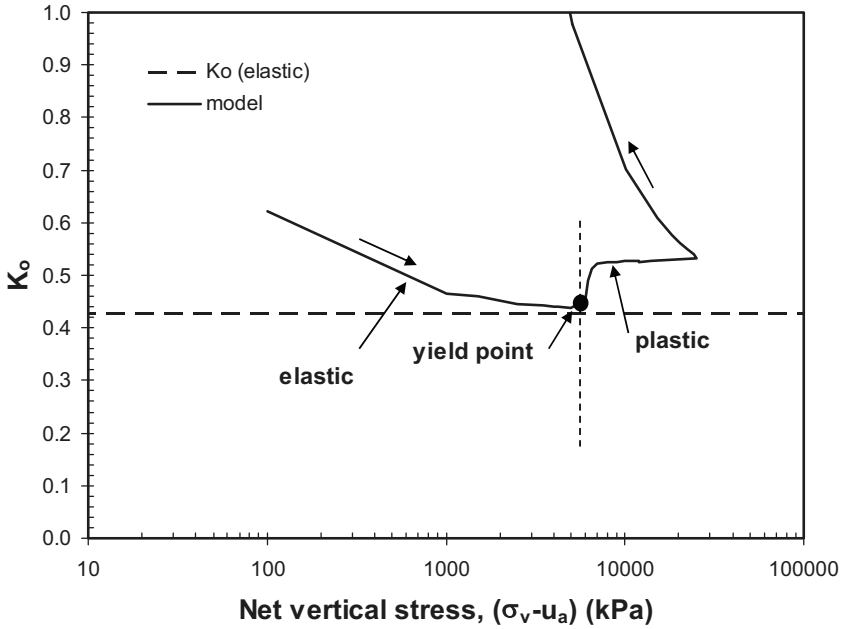

Figure 11.5 Evolution of K_o value during compression-rebound test on the as-prepared specimen (specimen CR-3)

11.2.4 Micro- and Macro-Structural Interaction Functions

The micro- and macro-structural interaction functions (i.e., f_I and f_D) can be derived from the results of cyclic wetting-drying tests under constant net vertical stresses (i.e., tests on specimen Cyclic-1 and Cyclic-2). Figure 11.6 shows a plot of the ratio of plastic to elastic deformation during wetting-drying cycles on specimens Cyclic-1 and Cyclic-2.

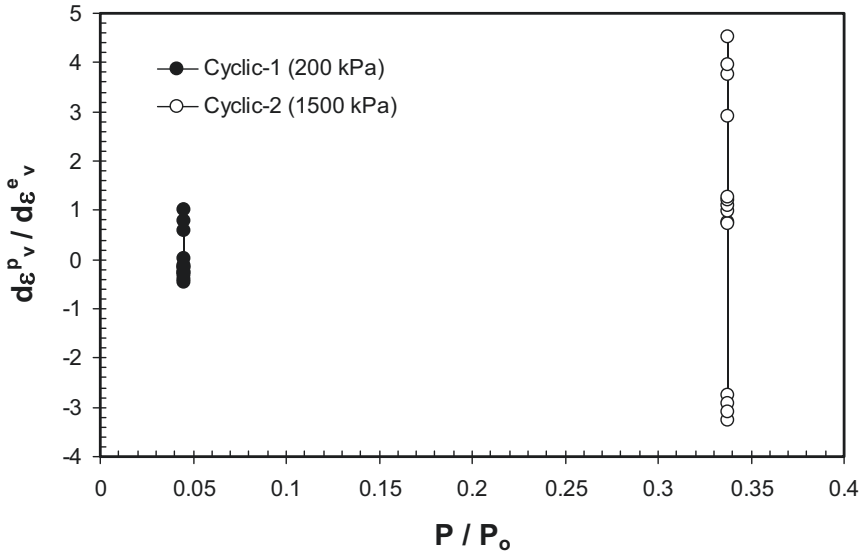

Figure 11.6 Ratio of plastic to elastic deformation during wetting-drying cycles

The volumetric deformation induced by changes in suction during wetting-drying cycles was insubstantial for both specimens. Therefore, the LC yield curve remained essentially the same during wetting-drying cycles since both the λ and κ values were constant. The derivation of interaction functions (f_I and f_D) using is not possible since the (P/P_o) value for each specimen is constant (Figure 11.6).

11.2.5 Inter-Aggregate and Intra-Aggregate Pore-Water

During compression-rebound, unconfined swelling, and constant volume swelling tests, the micro-structural effective stress changed inducing changes in the micro-structural void ratio (e_m) of the specimen. Since the micro-structural voids are considered to be saturated, the changes in water content of the microstructure can be inferred from the changes in e_m during compression-rebound and wetting tests. The computation of inter- and intra-aggregate water content is not described in the BBM and BExM. However, the micro-structural parameter derived based on the BExM can be utilised for this purpose. By assuming a constant micro-structural compressive index (κ_m) (i.e., equal to the average κ_m value (= 0.0102)), the changes in intra-aggregate water content (or micro-structural water content) and inter-aggregate (or macro-structural water content) can be computed. In the computation, the initial (or as-prepared) water content is assumed to be distributed according to the MIP test data. The intra-aggregate pore (i.e., the micro-pore) volume for the as-prepared specimen comprised 59% of the total pore volume. The proportion is assumed to be constant for all as-prepared specimens. Figure 11.7 shows the alteration of total, intra-aggregate, and inter-aggregate water contents during saturated compression-rebound tests (i.e., the tests on specimens SL-1 and CR-1). The change in intra-aggregate water content is only significant during swelling under 50 kPa loading on specimen SL-1 while a gradual decrease in the intra-aggregate water content with respect to changes in net vertical stress is observed.

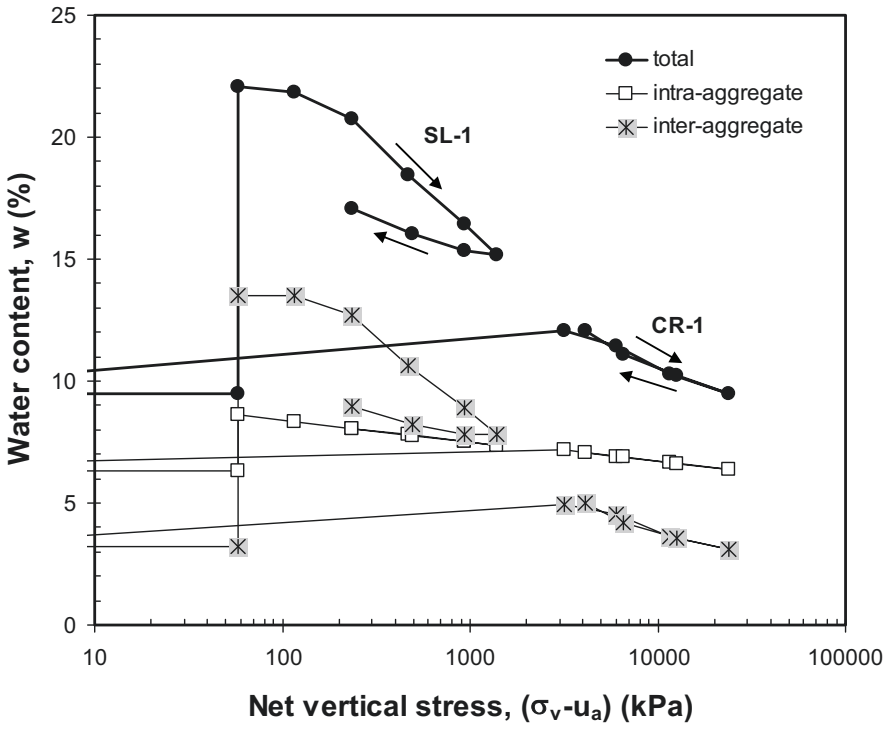

Figure 11.7 Change in total, intra-aggregate, and inter-aggregate water contents during saturated compression-rebound tests (specimens SL-1 and CR-1)

Figure 11.8 and Figure 11.9 show the change in total, intra-aggregate, and inter-aggregate water contents with suction during unconfined wetting and multi-step constant volume swelling pressure tests on the as-prepared specimens. Relative to the change in total water content change, the change in intra-aggregate water content is considered insignificant in both cases. In order to investigate the influence of boundary conditions on the micro-structural water sorption characteristics, a plot of intra-aggregate water content changes during unconfined and constant volume wetting is made and shown in Figure 11.10. The boundary conditions appear to affect the micro-structural change in water content when suction is reduced below 2000 kPa. Below this value, the increase in swelling pressure is almost equal or slightly lower than the decrease in suction inducing the low net increase in micro-structural effective stress.

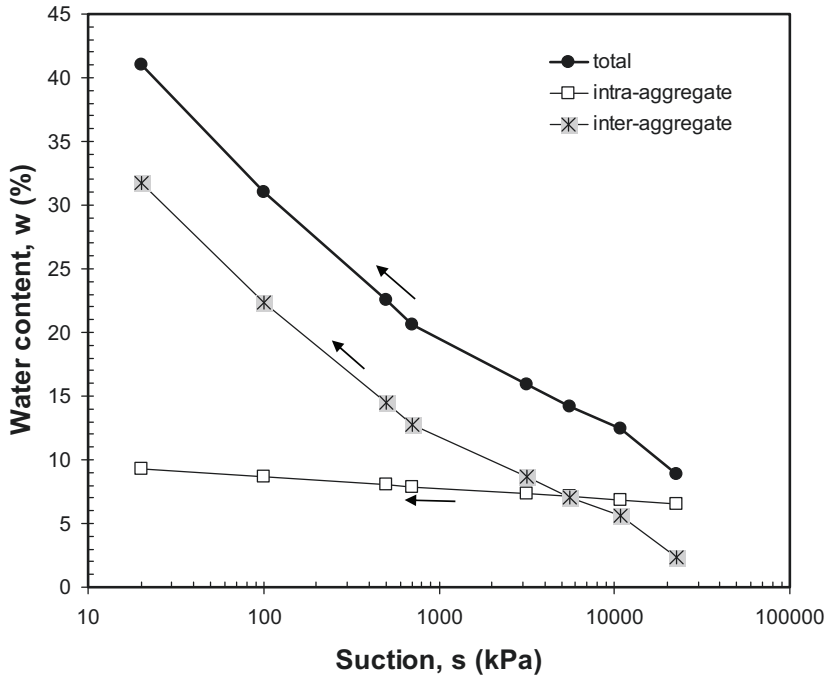

Figure 11.8 Change in total, intra-aggregate, and inter-aggregate water contents during unconfined wetting test from as-prepared conditions (specimens UC-7 and UC-9)

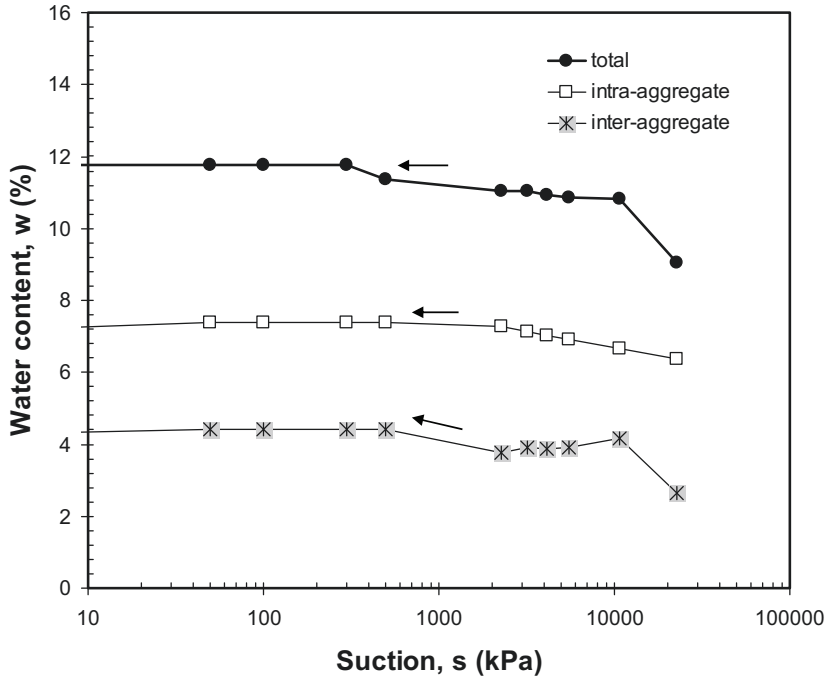

Figure 11.9 Change in total, intra-aggregate, and inter-aggregate water contents during constant volume wetting test from as-prepared conditions
(specimens SP-HC-50B-3 and 4)

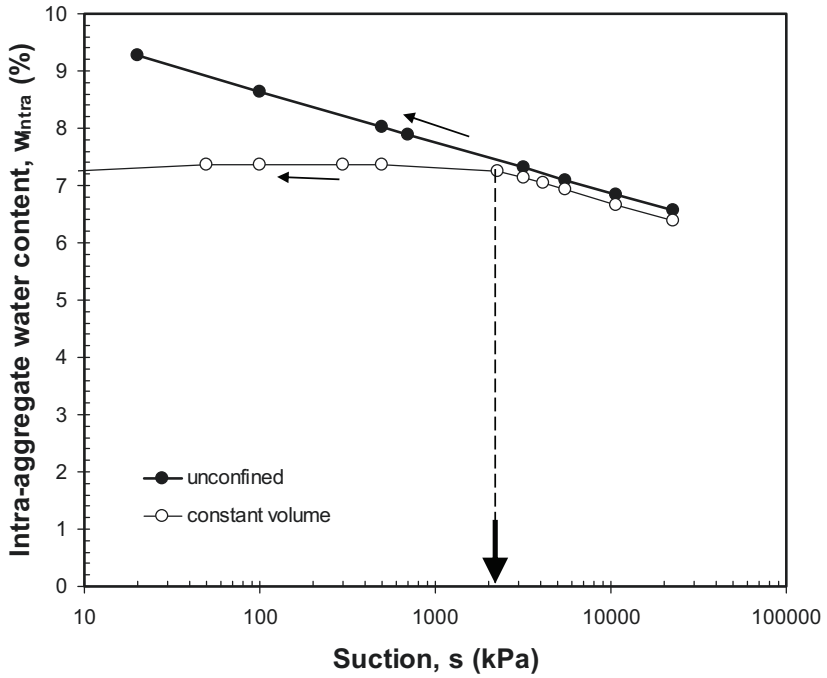

Figure 11.10 Comparison between changes in intra-aggregate water content from unconfined and constant volume wetting tests

11.3 Parameters for Constitutive Modelling II: A Non-Linear Elastic Volume Change Model Based on the Soil Phase Continuity Requirements

Parameters required for the non-linear elastic volume change model based in the soil phase continuity requirements consist of parameters associated with soil structure and water phase volumetric deformation (Fredlund and Rahardjo, 1993).

11.3.1 Elastic Parameters Associated with Soil Structure Volumetric Deformation

Elastic parameters associated with the soil structure volumetric deformation, which are required in the model, are modulus of elasticity with respect to changes in net vertical stress (E) and modulus of elasticity with respect to changes in suction (H). The E value of the material can be obtained from the one-dimensional compression-rebound test data (i.e., the tests on specimens CR-1, 2, and 3). In this case, the K_o value is assumed to be constant and the value can be computed from Poisson ratio (υ) using Equation (11.10).

The following general power law can be used to express the change in E value with net vertical stress with $(\sigma_v - u_a)_{ref}$ is the reference net vertical stress and β_E is a power which is a function of suction. At the reference net vertical stress, the soil has a modulus of elasticity of E_{ref}. The approach used herein in relating E with net vertical stress and suction is similar to formulation of the hardening soil model (Schanz, 1998).

$$E\left(\sigma_v - u_a\right) = E_{ref}\left[\frac{\left(\sigma_v - u_a\right)}{\left(\sigma_v - u_a\right)_{ref}}\right]^{\beta_E} \tag{11.11}$$

Figure 11.11 shows the variation of E with (σ_v - u_a) for specimens CR-1, 2, and 3 for loading case as computed using Equation (11.11). The plot indicates that the rate of increase in E with net vertical stress on loading decreases with increasing suction.

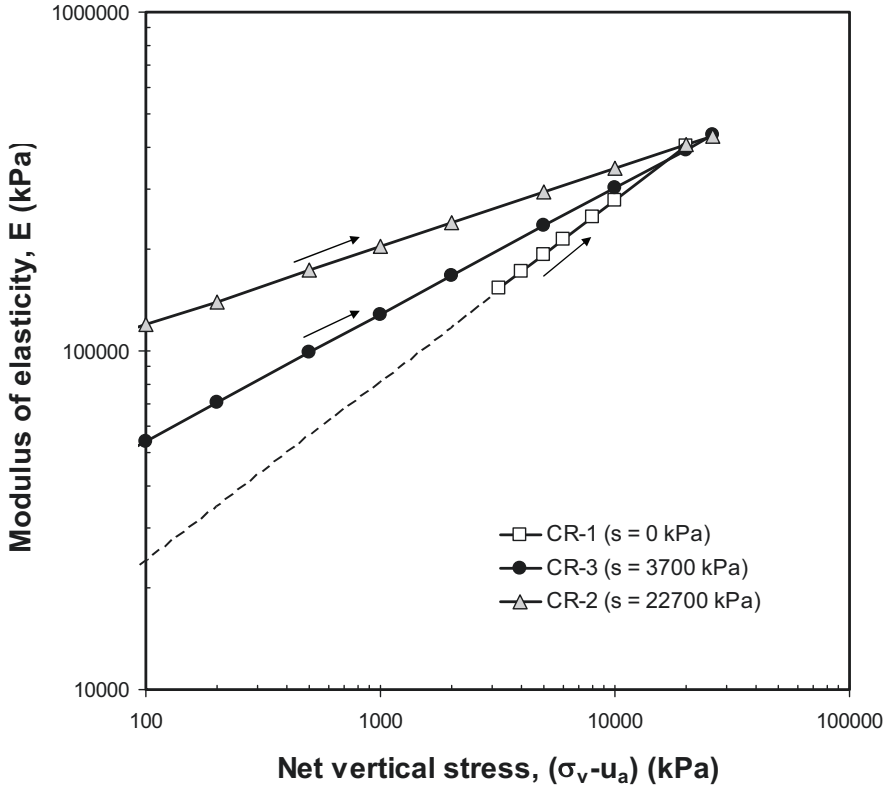

Figure 11.11 Variation of E with net vertical stress

Equation (11.12) expresses the variation of E value with net vertical stress for specimen CR-1 whereas Equation (11.13) and Equation (11.14) express the E versus (σ_v - u_a) for specimens CR-2 and CR-3, respectively.

$$E = 24487\left[\frac{\left(\sigma_v - u_a\right)}{100}\right]^{0.53} \tag{11.12}$$

$$E = 54214\left[\frac{\left(\sigma_v - u_a\right)}{100}\right]^{0.37} \tag{11.13}$$

$$E = 119205\left[\frac{\left(\sigma_v - u_a\right)}{100}\right]^{0.23} \tag{11.14}$$

In the above equations, the $(\sigma_v - u_a)_{ref}$ value is equal to 100 kPa. The E_{ref} value is equal to 24487 kPa, 54214 kPa, and 119205 kPa for suction equal to zero, 3700 kPa, and 22700 kPa, respectively. The β_E value is equal to 0.53, 0.37, and 0.23 for suction equal to zero, 3700 kPa, and 22700 kPa, respectively. Both E_{ref} and β_E values vary with suction.

A generalised relationship between E, s, and $(\sigma_v - u_a)$ can also be established. The variation of E value with s and $(\sigma_v - u_a)$ can be formulated by combining Equation (11.12) to Equation (11.14) resulting in the following equation with E, s, and $(\sigma_v - u_a)$ are in kPa.

$$E = 67800\left(\frac{s}{100}\right)^{0.041}\left[\frac{(\sigma_v - u_a)}{100}\right]^{0.315} \tag{11.15}$$

The variation of H value with suction can be computed from the unconfined wetting test from the as-prepared conditions (i.e., specimen UC-7 and 9) which is re-plotted in Figure 11.12. No experimental data for the material investigated herein are available to assess the change in H value with $(\sigma_v - u_a)$. Similar to the way by which the E versus $(\sigma_v - u_a)$ is formulated, the following general equation applies to relate H with suction.

$$H = H_{ref}\left(\frac{s}{s_{ref}}\right)^{\beta_H} \tag{11.16}$$

where s_{ref} is the reference suction and β_H is a power which is a function of $(\sigma_v - u_a)$.

The following equation is obtained by fitting Equation (11.16) to the experimental data presented in Figure 11.12 with H is in kPa.

$$H = 165\left(\frac{s}{10}\right)^{1.2} \tag{11.17}$$

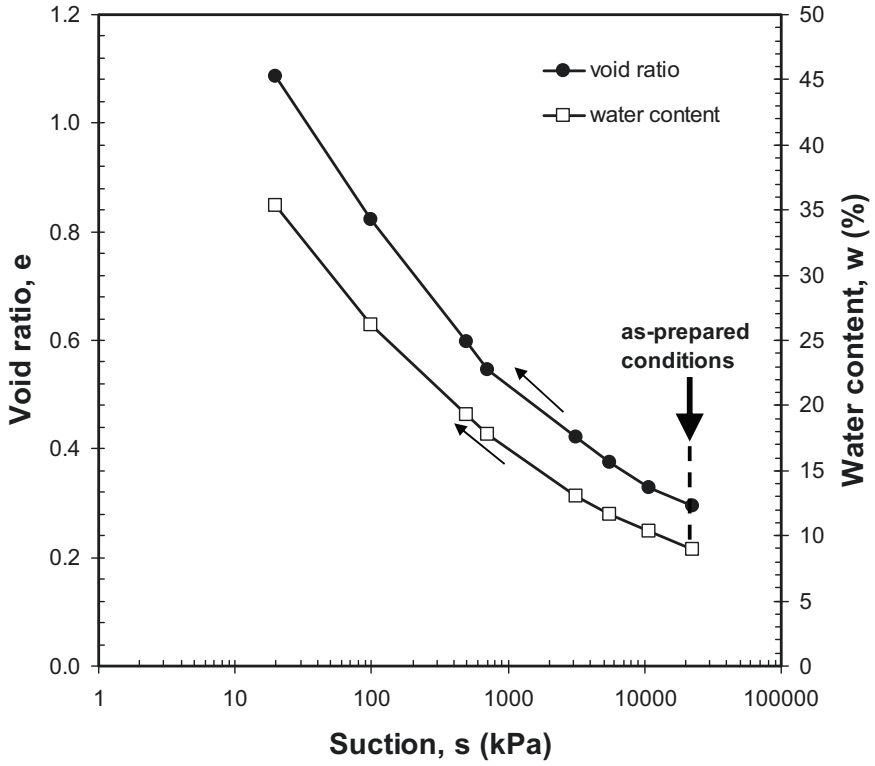

Figure 11.12 Void ratio and water content changes during unconfined wetting from the as-prepared conditions (specimens UC-7 and UC-9)

11.3.2 Elastic Parameters Associated with Water Phase Volumetric Deformation

Elastic parameters for the water phase are parameters relating the volumetric deformation of water phase with net vertical stress (E_w) and suction (H_w). Since the compression-rebound tests on specimens CR-2 and CR-3 were basically constant water content tests, the E_w versus (σ_v - u_a) relationship is only derived for the test on specimen CR-1. In the oedometer test on the saturated specimen (i.e., the test on specimen CR-1), the specimen volume change is assumed to be due to water being squeezed out during loading. Therefore, the following equation is obtained to express the change in E_w with (σ_v - u_a) during loading with E, E_w, and (σ_v - u_a) are in kPa.

$$E_w = 2.5\,E = 61218\left[\frac{(\sigma_v - u_a)}{100}\right]^{0.53} \tag{11.18}$$

The variation of H_w versus suction can be obtained by utilising the experimental data presented in Figure 11.12 and Equation (4.24). Figure 11.13 compares the variation of H and H_w with suction for the material tested in this investigation. Since degree of saturation of the specimen during unconfined wetting from the as-prepared state was fairly constant, the H versus suction and H_w versus suction curves are essentially parallel each other. Equation (11.19) can be used to express the variation of H_w versus suction.

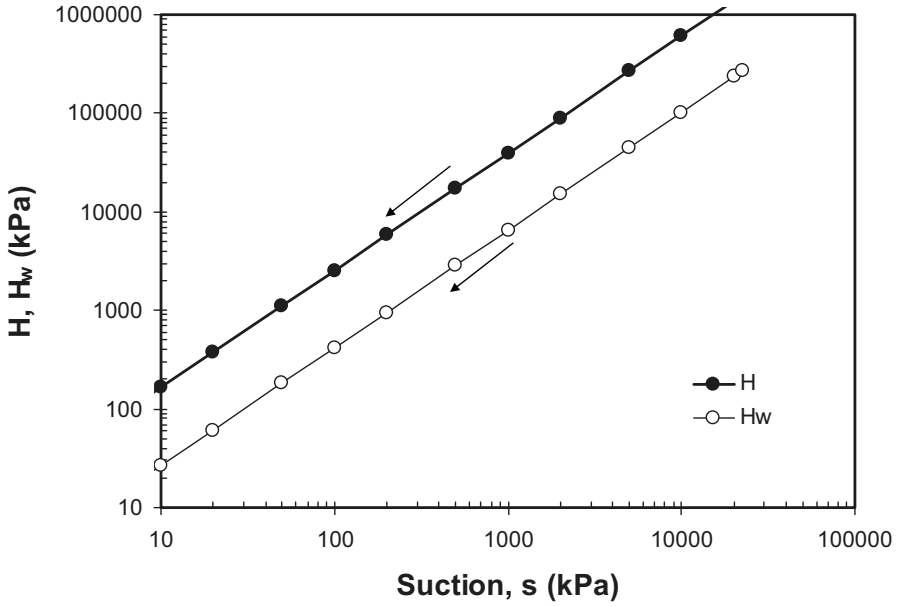

Figure 11.13 Variation of H and H_w with suction

$$H_w = 27\left(\frac{s}{10}\right)^{1.2} \tag{11.19}$$

11.4 Permeability Models

Saturated and unsaturated coefficients of permeability are required in modelling water (or liquid) transport through unsaturated compacted bentonite-sand mixture. The saturated permeability models brought out in this dissertation are the classical Kozeny-Carman (Kozeny, 1927 and Carman, 1938) and cluster model (Olsen, 1962). The unsaturated coefficient of permeability versus suction (i.e., the unsaturated permeability function) was computed from the saturated coefficient of permeability and wetting curve through statistical models such as van Genuchten-Mualem (van Genuchten, 1980 and Mualem, 1976) and Fredlund and Xing-Mualem models (Fredlund and Xing, 1994 and Mualem, 1976).

11.4.1 Saturated Permeability Models

11.4.1.1 Kozeny-Carman Model

Based on the measured total specific surface area presented in Chapter 6, the following Kozeny-Carman equation is obtained.

$$k_s = 6.61\times10^{-13}\left(\frac{e^3}{1+e}\right) \tag{11.20}$$

where k_s is in m/s.

Figure 11.14 shows the relationship between saturated coefficient of permeability (k_s) versus void ratio for compacted 50/50 bentonite-sand mixture. The permeability data obtained by Sitz (1997) at low void ratios are also plotted to compliment the permeability data computed from the saturated compression-rebound tests (i.e., the tests on specimens SL-1 and CR-1). The saturated coefficients of permeability derived from the MIP data are $1.74\text{x}10^{-6}$ m/s, $1.27\text{x}10^{-6}$ m/s, and $2.38\text{x}10^{-8}$ m/s for void ratio of 0.299, 0.319, and 0.6, respectively (i.e., the as-prepared, oven-dried, and swollen specimens). The data lie much above the trend-line of the k_s-e curve shown in Figure 11.14. The Kozeny-Carman prediction gives much lower values of k_s compared to the measured values and the computed k_s from the saturated compression-rebound test data (Equation (10.9)).

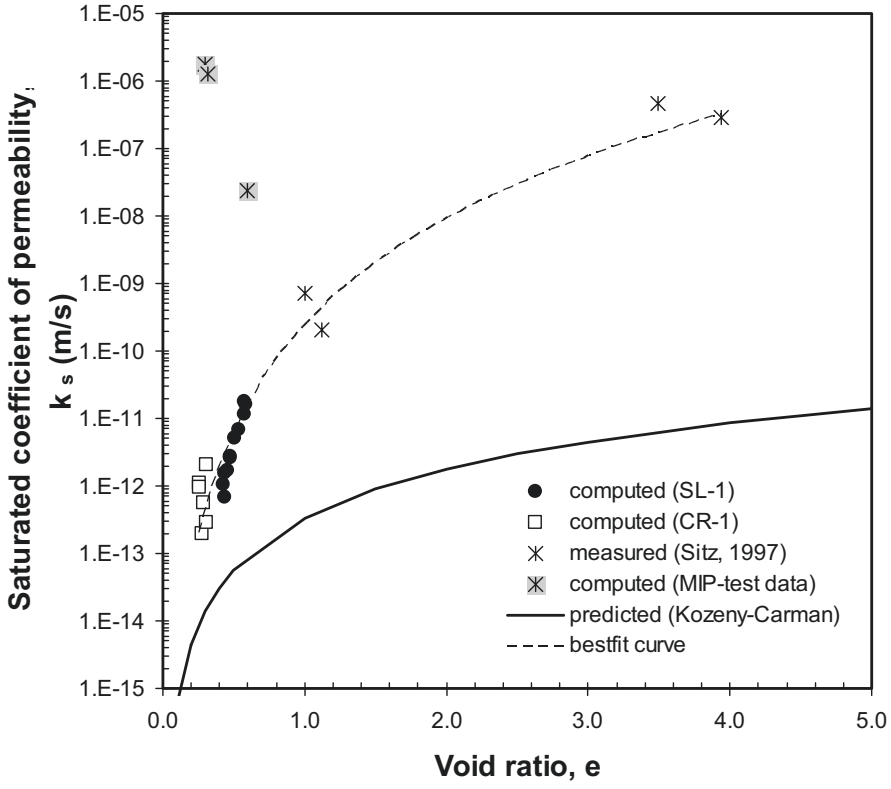

Figure 11.14 Saturated coefficient of permeability versus void ratio

11.4.1.2 Cluster Model

The Kozeny-Carman model has long been known to be insufficient in establishing the k_s-e relationship for clay soils (Olsen, 1962). Cluster model proposed by Olsen (1962) was used to derive the k_s-e relationship for the heavily compacted 50/50 bentonite-sand

mixture in this study. In the cluster model, information on cluster void ratio (i.e., intra-aggregate or micro-structural void ratio) (e_c or e_m), total void ratio (e_T or e), and average number of clay particles per cluster (N) are required. By utilising the elastic compressive index of micro-structural deformation (κ_m), variation of e_m during loading, unloading, and wetting can be computed and is shown in Figure 11.7, Figure 11.8, and Figure 11.9 for the saturated compression-rebound, unconfined swelling, and constant volume wetting tests, respectively. Figure 11.15 depicts the variation of intrinsic permeability (K) with void ratio during saturated compression-rebound tests estimated from cluster model in comparison with the Kozeny-Carman prediction. In the computation, N is assumed to be 10. The Kozeny-Carman predicts intrinsic permeability almost similar to that estimated using the cluster model prediction for void ratio 0.5. The difference between the two prediction results becomes apparent in the low void ratio range with the cluster model prediction being lower than the Kozeny-Carman prediction.

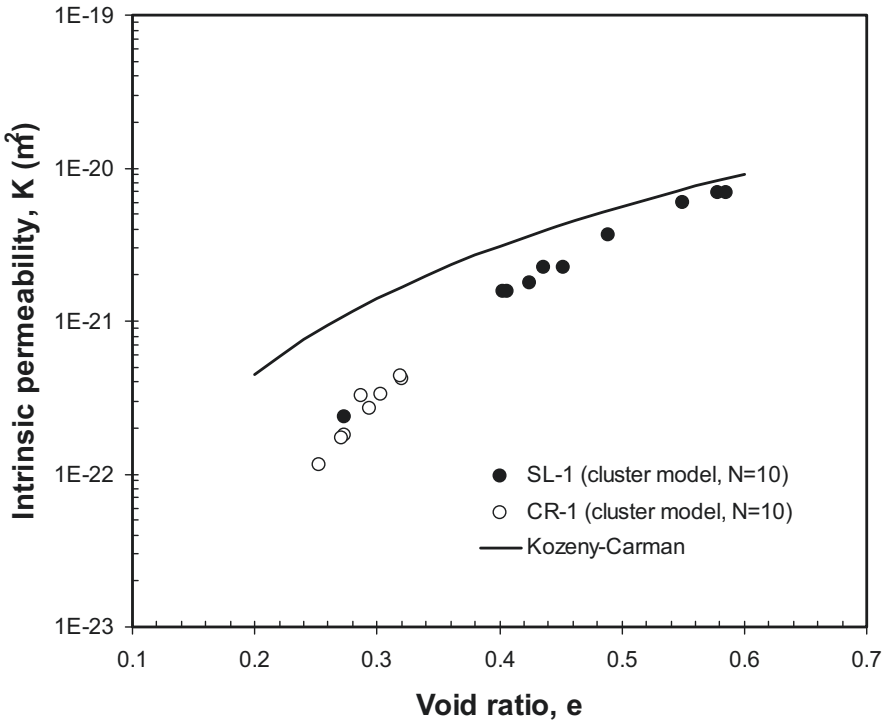

Figure 11.15 Intrinsic permeability estimated from cluster model in comparison with the Kozeny-Carman prediction for the saturated compression-rebound test data (specimens SL-1 and CR-1)

By taking the assumed relationship between total, cluster, and intra-cluster void ratio proposed by Olsen (1962) (Figure 4.7), the variation of intrinsic permeability (K) with void ratio for the saturated compression-rebound test data (i.e., specimens SL-1 and CR-1) can be computed. The relationship is given in Figure 11.16. Both models show the same trend of K-e relationship with a slight difference.

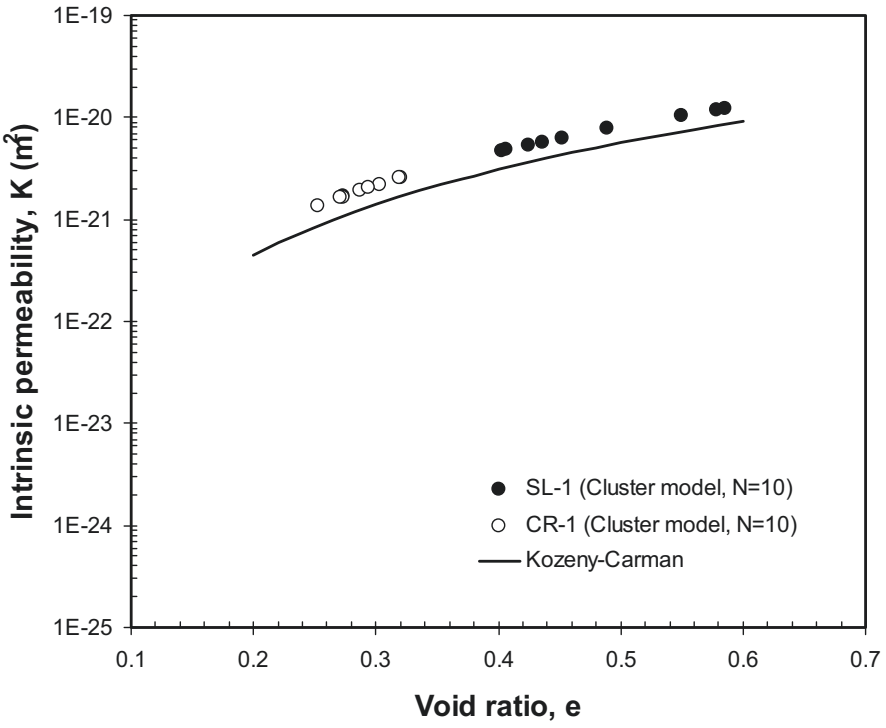

Figure 11.16 Intrinsic permeability estimated from cluster model in comparison with the Kozeny-Carman prediction for the saturated compression-rebound test data (specimens SL-1 and CR-1) assuming the e-e_m relationship as proposed by Olsen (1962)

Figure 11.17 and Figure 11.18 show the intrinsic permeability versus suction relationship during unconfined swelling and constant volume swelling tests on the as-prepared specimen, respectively. The changes in e_m value during tests are computed from the changes in micro-structural effective stress. At high void ratio (i.e., low suction), both methods give fairly similar estimate of K (Figure 11.17) indicating the less pronounced effects of changes in the micro-structural void ratio on the magnitude of K.

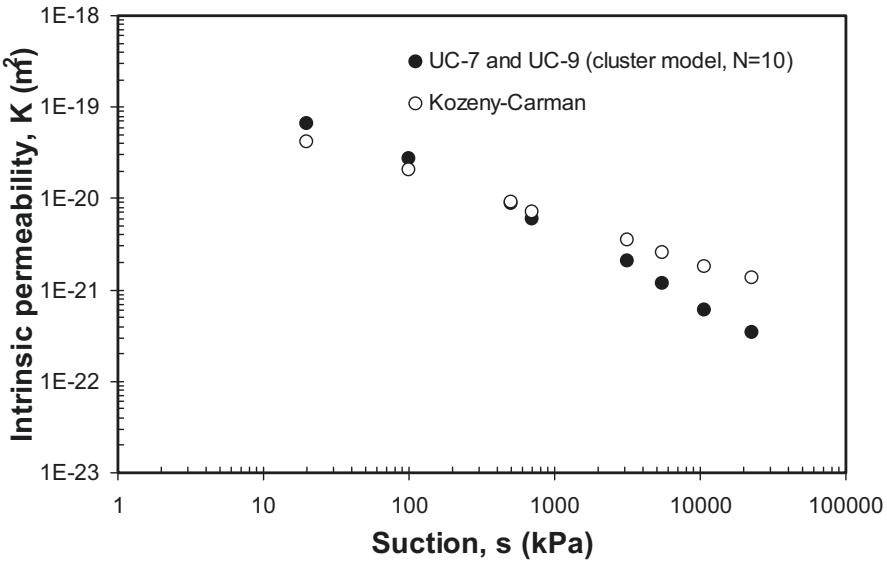

Figure 11.17 Intrinsic permeability versus suction estimated from cluster model in comparison with the Kozeny-Carman prediction during unconfined swelling test from as-prepared conditions (specimens UC-7 and UC-9)

Figure 11.18 shows that the K value decreases with decreasing suction up to about 2000 kPa suction during constant volume wetting (or swelling pressure) test and increases with decreasing suction afterward. The increase in K below 2000 kPa suction is mainly caused by a slight increase in void ratio of the specimen due to deformation of the equipment used. It is thought that the K value continued to decrease when the constant volume cell used was stiff enough to restrain deformation due to the development of high swelling pressure when the material approached its saturation. Thus, it could happen that the saturated coefficient of permeability (k_s) of an expansive soil wetted under constant volume conditions is even lower than its unsaturated coefficient of permeability (k_w). Generally, the k_w value of a soil is lower than its k_s value when void ratio is constant. In the case of expansive soil wetted under constant volume conditions, there is an expansion of clay clusters under constant total void ratio resulting in the macro-pores being blocked by the clay clusters.

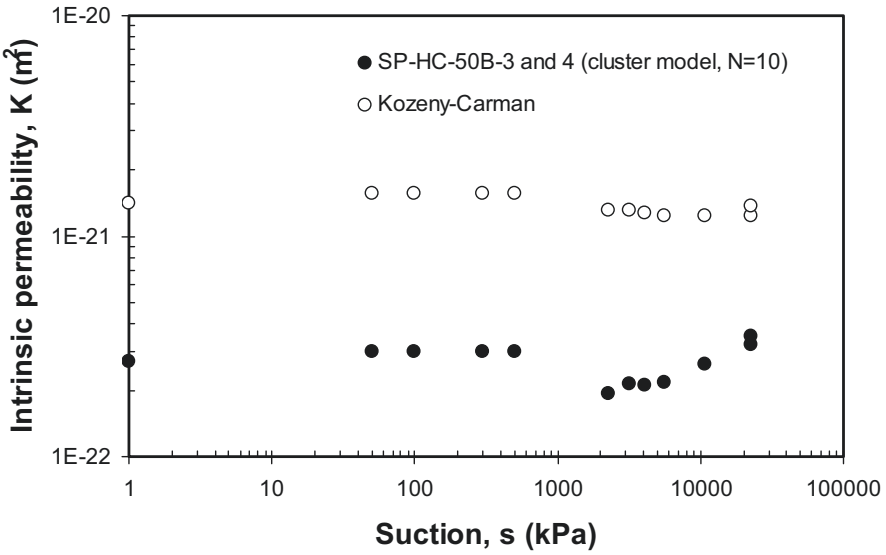

Figure 11.18 Intrinsic permeability versus suction estimated from cluster model in comparison with the Kozeny-Carman prediction during constant volume wetting test from as-prepared conditions (specimens SP-HC-50B-3 and 4)

Figure 11.19 shows a plot of intrinsic permeability versus $e_M^3/(1+e_M)$ of the as-prepared specimen computed using the cluster model in comparison with that predicted using the Kozeny-Carman equation for the three different types of test performed. The best-fit curve of the cluster model prediction data forms a straight line passing the origin, which is in agreement with the Kozeny-Carman postulation. The slope of the best-fitted cluster model prediction curve is 2.07×10^{-19} m^2 whereas that of the Kozeny-Carman permeability prediction is 6.75×10^{-20} m^2. Hence, at any value of e_M, both predictions give a less than one order difference in K value. This fact appears to indicate that the Kozeny-Carman K versus e relationship still holds provided that e_M is considered instead of e.

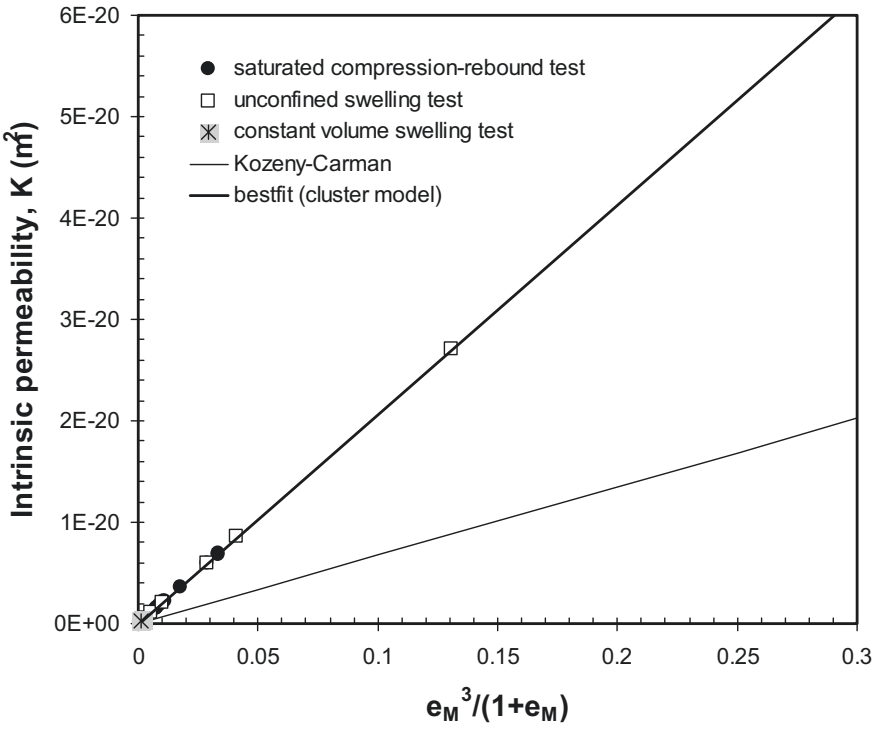

Figure 11.19 Intrinsic permeability versus $e_M^3/(1+e_M)$ for the as-compacted specimen

It should be noted that the k_s values predicted using the cluster model depends on the Kozeny-Carman prediction. In the model, the Kozeny-Carman prediction is modified using the number of clay particles per cluster (N) and the void ratio function. In the computation of k_s using the Kozeny-Carman equation, the specific surface area was assumed to be equal to the external specific surface area. However, the specific surface area used should be taken as the average specific surface area of the clay clusters. This can be done if there are enough experimental data on the permeability of the material so that the slope of K-e_M relationship can be computed. The slope indirectly accounts for the possible value of specific surface area used in the Kozeny-Carman equation.

11.4.2 Unsaturated Permeability Model

The unsaturated permeability function (i.e., unsaturated coefficient of permeability versus suction relationship) is defined for the unconfined swelling and multi-step constant volume swelling pressure tests of the as-prepared specimen.

11.4.2.1 Van Genuchten-Mualem Model

Derivation of unsaturated permeability function based on the van Genuchten-Mualem statistical model (van Genuchten, 1980 and Mualem, 1976) requires the van Genuchten fitting parameters for the soil-water chararacteristic (or the effective degree of saturation versus suction) curve. In this case, parameter n and m in the van Genuchten

SWCC equation are assumed to be correlated one to the other according to Equation (4.36). The residual degree of saturation (S_{res}) is taken as the minimum degree of saturation (i.e., the as-prepared degree of saturation). The maximum degree of saturation ($S_{r\ max}$) is taken as the maximum attainable degree of saturation of the specimen during wetting under the corresponding boundary conditions. Equation (11.21) and Equation (11.22) express the increase in S_e with decreasing suction during unconfined swelling test and multi-step constant volume swelling pressure test on the as-prepared specimen, respectively with S_e in percent and s in kPa.

$$S_e = 100\left[1+\left(\frac{s}{1201}\right)^{1.626}\right]^{-0.385} \qquad (11.21)$$
$$S_{r\max} = 86.1\%;\ S_{res} = 80\%$$

$$S_e = 100\left[1+\left(\frac{s}{272}\right)^{1.451}\right]^{-0.311} \qquad (11.22)$$
$$S_{r\max} = 100\%;\ S_{res} = 82\%$$

Based on the above equations, parameter *m* for the unconfined swelling test data is 0.386 and for the multi-step swelling pressure test data is equal to 0.311. The reference suction (s_{ref}) for the unconfined swelling test data is 1201 kPa and for the multi-step swelling pressure test data is equal to 272 kPa. Equation (11.21) has an r^2 of 0.982 with an *SEE* of 0.05% whereas Equation (11.22) has an r^2 of 0.81 with an *SEE* of 0.17%. The following equations express the change in coefficient of permeability with decreasing suction based on Equation (11.21) and Equation (11.22), respectively, both in combination with Equation (4.58) with S_e is in percent.

$$k_w\left(S_e\right) = k_s\sqrt{\frac{S_e}{100}}\left\{1-\left[\left(\frac{S_e}{100}\right)^{2.597}\right]^{0.385}\right\}^2 \qquad (11.23)$$

$$k_w\left(S_e\right) = k_s\sqrt{\frac{S_e}{100}}\left\{1-\left[\left(\frac{S_e}{100}\right)^{3.215}\right]^{0.311}\right\}^2 \qquad (11.24)$$

11.4.2.2 Fredlund and Xing-Mualem Model

Similar to the van Genuchten-Mualem model, in the Fredlund and Xing-Mualem statistical model (Fredlund and Xing, 1994 and Mualem, 1976), parameters describing the SWCC (or volumetric water content versus suction curve) are required. The best-fitting of parameters to the experimental data was performed by means of normalised volumetric water content (Θ) versus suction data for both the multi-step constant volume test and unconfined swelling from as-prepared conditions. Based on the experimental data, the *a*,

n, and *m* values for the unconfined swelling test data are 2607 kPa, 0.634, and 0.111, respectively and for the multi-step swelling pressure test data, the values are are 202 kPa, 1.147, and 0.106, respectively. The $S_{r\ max}$ and S_{res} as used in the van Genuchten-Mualem model are used as the upper and lower limits of integration that is performed based on Equation (4.56). Thus, Equation (11.25) and Equation (11.26) hold for the unconfined swelling and multi-step swelling pressure test data, respectively.

$$\Theta = \frac{0.86}{\left\{\ln\left[\exp(1)+\left(\frac{s}{2607}\right)^{0.634}\right]\right\}^{0.111}} \tag{11.25}$$

$$\Theta = \frac{1}{\left\{\ln\left[\exp(1)+\left(\frac{s}{202}\right)^{1.147}\right]\right\}^{0.106}} \tag{11.26}$$

The resulting relative permeability is a function of volumetric water content ($k_r(\theta_w)$). Using Equation (11.25) and Equation (11.26), the relative permeability can be expressed as a function of suction ($k_r(s)$).

11.4.2.3 Comparison between the van Genuchten-Mualem and Fredlund and Xing-Mualem Models

The saturated coefficient of permeability (k_s) as obtained using the cluster model can be used in the computation to derive the k_w-s relationship for both tests. Figure 11.20 shows a comparison between unsaturated permeability function obtained using the van Genuchten-Mualem model with that derived using the Fredlund and Xing-Mualem model for the unconfined wetting test on the as-prepared specimen. The Fredlund and Xing-Mualem statistical model predicts one to two order of magnitudes lower k_w than the van Genuchten-Mualem statistical model. Figure 11.21 shows the change in unsaturated coefficient of permeability during multi-step swelling pressure test on the as-prepared specimen. The two models predict almost similar unsaturated permeability function with variation of less than one order of magnitude.

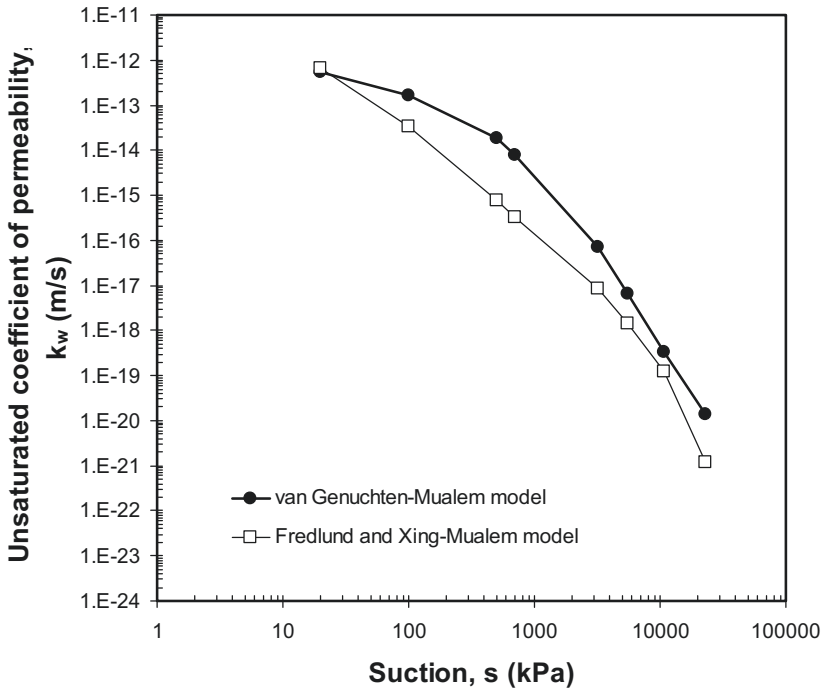

Figure 11.20 Variation of unsaturated coefficient of permeability during unconfined swelling test from as-prepared conditions (specimens UC-7 and UC-9)

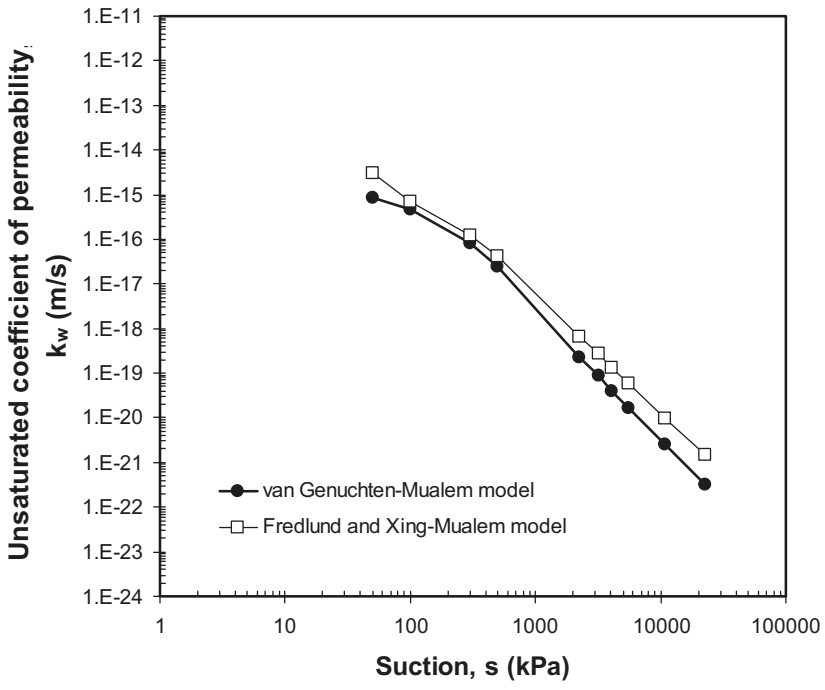

Figure 11.21 Variation of unsaturated coefficient of permeability during multi-step constant volume swelling pressure test from as-prepared conditions (specimens SP-HC-50B-3 and 4)

Figure 11.22 shows a three-dimensional plot of permeability function derived using the combination of cluster model and Fredlund and Xing-Mualem model for the multi-step swelling pressure, unconfined swelling, and saturated compression-rebound tests. The unsaturated coefficient of permeability of the as-prepared 50/50 bentonite-sand mixture is shown to be a function of void ratio and suction.

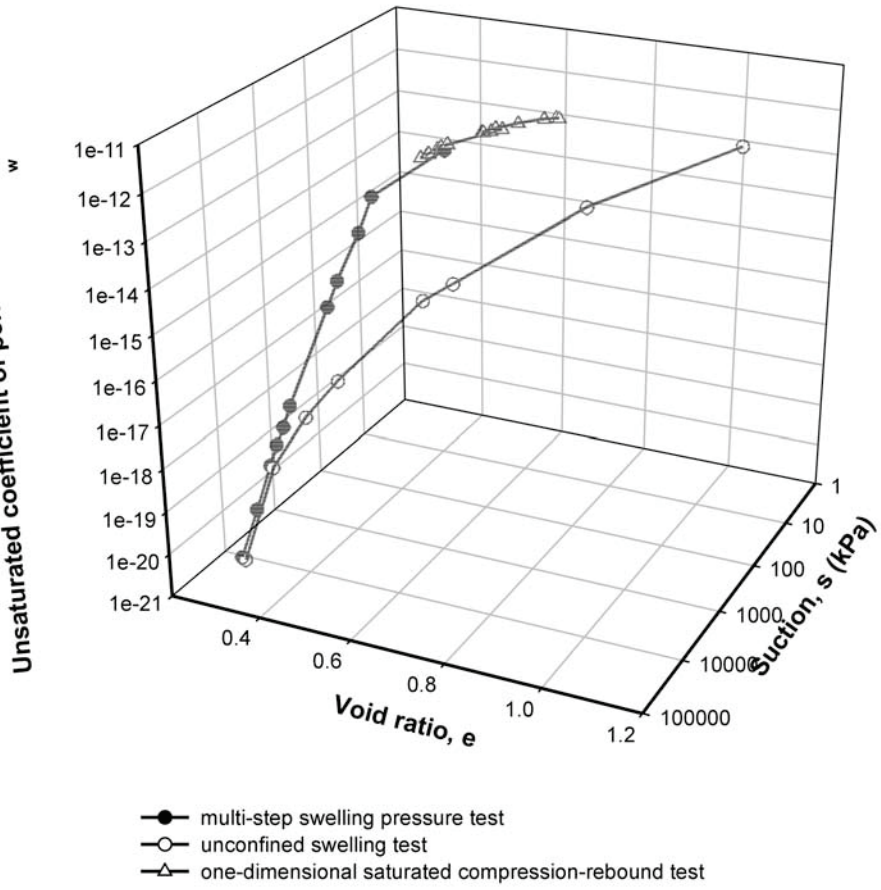

Figure 11.22 Three-dimensional plot of permeability function (cluster model and Fredlund and Xing-Mualem model)

11.5 Analysis of Crack Development due to Suction Increase

Cracking is an important issue when discussing the use of compacted 50/50 bentonite-sand mixture as sealing and buffer material in nuclear waste repository. The presence of cracks increases permeability of the material. Cracks are mainly caused by a rapid increase in suction during drying and/or an increase in temperature generated by the stored waste. Since this investigation did not focus on temperature effect, the analysis presented herein only aims at investigating possible development of cracks due to suction increase. The analysis uses parameters derived from the constitutive modelling II (i.e., the non-linear elastic volume change model based in the soil phase continuity requirements).

It is assumed in the analysis that suction is defined as the difference between pore-air and pore-water pressure in the soil (i.e., the capillary phenomenon).

The existence of cracks in the soil produce local tensile stresses at the crack tips when soil deformations in the direction perpendicular to the direction of crack strain are constrained (Morris et al., 1992). Before cracking starts, the net stress in the direction of cracking ($\sigma_{\parallel}$-u_a) is as follows:

$$\left(\sigma_{\parallel} - u_a\right) = K_o\left(\sigma_{\perp} - u_a\right) - \frac{E}{H\left(1-\upsilon\right)}s \tag{11.27}$$

where ($\sigma_{\perp}$ - u_a) is the net stress perpendicular to the crack direction.

For cracks to occur, the ($\sigma_{\parallel}$ - u_a) must exceed the tensile strength (t_s) of the soil and hence the occurrence of cracks depend on the magnitude of F function which is formulated as:

$$F = K_o\left(\sigma_{\perp} - u_a\right) - \frac{E}{H\left(1-\upsilon\right)}s - t_s \tag{11.28}$$

where F is a function having a value of less than zero when cracks occur.

The tensile strength of the soil increases with suction in according to the following equation with ϕ^b is the angle indicating an increase in shear strength with increasing suction (Morris et al., 1992).

$$\begin{aligned} t &= 0.5\left(c' + s\tan\phi^b\right) \\ \tan\phi^b &= \frac{S_e}{100}\tan\phi' \end{aligned} \tag{11.29}$$

In the equation, c' and ϕ' represent the saturated effective cohesion and effective angle of internal friction of the soil, respectively. The apparent effective cohesion (c_{app}) and the effective angle of internal friction of the as-prepared specimen (i.e., at a suction of 22700 kPa) have been reported by IfB (2001) and the values are equal to 2500 kPa and 40^o, respectively.

In this analysis, only one scenario is considered. The scenario considered is the cracks that develop on the saturated part of the material as caused by drying (or suction increase). The ($\sigma_{\perp}$ - u_a) which acts is therefore equal to the swelling pressure (P_s) of the material. The reduction of P_s with increasing suction is assumed to follow a relationship given in Equation (8.9). There may be other forces acting on the material, e.g., liquid pressure resulting from infiltrated water, however, the scenario considered herein provides the worst conditions of the material in the field. The variation of E value with suction and net stress follows the relationship given in Equation (11.15) whereas H is

derived from the wetting data (i.e., the void ratio-suction relationship) of the specimen which was subjected to suction increase after saturation under constant volume conditions (i.e., specimen UC-10).

$$H = 591200\left(\frac{s}{10}\right)^{1.114} \tag{11.30}$$

In the equation both H and s are in kPa.

Figure 11.23 shows the F value as a function of suction during drying (or suction increase) for non-constant t_s (i.e., according to Equation (11.29)) and constant t_s (i.e., the t_s value at saturation). The F value remains high even up to 1 000 000 kPa suction in both cases indicating that suction increase induce no cracks in the material. However, it should be noted that in this case the material is assumed to be always at mechanical and hydraulic equilibrium at each suction value. As discussed in the preceding chapter that hydraulic non-equilibrium can also induce crack on the saturated specimen.

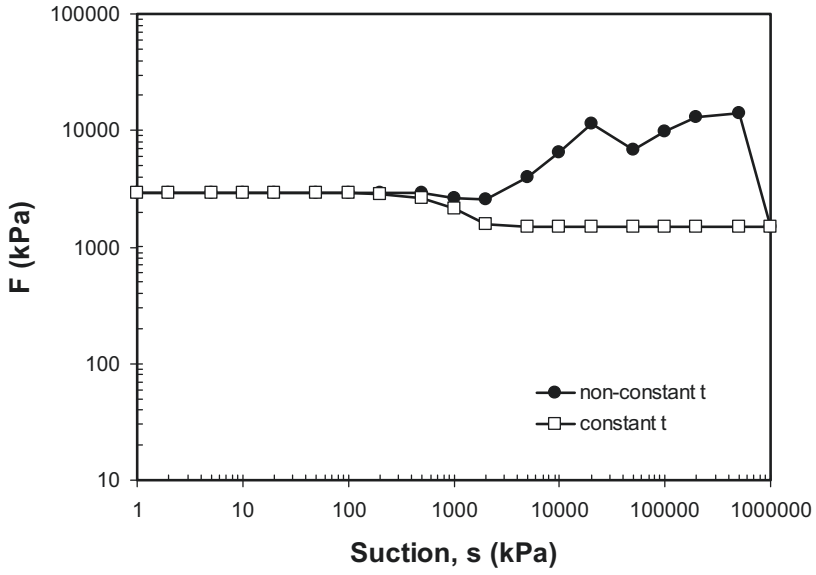

Figure 11.23 Variation of F with suction during drying

CHAPTER 12

CONCLUSIONS AND RECOMMENDATIONS

12.1 Conclusions

An experimental study on the hydro-mechanical characteristics of bentonite-sand mixtures has been presented. Based on the analysis of the experimental data presented (i.e., in Chapter 8 to Chapter 10) and the derivation of parameters (i.e., in Chapter 11), the following conclusions can be drawn.

12.1.1 Micro-structure and Fabric Studies

1. The as-prepared specimen exhibits a bimodal pore-size distribution curve indicating the presence of micro- and macro-pores. The fabric was preserved even after the specimen undergoes drying or wetting process.

2. Water was absorbed in the micro- and macro-pores during wetting under constant volume conditions without introducing any disintegration of clay clusters. The clay clusters separated each other while the volume of each individual cluster increase.

12.1.2 Suctions and Suction Measurements

1. Suction (or total suction) in expansive soils is composed by capillary (or surface tension) component, osmotic component, and the component due to sorptive forces. The capillary and sorptive forces components constitute the matric suction component of expansive soils.

2. Total suction of bentonite-sand mixtures is a function of mixture water content and mixture bentonite content or a function of bentonite water content and no apparent effects of void ratio and fabric are seen. It indicates that the contribution of capillary component of suction is insignificant.

3. Different techniques for measuring suction result in different values of suction. The chilled-mirror hygrometer is found to be the most accurate means of measuring total suction. The in-contact filter paper measures the capillary component of suction.

4. Hydration time appears to have effects on suction of expansive soils due to the presence of micro- and macro-pores in the soils. The process is thought to be related to the secondary behaviour (i.e., the time-dependent behaviour) in expansive soils.

12.1.3 Wetting and Drying Behaviour

1. The as-prepared 50/50 bentonite-sand mixture shows no general main wetting and drying curves for unconfined wetting and drying curves. Hysteresis is found in the water content and degree of saturation versus suction relationships whereas the void ratio versus suction relationship has insignificant hysteresis and shows a reversible response to drying and wetting under unconfined conditions.

2. There is a limiting degree of saturation for wetting under unconfined conditions, which is a function of the highest suction that ever experienced by the soil before the commencement of wetting process.

3. Cracks during drying under unconfined conditions occur due to the in-homogeneity of suction distribution at different levels of pores. The suction at which cracks start to occur is a function of stress level under which the soil is saturated prior to drying.

4. The wetting curve of the as-prepared specimen is affected by the specimen's boundary conditions (i.e., unconfined or constant volume conditions). The investigation of the changes in intra-aggregate water content with suction indicates that the boundary condition effects on wetting start to take place at 2000 kPa suction.

12.1.4 Swelling Pressure

1. Different methods used to measure swelling pressure result in different values of swelling pressure indicating the stress- and suction-path dependency of swelling pressure. The fact may indicate the effects of different fabrics of the specimens, which followed different paths, at equilibrium void ratio at the end of each test.

2. Swelling pressure of bentonite-sand mixtures is a function of mixture dry density and mixture bentonite content or is a function of bentonite dry density.

3. The delayed 'true' equilibrium state after wetting of the as-prepared specimen up to 2000 kPa suction resulted in insignificant development of swelling pressure. The behaviour is thought to be related to the internal redistribution of water caused by the suction gradient between the micro- and macro-pores.

4. There is a threshold suction below which a decrease in suction will be followed an increase in swelling pressure of the same magnitude. The magnitude of threshold suction is a function of bentonite content.

5. Similarly, there is also a threshold water content beyond which a small further increase in water content results in a significant increase in swelling pressure. The magnitude of threshold water content is also a function of bentonite content of the mixture.

12.1.5 One-Dimensional Compression and Rebound Behaviour under Constant Suction

1. The as-prepared 50/50 bentonite-sand mixture at saturated state behaves elastically in response to compression and rebound in the high range of net vertical stress (or low void ratio). The elastic behaviour diminishes as the material unsaturates or in the low range of net vertical stress.

2. The apparent pre-consolidation pressure increases with increasing suction. The influence of suction becomes unapparent with increasing suction.

3. The compressive index generally decreases with increasing suction. The slope of virgin compression line also decreases with increasing suction.

4. The parameters obtained from the one-dimensional test can be used in the Barcelona Basic Model with sufficient accuracy although the model was developed for isotropic stress conditions.

5. The modulus of elasticity of soil structure increases with increasing net vertical stress and suction according to a power law. The increase in modulus of elasticity of the material with net vertical stress becomes less apparent as suction increases.

6. The modulus of elasticity of soil structure with respect to changes in suction increases with increasing suction according to a power law and is also thought to increase with increasing net vertical stress.

7. The modulus of elasticity of water phase with respect to changes in net vertical stress as well as suction also increases with increasing net vertical stress according to a power law.

12.1.6 One-Dimensional Wetting-Drying Behaviour under Constant Load

1. The as-prepared specimen behaves elastically after four cycles of wetting and drying under constant net vertical stresses. The elastic deformation with respect to changes in suction under constant net vertical stresses signifies the elastic deformation of the micro-structures.

2. The compressive index for the micro-structure with respect to changes in suction is not significantly affected by net vertical stress.

12.1.7 Permeability Characteristics

1. The saturated coefficient of permeability of different mixtures is a function of bentonite dry density or bentonite void ratio.

2. The Kozeny-Carman equation predicts lower saturated coefficients of permeability than those computed using the saturated compression and rebound test data (assuming the applicability of Terzaghi's theory of consolidation).

3. The cluster model is found to be a promising permeability model for expansive soils. In the cluster model, the change in permeability with respect to changes in the intra-aggregate void ratio relative to the measurable changes in the total void ratio can be quantified whereas it cannot be captured by the Kozeny-Carman model.

4. The statistical models (in combination with the cluster model) can be used to calculate the unsaturated permeability of expansive soils.

12.2 Recommendations

Further experimental works are required to confirm several aspects that have not been clearly described by the present experimental data. Some characteristics of the compacted bentonite-sand mixtures investigated in this study have not been sufficiently incorporated in the current modelling approach. The following aspects are suggested for future studies on the bentonite-sand mixtures.

12.2.1 Future Experimental Works

1. Measurement of total suction should be performed on compacted specimens at different ages (not only at two different ages) to study more deeply the effects of hydration on the magnitude of total suction. The change in total suction with hydration time can accordingly be investigated. Similarly, an investigation of the effects of hydration time and aging on the swelling characteristics of the bentonite-sand mixtures used is desirable.

2. Measurement of matric suction using high suction probe is necessary to provide a better comparison with the total suction data of the compacted specimens measured using the chilled-mirror hygrometer.

3. Despite its dependency on the squeezing pressure used, the osmotic suction data for specimens with different water contents, dry densities, and bentonite contents compliment the total and matric suction data.

4. In this dissertation, the results of wetting and drying tests using the axis-translation and vapour equilibrium techniques are considered to be combinable assuming no

dilution of ions takes place during test using the axis-translation technique. It is thought that this is not that true for expansive soils since ions can always diffuse and dilute when the soil is in direct contact with liquid water. Water content of an expansive soil will be higher when it is wetted using the vapour equilibrium technique compared to that when wetted using the axis-translation technique in the low suction range. An assessment should be made regarding how far the assumption of no ion dilution conditions is reasonable in the case of expansive soils.

5. Drying tests from slurried conditions of the as-prepared 50/50 bentonite-sand specimen will provide the 'true' virgin compression curve with respect to changes in suction. Since the curve is dependent on the initial water content, it is recommended that the test be performed on the specimen with a water content as high as possible but low enough to prevent segregation of clay particles. The tests can also be considered to be done under different net vertical stress to study the influence of stress level on the drying behaviour. Similarly, one-dimensional compression test should be performed to provide the 'true' virgin compression curve with respect to changes in net vertical stress.

6. To compliment the data that have been obtained in this study, several one-dimensional compression and rebound tests should be performed under low suction values (i.e., lower than 1000 kPa) to study the transition from elastic to plastic behaviour of the as-prepared 50/50 bentonite-sand specimen.

7. The one-dimensional cyclic wetting-drying tests under constant net vertical stress should be performed in such a way to result in a greater swelling on wetting and a greater shrinking on drying. This way, the micro-macro interaction functions for the Barcelona Expansive Model (BExM) can be derived more realistically.

8. Measurement of saturated coefficients of permeability should be conducted as in the following. Several as-prepared 50/50 bentonite-sand specimens are subjected to different values of suction on wetting. After reaching equilibrium, the specimens are saturated under constant volume conditions and the saturated coefficients of permeability are measured. The initial cluster (or micro) void ratio of the specimens before wetting is constant. The change in the cluster void ratio can be computed by knowing the change in the micro-structural effective stress for each specimen. Accordingly, an iterative procedure can be setup to calculate the change in the number of clay particles per cluster for each specimen based on the measured coefficients of permeability and the computed values from the Kozeny-Carman model.

9. Since the transport of water in the vapour form is dominant in the low range of permeability (i.e., at high suction), diffusivity coefficient is more relevant to be measured. Measurement of unsaturated coefficients of permeability (and

diffusivity) should be performed using, for instance, instantaneous profile method. An expansive soil column (i.e., a hydro-mechanical cell) can be developed and instrumented with water content, relative humidity, and pressure sensors along its height. Water can be supplied from the bottom of the cell and distribution of water content and relative humidity in the soil is observed with time while also measuring its swelling pressure development. The permeability and diffusivity coefficients can be back-calculated from the experimental data.

10. Experimental studies extended to investigate the effects of temperature and different pore fluids are required for better understanding the material behaviour.

12.2.2 Perspective of Expansive Soil Modelling

1. Although the influence of osmotic suction on the expansive soil behaviour may indirectly be incorporated in the constitutive modelling approaches (i.e., the BExM and the volume change model based on the soil phase continuity requirements) by considering total suction instead of capillary suction, its role should be considered specifically. This is to account for possible ion exchanges between the material (i.e., the as-prepared 50/50 bentonite-sand mixture) with any liquids from its surrounding in the field (i.e., in the repository). Another approach that can be adopted is to consider total water potential instead of suction in the formulation of constitutive equations, which is in fact a thermodynamics approach (Iwata et al., 1995). In this approach, water or other solutions have a total water potential relative to the water potential of a pool of distilled deaired water. Flow of water and other solutions into or out of the sealing and buffer elements is caused by the difference in total water potential between the elements and the solutions and induces macroscopic volume change in the case of unconfined conditions or internal swelling in the case of constant volume conditions. The swelling pressure developed or the net vertical stress acting on a clay specimen at an equilibrium void ratio is a part of the total water potential (Iwata et al., 1995). However, this approach has not yet been well developed and related to the macroscopic measurable values such as void ratio and water content.

2. The hydraulic models, including the statistical models used to establish the unsaturated permeability function, have been derived by only considering the capillary component of suction. Since the capillary component has insignificant contribution in the magnitude of total suction of expansive soils, its role in the mechanism of unsaturated flow of water and other liquids is thought to be limited. Attempts could be made to include the osmotic flow (i.e., the flow of water or other liquids as a result of an osmotic gradient between the liquids and soil pore-water) in the formulation of hydraulic models of the material.

REFERENCES

Achari, G., Joshi, R.C., Bentley, L.R., and Chatterji, S. (1999) Prediction of the hydraulic conductivity of clays using the electric double layer theory. Canadian Geotechnical Journal, 36: 783-792.

AECL (2002) Atomic Energy of Canada Limited (AECL). Official Website. www.aecl.ca.

Ahlneck, C and Zografi, G. (1990) The molecular basis of moisture effects on the physical and chemical stability of drugs in the solid state. International Journal of Pharmaceutics, 62: 87-95.

Agus, S.S., Leong, E.C., and Rahardjo, H. (2001) Soil-water characteristic curve of Singapore residual soils. Geotechnical and Geological Engineering, 19: 285-309.

Agus, S.S., Leong, E.C., and Schanz, T. (2003a) Assessment of statistical models for indirect determination of permeability functions from soil-water characteristic curves. Géotechnique, 53(2): 279-282.

Agus, S.S., Leong, E.C., and Rahardjo, R. (2003b) A flexible wall permeameter for measurements of water and air coefficients of permeability of residual soils. Canadian Geotechnical Journal, 40: 559-574.

Agus S.S. and Schanz, T. (2003a) Vapour equilibrium technique for tests on a highly compacted bentonite-sand mixture. In Proceedings of the International Conference on Problematic Soils, Nottingham, United Kingdom, 2003: 467-474.

Agus, S.S. and Schanz, T. (2003b) The use of a relative humidity sensor for suction measurement of compacted bentonite-sand mixtures. In Proceedings of the Symposium on Geotechnical Measurements and Modelling (GTMM), Karlsruhe, Germany, 2003, Balkema, Rotterdam: 315-320.

Agus, S.S. and Schanz, T. (2004) Swelling pressure and wetting-drying curves of a highly compacted bentonite-sand mixture. In Proceedings of the International Unsaturated Soil Conference. From Experimental Evidence Towards Numerical Modelling of Unsaturated Soils, Weimar, Germany, 2003 (Ed. T. Schanz), Lecture Notes in Applied Mechanics, Springer: 241-256.

Aitchison, G.D. (1965) Moisture equilibria and moisture changes in soils beneath covered areas. A symposium in Print, (Australia), Butterworth (Ed. G.D. Aitchison).

AkEnd (2002) Site selection procedure for repository sites. Recommendation of the AkEnd Committee on a Site Selection Procedure for Repository Sites. Arbeitskreis Auswahlverfahren Endlagerstandort. W&S Druck GmbH, Collogne.

Albrecht, B.A., Benson, C.H. and Beuermann, S. (2003) Polymer capacitance sensors for measuring gas humidity in drier soils. Geotechnical Testing Journal, 26(1): 3-11.

Al-Khafaf, S. and Hanks, R.J. (1974) Evaluation of the filter paper method for estimating soil-water potential. Soil Science, 117(4): 194-199.

Allègre, M. (1999) The deep geological repository: an unavoidable and ethically correct solution. In the Proceedings of the Uranium Institute 24th Symposium, London: 1-11.

Al-Mukhtar, M. (1995) Macroscopic behavior and microstructural properties of a kaolinite clay under controlled mechanical and hydraulic state. In Proceedings of the 1st International Conference on Unsaturated Soils (UNSAT 95), Paris, France (Eds. E.E. Alonso and P. Delage), Balkema, Rotterdam: 3-9.

Alonso, E.E., Gens, A. and Josa, A (1990) A constitutive model for partially saturated soils. Geotechnique, 40(3): 405-430.

Alonso, E.E. (1998) Modelling expansive soil behaviour. In Proceedings of the 2nd International Conference on Unsaturated Soils, Beijing, China, Vol. 2: 37-70.

Alonso, E.E., Vaunat, J., and Gens, A. (1999) Modelling the mechanical behaviour of expansive clays. Engineering Geology, 54: 173-183.

Alonso, E.E., Romero, E., Hoffmann, C., and Garcia-Escudero, E. (2001) Expansive bentonite/sand mixtures in cyclic controlled-suction drying and wetting. In Proceeding of the 6th International Workshop on Key Issues in Waste Isolation Research (KIWIR 2001), Paris, Ecole National des Ponts et Chaussées, Paris: 513-541.

Amente, G., Baker, J.M., and Reece, F.C. (2000) Estimation of soil solution electrical conductivity from bulk soil electrical conductivity in sandy soils. Soil Science Society of America Journal, 64(6): 1931-1939.

ANDRA (2003) The French National Radioactive Waste Management Agency (ANDRA). Official Website. www.andra.fr.

ASTM (1997) Annual Book of Standards. Volumes 04.08 and 04.09, Soil and rock, ASTM International. West Conshohocken. PA.

ASTM (1997) Annual Book of Standards. Volumes 11.03, Standard test method for the atmospheric analysis, occupational health and safety, and protective clothing, ASTM International. West Conshohocken. PA.

Barbour, S.L. and Fredlund, D.G. (1989) Physico-chemical state variables for clay soils. In Proceedings of XII International Conference on Soil Mechanics and Foundation Engineering, Rio de Janeiro, Brazil, 1989, Balkema, Rotterdam: 1839-1843.

Barden, L., Madedor, A.D., and Sides, G.M. (1969) Volume change characteristics of unsaturated clay. Journal of Soil Mechanics and Foundation Division, ASCE, 95(SM1): 33-52.

Benson, C.H. and Bosscher, P.J. (1999) Time-domain reflectometry (TDR) in geotechnics: a review, nondestructive and automated testing for soil and rock properties. ASTM SPT 1350 (Eds. W.A. Marr and C.E. Fairhurst), ASTM, West Conshohochen, PA.

Bishop, A.W. and Henkel, D.J. (1962) The measurement of soil properties in the triaxial test. 2nd Edition. Edward Arnold, London.

Blatz, J.A., Graham, J. and Chandler, N.A. (2000) Influence of suction on the strength and stiffness of compacted sand-bentonite. Canadian Geotechnical Journal, 39: 1005-1015.

Blatz, J.A., Graham, J., and Chandler, N.A. (2002) Influence of suction on the strength and stiffness of compacted sand-bentonite. Canadian Geotechnical Journal, 39(5): 1005-1015.

Blatz, J.A. and Graham, J. (2003) Elastic-plastic modelling of unsaturated soil using results from a new traixial test with controlled suction. Géotechnique, 53(1): 113-122.

Bocking, K.A. and Fredlund, D.G. (1980) Limitations of the axis translation technique. In Proceedings of the 4th International Conference Expansive Soils, Denver, CO, 1980: 117-135.

Bolt, G.H. (1956) Physico-chemical analysis of the compressibility of pure clays. Géotechnique, 6(2): 82-93.

Bolt, G.H. and Miller, R.D. (1958) Calculation of total and component potentials of water in soils. Americal Geophysicist Union Transportaion, 39: 917-928.

Bolzon, G., Schrefler, B.A., and Zienkiewicz, O.C. (1996) Elastoplastic soil constitutive laws generalised to partially saturated states. Géotechnique, 46(2): 270-289.

Brenner, R.P. (1988) Bohrlochversiegelung in hochverdichtetem Bentonit mit Eignungsbeurteilung. Technischer Bericht 88-04, The Swiss National Cooperative for the Storage of Radioactive Waste (NAGRA), Wettingen, Switzerland.

Brooks, R.H. and Corey, A.T. (1964). Hydraulic properties of porous medium. Hydrology Papers. 3. Civil Engineering Department, Colorado State University, Colorado, Fort Collins.

Brown, R.W. (1970) Measurement of water potential with thermocouple psychrometers: construction and applications. U.S.D.A. Forest Service Research Paper INT-80.

Brown, R.W. and Bartos, D.L. (1982) A calibration model for screen-caged Peltier thermocouple psychrometers. U.S. Department of Agriculture Research Paper INT-293.

Brunaer, S., Emmett, P., and Teller, E. (1938) Adsorption of gases in multimolecular layers. Journal of American Chemist Society, 60: 309–319.

Brye, K.R. (2003) Long-term effects of cultivation on particle size and water-retention characteristics determined using wetting curves. Soil Science, 168(7): 459-468.

Bucher, F. and Spiegel, U. (1984) Quelldruck von hochverdichteten Bentoniten. Technischer Bericht 84-18, The Swiss National Cooperative for the Storage of Radioactive Waste (NAGRA), Wettingen, Switzerland.

Bucher, F., Jedelhauser, P., and Jeger, P. (1985) Schrumpfversuche an Bentonitproben. Technischer Bericht 85-24, The Swiss National Cooperative for the Storage of Radioactive Waste (NAGRA), Wettingen, Switzerland.

Bucher, F., Jedelhauser, P., and Mayor, P.A. (1986) Quell-, Durchlässigkeit-, und Schrumpfversuche and Quarzsand-Bentonit-Gemischen. Technischer Bericht 86-13, The Swiss National Cooperative for the Storage of Radioactive Waste (NAGRA), Wettingen, Switzerland.

Buckingham, E. (1907) Studies of the movement of soil moisture. USDA Bureau of Soils Bulletin, 38.

Burdine, N.T. (1953). Relative permeability calculation from pore-size distribution data. Petroleum Transactions. American Institute of Mining. Metallurgical and Petroleum Engineers, 198: 71-78.

Campbell, E.C., Campbell, G.S. and Barlow, W.K. (1973) A dew-point hygrometer for water potential measurement. Agricultural Meteorology, 12: 113-121.

Carman, P.C. (1938) Fundamental principles of industrial filtration-A critical review of present knowledge. Transaction of Institution of Chemical Engineering, 16: 168-188.

Carrier III, W.D. (2003) Goodbye, Hazen; Hello, Kozeny-Carman. Journal of Geotechnical and Geoenvironmental Engineering, 129(11): 1054-1056.

CEG (2002) The mock-up experiment. Centre of Experimental Geotechnics (CEG), Faculty of Civil Engineering, Czech Technical University (CTU), Czech Republic. Official Website. http://ceg.fsv.cvut.cz.

Cerato, A.B. and Lutenegger, A.J. (2002) Determination of surface area of fine-grained soils by the ethylene glycol monoethyl ether (EGME) method. Geotechnical Testing Journal, 25(3): 315-321.

Chandler, R.J. and Gutierrez, C.I. (1986) The filter paper method of suction measurement. Geotechnique, 36: 265-268.

Chandler, R.J., Crilly, M.S. and Montgomery-Smith, G. (1992) A low cost method of assessing clay desiccation for low-rise buildings. Proceedings of the Institution of Civil Engineer, 92(2): 82-89.

Chapman, D.L. (1913) A contribution to the theory of electro-capillarity. Philosophical Magazine, 25(6): 475-481.

Childs, E.C. and Collis-George, G.N. (1950). The permeability of porous materials. In Proceedings of The Royal Society, 210A: 392-405.

Chiou, C., Rutherford, D., and Manes, M. (1993) Sorption of N2 and EGME vapors on some soils, clays and mineral oxides and determination of sample surface areas by use of sorption data. Environmental Science Technology, 27: 1587–1594.

CODE_BRIGHT (2003) User's guide. Departamento de Ingeníeria del Terreno, E.T.S. Ingenieros de Caminos, Canales y Puertos de Barcelona, Universidad Politécnica de Cataluña, Spain.

Collins, K. and McGown, A. (1974) The form and functions of microfabric features in a variety of natural soils. Géotechnique, 24(2).

Corey, A.T. and Brooks, R.H. (1997) The Brooks-Corey relationships. In Proceedings of the International Workshop on Characterization and Measurement of the Hydraulic Properties of Unsaturated Porous Media, Riverside, CA (Eds. M.Th. van Genuchten and F.J. Leif), Part 1, the University of California, Riverside, CA: 13-18.

Croney, D., Coleman, J. D. and Bridge, P. (1952) The suction of moisture held in soil and other porous materials. Road Research Technical Paper, 24.

Croney, D. and Coleman, J.D. (1961) Pore pressure and suction in soil. In Proceedings of Conference on Pore Pressure and Suction in Soils, London, Butterworths: 31-37.

Cui, Y.J. and Delage, P. (1996) Yielding and plastic behaviour of an unsaturated compacted silt. Géotechnique, 46(2): 291-311.

Cui, Y.J., Loiseau, C., and Delage, P. (2002a) Microstructure changes of a confined swelling soil due to suction controlled hydration. In Proceedings of the 3rd International Conference on Unsaturated Soils (UNSAT 2002), Recife, Brazil (Eds. J.F.T. Jucá, T.M.P. de Campos, and F.A.M. Marinho), Swets & Zeitlinger, Lisse: 593-598.

Cui, Y.J., Yahia-Aissa, M., and Delage, P. (2002b) A model for the volume change behavior of heavily compacted swelling clays. Engineering Geology, 64: 233-250.

Cuisinier, O. and Masrouri, F. (2002) Influence of a suction cycle on the hydromechanical behaviour of a swelling soil. In Proceeding of the International Workshop on Environmental Geomechanics, Monte Verità, Switzerland (Eds. L. Vulliet, L. Laloui and B. Schrefler), EPFL Press, Lausanne: 175-180.

Cuisinier, O. and Masrouri, F. (2004) Testing the hydromechanical behaviour of a compacted swelling soil. Geotechnical Testing Journal, 27(6).

Cunningham, M.R., Ridley, A.M., Dineen, K., and Burland, J.B. (2003) The mechanical behaviour of a reconstituted unsaturated silty clay. Géotechnique, 53(2): 183-194.

Dalton, F.N., Herkelrath, W.N., Rawlins, D.S., and Rhoades, J.D. (1984) Time-domain reflectometry: simultaneous measurement of soil water content and electrical conductivity with a single probe. Science, 224(4652): 989-990.

Deka, R.N., Wairiu, M., Mtakwa, P.W., Mullins, C.E., Veenendaal, E.M., and Townend, J. (1995) Use and accuracy of the filter-paper technique for measurement of soil matric potential. European Journal of Science, 46: 233-238.

Delage, P., Suraj de Silva, G.P.R., and Vicol, T. (1992) Suction controlled testing of non saturated soils with an osmotic consolidometer. In Proceedings of the 7th International Conference on Expansive Soils, Dallas, Texas, 1992: 206-211.

Delage, P. and Graham, J. (1996) Mechanical behaviour of unsaturated soils: Understanding the behaviour of unsaturated soils requires reliable conceptual models. In Proceedings of the 1st International Conference on Unsaturated Soils (UNSAT 95), Paris, France (Eds. E.E. Alonso and P. Delage), Balkema, Rotterdam: 1223-1256.

Delage, P., Audiguier, M., Cui, Y.J., and Howat, M. (1996) The microstructure of a compacted silt. Canadian Geotechnical Journal, 33: 150-158.

Delage, P., Hawat, M., and Cui, Y.J. (1998) The relationship between suction and swelling properties in a heavily compacted unsaturated clay. Engineering Geology, 50(1-2): 31-48.

Derjaguin, B.V. and Landau, L. (1941) Theory of the stability of strongly charged lyophobic sols and of the adhesion of strongly charged particles in solutions of electrolytes. Acta Physicochim, URSS 14: 633-662.

Dif, A.E. and Bluemel, W.F. (1991) Expansive soils under cyclic drying and wetting. Geotechnical Testing Journal, 14: 96-102.

DIN (1987) Baugrund und Grundwasser. Benenen und Beschreiben von Boden und Fels. Deustche Institut für Normung e.V., Beuth Verlag GmbH, Berlin.

Dixon, D., Chandler, N., Graham, J. and Gray, M.N. (2002) Two large-scale sealing tests conducted at Atomic Energy of Canada's underground research laboratory: the buffer-container experiment and the isothermal test. Canadian Geotechnical Journal, 39: 503-518.

DOE (2002) Yucca mountain science and engineering report. Technical information. U.S. Department of Energy (DOE), Office of Civilian Radioactive Management (OCRWM). Report Revision 1 No. DOE/RW-0539-1, February 2002, www.ocrwm.doe.gov/document/ser_b/index.html.

Doehne, E., Stulik, D.C. (1990) Applications of the environmental scanning electron microscope to conservation science. Scanning Microscopy, 4: 275-286.

Duliu, O.G. (1999) Computer axial tomography in geosciences: an overview. Earth Science Review, 48: 265–281.

Edlefsen, N.E. and Anderson, A.B.C. (1943) Thermodynamics of soil moisture. Hilgardia, 15: 31-298.

ENRESA (2000) FEBEX project—full-scale engineered barriers experiment for a deep geological repository for high level radioactive waste in crystalline host rock. Final Report, Publicatión Técnica 1/2000, Empresa Nacional de Residuos Radiactivos SA (ENRESA), Madrid, Spain.

Enviros (2003) The virtual repository of nuclear information. Public Access Area. Enviros Consulting Ltd. www.enviros.com/repository.

Fawcett, R.G. and Collis-George, N. (1967) A filter paper method for determining the moisture characteristics of soil. Australian Journal of Experimental Agriculture and Animal Husbandry, 7: 162-167.

Feng, M., Fredlund, D.G., and Shuai, F. (2002) A laboratory study of hysteresis of a thermal conductivity soil suction sensor. Geotechnical Testing Journal, 25(3): 1-9.

Fleureau, J.M., Verbrugge, J.C., Huergo, P.J., Correia, A.G., and Kheirbek-Saoud, S. (2002) Aspects of the behaviour of compacted clayey soils on drying and wetting paths. Canadian Geotechnical Journal, 39: 1341-1357.

Fredlund, D.G. and Morgenstern, N. (1977) Stress state variables for unsaturated soils. Journal of the Geotechnical Engineering Division, ASCE, 103(GT5): 447-466.

Fredlund, D.G. (1979) Appropriate concepts and technology for unsaturated soils. 2nd Canadian Geotechnical Colloquium. Canadian Geotechnical Journal, 16(1): 121-139.

Fredlund, D.G. (1989) Negative pore-water pressures in slope stability. In Simposio Suramericano de Deslizamiento, Paipa, Columbia, 1989: 1-31.

Fredlund, D.G. and Wong, D.K.H. (1989) Calibration of thermal conductivity sensors for measuring soil suction. Geotechnical Journal, 12(3): 188-194.

Fredlund, D.G. and Rahardjo, H. (1993) Soil mechanics for unsaturated soils. John Wiley & Sons Inc., NY.

Fredlund, D.G. and Xing, A. (1994). Equation for the soil-water characteristic curve. Canadian Geotechnical Journal, 31: 521-532.

Fredlund, D.G., Xing, A., and Huang, S. (1994) Predicting the permeability function for unsaturated soils using the soil-water characteristic curve. Canadian Geotechnical Journal, 31:533-546.

Fredlund, D.G., Gan, J.K.-M., and Gallen, P. (1995) Suction measurements on compacted till specimens and indirect filter paper calibration technique. Transportation Research Board, Record (1481): 3-9.

Friedel, R.R. and Cundell, A.M. (1998) The application of water activity measurement to the microbiological attributes testing of nonsterile over-the-counter drug products. Pharmacopeial Forum, 24(2): 6087-6090.

Gan, J.K.M. and Fredlund, D.G. (1988) Multistage direct shear testing of unsaturated soils. Geotechnical Testing Journal, 11(2): 132-138.

Garcia-Begochea, I., Lovell, C.W., Altschaeffl, A.G. (1979) Pore distribution and permeability of silty clay. Journal of Geotechnical Engineering, 105(7): 839-856.

Gardner, R. (1937) A method of measuring the capillary tension of soil moisture over a wide moisture range. Soil Science, 43: 227-283.

Gattermann, J.H. (1998) Theorie und Modellversuch für ein Abdichtungsbauwerk aus hochverdichteten Bentonit-formsteinen. Verlag Glückauf, Essen, Germany.

Gee, G., Campbell, M., Campbell, G. and Campbell, J. (1992) Rapid measurement of low soil potentials using a water activity meter. Soil Science Society of America Journal, 56: 1068-1070.

Gens, A. and Alonso, E.E. (1992) A framework for the behaviour of unsaturated expansive clays. Canadian Geotechnical Journal, 29: 1013-1032.

Graham, J., Wiebe, B., Tang, X. and Onofrei, C. (1995) Strength and stiffness of unsaturated sand-bentonite 'buffer'. In Proceedings of the 1st International Conference on Unsaturated Soils (UNSAT 95), Paris, 1995 (Eds. E.E. Alonso and P. Delage), Balkema, Rotterdam: 89-94.

Grauer, R. (1988) Zum chemischen Verhalten von Montmorillonit in einer Endlagerverfüllung. Technischer Bericht 88-24, The Swiss National Cooperative for the Storage of Radioactive Waste (NAGRA), Wettingen, Switzerland.

Gray, M.N. (1993) OECD/NEA International Stripa Project Overview-Volume III: Engineered barriers. The Swedish Nuclear Fuel and Waste Management Company (SKB), Stockholm, Sweden.

Greacen, E.L., Walker, G.R. and Cook, P.G. (1987) Evaluation of the filter paper method for measuring soil water suction. In Proceedings of the International Conference on Measurement of Soil and Plant Water Status: 137-143.

Greenspan, L. (1977) Humidity fixed points of binary saturated aqueous solutions. Journal of Research of the National Bureau Standards—A Physics and Chemistry, 81A: 89-96.

Griffiths, F.J., Joshi, R.C. (1989) Change in pore-size distribution due to consolidation of clays. Géotechnique, 39(1): 159-167.

Grim, R.E. (1968) Clay Mineralogy. 2nd ed. McGraw-Hill, NY.

Grimsel (2003) The Grimsel test site. Official Website. www.grimsel.com.

Guan, Y. and Fredlund, D.G. (1997) Use of the tensile strength of water for the direct measurement of high soil suction. Canadian Geotechnical Journal, 34: 604-614.

Guoy, G. (1910) Sur la constitution de la charge électrique á la surface d'un électrolyte. Anniue Physique, Paris, 9(4): 457-468.

Haas, R. (1991) Bedeutung der Isothermenmessung an Tonen. Mitteilung des Institut für Bodenforschung und Baugeologis der Universität für Bodenkultur Wien, Reihe Angewandte Geowissenschaft, Heft 1, Vienna.

Hamblin, A.P. (1981) Filter paper method for routine measurement of field water potential. Journal of Hydrology, 53: 355-360.

Hamilton, J.M., Daniel, D.E. and Olson, R.E. (1981) Measurement of hydraulic conductivity of partially saturated soils. In Permeability and Groundwater Contaminant Transport, ASTM Special Technical Publication 746 (Eds. T.F. Zimmie and C.O. Riggs), ASTM: 182-196.

Hand, L. (1994) Controlling water activity and pH in snack sticks. Meat Marketing and Technology, May: 55-56.

Harrison, B.A. and Blight, G.E. (2000) A comparison of in-situ soil suction measurements. In Proceedings of the 1st Asian Conference on Unsaturated Soils (UNSAT-ASIA 2000), Singapore, 2000 (Eds. H. Rahardjo, D.G. Toll, and E.C. Leong), Balkema, Rotterdam: 281-286.

Hasenpatt, R. (1988) Bodenmechanische Veränderungen reiner Tone durch Adsorption chemischer Verbindungen. Mitteilung des IGB der ETH Zürich, No. 134. Swiss Federal Institute of Technology, Zurich, Switzerland.

Hazen, A. (1892) Some physical properties of sands and gravels, with special reference to their use in filtration. 24th Annual Report. Massachusetts State Board of Health. Publication Document No. 34: 539-556.

Herbert, H.J. and Moog, H.C. (2002a) Untersuchungen zur Quellung von Bentoniten in hochsalinaren Lösungen. Abschlussbericht GRS-179, Förderkennzeichen 02 E 8986 5 (BMBF). Gesellschaft für Anlagen und Reaktorsicherheit (GRS)mbH, Germany.

Herbert, H.-J. and Moog, H.C. (2002b) Modelling of saturation and swelling effects in clays under different saline conditions. Eurosafe Forum 2002, http://www.eurosafe-forum.com.

Hilf, J.W. (1956) An investigation of pore water pressure in compacted cohesive soils. US Bureau of Reclamation. Technical Memo No. 654, Denver, Colorado.

Holtz and Gibbs (1956) Engineering properties of expansive soils. Transaction ASCE, 121.

Houston, S.L., Houston, W.N. and Wagner, A.-M. (1994) Laboratory filter paper suction measurements. Geotechnical Testing Journal, GTJODJ, 17(2): 185-194.

Hovart, A.L. (1985) Handbook of aqueous electrolyte solutions: physical properties, estimation and correlation methods. Ellis Horword Limited, John Wiley & Sons, NY.

Huang, S., Barbour, S.L., and Fredlund, D.G. (1998) Development and verification of a coefficient of permeability function for a deformable unsaturated soil. Canadian Geotechnical Journal, 35: 411-425.

IAEA (1994) Classification of radioactive waste-A safety guide. Safety Series No. 111-G-1.1. International Atomic Energy Agency (IAEA), Vienna.

Institut für Bergbau (IfB) (2001) Untersuchung zum statischen Verhalten des Streckenverschlussbauwerkes in der EU1 der Grube Sondershausen (Zusammenwirken von Dichtelement und statischen Widerlager), IfB Freiberg, Germany.

Iwata, S., Tabuchi, T. and Warkentin, B.P. (1995) Soil-water interactions: mechanisms and applications. Marcial Dekker, NY.

Iyer, B. (1990) Pore water extraction: comparison of saturation extract and high-pressure squeezing. In Physico-Chemical Aspects of Soil and Related Material (Eds. K.B. Hoddinott and R.O. Lambs), ASTM STP 1095: 159-170.

JNC (1999a) H12: Project to establish the scientific and technical basis for HLW disposal in Japan. Project overview report. Japan Nuclear Cycle Development Institute (JNC).

JNC (1999b) H12: Project to establish the scientific and technical basis for HLW disposal in Japan. Supporting report 2: Repository design and engineering technology. Japan Nuclear Cycle Development Institute (JNC).

Johnston, L.N. (1942) Water permeable jacketed thermal radiators as indicators of field capacity and permanent wilting percentage in soils. Soil Science, 54: 123-126.

Josa, A., Alonso, E.E., Lloret, A., and Gens, A. (1987) Stress-strain behaviour of partially saturated soils. In Proceedings of the 9th European Conference on Soil Mechanics and Foundation Engineering, Dublin, 1987, Vol. 2: 561-564.

Kahr, G., Kraehenbuehl, F., Müller-Vonmoos, M., and Stöckli, H.F. (1986) Wasseraufnahme und Wasserbewegung in hochverdictetem Bentonit. Technischer Bericht 86-14, The Swiss National Cooperative for the Storage of Radioactive Waste (NAGRA), Wettingen, Switzerland.

Kalinski, R.J. and Kelly, W.E. (1993) Estimating water content of soils from electrical resistivity. Geotechnical Testing Journal, 16(3): 323-329.

Kassiff, G. and Ben Shalom, A. (1971) Experimental relationship between swell pressure and suction. Géotechnique, 21(3): 245-255.

Khalili, N., Geiser, F., and Blight, G.E. (2004) Effective stress in unsaturated soils: review with new evidence. International Journal of Geomechanics, 4(2): 115-126.

Kohgo, Y., Nakano, M., and Miyazaki, T. (1993) Theoretical aspects of constitutive modelling for unsaturated soils. Soil Mechanics and Foundation Engineering, 33(4): 43-63.

Komine, H. and Ogata, N. (2003) New equations for swelling characteristics of bentonite-based buffer materials. Canadian Geotechnical Journal, 40: 460-475.

Komornik, A. and Zeitlen, J.G. (1985) An apparatus for measuring lateral swelling pressure in the laboratory. In Proceedings of the 6th ICSMFE: 278-284.

Kozeny, J. (1927) Über kapillare Leitung des Wassers im Boden. Akademie der Wissesschaften. Wien, 136(2a): 271.

Kraehenbuehl, F., Stoeckeli, H.F., Brunner, F., Kahr, G., and Mueller-Vonmoos, M. (1987) Study of the water-bentonite system by vapor adsorption, immersion calorimetry and X-ray techniques: Micropore volumes and internal surface areas following DUBININ's theory. Clay Minerals, 22: 1-9.

Krahn, J. and Fredlund, D.G. (1972) On total, matric and osmotic suction. Soil Science, 115(5): 339-348.

Lambe, T.W. and Whitman, R.V. (1969) Soil mechanics. Wiley, NY.

Lang, A.R.G. (1967) Osmotic coefficients and water potentials of sodium chloride solutions from 0 to 40°C. Australian Journal of Chemistry, 20: 2017-2023.

Lee, R.K.C. and Fredlund, D.G. (1984) Measurement of soil suction using the MCS 6000 gauge. In Proceedings of the 5th International Conference on Expansive Soils, Institution of Engieers, Adelaide, Australia, 1984: 50-54.

Lee, H.C. and Wray, W.K. (1995) Techniques to evaluate soil suction – a vital unsaturated soil variable. In Proceedings of the 1st International Conference on Unsaturated Soils (UNSAT 95), Paris, 1995 (Eds. E.E. Alonso and P. Delage), Balkema, Rotterdam: 615-622.

Leong, E.C. and Rahardjo, H. (1997a) Review of soil-water characteristic curve equations. Journal of Geotechnical and Geoenvironmental Engineeing, 123(12): 1106-1117.

Leong, E.C. and Rahardjo, H. (1997b) Permeability functions for unsaturated soils. Journal of Geotechnical and Geoenvironmental Engineeing, 123(12): 1118-1826.

Leong, E. C., He, L. and Rahardjo, H. (2002) Factors affecting the filter paper method for total and matric suction measurements. Geotechnical Testing Journal, 25 (3): 321-332.

Leong, E.C., Tripathy, S., and Rahardjo, R. (2003) Total suction measurement of unsaturated soils with a device using the chilled-mirror dew-point technique. Géotechnique, 53(2): 173-182.

Leong, E.C., Tripathy, S., and Rahardjo, H. (2004) A modified pressure plate apparatus. Geotechnical Testing Journal, 27(3): 322-331.

Lide, D.R. and Frederikse, H.P.R. (1994) CRC Handbook of Chemistry and Physics. CRC Press Inc., Boca Raton, FL.

Likos, W.J. and Lu, N. (2003) Automated humidity system for measuring total suction characteristics of clay. Geotechnical Testing Journal, 26(2): 179-190.

Lloret, A., Villar, M.V., Sánchez, M., Gens, A., Pintado, X., and Alonso, E.E. (2003) Mechanical behaviour of heavily compacted bentonite under high suction changes. Géotechnique, 53(1): 27-40.

Low, P.F. (1961) Physical chemistry of clay-water interaction. Advances in Agronomy, 13: 269-327.

Lu, L. and Likos, W.J. (2003) Unsaturated soil mechanics. Wiley, NY.

Madsen, F.T. and Müller-Vonmoos, M. (1989) The swelling behaviour of clays. Applied Clay Science, 4: 143-156.

Marcial, D., Delage, P., and Cui, Y.J. (2002) On the high stress compression of bentonites. Canadian Geotechnical Journal, 39:812-820.

Marinho, F. and Chandler, R.J. (1995) Aspects of the behaviour of clays on drying. Unsaturated Soils, ASCE Geotechnical Special Publication, 39: 77-90.

Marshall, T.J. (1958) A relation between permeability and size distribution of pores. Journal of Soil Science, 9: 1-8.

Matyas, E.L. and Radhakrishna, M.S. (1968) Volume change characteristics of partially saturated soils. Géotechnique, 18(4): 432-448.

McKeen, R.G. (1980) Field studies of airport pavements on expansive soils. In Proceedings of the 4th International Conference on Expansive Soils: 242-261.

Meilani, I. Rahardjo, H., Leong, E.C., and Fredlund, D.G. (2002) Mini suction probe for matric suction measurements. Canadaian Geotechnical Journal, 39: 1427-1432.

Mesri, G. and Olson, R.E. (1971) Consolidation characteristics of montmorillonite. Géotechnique, 21(4): 341-352.

Mesri, G., Pakbaz, M.C. and Cepeda-Diaz, A.F. (1994) Meaning, measurement and field application of swelling pressure of clay shales. Geotechnique, 44(1): 129-145.

Milodowski, A.E., Hughes, C.R., Kemp, S.J., and Pearce, J.M. (1990) Characterization of bentonite alteration in reacted blocks from swelling-test experiments. British Geological Survey Report No. WG/90/39C.

Mitchell, J.K. (1993) Fundamentals of Soil Behavior. 2nd Edition. John Wiley & Sons Inc., NY.

Mongiovi, L. and Tarantino, A. (1998) An apparatus to investigate the two effective stresses in unsaturated soils. In Proceedings of the 2nd International Conference on Unsaturated Soils, Beijing, China, 1998, International Academic Publisher, Beijing: 422-425.

Morris, P.H., Graham, J., and Williams, D.J. (1992) Cracking in drying soils. Canadian Geotechnical Journal, 29: 263-277.

Mualem, Y. (1976). A new model for predicting the hydraulic conductivity of unsaturated porous media. Water Resources Research, 12: 513-522.

Müller-Vonmoos, M. and Kahr, G. (1982) Bereitstellung der Bentonite für die Laboruntersuchung. Technischer Bericht 82-04, The Swiss National Cooperative for the Storage of Radioactive Waste (NAGRA), Wettingen, Switzerland.

Müller-Vonmoos, M., Bucher, F., Kahr, G., Madsen, F., and Mayor, P.A. (1991) Wechsellagerung und Quellverhalten von Kalium-Bentoniten. Technischer Bericht 91-31, The Swiss National Cooperative for the Storage of Radioactive Waste (NAGRA), Wettingen, Switzerland.

Nagaraj, T.S. and Srinivasa Murthy, B.R. (1985) Prediction of preconsolidation pressure and recompression index of soils. Geotechnical Testing Journal, 8(4): 199-203.

Nagaraj, T.S., Pandian, N.S., Sashikumar, B.M., and Sivakumar Babu, G.L. (1988) An approach to predict tropical soil behaviour. In Proceedings of the 2nd International Conference on Geomechanics of Tropical Soils, Singapore, Vol. 1: 167-174.

Nagaraj, T.S. and Miura, N. (2001) Soft clay behaviour─analysis and assessment. Balkema, Rotterdam.

Navarro, V. and Alonso, E.E. (2001) Secondary compression of clays as a local dehydration process. Géotechnique, 51(10): 859-869.

Nelson, J.D. and Miller, D.J. (1992) Expansive soils: problems and practice in foundation and pavement engineering. John Wiley & Sons, NY.

Olsen (1962) Hydraulic flow through saturated clays. Clays and Clay Minerals, 9: 131-161.

Olson, R.E. and Langfelder, L.J. (1965) Pore-water pressures in unsaturated soils. Journal of Soil Mechanics and Foundation Division, Proceedings of American Society of Civil Engineers, 91(SM4): 127-160.

Olson, R.E. (1986) State of the art: consolidation testing. Consolidation of Soils: Testing and Evaluation (Eds. R.N. Yong and F.C. Townsend, ASTM STP 892, Philadelphia: 7-70.

ONDRAF/NIRAS (2001) Safety assessment and feasibility interim report (SAFIR) 2. Report No. NIROND 2001-06 E, Belgian Agency for Radioactive Waste and Fissile Materials (ONDRAF/NIRAS), December 2001.

ONDRAF/NIRAS (2003) Belgian Agency for Radioactive Waste and Fissile Materials (ONDRAF/NIRAS). Official Website. www.nirond.be.

Orsi, T.H., Edwards, C.M., Anderson, A.L. (1994) X-ray computed tomography: a nondestructive method for quantitative analysis of sediment cores. Journal of Sedimentary Research, A64: 690–693.

Peck, A.G. and Rabbidge, R.M. (1966) Design and performance of an osmotic tensiometer for measuring capillary potential. In Proceedings of Soil Science Society of America, 33(2): 196-202.

Phene, C.J., Hoffmann, G.J., and Rawlins, S.L. (1971) Measuring soil matric potential in situ by sensing heat dissipation with a porous body: theory and sensor construction. In Proceedings of Soil Science Society of America, 35: 27-32.

Pusch, R. (1979) Highly compacted sodium bentonite for isolating rock-deposited radioactive waste products. Nuclear Technology, 45: 153-157.

Pusch, R. (1985) Final report of the Buffer Mass Test-Volume III: Chemical and physical stability of the buffer materials. Stripa Project 85/14, The Swedish Nuclear Fuel and Waste Management Company (SKB), Stockholm, Sweden.

Pusch, R. and Güven, M. (1988) Electronmicroscopic examination of hydrothermal treated bentonite. In Proceedings of the Workshop of Artifical Clay Barriers for High Level Radioactive Waste Repositories, Lund, Sweden: 35-46.

Pusch, R. (2001) The microstructure of MX-80 clay with respect to its bulk physical properties under different environmental conditions. SKB Technical Report, TR-01-08. The Swedish Nuclear Fuel and Waste Management Company (SKB), Stockholm, Sweden.

Rawlins, S.L. and Dalton, F.N. (1967) Psychrometric measurement of soil water potential without precise temperature control. Proceedings of Soil Science of America, 31: 297-301.

Richards, L.A. (1931) Capillary conduction of liquids through porous medium. Journal of Physics, 1: 318-333.

Richards, B.G. (1965) Measurement of the free energy of soil moisture by the psychrometric technique using thermistors. In Moisture Equlibria and Moisture Changes in Soils Beneath Covered Areas, A Symposium in Print, Butterworths, Australia: 39-46.

Richards, B.G. (1974) Behaviour of unsaturated soils. In Soil Mechanics—New Horizons (Ed. I.K. Lee), American Elsevier, NY.

Ridley, A.M. and Burland, J.B. (1993) A new instrument for the measurement of soil moisture suction. Géotechnique, 43(2): 321-324.

Ridley, A.M. (1995) Discussion on "Laboratory filter paper suction measurements" by Houston et al. Geotechnical Testing Journal, GTJODJ, 18(3): 391-396.

Ridley, A.M. and Wray, W.K. (1996) Suction measurement: a review of current theory and practices. In Proceedings of the 1st International Conference on Unsaturated Soils (UNSAT 95), Paris, 1995 (Eds. E.E. Alonso and P. Delage), Balkema, Rotterdam: 1293-1322.

Romero, E., Gens, A., and Lloret, A. (1999) Water permeability, water retention and microstructure of unsaturated compacted Boom clay. Engineering Geology, 54: 117-127.

Romero (2001) Controlled suction techniques. In 4^{o} Simposio Brasileiro de Solos Nâo Saturados, Porto Alegre, Brasil, 2001 (Eds. W.Y.Y. Gehling and F. Schnaid): 535-542.

Romero, E., Alonso, E., García, I., and Knobelsdorf, J. (2002) Microstructural changes affecting air permeability through an unsaturated 80/20 sand-bentonite mixture. In Proceedings of Workshop on Clay Microstructure and Its Importance to Soil Behaviour, Lund, Sweden, 2002 (Ed. R. Pusch), SKB, Sweden: 1-8.

Romero (2003) The UPC pneumatic oedometer cell. Personal communication.

Romero, E., Gens, A., and Lloret, A. (2003) Suction effects on a compacted clay under non-isothermal conditions. Géotechnique, 53(1): 65-81.

Schanz, T. (1998) Zur Modellierung des Mechanischen Verhaltens von Reibungsmaterialen. Habilitation, University of Stuttgart, Germany.

Schanz, T. and Tripathy, S. (2003) Development of a high pressure oedometer system for testing expansive soils. De-sign and Specifications. Laboratory of Soil Mechanics, Bauhaus-University Weimar, Germany.

Schanz, T. Agus, S.S. and Tscheschlok, G. (2004) Determination of hydro-mechanical properties of Trisoplast®. Research Report Bo-015/03. Laboratory of Soil Mechanics, Bauhaus-University Weimar, Weimar, Germany.

Schick (2004) The pF-curve of fine-grained soils at high pore water suction. In Proceedings of the International Unsaturated Soil Conference. From Experimental Evidence Towards Numerical Modelling of Unsaturated Soils, Weimar, Germany, 2003 (T. Schanz ed.), Lecture Notes in Applied Mechanics, Springer: 69-89.

Schmidt, W., Sitz, P., and Kessler, J. (1992) Physikalische und chemische Eigenschaften von Bentonite als Verfüll- und Versigelungsmaterial bei der Endlagerung radioaktiver Abfälle. Technischer Bericht 93-37, The Swiss National Cooperative for the Storage of Radioactive Waste (NAGRA), Wettingen, Switzerland.

Schofield, R.K. (1946) Ionic forces in thick films of liquid between charged surface. Transaction of Faraday Society, 42B: 219.

Schofield, A.N. and Wroth, C.P. (1968) Critical state soil mechanics. McGraw-Hill, London.

Shaw, B. and Baver, L.D. (1939) An electrothermal method for following moisture changes of the soil insitu. In Proceedings of Soil Science Society of America, 4: 78-83.

Shuai, F. and Fredlund, D.G. (1998) Model for the simulation of swelling pressure measurements on expansive soils. Canadian Geotechnical Journal, 35: 96-114.

Slade, P.G. and Quirk, J.P. (1991) The limited crystalline swelling of smectite in $CaCl_2$, $MgCl_2$, and $LaCl_3$ solutions. Journal of Colloid Interface Science, 144: 18-26.

Slichter, C.S. (1898) Theoretical investigation of the motion of ground waters. 19th Annual Report. U.S. Geology Survey.

Sitz, P. (1997) Materialuntersuchungen für Mehrkomponentensysteme auf Ton/Bentonit Basis für Dichtung und Lastabtrag, mit hohem Ruckhaltvermögen, für den langzeitsicheren Verschluß von UTD und Endlagern im Salinar. Abschlußbericht 02 C 0193 (BMBF), TU Bergakademie Freiberg, Germany.

Sitz, P. (2003) Entwicklung eines Grundkonzeptes für langzeitstabile Streckenverschlussbauwerke für UTD im Salinar, Bau und Test eines Versuchsverschlussbauwerkes unter realen Bedingungen. Forschungsvorhaben 02 C 05472 (BMBF), TU Bergakademie Freiberg, Germany.

SKB (2003) The Swedish Nuclear Fuel and Waste Management Company. Official Website. www.skb.se.

Soilmoisture Equipment Corp. (2002) Commercial Publications. P.O. Box 30025, Santa Barbara, CA.

Spanner, D.C. (1951) The Peltier effect and its use in the measurement of suction pressure. Journal of Experimental Botany, 2: 145-168.

Sridharan, A., Altschaeffl, A. G., and Diamond, S. (1971) Pore size distribution studies. Journal of Soil Mechanics and Foundation Engineering, 97, (SM 5): 771–787.

Sridharan, A. and Jayadeva, M.S. (1982) Double layer theory and compressibility of clays. Geotechnique, 32(2): 133-144.

Sridharan, A., Sreepada Rao, A. and Sivapullaiah, P.V. (1986) Swelling pressure of clays. Geotechnical Testing Journal, GTJODJ, 9(1): 24-33.

Sridharan, A., Murthy, N.S., and Prakash, K. (1987) Rectangular hyperbola method of consolidation analysis. Géotechnique, 37(3): 335-368.

Sridharan, A. and Nagaraj, H.B. (1999) Absorption water content and liquid limit of soils. Geotechnical Testing Journal, GTJODJ, 22(2): 121-127.

Sridharan, A. and Prakash, K. (2000) Percussion and cone methods of determining liquid limit of soils: controlling mechanisms. Geotechnical Testing Journal, 23(2): 242-250.

Sridharan, A. and Gurtug, Y. (2004) Swelling behaviour of compacted fine-grained soils. Engineering Geology, 72: 9-18.

Srinivasa Murthy, B.R., Nagaraj, T.S. and Bindhumadhava (1987) Influence of coarse particles on compressibility of soils. In Proceedings of the International Symposium on Prediction and Performance in Geotechnical Engineering, Calgary, Canada, 1987, Balkema, Rotterdam: 195-200.

Stern (1924) Zur Theorie der elektrolytischen Doppelschicht. Zeitschrift Elektrochemie, 30: 508-516.

Stewart, D.I., Cousens, T.W., Studds, P.G. and Tay, Y.Y. (1999) Design parameters for bentonite-enhanced sands as a landfill liner. Proceedings of Institution of Civil Engineers Geotechnical Engineering, 137: 189-195.

Struder, J., Amman, W., Meier, P., Muller, Ch., and Glauser, E. (1984) Verfüllen und Versiegeln von Stollen, Schächten und Bohrlöchern. Technischer Bericht 84-33, The Swiss National Cooperative for the Storage of Radioactive Waste (NAGRA), Wettingen, Switzerland.

Studds, P.G., Stewart, D.I. and Cousens, T.W. (1998) The effects of salt solutions on the properties of bentonite-sand mixtures. Clay Minerals, 33: 651-660.

Subba Rao, K.S. and Tripathy, S. (2003) Effect of aging on swelling and swell-shrink behaviour of a compacted expansive soil. Geotechnical Testing Journal, 26(1): 1-11.

Tang, X., Graham, J., and Wan, A.W.L. (1997) Measuring total suctions by psychrometer in triaxial tests. In Proceedings of the XIVth International Conference on Soil Mechanics and Foundation Engineering, Hamburg, Germany, 1997, Vol. 1: 213-216.

Tang, G.X., Graham, J., Blatz, J., Gray, M., and Rajapakse, R.K.N.D. (2002) Suctions, stresses and strengths in unsaturated sand-bentonite. Engineering Geology, 64: 147-156.

Terzaghi, K. (1925). Erdbaumechanik auf bodenphysikalischer Grundlage. Franz Deuticke. Leipzig und Wien.

Terzaghi, K. (1936) The shear resistance of saturated soils. In the Proceedings of the 1st International Conference on Soil Mechanics, Vol. 1: 54-56.

Topp, G.C., Davis, J.L., and Annan, A.P. (1980) Electromagnetic determination of soil water content: Measurements in coaxial transmission lines. Water Resources Research, 6(3): 574-582.

Tripathy, S., Schanz, T., and Sridharan, A. (2004) Swelling pressures of compacted bentonites from diffuse double layer theory. Canadian Geotechnical Journal, 41: 437-450.

U.S.D.A (1950) U.S.D.A. Agricultural Handbook No. 60, Diagnosis and Improvement of Saline and Alkali Soils.

Vaisala (2002) HMP240 series transmitters. User's guide. Vaisala Oyj., Helsinki, Finland.

van Genuchten, M.T. (1980). A closed-form equation for predicting the hydraulic conductivity of unsaturated soils. Soil Science Society of America Journal, 44: 892-898.

van Olphen, H. (1977) An introduction to clay colloid chemistry. 2nd Edition, Wiley Interscience, NY.

Verwey, E.J.W. and Overbeek, J.T.G. (1948) Theory of the stability of lyophobic colloids. Elsevier, NY.

Vu, H.Q. and Fredlund, D.G. (2004) The prediction of one-, two-, and three-dimensional heave in expansive soils. Canadian Geotechnical Journal, 41: 713-737.

Wang, X. and Benson, C.H. (2004) Leaf-free pressure plate extractor for measuring the soil water characteristic curve. Geotechnical Testing Journal, 27(2).

Wanner, H. (1986) Modelling interaction of deep groundwaters with bentonite and radionuclide speciation. Technical Report 86-12, The Swiss National Cooperative for the Storage of Radioactive Waste (NAGRA), Wettingen, Switzerland.

Washburn, E.W. (1921) A method of determining the distribution of pore sizes in a porous material. Proceedings of the National Academy of Sciences, 7: 115.

Wellington, S.L. and Vinegar, H.J. (1987) X-ray computerized tomography. Journal of Petroleum Technology, 39(8): 885–898.

Wescor Inc. (1986) HR 33T Dew point microvoltmeter: Instruction/service manual. Wescor Inc., Utah.

White, I., Zegelin, S.J., Topp, G.C., and Fish, A. (1994) Effect of bulk electrical conductivity on TDR measurement of water content in porous media. In Proceedings of the Symposium on Time Domain Reflectometry in Environmental, Infrastructure, and Mining Applications, Evanston, Illinois, 1994, U.S. Bureau of Mines, Special Publication SP 19-94: 294-308.

Wiederhold, P.R. (1997) Water vapour measurement—methods and instrumentation. Marcial Dekker, NY.

Williams, T.M. and Miknis, F. P. (1997) Use of Environmental SEM to study asphalt-water interaction. Journal of Materials in Civil Engineering, Vol. 10 (2).

Wittke, W. (1996) Abdichtung von Strecken im Endlager Morsleben mit hochverdichtetem Bentonit. Geotechnik, 19(4): 304-311.

Wittke, W., Schmitt, D., Gattermann, J. (1998) Verschließkonzept für Untertagedeponien—Entwurf und geotechnische Nachweis. Geotechnik, 21(3): 212-216.

Wong, J.C., Rahardjo, H., Toll, D.G., and Leong, E.C. (2001) Modified triaxial apparatus for shearing infiltration test. Geotechnical Testing Journal, GTJODJ, 24(4): 370-380.

Xie, M., Wang, W., de Jonge, J., and Kolditz, O. (2003) Numerical modeling of swelling processes in highly compacted bentonites. In Proceedings of GeoProc 2003 (Eds. Stephanson et al.): 315-320.

Xie, M., Agus, S.S., Schanz, T., and Kolditz, O. (2004) An upscaling method and a numerical analysis of swelling/shrinking processes in a compacted bentonite/sand mixture. International Journal for Numerical and Analytical Methods in Geomechanics, 28(15): 1479-1502.

Yong, R.N., Boonsinsuk, P., and Wong, G. (1986) Formulation of backfill material for a nuclear fuel waste disposal fault. Canadian Geotechnical Journal, 23: 216-228.

Yong, R.N. (1999) Soil suction and soil-water potentials in swelling clays in engineered clay barriers. Engineering Geology, 54: 3-13.

Yu, X. and Drnevich, V.P. (2004) Soil water content and dry density by time domain reflectometry. Journal of Geotechnical and Geoenvironmental Engineering, 130(9): 922-934.

Zhang, X.W., Liu, X., Gu, D.X., Zhou, W., Wang, R.L., and Liu, P. (1996) Desorption isotherms of some vegetables. Journal of the Science of Food and Agriculture, 70: 303-306.

Zerhouni (1995) Triaxial testing using psychrometers (In French). In Proceedings of the 1st International Conference on Unsaturated Soils (UNSAT 95), Paris, 1995 (Eds. E.E. Alonso and P. Delage), Balkema, Rotterdam: 673-678.

Zur, B. (1966) Osmotic control of the matric soil water potential. Soil Science, 102: 394-398.